

ADVANCED NONDESTRUCTIVE MONITORING AND EVALUATION OF  
DAMAGE IN CONCRETE MATERIALS

By

CHRISTOPHER C. FERRARO

A THESIS PRESENTED TO THE GRADUATE SCHOOL  
OF THE UNIVERSITY OF FLORIDA IN PARTIAL FULFILLMENT  
OF THE REQUIREMENTS FOR THE DEGREE OF  
MASTER OF ENGINEERING

UNIVERSITY OF FLORIDA

2003

Copyright 2003

by

Christopher C. Ferraro

This thesis is dedicated to my loving family, my parents, Ronald and Victoria Ferraro, my sister Alicia Ferraro, my brother Ronald Ferraro Jr. and to my loving girlfriend Aliza Bar-David as they have offered their support and love throughout this endeavor. It is with the love and support of my family and friends that I am able to reach my goals.

## ACKNOWLEDGMENTS

The author would like to thank all of the members of his supervisory committee for their help and ideas throughout this effort. Dr. Andrew Boyd, the committee chair, provided valuable time and knowledge of the subject, as well as financial support, making this research successful.

Acknowledgement is owed to Dr. H.R. Hamilton and Dr. David Bloomquist for their contribution of time and knowledge, which provided to be invaluable assistance and guidance during this effort.

The author would also like to express gratitude to all of those within the Department of Civil and Coastal Engineering Department including George Lopp, Chuck Broward and Scott Cumming.

For her enormous efforts the author would like to extend his gratitude to Ms. Eileen Czarnecki. Her time and assistance were crucial to the completion of this research in a timely manner.

The author would also acknowledge PhD candidates Christos Drakos and Forrest Masters. Their mentoring and assistance on a professional and personal level were greatly appreciated.

The author would also like to thank his best friend, Aliza Bar-David, for the unyielding support and patience she offered me during the research and writing of this thesis.

## TABLE OF CONTENTS

	<u>page</u>
ACKNOWLEDGMENTS .....	iv
LIST OF TABLES .....	viii
LIST OF FIGURES .....	ix
ABSTRACT .....	xv
CHAPTER	
1 INTRODUCTION .....	1
2 LITERATURE REVIEW .....	4
Introduction to Nondestructive Testing .....	4
Literature Review .....	4
Visual Inspection .....	4
Liquid Penetrant Methods .....	10
Acoustic Sounding .....	13
Surface Hardness Methods .....	18
Penetration Resistance Methods .....	20
Pullout Test .....	21
Break-Off Test .....	23
Ultrasonic Testing .....	25
Impact Echo .....	53
Acoustic Emission .....	81
Impulse Response .....	95
Magnetic Methods .....	102
Ground Penetrating Radar .....	107
Resonant Frequency .....	111
Infrared Thermography .....	115
Radioactive Testing .....	123
3 SURVEY OF RELEVANT BRIDGE STRUCTURES IN FLORIDA .....	129
Definition of Sufficiency Rating .....	130
Methodology .....	131
Results .....	134
Conclusions .....	135

4	BRIDGE INSPECTIONS.....	137
	Document Review .....	137
	NDT Methods Used for Inspection.....	138
	Bahia Honda Bridge .....	138
	Site Information.....	138
	Procedures .....	138
	Results .....	139
	Conclusions .....	141
	Niles Channel Bridge.....	147
	Site Information.....	147
	Procedures .....	147
	Results .....	148
	Conclusions .....	150
	Sebastian River Bridge .....	153
	Site Information.....	153
	Procedures .....	153
	Results .....	153
	Conclusions .....	155
	Wabasso Bridge.....	158
	Site Information.....	158
	Procedures .....	158
	Results .....	159
	Conclusions .....	160
	Sebastian Inlet Bridge.....	163
	Site Information.....	163
	Procedures .....	164
	Results .....	165
	Conclusions .....	166
5	NONDESTRUCTIVE LABORATORY SPECIMEN TESTING.....	169
	Prior Research.....	169
	Methodology.....	170
	Procedure.....	170
	Results and Discussion .....	173
	Conclusions.....	179
6	LABORATORY SIMULATION OF DAMAGE OBSERVED IN THE FIELD....	181
	Prior Research.....	181
	Methodology.....	182
	Procedure.....	182
	Results and Discussion .....	186
	Conclusions.....	192

## APPENDIX

A	SUMMARY OF PONTIS RESULTS .....	193
B	SUMMARY OF DEFICIENT BRIDGES.....	211
C	NDT DATA AND RESULTS FROM BRIDGE TESTING .....	212
D	LABORATORY DATA OF CYLINDER SPECIMENS.....	225
E	LABORATORY DATA AND GRAPHICAL RESULTS OF LARGE SCALE SPECIMENS .....	231
F	SUMMARY OF STASTICAL RESULTS OF ULTRASONIC PULSE VELOCITY DATA .....	282
	LIST OF REFERENCES.....	286
	BIOGRAPHICAL SKETCH .....	293

## LIST OF TABLES

<u>Table</u>	<u>page</u>
2.1 Standard sizes of pin and probe used for penetration tests. ....	21
2.2 Acoustic velocities of common materials used in construction .....	37
2.3 Relationship between pulse velocity and concrete quality.....	52
2.4 Emissivities of common engineering materials .....	118
5.1 Mixture proportions for NDT and strength tests. ....	170
5.2 Compressive strength vs. resonant frequency of concrete samples. ....	178
6.1 Mixture proportions for NDT and strength tests.....	183

## LIST OF FIGURES

<u>Figure</u>	<u>page</u>
2.1 Flexible borescope.....	7
2.2 Flexible borescope and monitor .....	7
2.3 Rigid borescope.....	7
2.4 Robot used for visual survey at the WTC disaster site .....	9
2.5 Robot used for visual survey at the WTC disaster site .....	10
2.6 Cracks in concrete pavement with moisture present.....	11
2.7 Contact angles for various liquids.....	12
2.8 Coin tap test results (a) Force-time histories of solid and disbonded areas of a carbon fiber reinforced skinned honeycomb structure, (b) Spectra of time histories .....	14
2.9 Illustration of typical pullout test .....	22
2.10 Typical cross section of the breakoff test, all dimensions in mm .....	24
2.11 Sinusoidal oscillation of a loaded spring.....	27
2.12 Model of an elastic body .....	28
2.13 Graphical illustration of Snell's law.....	30
2.14 A portable ultrasonic testing device used at the University of Florida .....	32
2.15 Schematic of a pulse velocity apparatus .....	34
2.16 Idealized scans of a material defect: a) A-scan, b) B-scan, c) C-scan, .....	35
2.17 Typical ultrasonic test procedure .....	36
2.18 Methods of pulse velocity measurements: a) direct method, b) indirect method, c) surface method .....	39

2.20	Schematic of pulse-echo and pitch and catch techniques.....	42
2.21	Pulse echo schematic (a)Typical test setup, and (b) resulting display .....	43
2.22	Reflections of stress waves from internal discontinuities .....	44
2.23	Signal scatter due to uneven reflecting surface morphology .....	44
2.24	Setup of ultrasonic tomographic ray paths .....	48
2.25	Measurement of crack depth .....	50
2.26	Schematic of a typical piezoelectric transducer used for impact echo testing .....	55
2.27	View of a typical impact-echo equipment system.....	57
2.28	Illustration of typical wave propagation through a cross section of a solid.....	58
2.29	Illustration of wave propagation model through a cross section of a solid.....	59
2.30	The typical force-time function for the elastic impact of a sphere on a solid.....	60
2.31	Example of frequency analysis using FFT (a) represents the frequency distribution, (b) represents the corresponding amplitude spectrum .....	62
2.32	Plots of P, S and R-waves at various times after an impact (a) 125 $\mu$ s, (b)150 $\mu$ s, (c)200 $\mu$ s and (d) 250 $\mu$ s.....	64
2.33	The ray path of typical P-wave propagation through a solid media.....	64
2.34	Impact echo ray paths (a) A phase change at both boundaries(b) A phase change at upper boundary only .....	67
2.35	Schematic representations of (a) P-wave ray reflections and (b) the resulting idealized waveform .....	68
2.36	Actual waveform on an impact-echo test plate .....	70
2.37	Schematic representation of the test set up for wave speed measurements .....	71
2.38	Example waveform obtained in wave speed measurements .....	72
2.39	Illustration of the smallest detectable crack and its dependency on depth.....	73
2.40	A crack at depth ‘d’ gives the same response as a void at that depth .....	74
2.41	Surface-opening cracks: (a) perpendicular, (b) inclined, and (c) curved .....	76

2.42	Measuring the depth of a surface-opening crack: (a) schematic of experimental test setup, and (b) sample waveforms .....	76
2.43	The impact-echo response of a concrete slab on soil subgrade: (a) cross-section, (b) waveform, and (c) spectrum .....	78
2.44	The impact-echo response obtained from a concrete slab at a location where a void exists in the soil subgrade (a) cross-section; (b) waveform; and (c) spectrum .....	78
2.45	Burst acoustic emission signal with properties .....	82
2.46	Acoustic emission process .....	82
2.47	Basic setup of acoustic emission equipment .....	85
2.48	Various acoustic emission sensors .....	85
2.49	Transient recorder with multiple output acoustic emission signals .....	88
2.50	Acoustic emission calibration block .....	89
2.51	Placement of sensors on a concrete cube .....	92
2.52	The instrumented sledgehammer and geophone used in the IR method .....	97
2.53	Schematic of the impulse response technique .....	97
2.54	Theoretical impulse response mobility spectrum .....	98
2.55	Typical mobility plot for sound concrete .....	99
2.56	Mobility plots for sound and debonded concrete .....	100
2.57	Mobility plots for sound and delaminated concrete .....	101
2.58	Schematic of a typical magnetic field induced by an electric current .....	103
2.59	Covermeter used by the Civil Engineering Department at the University of Florida .....	106
2.60	Typical configuration of covermeter testing apparatus .....	107
2.61	Typical display of a GPR Scan. The white portion denotes an anomaly .....	110
2.62	Typical forced resonant frequency setup .....	113
2.63	Dynamic modulus of elasticity vs. cylinder compressive strength .....	114

2.64	The electromagnetic spectrum .....	116
2.65	Typical thermograph revealing defects .....	118
2.66	Schematic of a scanning radiometer IR camera .....	121
2.67	Schematic description of thermographic void detection process.....	122
2.68	Radiography schematic .....	124
2.69	Schematics of direct radiometry: (a) with an internal signal detector and external source, (b) with an external signal detector and source .....	126
2.70	Schematic of backscatter radiometry .....	126
2.71	Image of prestressing cable anchorage in concrete (a) X-radioscopic image of a prestressing cable anchorage embedded in a concrete, (b) schematic and brief explanation of the radiographic image .....	127
3.1	Summary of sufficiency rating factors .....	130
3.2	The result of a typical bridge query by sufficiency rating .....	132
3.3	Examples of Pontis codes vs. sufficiency ratings. ....	133
4.1	Plan view of Bahia Honda bridge pilecap and column 54 .....	144
4.2	Photo location plan Bahia Honda bridge pile cap and column 54 .....	144
4.3	View of bridge superstructure from water-level .....	145
4.4	View of footing .....	145
4.5	View of crack in column .....	146
4.6	View of crack in column. Efflorescence of the gunite topping on the strut can be seen in the background .....	146
4.7	Plan view of crack orientation on column 54.....	147
4.8	Plan view of Niles Channel Bridge column line 20 .....	151
4.9	General view of Niles Channel Bridge underside, column line 20 in foreground .....	151
4.10	Impact-echo testing on bridge column .....	152
4.11	View of typical strut and column repair .....	152

4.12	Plan view of Sebastian River Bridge column line 11.....	156
4.13	General view of Sebastian River Bridge.....	156
4.14	Column line 11 with column 11-5 in foreground.....	157
4.15	Column 11-4.....	157
4.16	Cracked and delaminated repair in column 11-4 .....	158
4.17	Plan view of Wabasso Bridge column .....	162
4.18	General view of Wabasso Bridge.....	162
4.19	Column / pilecap 5 .....	163
4.20	Close-up of exposed seashell aggregate on pile cap 5 .....	163
4.21	Plan view of column / pile cap of Sebastian Inlet Bridge.....	167
4.22	General view of Sebastian Inlet Bridge underside. Column line 7 in foreground adjacent to stairs .....	167
4.23	Column line 6 .....	168
4.24	Plan view of crack orientation on column 12.....	168
5.1	Ultrasonic pulse velocity experimental setup.....	171
5.2	Resonant frequency experimental setup.....	172
5.3	Impact echo experimental setup.....	172
5.5	Frequency spectrum of outlying data point.....	176
5.6	Frequency spectrum of typical impact echo data point.....	176
5.7	Compressive strength vs. resonant frequency for Mixtures A and B.....	178
6.1	Setup of laboratory experiment.....	183
6.2	Ultrasonic pulse velocity testing on specimen .....	185
6.3	Impact-echo testing on specimen .....	186
6.4	Wave velocity vs. age for a sample from Mixture A exposed to limewater. ....	187
6.5	Wave velocity vs. age for a sample from Mixture A exposed to sulfate solution.....	187

6.6	Close up view of a sample exposed to sulfate solution. The arrow denotes the area of precipitated salt crystals. ....	189
6.7	Wave velocity vs. age for a sample from Mixture B exposed to limewater .....	190
6.8	Wave velocity vs. age for a sample from Mixture B exposed to sulfate solution .....	190

Abstract of Thesis Presented to the Graduate School  
of the University of Florida in Partial Fulfillment of the  
Requirements for the Degree of Master of Engineering

ADVANCED NONDESTRUCTIVE MONITORING AND EVALUATION OF  
DAMAGE IN CONCRETE MATERIALS

By

Christopher Charles Ferraro

December 2003

Chair: Andrew J. Boyd

Major Department: Civil and Coastal Engineering

The objective of this work is to perform research that will enable the FDOT to nondestructively assess and monitor the quality of *in-situ* concrete bridge structures. As part of the research, a literature review of relevant nondestructive methods was performed. Also survey of relevant bridge structures within the FDOT's bridge database system was conducted in an attempt to categorize prevalent bridge deficiencies occurring throughout the state.

Field research concentrated on the application of the most appropriate nondestructive testing (NDT) methods and their application to materials assessment and interpretation of typical NDT data. The attempt of qualifying the onset of damage was attempted using the applicable NDT method. General material properties of good quality bridge materials were tested nondestructively.

Laboratory research focused on the establishment of the nondestructive material properties and their relationship to strength properties, which were obtained via the use of

destructive tests after NDT was performed. Other laboratory research monitored the changes of NDT data within concrete samples under constant exposure to severe environments. This experiment was designed to differentiate the effects certain solutions have on field-size samples of concrete when exposed over periods of time. The primary objective of this experiment was to observe the effect of exposure of concrete to sulfate solutions with respect to surface wave velocity and through wave velocity.

Field studies suggest that the wave velocity of concrete samples decreases with increasing damage. However, the lack of controlled experiments, involving continuous laboratory monitoring, with respect to stress wave velocity and damage prevents the quantification of the two parameters.

## CHAPTER 1 INTRODUCTION

Performance testing of Portland cement concrete materials dates back to the early 1830's, when systematic tests were performed on concrete samples in Germany. Since then, standards for Portland concrete have been created and published by various organizations throughout the world.

The concept of nondestructive testing (NDT) is to obtain material properties of in-place specimens without the destruction of the specimen nor the structure from which it is taken. However, one problem that has been prevalent within the concrete industry for years is that the true properties of an in-place specimen have never been tested without leaving a certain degree of damage on the structure. For most cast-in-place concrete structures, construction specifications require that test cylinders be cast for 28-day strength determination. Usually, representative test specimens are cast from the same concrete mix as the larger structural elements. Unfortunately, test specimens are not an exact representation of *in-situ* concrete, and may be affected by variations in specimen type, size, and curing procedures (Neville 1996).

Virtually all concrete structures exposed to nature experience deterioration over time. Inspection personnel have difficulty determining the quality of *in-situ* concrete that has experienced decay without direct material sampling. The disadvantage to material sampling is that an inspector must remove a portion of the structure, usually by means of coring, and make repairs to the sample area. Removing cores from a concrete structure is

an intrusive process that can weaken the structure and usually leads to long-term durability concerns.

The majority of bridges in the state of Florida are constructed of concrete. The Florida Department of Transportation (FDOT) has been experiencing increased costs for bridge rehabilitation and reconstruction due to deterioration of concrete bridge elements as a result of exposure.

The objective of this work is to perform research that will enable the FDOT to nondestructively assess and monitor the quality of *in-situ* concrete bridge structures. As part of the research, a literature review of any relevant nondestructive methods was performed. Also, relevant bridge structures within the FDOT's bridge database system were reviewed in an attempt to categorize prevalent bridge deficiencies occurring throughout the state.

Field research concentrated on the application of the most appropriate NDT methods and their application to the materials assessment and the interpretation of typical NDT data. The attempt of qualifying the onset of damage was attempted using applicable NDT methods. General material properties of good quality bridge materials were established nondestructively.

Laboratory research focused on the establishment of the nondestructive material properties and their relation to strength properties, which were obtained via the use of destructive tests after NDT was performed. Other laboratory research monitored the changes in NDT data within concrete samples under constant exposure to severe environments.

Concrete specimens of dimensions were created to simulate the effect of curing and damage on field-sized specimens. Two different mixtures of specimens were cast and placed in solutions to observe changes in the material properties. One set of specimens was partially submerged in sulfate solution to simulate the effect of a harsh environment and its effects on concrete specimens with age. The other set of specimens was partially submerged in limewater solution to simulate the effect of a control group.

The testing regimen consisted of weekly NDT testing of the concrete samples, at ages of one day, one week, two weeks, three weeks, four weeks, six weeks, eight weeks, 10 weeks 12 weeks and 13 weeks. The samples were removed from their respective solutions at the age of 90 days. Nondestructive testing was carried out to assess the material property changes over time.

## CHAPTER 2 LITERATURE REVIEW

### **Introduction to Nondestructive Testing**

The purpose of establishing standard procedures for nondestructive testing (NDT) of concrete structures is to qualify and quantify the material properties of in-situ concrete without intrusively examining the material properties. There are many techniques that are currently being researched for the NDT of materials today. This chapter focuses on the NDT methods relevant for the inspection and monitoring of concrete materials.

### **Literature Review**

#### **Visual Inspection**

Visual inspection refers to evaluation by means of eyesight, either directly or assisted in some way. The visual inspection of a structure is the “first line of defense” and typically involves the search for large-scale deficiencies and deformities. Perhaps the most important aspect related to the preparation for visual inspection is the review of available literature related to the structure or structural element. This should include original drawings, notes and reports from previous inspections, and interviews with personnel familiar with the structure or structural element to be inspected. Although interviews are usually not in themselves considered a type of visual inspection, the interview process can often precipitate a visit to the structure or structural element that can then focus on visible defects noted by site personnel, who usually have the most familiarity with the structure.

**Direct visual inspection**

The basic principle of direct visual inspection is a meticulous attention to detail. The most common tools used by inspectors include calipers, gauges, templates, micrometers, rulers, levels, chalk, illumination devices, cameras, note taking devices, and other miscellaneous equipment.

Direct visual inspection can be applied to most methods of preventative maintenance and rehabilitation work. Many inspectors are usually so involved with the search for small-scale deficiencies within a structure that large-scale deficiencies are sometimes overlooked. It is important for the inspector to periodically take a step back and look for larger scale deficiencies. This “can’t see the forest for the trees” syndrome occurs more often in the consulting industry than most people realize, especially when lesser-experienced inspection personnel are involved.

**Remote visual inspection**

Often, field conditions are not conducive to the direct inspection of a structure or its component elements. Sight limitations could be a result of inaccessibility due to obstructions, hazardous conditions or deficiencies of a scale not visible to the naked eye. When such unfavorable field conditions arise, aids may be required to permit effective visual inspection. Usually, remote visual inspection involves the effective use of optical instruments. These instruments include mirrors, borescopes, charged coupled devices (CCD), and remote miniature cameras.

**Borescopes**

A borescope is an optical instrument composed of a tube designed for the remote inspection of objects. A person at one end of the tube can view an image obtained at the other end. The image is transmitted through the tube via fiber optic bundles, running

though the tube, camera, video projection system, or lenses. A borescope that utilizes fiber bundles for its image projection is commonly referred to as a fiber optic borescope or fiberscope. Another method of image transfer is through the use of a small camera at one end of the tube and a monitor at the other end. Lenses can also be used to convey the image to the observer through an eyepiece.

Due to the variety of needs created by industry, there are several types of borescopes. The basic categories are rigid or flexible, as dictated by the configuration of the tube. Figures 2.1 through 2.3 illustrate flexible and rigid borescopes. The borescopes most commonly used today are: fiber optic borescopes, camera borescopes, lens borescopes and microborescopes. The fiber optic and camera variety are usually of the flexible type, while the lens borescope is typically rigid. Microborescopes can be either rigid or flexible.

Borescopes are commonly used for the inspection of objects that have areas of inaccessibility. They are prevalent in the mechanical engineering field more than any other area and are instrumental in the inspection and condition assessment of engines and engine parts. However, borescopes are valuable to civil/structural inspectors and are commonly employed in the inspection of inaccessible structural elements, such as the interior of masonry block or multi-wythe brick walls. Borescopes were instrumental in the Statue of Liberty restoration project, which began in 1984 and was completed in 1990. Olympus Corporation donated flexible fiberscopes, rigid borescopes, halogen light sources and photo recording accessories to the project. The equipment was used by the National Parks Service engineers to examine the Lady's iron skeleton. In depth observations revealed a hazardous array of warps, sags, leaks, and failed joints (Hellier

2001). Without the use of borescopes, the inspectors' efforts would have resulted in an incomplete assessment of the structure. Figures 2.1-2.3 are photographs of the most commonly used borescopes.

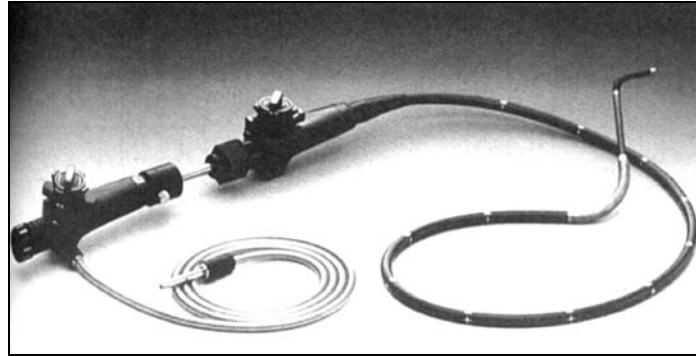


Figure 2.1: Flexible borescope (Hellier 2001)

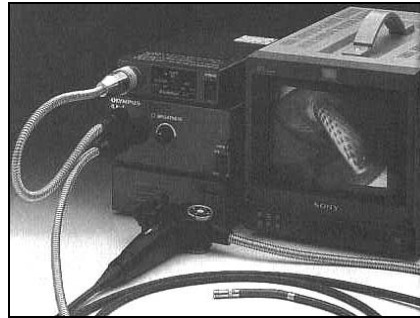


Figure 2.2: Flexible borescope and monitor (Hellier 2001)

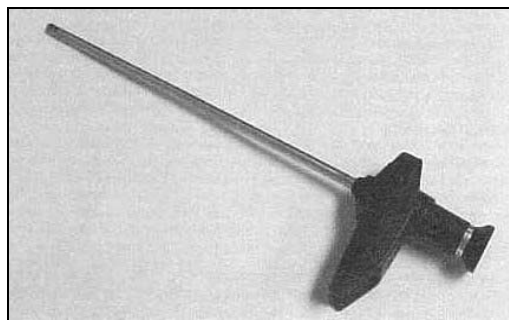


Figure 2.3: Rigid borescope (Hellier 2001)

### **Charged coupled device**

Willard Boyle and George Smith of Bell Laboratories invented the Charged Coupled Device (CCD) in 1970. Since then, CCDs have been used in many of the

computer-based optical equipment in use today. CCDs can be found in photocopiers, facsimile machines, cameras, scanners and other optical computer based products.

A CCD is composed of thousands of light sensitive cells, usually referred to as pixels that produce an electrical charge proportional to the amount of light they receive. These pixels can be arranged in either a linear or two-dimensional array, which in turn can be used to produce a digital image. The typical facsimile machine and computer scanner used today have a linear arrangement of CCDs, which progressively traverses the original object in order to progressively build a digital copy. Digital cameras use a two dimensional CCD, also called an area CCD, to instantly create a digital image.

CCDs are of value to the inspection industry as they allow inspectors to capture images of specimens as the traditional camera has done for decades. The advantage of using CCD based technology over film-based cameras is primarily the speed in which the images are developed. Digital photos are usually viewable through the camera instantaneously, which allows personnel on site to observe the image without delay. The person taking the digital photo can then make an on-site decision concerning the quality of the image and whether it needs to be recaptured.

### **Robotic cameras**

Miniature cameras are sometimes considered a variation of fiber optic cameras. In the recent past, both miniature cameras and fiber optic cameras both required a wire or some physical connection to the monitor or viewing device. However, as technology progresses, limitations diminish. Miniature robotic cameras were instrumental in the initial stages of the inspection of the World Trade Center (WTC) disaster site in September 2001. The robots deployed at the WTC site were completely free of cables and were able to gain access to areas where human access was impossible or hazardous.

The equipment used in this case employed artificial intelligence, robotics, and CCD technology. Dr. Robin Murphy, an Associate Professor at the University of South Florida, is also the Director of Research for the Center for Robot-Assisted Search and Rescue (CRASAR) in Tampa, Florida. Her research primarily encompasses artificial intelligence in robotics and robot tasking (Murphy 2000).

The robots employed at the WTC disaster site, depicted in 2.4 and 2.5, were used to explore and inspect the inner areas of the wreckage. Remote exploration of the site allowed inspectors to locate victims and visually inspect the structural integrity of the wreckage. The robots were used in several areas of the site, including the collapsed Towers One and Two. This was the first known robot-assisted search and rescue response, and represented the culmination of six years of research and training. The robots were successfully used to find at least five victims, helped rescue teams select voids for further searching, and assisted in the building clearing efforts. Videos of the robots, their interfaces, and views from their sensors were used to illustrate key findings on mobility, sensing, control, and human-robot interaction.



Figure 2.4 : Robot used for visual survey at the WTC disaster site (Casper 2002)

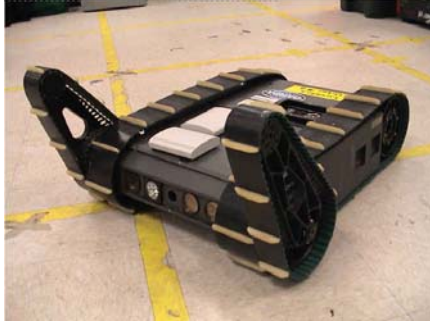


Figure 2.5 : Robot used for visual survey at the WTC disaster site (Casper 2002)

Although disaster inspection is a highly specialized and limited field of research, the technology developed and implemented for this work will become more prevalent in the visual inspection industry.

### **Applications of Visual Inspection**

Visual inspection is a fast, convenient and relatively inexpensive technique used to evaluate the overall condition of structures. This technique allows inspectors to make real-time evaluations and recommendations of a given structure, which is particularly valuable in emergency or safety inspections.

Some limitation of the visual inspection technique is sight obstructions, which can be due to lighting, access or obstruction. Another disadvantage of visual inspection is the “human factor” that is often encountered. The susceptibility to human misinterpretation and the requirement for establishing a baseline for defects in general, especially under poor conditions, can lead to inconsistent identification of anomalies, which can give rise to contradicting evaluations (Qasrawi 2000).

### **Liquid Penetrant Methods**

The liquid penetrant examination method can be used to nondestructively evaluate certain nonporous materials. The American Society for Testing and Materials (ASTM) has developed material specific test standards for the penetrant examination of solids

(ASTM E165 – 95). Liquid penetrant methods are nondestructive testing methods for detecting discontinuities open to the surface, such as cracks, seams, laps, cold shuts, laminations, through leaks, or lack of fusion. These methods are applicable to in-process, final, and maintenance examinations. They can be effectively used in the examination of nonporous, metallic materials, both ferrous and nonferrous, and of nonmetallic materials such as glazed or fully densified ceramics, certain nonporous plastics, and glass.

Hardened Portland cement concrete is a permeable material due to the properties of the cement matrix. As concrete is batched and mixed, capillary pores are formed in the hydrated cement matrix; penetrant methods of investigation, as described in the relevant ASTM standard, do not apply to concrete because they were developed for testing of nonporous materials. At present, there is no standardized test method available for liquid penetrant examination of porous materials.

However, it is possible to use water as an aid to detect surface flaws in concrete. Inspectors can apply water to a concrete surface and observe the rate of drying. As the water evaporates from the surface, areas containing cracks will hold moisture. As illustrated in Figure 2.6, these moist areas will result in local discoloration of the concrete, which facilitates the visual detection of cracks.

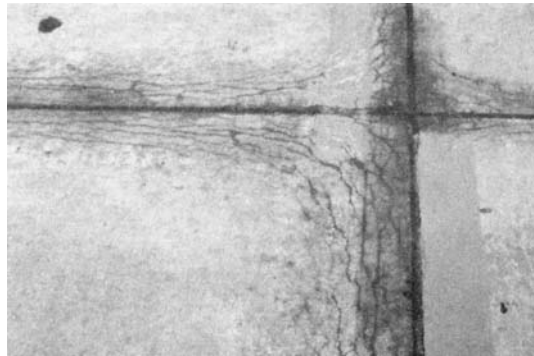


Figure 2.6: Cracks in concrete pavement with moisture present (ACI 201.1 R92)

The principle upon which the liquid penetration method is based is that of capillary suction, a physical phenomenon in which the surface tension of liquids causes them to be drawn into small openings such as cracks, seams, laps, cold shuts, laminations and other similar material deficiencies.

The most important property affecting the ability of a penetrant to enter an opening is “wettability”. Wettability refers to a liquid's behavior when in contact with a surface (Hellier 2001). The angle created between the free surface of a liquid and a solid surface is referred to as the contact angle. It is an important characteristic related to the penetrability of the liquid. Liquids that have small contact angles have better penetrability than those liquids exhibiting large contact angles. Figure 2.7 depicts contact angles for various liquids.

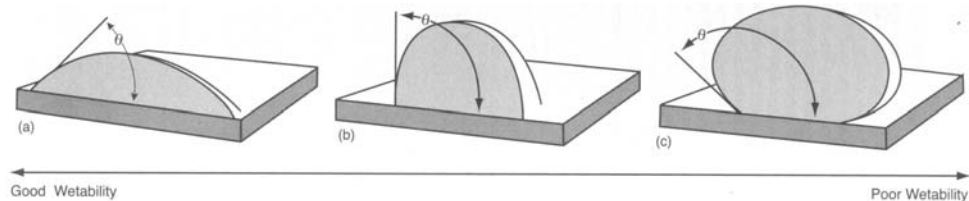


Figure 2.7: Contact angles for various liquids (Hellier, 2001)

Viscosity is another significant property of liquid penetrants. Viscosity is defined as the resistance to flow in a fluid, or semifluid. Liquids with lower viscosities are more desirable for use in liquid penetrant examination since they have superior flow properties.

The visibility of the liquid penetrant is a valuable quality in the penetrant examination procedure. Usually, the visibility or contrast of a liquid penetrant is measured by the dye concentration, which makes the liquid penetrant more visible. Contrast ratio is used to measure the visibility of a penetrant. The contrast ratio scale ranges from 50:1 to 1:1, where a contrast ratio of 1:1 would represent a color in reference

to itself, for example, red dye on a red solid surface. Contrast ratios of 40:1 can be achieved through the use of fluorescent dye penetrants under ultraviolet illumination. As a result, ASTM has recognized fluorescent penetrant examination, and standard test methods have been developed. ASTM D4799-03 is the standard test that describes the conditions and procedures for fluorescent penetrant testing for bituminous materials.

Although liquid penetrant methods have been beneficial in the location of surface defects in solids, they have several limitations. Existing liquid penetrant examination techniques are applicable to the inspection of nonporous solids and are thus not applicable to the survey and inspection of concrete structures and buildings. The majority of these are composed of concrete and masonry; both of which are porous materials.

### **Acoustic Sounding**

Acoustic sounding is used for surveying concrete structures to ascertain the presence of delaminations. Delaminations can be a result of poor concrete quality, debonding of overlays or applied composites, corrosion of reinforcement, or global softening. The test procedures used for delineating delaminations through sounding include: coin tap, chain drag, hammer drag, and an electro-mechanical sounding device. The purpose of each test is to sonically detect deficiencies in the concrete. ASTM has created a standard, *ASTM D 4580 – 86*, which covers the evaluation of delaminations. The standard describes procedures for both automated and manual surveys of concrete.

A major advantage to sonic testing is that it produces immediate results on near surface anomalies. The effectiveness of sonic testing relies heavily on the user's expertise in signal interpretation and consistency.

### Coin tap test

The coin tap test is one of the oldest and most widely researched methods of sonic testing. The test procedure requires the inspector to tap on the concrete sample with a small hammer, coin, or some other rigid object while listening to the sound resulting from the impact. Areas of nondelaminated concrete will create a clear ringing sound upon impact while regions of delaminated, disbonded, or softened concrete will create a dull or hollow sound. This change in sonic characteristics is a direct result of a change in effective stiffness of the material. As a result, the force-time function of an impact and its resulting frequencies of an impact differ between areas of good and poor quality concrete (Cawley & Adams, 1988). *ASTM D 4580-86* describes the procedure for manually surveying concrete structures for delaminations using the coin tap procedure.

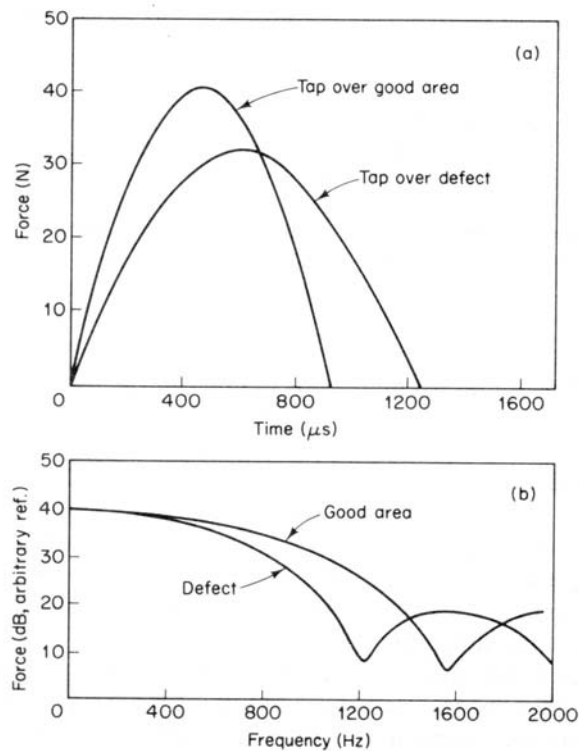


Figure 2.8: Coin tap test results (a) Force-time histories of solid and disbonded areas of a carbon fiber reinforced skinned honeycomb structure, (b) Spectra of time histories (Cawley & Adams, 1988)

Figure 2.8 illustrates the shorter force-time history and larger resulting frequency produced by impacts on solid material as opposed to disbanded/delaminated material. Understanding the force-time function aids an inspector's abilities to sonically evaluate a material, as it takes less time for two elastic solids to separate subsequent to a collision. A similar analogy could be made by comparing the effect of walking on a sidewalk to walking in the mud. The sinking phenomenon that one experiences in the mud is similar to the extended time length of impact produced by a delaminated material. The "sinking" of the hammer or coin into the delaminated material results in a plastic deformation of the material, resulting in a more dull or hollow sound.

The electronics industry has provided inspectors with equipment that is capable of detecting and recording the sonic wave signals that are produced by an impact. As a result, there are currently several commercially available products available for such signal acquisition. The most common devices for sonic data acquisition are the instrumented hammer and the smart hammer.

The instrumented hammer was developed for the airline industry to be used in the detection of anomalies in airplane materials. It measures and records the force-time history and amplitude frequency of an impact via the use of an accelerometer embedded in the head of the hammer.

The smart hammer was developed for the shipbuilding industry. This instrument measures and records the sonic response of an impact through a microphone. The microphone uses the sonic data, instead of the force data, to create an acoustic signal.

Both impact-force data generators and impact-sound data generators have been proven to generate useful signals for nondestructive sonic testing. The information gained

from both sources has demonstrated their capability of producing consistent and valid experimental results. At the present time, research is being conducted into both impact-force and impact-sound devices to develop improved testing methods. Both devices have created the opportunity for improved standardization of acoustic sounding tests. The objective nature of testing with mechanical devices that are capable of producing consistent and repeatable results can help to improve testing standards for structural and material inspectors. Although the instrumented hammer and smart hammer are considered to be automated delamination inspection equipment, the testing data and procedures produced by these devices are still in the initial stages and an ASTM standard test method for these devices has not yet been created.

### **Chain drag survey**

The chain drag survey provides a low-cost method to inspect delaminated areas in concrete surfaces. The survey allows inspectors to traverse a large area with reasonable accuracy in a short period of time. Since the test is quick and inexpensive it may be used for an initial evaluation to determine the need for further investigation. Like the coin tap and hammer sounding methods, the chain drag test is subjective, and therefore requires an experienced inspector to perform the survey. Due to the nature of the test, localized areas of delaminations are more difficult to detect. Concrete decks or slabs that have comparatively large percentages of deficiencies may require the use one of the more localized tests, like the coin tap or hammer sounding methods, to provide a more accurate picture of the tested structure.

The chain drag survey consists of dragging a chain over the concrete surface. This approach suffers from limitations similar to the electro-mechanical sounding device. The chain drag survey cannot be performed on vertical members of a structure and thus is

limited to the topside of concrete slabs and decks. Similar to the coin tap test, areas of nondelaminated concrete will create a clear ringing sound upon contact, and areas of delaminated, disbonded or softened concrete will create a dull or hollow sound. The typical chain used for inspection is composed of four or five segments of 1 inch link chain of ¼” diameter steel approximately 18 inches long attached to an aluminum or copper tube two to three feet in length. The test is performed by dragging the chain across the entire surface of the concrete slab and marking the areas that produce a dull sound. The deficient areas can be recorded and further investigated using other techniques.

### **Electro-mechanical sounding device**

The Electro-Mechanical sounding device is a small, wheeled device equipped with tapping wheels and sonic receivers. Two rigid steel tapping wheels provide the impacts for the delamination survey. The sonic receivers are composed of oil filled tires coupled with piezoelectric transducers. The data acquisition equipment is composed of a data recorder that stores the signals from the sonic receivers (ASTM D4580-86). The electro-mechanical sounding device has become somewhat antiquated as the development of other, more reliable and more efficient, delamination survey techniques have been developed. ASTM D 4580-86 (procedure A) defines the standard practice for performing a delamination survey using this device. It is primarily limited by the nature of the equipment employed, as it cannot perform tests on vertical concrete surfaces, and is thus restricted to the top surface of concrete decks and slabs.

### **Applications of acoustic sounding**

Acoustic sounding has proven to be a reliable supplement to visual and other forms of evaluation due to its capability to conduct near-surface investigations at a relatively rapid rate. These techniques are also valuable in that they are usually relatively low in

cost and can be conducted in conjunction with most visual inspections. However, the method is limited in several respects. It remains largely subjective to human interpretation and can be a confusing technique when background noise is prevalent. The method lacks the ability to detect small defects and subsurface defects, as it is strictly a near-surface investigation method.

### **Surface Hardness Methods**

Essentially, the surface hardness methods for nondestructive testing of concrete consist of impact type tests based on the rebound principle. Some of these methods have been effectively used to test concrete since the 1930's. Due to the complexity of concrete as a material and the disparity between the concrete surface and the inner structure, surface methods are inherently limited in their results. However, surface methods have been proven to give an effective evaluation of the uniformity of a concrete member and in comparing concrete specimens in a relative sense.

The most widely used surface hardness methods are the testing pistol by Williams, the pendulum hammer by Einbeck, the spring hammer by Frank and the rebound hammer by Schmidt. The Schmidt rebound hammer has become the industry favorite in the use of surface hardness measurements today. The Schmidt hammer is basically a hand-held spring plunger that is suitable for lab or field-testing. The capabilities of the Schmidt hammer have been extensively tested, and there are over 50,000 Schmidt hammers in use world-wide (Malhotra & Carino 1991).

The basic rebound principle consists of a spring-driven mass that is driven against the surface of a concrete specimen with a known energy. The rebound distance of the mass is measured and the "hardness" of the concrete surface is estimated from this value. A harder surface results in a longer rebound distance due to the increase in energy

reflected back to the impinging mass. However, despite its apparent simplicity, the rebound hammer test involves complex problems of impact and the associated stress wave propagation (Neville 1995). The energy absorbed by a concrete sample is related to both its strength and its stiffness. Therefore, it is the combination of concrete strength and stiffness that influences the rebound number.

There is no unique relation between surface hardness and in-situ strength of concrete. This relationship is dependent upon any factor affecting the concrete surface, such as surface finish, degree of saturation, and surface preparation. The concrete mix design, including the type of aggregate, water/cementitious materials ratio and cement type can also affect hammer results. The method cannot accurately determine the subsurface condition of concrete. It tests only a localized area of concrete to a depth of perhaps 20 or 30mm (BSI, 1986). The condition of the concrete will further affect the rebound number. Areas of honeycombing, scaling, rough surfaces and high porosity will decrease the rebound number. Areas of carbonation will increase the rebound number. Therefore, the user must insure careful selection of a representative area of concrete and must understand the limitations inherent in the test.

The Schmidt rebound hammer is, in principle, a surface hardness tester with little apparent theoretical relationship between the strength of concrete and the rebound number of the hammer. However, within limits, empirical correlations have been established between strength properties and the rebound number (Malhotra & Carino 1991). The accuracy of the rebound hammer has been estimated between  $\pm 15-20\%$  under laboratory testing conditions and  $\pm 25\%$  in field-testing conditions. Such accuracy, however, requires a proper calibration of the hammer with the concrete in question.

The American Society for Testing and Materials (ASTM) has created a standard test for the Rebound Number of Hardened Concrete (ASTM C 805-97). This test specification should be referenced and strictly followed for proper testing procedures.

### **Penetration Resistance Methods**

The basic principle behind penetration resistance methods is the application of force to a “penetrating object,” and then determining the resistance of a specific concrete to such penetration by measuring the depth of penetration. Penetration resistance methods have been effectively used to test concrete since the 1960’s. The limitations of penetration methods are similar to the limitations of surface hardness methods. The depth of penetration is usually only a small percentage of the full depth of the concrete member. Penetration methods have been proven to give an effective near surface evaluation of *in-situ* compressive strength, uniformity of concrete and soundness at different locations. The two most commonly used penetration resistance methods are the Pin Penetration Method and the Windsor Probe.

The Pin Penetration method uses a spring-driven mechanism to drive a 30 mm long, 3.6 mm diameter steel pin into the concrete surface. The pin is subsequently removed and the depth of the resulting hole is measured. The Windsor Probe test uses the same principle, although larger diameter steel probe is used. Table 2-1 contains a schedule of probe sizes for each test. The Windsor Probe test requires a larger driving force and employs a gunpowder charge to develop the necessary impetus. ASTM has approved a standard test for the Penetration Resistance of Hardened Concrete (ASTM C 803-97), which covers both tests. This test specification should be referenced for proper testing procedures.

Table 2.1: Standard sizes of pin and probe used for penetration tests.

	Pin Penetration Method	Windsor Probe Test
Size of Penetration:	30 mm length 3.6 mm diameter	80mm length 6.3/7.9mm diameter
Usable Range of Concrete Strength:	450 – 4000 psi 3-28 MPa	450 – 6000psi 3 – 40 MPa

The ASTM standard requires three firmly embedded test probes in a given test area to constitute as one test for both penetration test methods (ASTM C803-97). The penetration methods are still near-surface tests but do offer reliable empirical relationships between concrete strength and penetration resistance. Consistent empirical correlations have been successfully established between strength and penetration resistance. The penetration methods have been estimated to be within  $\pm 5\%$  accuracy under both laboratory and field-testing conditions when the test procedure is performed properly and a valid correlation has been developed.

The primary limitation of penetration methods is that they do not offer a full-depth appraisal of the concrete that they are testing. They are considered to be surface-testing methods only and they do not yield absolute values for the strength of concrete in a structure. They are effective at estimating *in situ* concrete strength only when the proper correlations are performed subsequent to testing. Penetration methods are not purely nondestructive in nature since they induce some damage to the tested specimen. It is more accurate to consider penetration tests as semi-destructive.

### **Pullout Test**

The basic purpose of the pullout test is to estimate the *in situ* strength of a concrete structure. Pullout tests consist of measuring the force required to extract a mechanical insert embedded in a concrete structure. The measured pullout force can then be used to

estimate the compressive, tensile and shear strength of the concrete. The pullout test was originally developed in the former Soviet Union in the 1930's and later independently developed in the United States in the early 1940's. Further research has led to several modifications since then. The test that is most commonly used in industry today is the pullout test as modified by Kaindl in the 1970's.

The pullout test, illustrated in Figure 2.9, uses a metal insert that is inserted into fresh concrete or mechanically installed into hardened concrete. The tensile or “pullout” force required to extract the embedded insert, and the core of concrete between the insert and the surface, can give accurate estimates of the concrete's compressive, tensile and shear strengths. The pullout test has become a proven method for the evaluation of the *in situ* compressive strength of concrete and has several industry applications. The pullout test is used to determine whether the strength of the concrete has reached a sufficient level such that post-tensioning may commence; cold weather curing of concrete may be terminated or forms and shores may be removed.

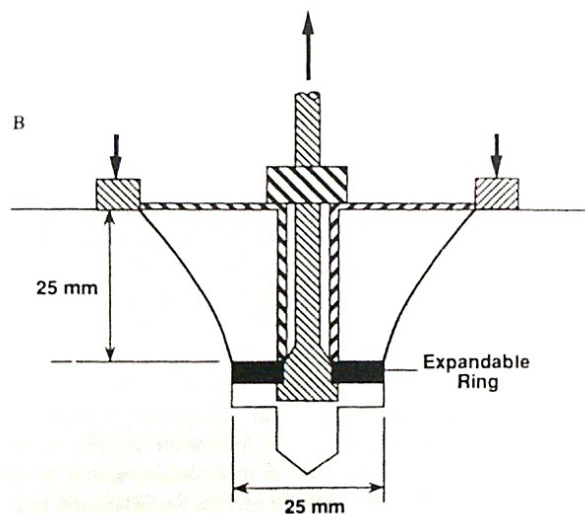


Figure 2.9: Illustration of typical pullout test (Malhotra & Carino 1991)

Consistent empirical correlations can be established between strength properties and pullout test methods. Pullout test results have been estimated to be within  $\pm 8\%$  accuracy for laboratory and field-testing conditions when the test procedure has been performed properly and a proper correlation has been developed.

The pullout test method does not provide a full-depth appraisal of the concrete structure that is being tested. It is not truly nondestructive in nature since it induces significant damage to the tested member. It is more accurate to consider the pullout test as semi-destructive. The damage incurred during pullout testing is usually more significant than most other “NDT” methods and patching of the tested structure is usually required. Figure 2.9 shows a schematic of the pullout test.

ASTM has created a standard test for the Pullout Strength of Hardened Concrete (ASTM C 900-99). This test specification should be referenced for proper testing procedures.

### **Break-Off Test**

The primary purpose of the break-off test is to estimate the strength of a concrete structure. This test involves the breaking off of an internal cylindrical piece of the *in situ* concrete at a failure plane parallel to the surface of the concrete component. The measured break-off force can then be used to estimate the compressive and tensile strength of the concrete. The break-off test was originally developed in Norway in 1976. It was later introduced into the United States in the early 1980's. The test procedure used today is essentially the same as when the test was originally introduced.

The break-off test can use a cylindrical sleeve that is inserted into fresh concrete to create the embedded cylinder. Alternatively, the embedded concrete cylinder can be

drilled into hardened concrete using a core drill bit. The embedded cylinder size is usually 55mm in diameter and 70mm in height. Figure 2.10 illustrates a typical cross section of the breakoff test.

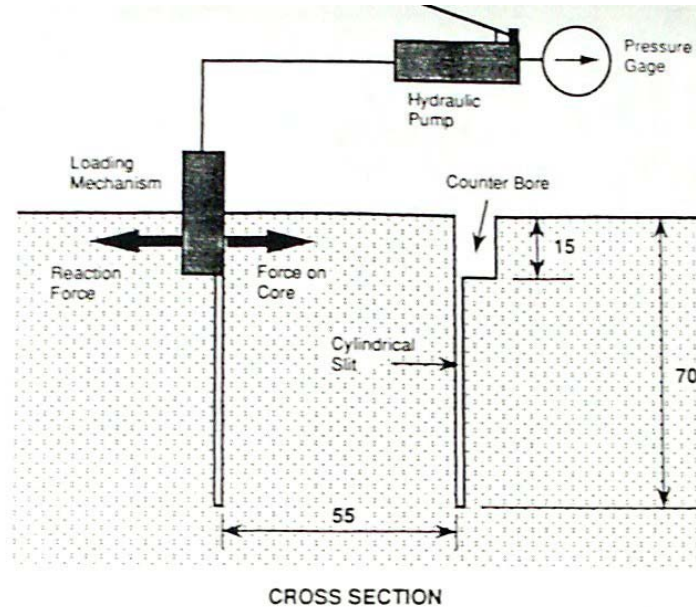


Figure 2.10: Typical cross section of the breakoff test, all dimensions in mm (Malhotra & Carino 1991)

The actual test method involves the application of a horizontal force to the upper edge of the embedded concrete cylinder, which is slowly increased until failure. The force required to break the embedded cylinder is then used to estimate the concrete compressive and tensile strength. The break-off test is a proven method of evaluation of the *in situ* compressive strength of concrete and has several industry uses. Like the pullout test (described later) it is used to determine whether the strength of the concrete has reached a specified value so that post-tensioning of a bridge structure may commence, cold weather curing of concrete may be terminated, or forms and shores can be removed.

Consistent empirical correlations have been established between strength properties and break-off test methods. The break-off test results have been estimated to be within

$\pm 7\%$  accuracy for laboratory and field-testing conditions when the test procedure has been performed properly and sufficient data is available to formulate a proper correlation.

The primary limitation of the break-off test is that it is not truly nondestructive in nature. It induces significant damage to the tested member. Thus, it is more accurate to consider the break-off test as semi-destructive. The volume of removed material is 667 cm<sup>3</sup> or 41 in<sup>3</sup>. Thus, the damage incurred during break-off testing is typically more extensive than other “NDT” methods, and patching of the tested structure is usually required.

ASTM has approved a standard test for the Break-Off Number of Hardened Concrete (ASTM C 1150-96). This test specification should be referenced for proper testing procedures.

### **Ultrasonic Testing**

Ultrasonic testing is a NDT method that is used to obtain the properties of materials by measuring the time of travel of stress waves through a solid medium. The time of travel of a stress wave can then be used to obtain the speed of sound or acoustic velocity of a given material. The acoustic velocity of the material can enable inspectors to make judgments as to the integrity of a structure.

The term ultrasonic is defined as a sound having a frequency above the human ear's audibility limit of about 20,000 hertz. Ultrasonics are very popular in the medical industry and have been used there for over thirty years, allowing doctors to non-intrusively investigate internal organs and monitor blood flow in the human body. The materials industry has also been able to utilize ultrasonics for non-intrusive investigation

of assorted materials such as metals, composites, rock, concrete, liquids and various other nonmetals.

The first studies of ultrasonics are recorded as far back as the Sixth Century B.C. when Greek philosopher, Pythagorus performed experiments on vibrating strings. Galileo Galilei is credited with performing the first of the modern studies of acoustics. He was the first scientist to correlate pitch with frequency of sound. The earliest known study of the speed of sound in a liquid medium took place in 1822 when Daniel Colladen, a Swiss physicist/engineer, and Francois Sturm, a Swiss mathematician, used flash ignition and a bell to successfully estimate the speed of sound in Lake Geneva, Switzerland. In 1915, Paul Langevin pioneered the study of high-frequency acoustic waves for submarine detection during the outbreak of World War I (Guenther 1999).

The age of ultrasonic testing of materials was established in 1928 by Sergei Y. Sokolov, a scientist at the Lenin Electrotechnical Institute in Leningrad, Russia. Sokolov proposed and demonstrated that he could translate ultrasonic waves or sound pressures into visual images. In the 1920's he advanced the idea of creating a microscope using high frequency sound waves. He then applied his ideas to detect abnormalities in metals and other solid materials. As technologies have developed over the twentieth century, the knowledge gained through the use of the high frequency microscope has been applied to other ultrasonic systems (e.g. radar) (Guenther 1999).

In the United States, the development of the ultrasonic test is attributed to Dr. Floyd Firestone, who, in 1942, introduced what is now called the pulse echo technique (described later) as a method of nondestructive testing. Dr. Firestone successfully used the pulse echo technique for ultrasonic flaw detection. Ultrasonics have since been used

to evaluate the quality of concrete for approximately 60 years. The method can be used for non-intrusively detecting internal defects, damage, and deterioration in concrete. These flaws include deterioration due to sulfate and other chemical attacks, cracking, and changes due to freeze-thaw cycling.

### Theory

Ultrasonic testing of materials utilizes the vibrations of the particles that comprise a given medium. Sound waves and ultrasonic waves are simply the vibrations of the particles that make up a solid, liquid, or gas. As an energy form, the waves are an example of mechanical energy.

The motion of vibration is described as a periodic motion of the particles of an elastic body or medium, in alternately opposite directions from the position of equilibrium when that equilibrium was disturbed. However, vibration can also be described as an oscillation, which is the act of swinging back and fourth between points. An elastic oscillation is one in which the driving force behind the oscillation (e.g. a spring) is proportional to the displacement of the object. Figure 2.11 illustrates the basic sinusoidal oscillation of a free body on a loaded spring and the resulting sine curve that can be achieved when the motion is plotted with respect to time.

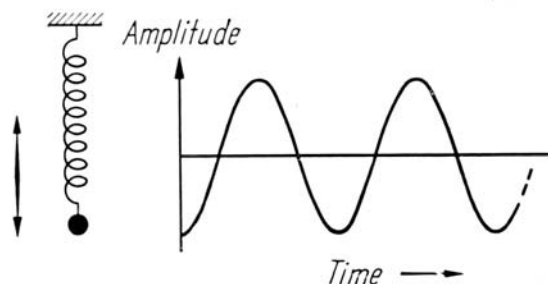


Figure 2.11: Sinusoidal oscillation of a loaded spring (Krautkramer 1979)

The sinusoidal waveform that is created by sound waves is a convenient characteristic of the wave motion that allows scientists to quantify sound in terms of amplitude and frequency. The frequency of these waves differentiates sonic from ultrasonic waves. The unit of frequency is the hertz or Hz, and is defined as one cycle of vibration per second. Sounds below approximately 16 Hz are below the lower limit of human audibility, whereas sounds of 20,000 Hz are above the upper limit of human audibility.

The basis of ultrasonic testing is particle vibration within a medium upon the application of mechanical energy. Figure 2.11 shows the free body motion of a single mass and its interaction with a single spring. Considering the mass from the diagram in Figure 2.11 to be a particle, and the spring to be the connection of particles, the simple principle of free body motion to fit a particle interaction model can be expanded as seen in Figure 2.12.

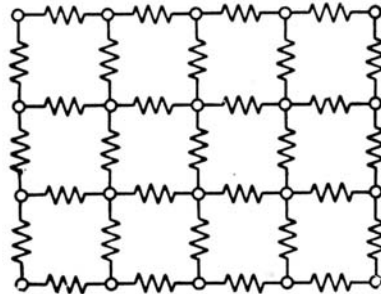


Figure 2.12: Model of an elastic body (Krautkramer 1979)

The model depicted in Figure 2.12 is the basic model used in wave science. Mechanical waves propagate through materials by means of particle motion. Wave propagation is largely dependent upon the type of excitation or energy input, the mass of the individual particles, and the spring stiffness of their internal connections. A wave initiated by an external event such as normal or shear force, travels by vibratory

movement transmitted from particle to particle. If the springs that connect the particles were infinitely stiff, all particles of the material would start to oscillate at the same instant and the wave would be transmitted at an infinite speed. Hence, the material's elasticity and density play an important role in wave propagation (Kaiser & Karbhari 2002). Internal friction and other forces resist particle motion upon excitation, and wave propagation occurs at a finite rate. This rate is referred to as its wave velocity and is dependent upon material composition.

Although sound waves can propagate through all three forms of matter (solids, liquids and gases), the type of waveform able to move through a material is dependent on the material phase. For materials in the gaseous or liquid phase, dilatational waves are typically the only form that travels well. Dilatational waves are also referred to as compression or longitudinal waves and are the primary stress waves produced by material excitation. The particle motion in a longitudinal wave is parallel to the direction of propagation. The result is a compressive or tensile stress wave.

Distortional waves are the secondary stress waves that are produced upon forced contact. These waves are also called shear or transverse waves. In shear waves, the particle motion of the wave front is normal to the direction of propagation, resulting in shear stress.

Rayleigh waves, also called surface waves, differ from longitudinal and shear waves because they do not propagate through a solid. Rayleigh waves propagate along the surface in an elliptical motion.

Lamb waves are similar to Rayleigh waves because they also do not travel through a material and are also considered surface waves. Lamb waves, however, occur only in

solids that are a few wavelengths in thickness and have a uniform thickness. Common objects subject to the development of lamb waves are plates, pipes, tubes, and wires.

### The behavior of waves at material interfaces

The term *interface* is defined as a surface forming a common boundary of two bodies, spaces, densities or phases. One of the most common interfaces people are familiar with is the oil-water interface. In materials science, an interface is usually defined as a fringe between two materials, which have different properties such as density or phase. Another possible difference in material properties is acoustic impedance, which is defined as a material's density multiplied by its wave speed. When stress waves collide with material interfaces, portions of the waves are reflected and refracted. The principle of refraction is best described by Snell's law, which relates the angle of refraction and the wave velocity to the refraction angle of two materials.

$$\frac{\sin i^\circ}{V_1} = \frac{\sin R^\circ}{V_2} \quad (1)$$

where:  $i^\circ$  = angle of incidence

$R^\circ$  = angle of refraction

$V_2$  = wave velocity in Medium 2

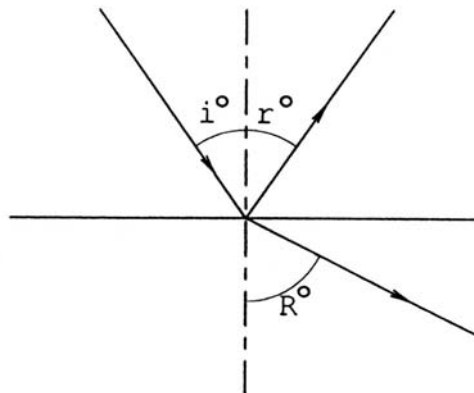


Figure 2.13: Graphical illustration of Snell's law (Hellier 2001)

Figure 2.13 shows a typical example of the refraction angle of an ultrasonic wave as it enters a different material. The concrete-air and the concrete-steel interfaces are the two most common interfaces encountered in nondestructive testing of civil engineering structures.

Most of the illustrations used to describe the characteristics of ultrasonics consider the sound or ultrasound as a two-dimensional ray, which is somewhat simplified for the study of ultrasonics and nondestructive testing. A more accurate representation of the sound energy is a three dimensional beam. The study of a sound beam is more complicated than a sound ray. As the complexity of the physical characteristics in a material increases, different mechanical mechanisms become factors in their analysis.

Scientists define attenuation as the gradual loss of sound wave energy through a medium. Attenuation can be more accurately described as the combined effect of a number of parameters:

- Interference from diffraction effects
- Interference adsorption (friction and heat)
- Interference scatter
- Interference beam spread (Hellier 2001)

The combination of these effects can create disturbances and erratic signals within a material. One of the early challenges of scientists using ultrasonic equipment was deciphering and filtering the interference signals created by material properties.

### **Instrumentation**

Commercial ultrasonic equipment has been under development since World War II. The first equipment available to the materials engineering industry was produced in the 1950's. Since then, a variety of ultrasonic detection devices have become available. Most of the ultrasonic devices used for material inspection and flaw detection are portable and

battery powered. A portable ultrasonic testing device is illustrated in 2.14. Portability enables material inspection in the field and a high degree of user flexibility.



Figure 2.14: A portable ultrasonic testing device used at the University of Florida

The typical testing apparatus used for ultrasonic testing consists of the following:

- Transducer
- Time Measuring Circuit
- Receiver/Amplifier
- Display
- Reference Bar
- Coupling Agent

### **Transducer**

A transducer is used for transforming electrical pulses into bursts of mechanical energy. A typical pulse velocity apparatus consists of a transmitting transducer and a receiving transducer. The transmitting transducer generates an ultrasonic pulse through the test specimen, and the receiving transducer receives the pulse. The generation and reception of ultrasonic waves is accomplished using piezoelectric crystals. Piezoelectric elements are reciprocal, which means an applied voltage generates a deformation, or an

impinging stress generates a voltage. This physical property makes piezoelectric elements ideal as transducers (Papadakis 1999).

### **Time measuring circuit**

The time measuring circuit or clock is an essential component of the ultrasonic pulse velocity equipment. It controls the frequency output of the pulse by signaling the pulser to provide a high-voltage pulse to the transducer. The time measuring circuit measures the time of travel of a pulse or stress wave through the test specimen. Since the primary function of the time measuring circuit is to regulate pulse generation, it is commonly referred to as a pulser. It provides an output to the display when the receiving transducer receives a pulse. The time measuring circuit is capable of producing an overall time-measurement resolution of 1 microsecond ( $\mu\text{s}$ ). ASTM C597-97 requires a constant signal with a varying voltage of  $\pm 15\%$  at a temperature range of  $0^\circ\text{C} - 40^\circ\text{C}$ .

### **Receiver/amplifier**

The receiver is the term applied to all of the circuit functions that amplify the weak echoes and determine their amplitude. It has four basic components, the preamplifier, the logarithmic amplifier, the rectifier and the low pass amplifier.

The function of the preamplifier is to ensure that any signal from the receiving transducer arrives at the time measuring circuit. Since electrical outputs from the transducer are relatively small, signal amplification is necessary to overcome the resistance in the transducer cable, which can be relatively long. The function of the logarithmic amplifier is to process weak echo signals. Once the weak signals are amplified, the rectifier and the low pass filter process the signals. After processing by the

receiver/amplifier, a useable signal can be sent to the display. A schematic of a typical ultrasonic pulse velocity meter is shown in Figure 2.15.

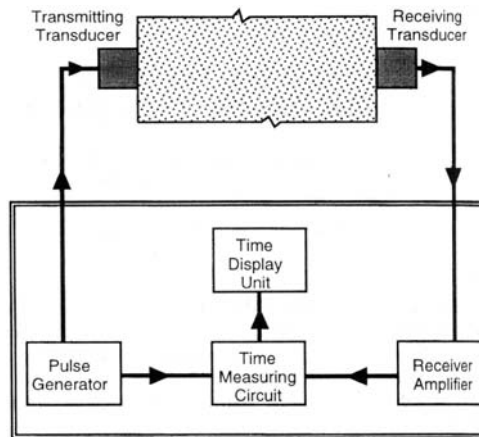


Figure 2.15: Schematic of a pulse velocity apparatus (ASTM C597-97 2001)

### Display

The signal received by the ultrasonic test equipment is typically displayed digitally with modern equipment. The results consist of a direct reading of display time on an x-y coordinate system. The x-axis becomes the time trigger and the y-axis represents the mechanical energy received. The display units can also illustrate defect or anomaly locations and sizes, depending on the type of data requested by the user.

The information obtained in the ultrasonic test is referred to as a scan. Currently there are three types of scans that are applicable to ultrasonic testing: A-scans, B-scans, and C scans.

The A-scan is the simplest scan form. It is a spot scan of the material and results in the most basic form of displayed information. The resulting scan is a waveform where regions of high frequency sound waves are recorded and displayed as peaks on the screen. B-scans are a bit more sophisticated. They incorporate a linear scan instead of a point or spot scan. B-scans are essentially the summation of a series of A-scans that are produced by “sweeping” the transducer over the material specimen. C-scans are even

more complicated than B-scans because they incorporate a two dimensional grid system. C-scans are comprehensive scans that are most applicable to nondestructive testing of materials. Figure 2.16 illustrates the differences between these three types of scans.

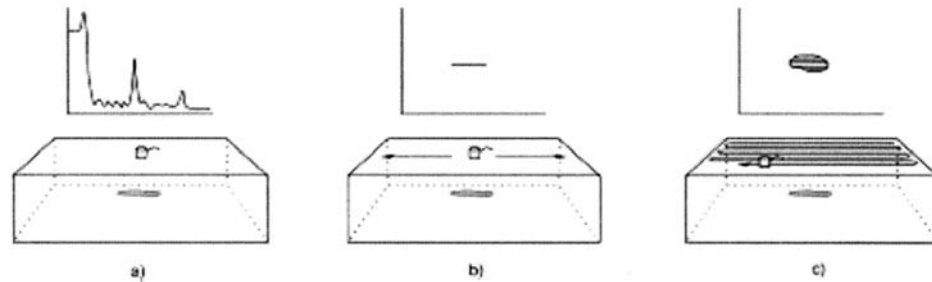


Figure 2.16: Idealized scans of a material defect: a) A-scan, b) B-scan, c) C-scan, (Kaiser & Karbhari 2002)

### Reference bar

The reference bar is a piece of material that is used to calibrate the ultrasonic apparatus. Ultrasonic instruments, which use a microprocessor to record delay time, do not require a reference bar. These instruments can be calibrated by compressing both transducer together to obtain a zero reading. Otherwise, ASTM C597-97 requires that a bar of metal or some other material for which the transit time of compressional waves is known. The reference bar is used as a functional check of ultrasonic equipment prior to testing.

### Coupling agent

A coupling agent is usually required to ensure the efficient transfer of mechanical energy between the transducer and the tested material. The purpose of placing the coupling material between the transducer and test specimen is to eliminate air between the respective surfaces. Typically, coupling agents consist of viscous liquids such as grease, petroleum jelly, or water-soluble jelly. Pounded surface water is also considered an

acceptable couple. Water is considered as an acceptable couple for underwater ultrasonic testing.

### Acoustic velocity calculation

The acoustic velocity wave speed of a given concrete specimen can easily be obtained with the travel time of a stress wave and the length of the specimen. The pulse is sent from the sending transducer to the receiving transducer through the concrete specimen as see in Figure 2.17. The relationship of a specimen's acoustic velocity is simply calculated from a time and a length measurement. It should be noted that cracks, flaws, voids and other anomalies within a material specimen could increase time of travel therefore decreasing the materials acoustic velocity. However, assuming the specimen in Figure 2.17 is free of anomalies, its acoustic velocity can be calculated simply by. The length of the specimen is 200 mm.

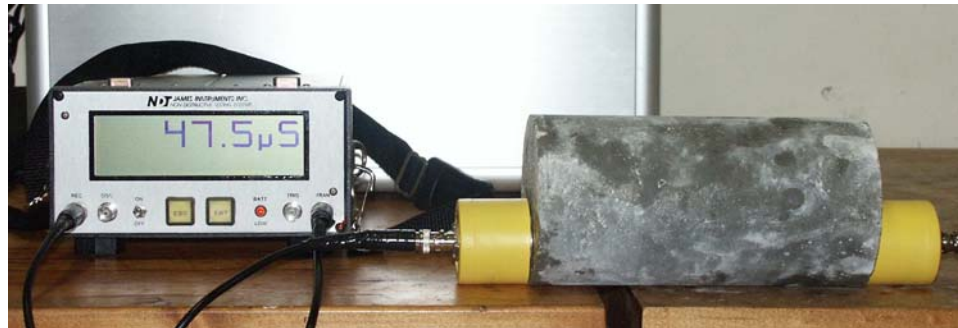


Figure 2.17: Typical ultrasonic test procedure

$$V = L/T; \quad V = 0.2\text{m}/47.5\mu\text{s} = 4210 \text{ m/s (2)}$$

The experiment shown in Figure 2.17 provides the user with a quantitative result. The pulse velocity acoustic velocity,  $V$ , of stress waves through a concrete mass is related to its physical properties (ASTM C597-97). is a function of Young's Modulus of

Elasticity  $E$ , the mass density  $\rho$ , and Poisson's Ratio  $\nu$ . The relevant equation for wave

$$\text{speed is: } V = \sqrt{\frac{E(1-\nu)}{\rho(1+\nu)(1-2\nu)}} \quad (3)$$

The acoustic velocity of a solid varies given its composition. Therefore, different materials have different acoustic velocities. The acoustic velocities of common materials are shown in Table 2.2 (Krautkramer 1991).

Table 2.2 Acoustic velocities of common materials used in construction

Material	Acoustic Velocity (m/s)
Aluminum	6320
Cast Iron	3500-5800
Concrete	2000-5500
Glass	4260-5660
Iron	5900
Steel	5900
Water	1483
Ice (water)	3980

### Flaw detection

The immersion testing method involves typical ultrasonic equipment, though the test specimen is completely submerged in water. The water acts as a coupling agent, which aids in the transfer of a clear signal from the transducer to the material being tested. Immersion testing is usually performed in a laboratory on relatively small test specimens, but can be applied to structures in the field. It is possible to perform immersion testing on structures using a technique called ponding. This technique involves the creation of a layer of water or pond between the specimen and the transducer

and thus is only applicable to the upper surface of structures or submerged sections of underwater structures.

Contact methods are the most commonly used methods in the ultrasonic nondestructive testing of materials. Contact methods require the use of a coupling agent, as described in the Coupling Agent section. The development of contact methods allow more versatility in the ultrasonic testing of specimens, since they enable inspectors to test structures and components regardless of orientation. The ultrasonic pulse velocity testing method, as described in ASTM C597-97, is a contact method.

As illustrated in Figure 2.18, there are three possible transducer arrangements in ultrasonic pulse velocity testing. These variations include through or direct transmission, semidirect transmission, and surface or indirect transmission.

The through transmission arrangement is considered to be the preferred approach. It is the most energy efficient arrangement because the pulse receiver is directly opposite the pulse transmitter. Since the distance between the two transducers is minimized, the amount of pulse energy lost through material friction is also minimized.

The semidirect arrangement is less energy efficient than the through transmission arrangement due to the geometry of the transducer arrangement. The angles involved cause signal interference and therefore are more likely to produce errors. The semidirect arrangement is still useful for inspections where through transmission testing is not due to unfavorable structure configuration. The method is also useful for testing of composite columns that contain heavy reinforcing steel within their core. The semidirect transducer arrangement facilitates ultrasonic testing of the concrete in the column while avoiding interference from the embedded steel.

The surface method is the least efficient of the three ultrasonic pulse velocity configurations. This is due to the nature of the waves that travel through the surfaces of materials. The amplitudes of waves received via the receiving transducer are typically less than 5% of waves received by the direct transmission method. Such a small amount of wave energy obtained by the receiving transducer can result in errors in the measurement and analysis of a wave signal. Although the arrangement is the least efficient of the three methods, it is useful in situations where only one surface of a structure or specimen is accessible, such as a floor slab. Surface wave speed and surface crack depth are acquirable through the surface method as well. These methods are explained in the impact echo section of this chapter. Impact-echo and ultrasonics utilize the same principle for crack depth measurement.

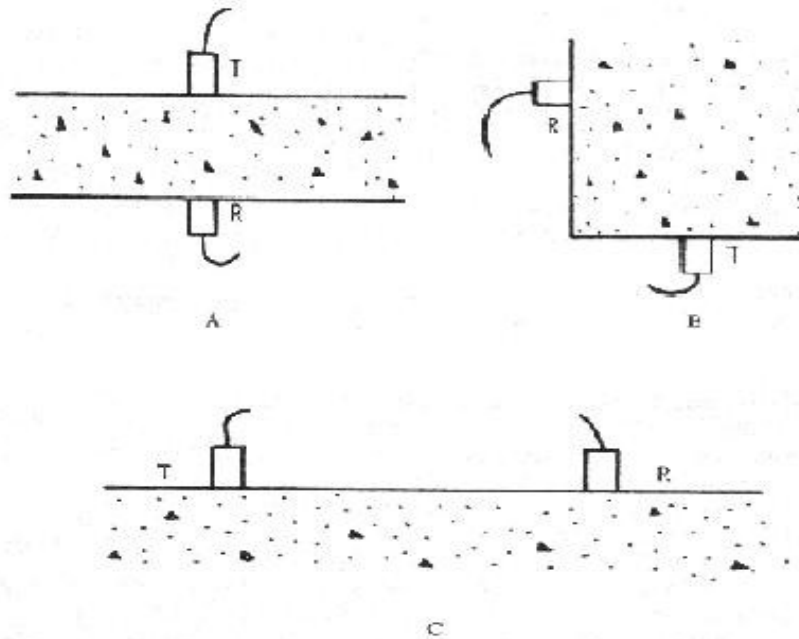


Figure 2.18: Methods of pulse velocity measurements: a) direct method, b) indirect method, c) surface method, (Malhotra & Carino 1991)

Noncontact methods of ultrasonic testing are under continuous research. This field of study has many desirable attributes and similar fields of study include acoustic levitation and transportation.

At the present time, there are several noncontact acoustical techniques being developed for the nondestructive testing of materials and structures. New acoustical techniques are now available as a result of the development of the piezoelectric transducer. Three techniques exist: electromagnetic transducers (EMATs), laser beam optical generators, and air or gas-coupled transducers (Bergander 2003).

Most contact ultrasonic testing requires the use of a piezoelectric transducer to send and receive the stress wave signals. The signals are introduced into and received from the test specimen through physical contact of the transducers coupled to the test surface. EMATS are composed of an RF coil and a permanent magnet. The RF coil is excited by an electric pulse which sends an electromagnetic wave along the surface. The EMATS technique requires the test surface to be magnetically conductive. (Green 2002).

Laser ultrasound facilitates the non-contact ultrasonic testing of materials regardless of the materials' electrical conductivity. It provides the opportunity to make truly non-contact ultrasonic measurements in both electrically conducting and electrically nonconducting materials, in materials at elevated temperatures, in corrosive and other hostile environments, and in locations generally difficult to reach, all at relatively large distances from the test surface (Green 2002). Laser ultrasound techniques are able to produce compression, shear, Rayleigh and Lamb waveforms, increasing the test's versatility and serviceability. Laser generated and air coupled ultrasonics have been successful in the characterization of materials which are non-electrically conducting but

are not yet serviceable for flaw detection and material investigation. However, the contemporary non-contact ultrasonic methods have been proven to be scientifically applicable in the aeronautics and metallurgical disciplines. A schematic representation of contact transducers vs. non-contact transducers is illustrated in Figure 2.19

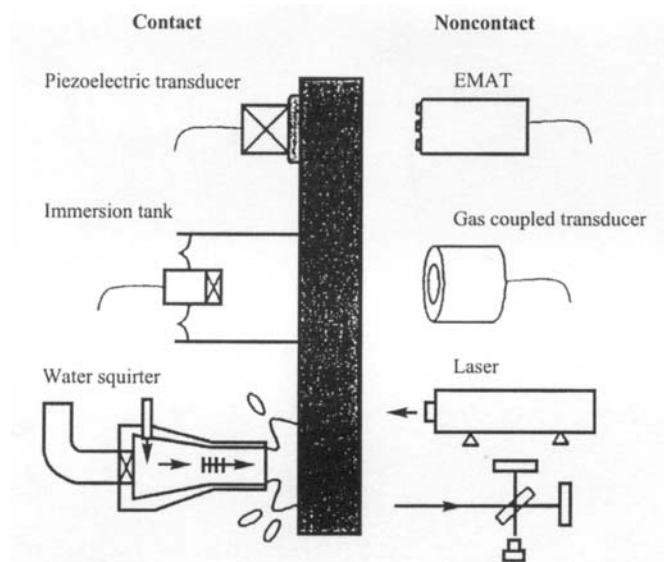


Figure 2.19: Illustration of contact and noncontact techniques (Green 2002)

### **Pulse-echo testing**

The pulse-echo test is based upon stress wave propagation. It uses the same principles and concepts as the impact-echo method (described later). The basic principle behind both methods is referred to as the “pitch and catch” technique. In pulse-echo testing, a stress wave or pulse is created by a transmitting transducer, just as it is with ultrasonic pulse velocity method. Some types of pulse-echo equipment utilize the same transducer to receive while others require separate sending and receiving transducers. This latter type of arrangement is often termed as "pitch and catch." However, the receiver and transmitter need not necessarily be separate transducers placed at different points on the test specimen but can be combined to a single transducer. This type of

testing is referred to as “true pulse echo.” Figure 2.20 provides a schematic of the pulse echo principle.

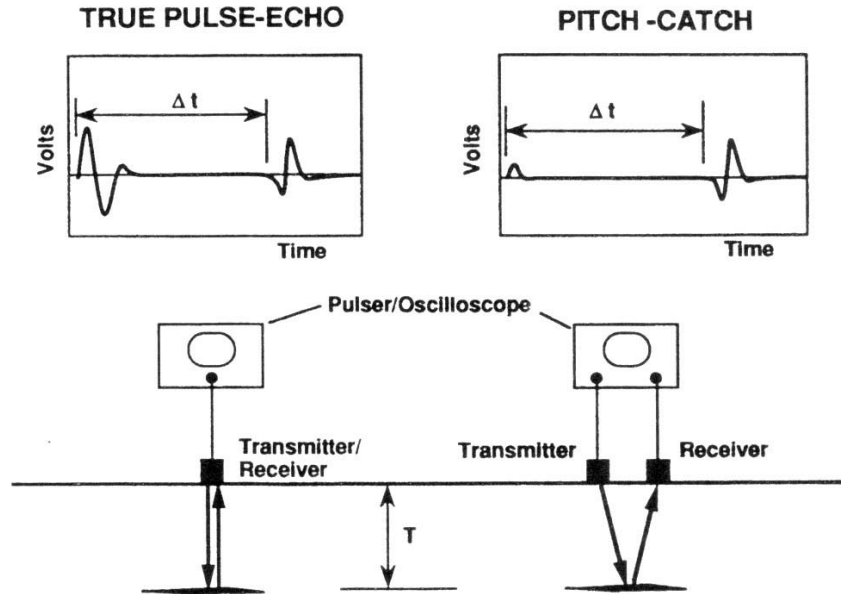


Figure 2.20: Schematic of pulse-echo and pitch and catch techniques (Malhotra & Carino 1991)

The echo wave coming from the flaw is described by its transit time from the transmitter to the flaw and back to the receiver. Later, the reflected wave from the back side of the specimen, for example the back echo or bottom echo, arrives after a correspondingly longer delay. Both echoes are indicated according to the intensity, or rather amplitude, which is referred to as echo height because of their usual presentation as peaks above the horizontal zero line. (Krautkramer 1990). Figures 2.21 a and b provides a schematic of the typical setup and results from pulse echo scans.

The primary difference between the pulse-echo method and the impact-echo method is that the former technique utilizes a transmitting transducer while the latter employs a mechanical impactor. Both methods use a receiving transducer, which is used to detect the reflected waveform. The difference between the transmitting transducer and

the mechanical impactor is the waveform created. The mechanical impact creates a spherical wave front, whereas the transmitting transducer creates a pulse wave beam, resulting in a much smaller material examination area.

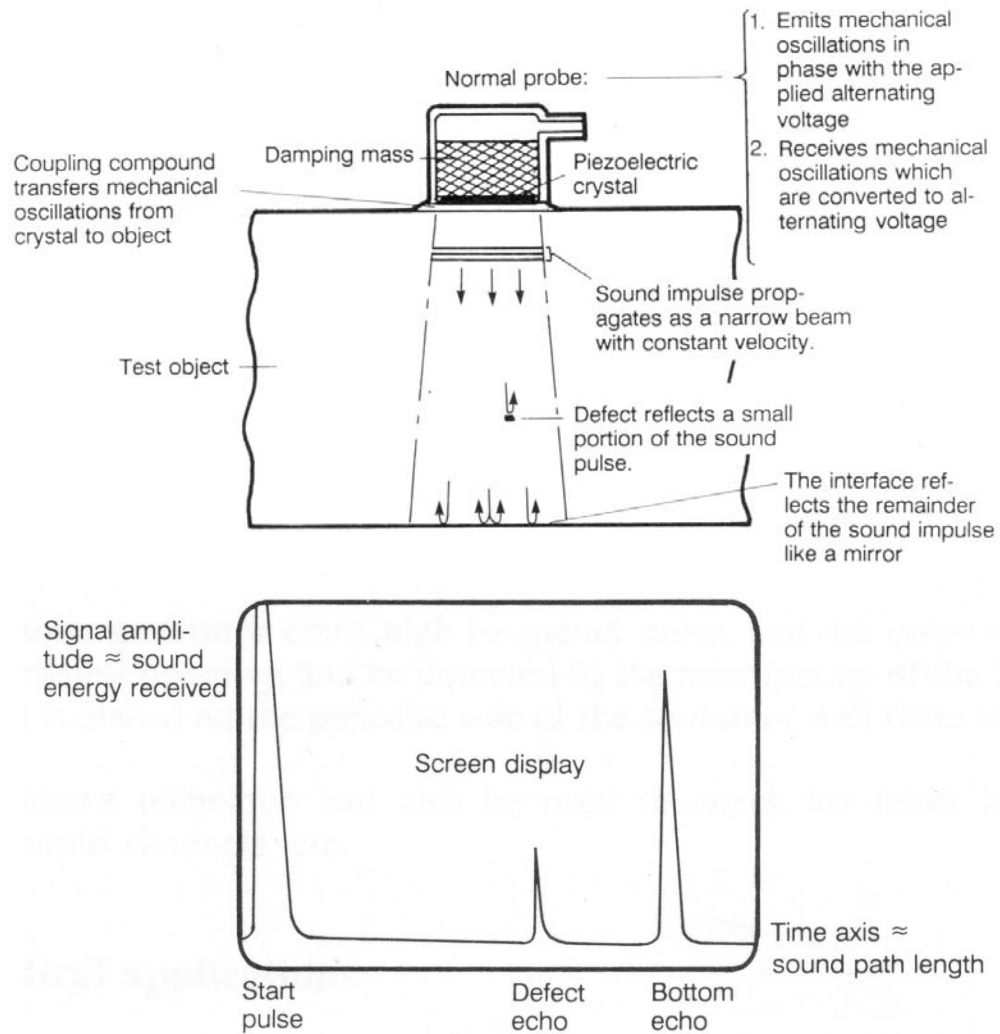


Figure 2.21: Pulse echo schematic (a)Typical test setup, and (b) resulting display (Boving 1989)

The biggest limitation to the pulse-echo method can be attributed to the geometry of the specimen. The reflections of internal anomalies are dependent upon their orientation. In cases where discontinuities, and opposite surfaces, are oriented unfavorably or parallel to the ultrasonic ray path, it may be unable to receive reflected

pulse wave signals. The orientation of anomalies and defects is equally important to size in the pulse echo method. The most favorable orientation for an anomaly is perpendicular to the ultrasonic ray path. Figure 2.22 provides an illustration of the signal response due to the orientation of an anomaly. Reflections due to uneven surface morphology can cause *signal scatter*, as shown in Figure 2.23, resulting in the test missing the backwall echoes. This phenomenon can make it difficult to determine anomaly location.

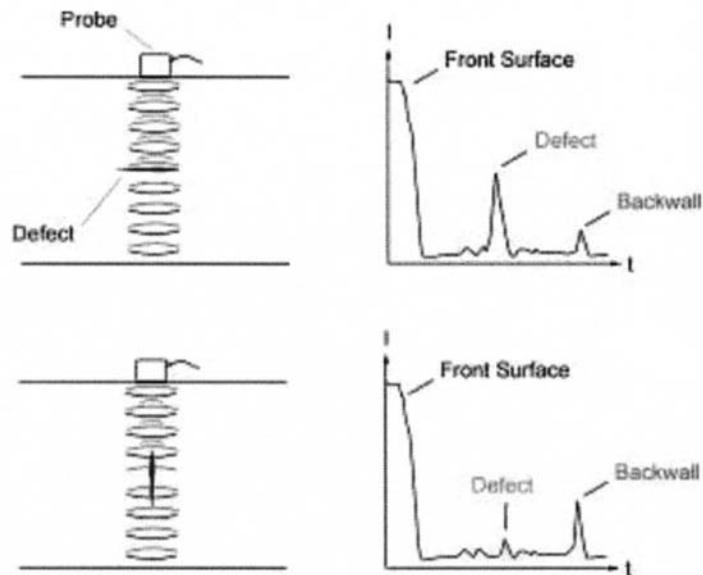


Figure 2.22: Reflections of stress waves from internal discontinuities (Kaiser & Karbhari 2002)

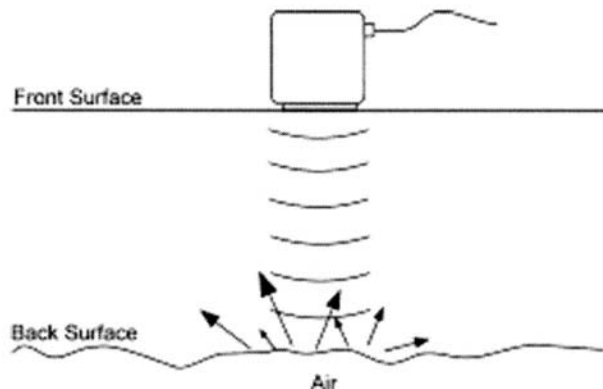


Figure 2.23: Signal scatter due to uneven reflecting surface morphology (Kaiser & Karbhari 2002)

### **Applications of ultrasonics**

Ultrasound has been used to determine the integrity of various materials including metal and alloys, welds, forgings and castings. Ultrasound has also been applied to concrete in an attempt to nondestructively determine *in situ* concrete features such as:

- Compressive strength
- Defect location
- Surface crack measurement
- Corrosion damage

### **Strength determination**

The material properties of concrete are variable, and strength determination is a difficult and complicated process. The basic ingredients of concrete are hydrated cement paste, aggregates, water and air. The hydrated cement paste is a highly complex multiphase material. The mineral aggregates are porous composite materials differing greatly from the cement paste matrix. The interface between paste and aggregate particles has its own special properties. Concrete can aptly be considered a composite of composites, heterogeneous at both the microscopic and macroscopic levels (Popovics 2001). Concrete, unique in its placement, is one of the only materials used in construction that is usually batched and transported to a construction site for placement in the form of a viscous liquid. The concrete liquid is then formed and left to form a hardened paste. It is this hardened concrete for which material properties can be estimated in construction practice.

Minimum concrete strengths can be accurately predicted and estimated. However, the most commonly accepted method of measuring the compressive strength of *in situ* concrete is through core testing. Many studies have shown that there is no particular correlation between the strength of concrete defined by ASTM standards and the strength

of concrete actually in a structure (Mindess et al. 2003). Since some of the material properties of concrete, like strength, change with time and exposure, determining the strength of *in situ* concrete nondestructively is a valuable ability. Concrete is the only engineering material in which strength determination is attempted by ultrasonic measurements. The demand to test ultrasonically has been created by industry needs. Using NDT methods to achieve a reliable conclusion regarding the condition of a structure allows engineers to more efficiently plan repairs.

At the present time, there is no theoretical relationship between ultrasonic pulse velocity, or wave velocity and the compressive strength of concrete. However, in infinitely elastic solids, the P-Wave  $C_p$  is a function of Young's Modulus of Elasticity  $E$ , the mass density  $\rho$ , and Poisson's Ratio  $\nu$ . The relevant equation for wave speed is:

$$C_p = \sqrt{\frac{E(1-\nu)}{\rho(1+\nu)(1-2\nu)}} \quad (4)$$

Using this formula, it is possible to use the wave speed from ultrasonic testing to obtain other physical properties of concrete, such as compressive strength. However, most prior studies have been laboratory controlled and were performed on concretes with consistent mix parameters. These studies tend to neglect the effects of age and weathering on hardened concrete, which is a limiting factor when considering ultrasonic testing for strength determination in older structures (Lemming 1996, Popovics et al.1999, 2000, Popovics 2001, Gudra & Stawiski 2000, Lane 1998, Krautkramer 1990, Malhotra 1984, 1994, Malhotra & Carino1991).

The ultrasonic determination of concrete strength has been intensively researched. Although some studies have shown positive results (Lemming 1998, Popovics et al.1999, 2000, Popovics 2001, Gudra & Stawiski 2000, Lane 1998, Krautkramer 1990, Malhotra

1984, 1994, Malhotra & Carino 1991), there is no completely acceptable method for the determination of concrete strength using ultrasonics. This is due to the complexities of the material, the generated waveform, and the structure. Thus, continued research toward the development of a concrete strength versus ultrasonic pulse velocity relationship is justified (Popovics 2001).

### **Defect detection**

The most successful application of ultrasonics has been in the detection and location of the presence of discontinuities in concrete specimens and structures. Ultrasonic testing has been proven to be capable of detecting various anomalies including rebar, prestressed tendons, conduit delaminations, voids, and cracks. The reliability of ultrasonic tests has been confirmed when applied to the testing of concrete and masonry structures.

Ultrasonics are useful in the evaluation of construction and in the rehabilitation of structures. The sonic test is a reliable technique used to evaluate the effectiveness of grout injection. Investigations, repeated before and after repair, allow for control of the distribution of the grout in the masonry. Nevertheless, in the tested case, it was impossible to distinguish between the effects of each grout, the materials being injected having similar modalities (Binda 2001).

Recent research has been conducted using array systems and ultrasonic tomography to evaluate concrete specimens and structures. Tomography is defined as a method of producing a three-dimensional image of the internal structure of a solid object by the observation and recording of the differences in the effects on the passage of waves of energy impinging on those structures. Ultrasonic tomography can be performed by measuring the times-of-flight of a series of stress pulses along different paths of a

specimen. The basic concept is that the stress pulse on each projection travels through the specimen and interacts with its internal construction. Figure 2.24 illustrates the basic concept behind ultrasonic tomography. Variations of the internal conditions result in different times of flight being measured (Martin et al. 2001).

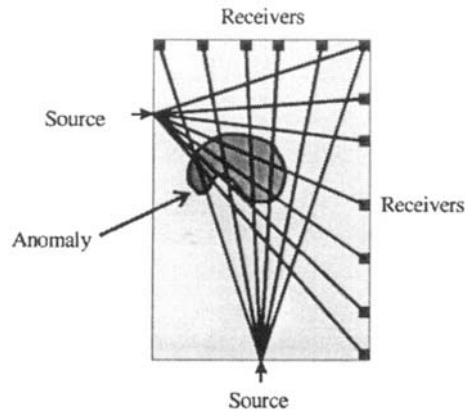


Figure 2.24: Setup of ultrasonic tomographic ray paths (Martin et al. 2001)

Field research has revealed that ultrasonic tomography constitutes a reliable method for investigating concrete structures. However, it is time consuming, and thus the practicality of using this method for global inspection of structures is limited.

Ultrasonic imaging and tomography methods have incorporated the use of array systems for transducer arrangements to be utilized for the inspection and defect detection. The practical application of the system shows that it is possible to measure the concrete cover of large construction elements, even behind dense reinforcing bars. The data is evaluated by means of time-of-flight corrected superposition. The array system together with a three-dimensional reconstruction calculation can be used for the examination of transversal prestressing ducts. The system has already been used successfully on site (Krause et al. 2001).

The most recent research in ultrasonics and its uses in nondestructive testing has been the automated interpretation of data. The interpretation of NDT data is a difficult

task, and those who do so must be trained and skilled in the NDT discipline. However, when large engineering structures are inspected, the amount of data produced can be enormous and a bottle neck can arise at the manual interpretation stage. Boredom and operator fatigue can lead to unreliable, inconsistent results where significant defects are not reported. Therefore, there is great potential for the use of computer systems to aid such interpretation (Cornwell & Mc Nab 1999). At present, the automated data analysis systems are unreliable for industry use. However, the value of automated flaw analysis has been successfully demonstrated on examples of real defects and made correct flaw diagnoses (Cornwell & McNab 1999). It appears as though the biggest limiting factor of the automated interpretation of NDT data is a general lack of knowledge involving defect and flaw detection. The information obtained via the use of ultrasonics and other NDT methods requires the interpretation of an experienced technician or engineer. Scientists have yet to find the simple answers with respect to ultrasonic data that allow computers and computer programs to be utilized for interpretation.

### **Surface crack measurement**

Surface crack measurement has been studied by several researchers and the results are considered to be reliable when the testing procedure is properly performed. In a concrete specimen with a known wave speed, a crack that is present will cause the path length of the ultrasonic pulse to become larger. Using simple geometric calculations, it is possible to obtain the depth of a surface initiated crack within a specimen, as long as that crack represents significant void space (i.e. is wide enough to eliminate contact of the sides). The limitation of this method is smaller cracks that lack large void space. In such cases, the pulse may be able to cross the crack due to the small discontinuity in the

concrete, thus shortening the path length. Figure 2.25 illustrates the concept of crack depth measurement.

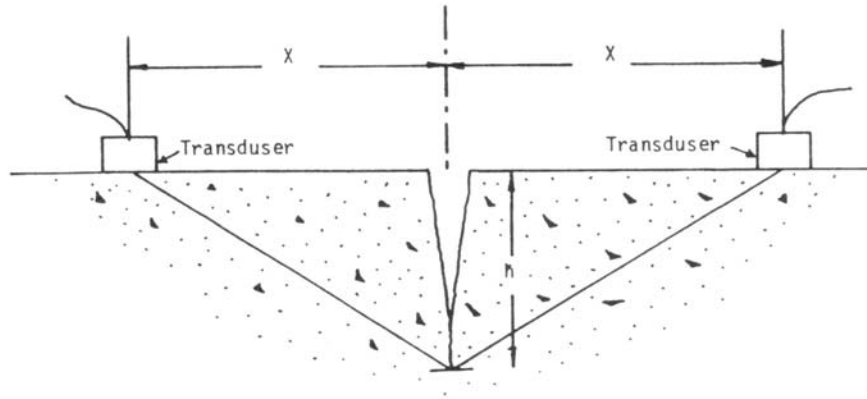


Figure 2.25: Measurement of crack depth (Malhotra 1991)

### **Detection of corrosion damage**

Corrosion of reinforcing steel is one of the most prevalent problems plaguing concrete structures. The most commonly used methods of corrosion detection are electrochemical methods, such as the DC polarization method, the AC impedance method, and the open circuit potential method. Such electrochemical methods can only obtain overall information theoretically. However, pitting corrosion often occurs in reinforcing steel in reinforced-concrete members. The local environment surrounding the metal surface is not uniform, and inappropriate loading may induce cracks in concrete that allow, or even draw, chloride ions from the environment. These ions can penetrate the concrete along the cracks faster than at other, uncracked areas. Electrochemical measurements for the detection of corrosion damage in reinforced concrete members may underestimate the local pitting corrosion rate because the electrochemical parameters represent global information obtained by taking an average of the total amount of local corrosion on the whole metal surface area (Yeih & Huang 1998).

Laboratory research has been performed that has correlated ultrasonic wave amplitude attenuation to corrosion damage in reinforced concrete specimens. Some of the limitations of this approach include the test control conditions. Most of the research involving corrosion degradation in reinforced concrete specimens has involved the corrosion of steel in intact concrete specimens. However, structures observed in the field typically exhibit corrosion damage as a result of material deficiencies in the concrete that encases it, usually a result of both the concrete and the steel. This problem requires further analysis of the combined effect of both materials for field applications.

Laboratory studies have yet to incorporate both materials. The ultrasonic investigation of a deteriorated reinforced concrete specimen essentially requires the comprehension of ultrasonic wave forms that account for dissimilar material effects from the steel and complex multiphase heterogeneous material that is concrete. Ultrasonic testing analysis of the resulting damage of such complex conditions is difficult to perform. Further research and testing is needed before ultrasonic testing can be reasonably applied in field use for the detection of corrosion effects in reinforcing steel. Engineers need to understand the shortcomings of nondestructive testing tests so that they can make proper determinations and accurate evaluations of structures (Boyd et al. 2002).

### **Structural health monitoring**

Structural health monitoring is at the forefront of structural and materials research. Structural health monitoring systems enable inspectors and engineers to gather material data of structures and structural elements used for analysis. Ultrasonics can be applied to structural monitoring programs to obtain such data, which would be especially valuable since the wave properties could be used to obtain material properties. There is scarce

literature available on the monitoring of in-place concrete structures and structural elements.

Current research in structural monitoring relates to the performance of fiber reinforced polymer composites and other structural strengthening methods. Fiber optics have given rise to remote structural health monitoring, remote sensing, and nondestructive load testing. Ultrasound has been applied to concrete strength, crack detection, thickness measurements, and wave speeds of concrete structures.

The concept behind using ultrasonics for structural health monitoring is observing changes in the structure's wave speed over time. As previously discussed, the wave speed is a function of Young's Modulus of Elasticity  $E$ , the mass density  $\rho$  and Poisson's Ratio  $\nu$ . The overall quality of the concrete is associated with the ultrasonic wave speed (Ryall 2001).

Table 2.3 Relationship between pulse velocity and concrete quality

Longitudinal Pulse Velocity (m/s)	Quality of Concrete
> 4500	excellent
3500-4500	good
3000-3500	doubtful
2000-3000	poor
< 2000	verypoor

This testing approach may be used to assess the uniformity and relative quality of the concrete, to indicate the presence of voids and cracks, and to evaluate the effectiveness of crack repairs. It may also be used to indicate changes in the properties of concrete, and in the survey of structures, to estimate the severity of deterioration or cracking. When used to monitor changes in the condition over time, tests are repeated at the same positions (ASTM C597-97). Decreases in ultrasonic waves speeds over time can

reveal the onset of damage before visible deficiencies become evident. This allows inspectors and engineers to implement repair recommendations before minor deficiencies become safety hazards.

### **Impact Echo**

The term “ultrasonic” refers to sound waves having a frequency above the human ear's audibility limit, which is about 20,000 Hz. Ultrasonic testing has been used to successfully evaluate the quality of concrete for approximately 60 years. This method can be used for non-intrusively detecting internal defects in concrete. Some of these flaws include deterioration due to sulfates or other mineral attack, and cracking and changes due to freeze-thaw cycling. One type of ultrasonic testing is the impact-echo method.

### **Development of method**

Nicholas Carino of the National Bureau of Standards (NBS) developed the impact-echo method in the 1970's and 1980's for assessment of buildings and bridges that failed during construction (Sansalone & Streett, 1997). Mary Sansalone focused her research on the refinement and application of the impact-echo method for her Ph. D thesis at Cornell University. Their research comprises the majority of impact-echo research and development performed in the United States applicable to concrete and concrete structures.

Early research focused on laboratory studies involved the location of defects and voids in concrete. There have been four key research breakthroughs since research began to successfully develop impact echo as an NDT method (Sansalone & Streett, 1997). The concerns utilization of the numerical simulation of stress waves in solids using finite element computer models. This method was implemented to help facilitate the interpretation of early experimental results. The models created were two-dimensional

finite element models based on Green's functions, which simulate stress wave propagation in plates. Green's functions are widely used in determining responses in solids to an applied unit force. These functions can be used to obtain the propagation of elastic waves in solids. This mathematical formulation was essential in the interpretation of results obtained through experimentation.

The second key research breakthrough relates to the use of steel ball bearings to produce impact generated stress waves. The impacting of objects on the surface of a given solid produces stress waves that facilitate signal acquisition. This elastic impact results in a force-time function that is defined and mathematically applicable. The impact-echo method does not use a pulse-generating transducer to generate stress waves, rather, the impacting of an object, typically a small steel ball, provides the stress wave. The development of the impact method overcame the need for a pulse generating transducer. Typical steel balls range from 4 to 15 mm in diameter but can be larger or smaller depending on the desired waveform needed for the test. Typical impact speeds are 2 to 10 meters per second but can also vary depending upon the desired waveform. The contact time typically ranges from 15 to 80  $\mu$ s. Proper selection of steel ball diameter and impact speed is essential in flaw detection to create the correct wave frequency, which is typically less than 80 kHz. This range can vary depending on the properties and dimensions of the test sample.

The third key research advancement was the development of a transducer that can acquire impact generated stress waves. The development of the correct receiving transducer was an integral phase in the advancement of the impact-echo method. The receiving transducer was developed by T.M. Proctor (Hamstad and Fortunko, 1995). The

intended use for the receiving transducer was the acoustic emission testing of metals. However, it was discovered that the transducer was compatible with impact-echo testing of concrete. The receiving transducer is composed of a small conical piezoelectric element bonded to a larger brass block. For protection of the transducer tip, a lead element is fitted between the transducer tip and the material to be tested. Some tests use coupling materials such as gels to provide an effective test surface. In areas where a smooth concrete surface is not available, the concrete is usually grinded to a smooth surface to ensure proper transducer-to-surface coupling. Figure 2.26 is a schematic of a typical piezoelectric transducer.

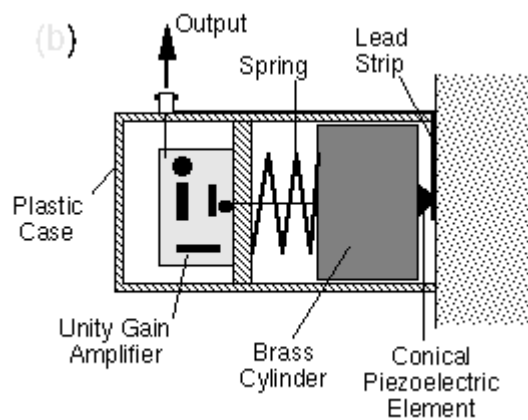


Figure 2.26: Schematic of a typical piezoelectric transducer used for impact echo testing (Carino 2001)

The final key research advance pertains to the use of frequency domain analysis for signal interpretation. Waveform analysis is the determining component in the use of NDT. In many cases the operator has difficulty in interpreting the wave signals received in the time-domain by the piezoelectric transducer. Using a Fourier transform on the time-domain signals, it is possible to graph the wave's frequency-domain signal. The result is a frequency vs. amplitude plot, also called an amplitude spectrum.

**Recent research advances**

Much of the research and development of the impact-echo method has been carried out at Cornell University. This research primarily involves the relevant application of impact-echo to the evaluation and inspection of concrete and masonry materials (Sansalone & Streett, 1997). Through this research, the methods for determining wave speeds in concrete, grout, and masonry were improved for industry use. The research also helped develop applicable methods for locating and determining flaws in concrete and masonry. Some of the flaw types that have been accurately detected using the impact-echo method include cracks, voids, bonding voids, honeycombing, and concrete damage. The method can also be used to obtain the thickness of a material such as concrete or asphalt pavement.

The advances in the impact-echo method made at Cornell University used a combination of research techniques. These techniques include numerical models, finite-element analysis, eigenvalue analysis, resonant frequency analysis and laboratory testing. The first portable impact-echo system was developed by Mary Sansalone and Donald Pratt and was patented by Cornell University. The patented system has five basic components including spring-mounted impactors (ball bearings), a receiving transducer, a high-speed digital-to-analog data-acquisition system, a rugged and powerful laptop-size computer, and software for transferring analyzing and storing test data (Sansalone & Streett, 1997). Figure 2.27 is an illustration of a typical impact-echo equipment system.

The portable impact-echo system has been successfully developed as a commercial product and is available for retail purchase. Most portable impact-echo systems that are available for consumer use are purchased with four components, with the laptop computer being omitted.



Figure 2.27: View of a typical impact-echo equipment system

### **Stress wave theory**

The effective use of the impact-echo system requires that the user have a basic understanding of the properties and fundamentals of stress waves. In solid mechanics, when any two objects collide local disturbances take place within a given material. The disturbances can cause deformations that may be plastic or elastic in nature. A plastic deformation is defined as a deformation in which the material is permanently deformed. Elastic deformations are the type in which the material is temporarily deformed but then returns to its original shape. When an elastic collision occurs between objects, a disturbance is generated that travels through the solid in the form of stress waves. There are three primary modes of stress wave propagation through elastic media: dilatational, distortional, and Rayleigh waves (Sansalone & Carino, 1989).

Dilatational waves are the primary stress waves produced upon impact. They are also referred to as primary waves, P-waves, or compression waves. The particle motion of the wavefront of P-waves is parallel to the direction of impact propagation. The result is a compressive or tensile stress wave (Sansalone & Streett 1997). The P-wave velocity is the fastest of the three stress waves produced from the impact. Typical P-wave speeds

for concrete ranges from approximately 3000 m/s to 5500 m/s. For normal strength concrete, P-wave speed usually ranges from 3500 m/s-4500 m/s.

Distortional waves are the secondary stress waves that are produced upon forced contact. These waves are also called shear waves or S-waves. In S-waves, the particle motion of the wave front is normal to the direction of propagation producing shear stress. (Sansalone & Streett 1997). S-wave speed in normal concrete is usually about 62 percent of the P-wave speed.

Rayleigh waves are also called R-waves or surface waves. Rayleigh waves, unlike P-waves and S-waves, do not propagate through the solid. Rayleigh waves propagate along the surface of a given concrete specimen in an elliptical motion. P-waves and S-waves propagate through a concrete specimen in spherical wavefronts. Rayleigh wave speed is usually 56 percent of P-wave speed. Figures 2.28 and 2.29 illustrate the typical relationship between stress wave types.

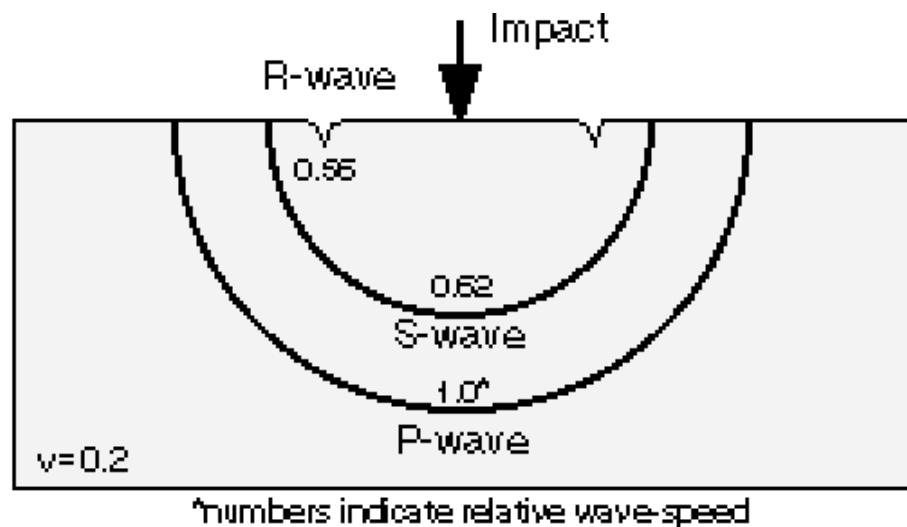


Figure 2.28: Illustration of typical wave propagation through a cross section of a solid (Carino 2001)

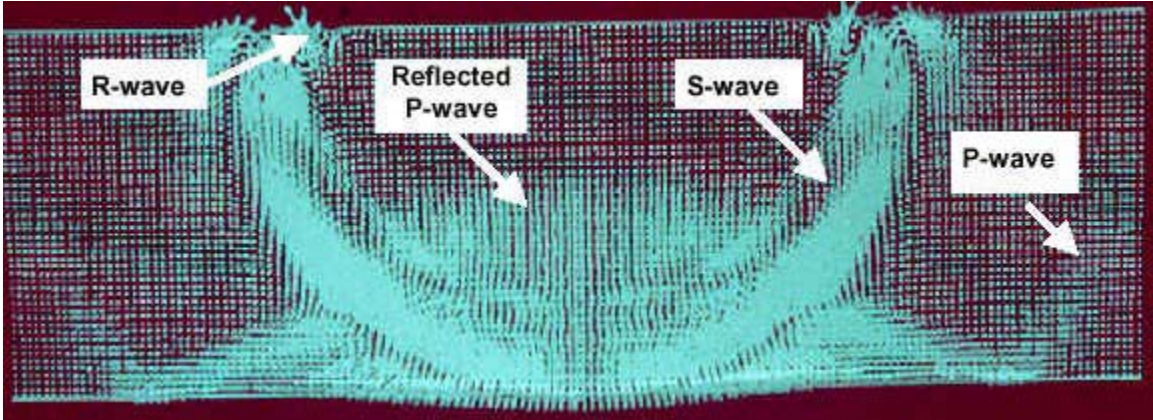


Figure 2.29: Illustration of wave propagation model through a cross section of a solid (Carino 2001)

The wave speeds in elastic solids are related to Young's Modulus of Elasticity  $E$ , Poisson's ratio  $\nu$ , and the density  $\rho$  (Sansalone & Streett, 1997). In the equations below  $C_p$ ,  $C_s$  and  $C_r$ , describe the P-wave, S-wave and R-wave speeds respectively.

$$C_p = \sqrt{\frac{E(1-\nu)}{\rho(1+\nu)(1-2\nu)}} \quad (5)$$

$$C_s = \sqrt{\frac{G}{\rho}} \quad ; \quad C_s = \sqrt{\frac{1-2\nu}{2\rho(1+\nu)}} \quad (6)$$

$$C_r = \left( \frac{0.87 + 1.12\nu}{1 + \nu} \right) C_s \quad (7)$$

Where  $G$  is the Shear Modulus of Elasticity.

The typical range of values for Poisson's ratio " $\nu$ " is typically 0.17-0.22. Inserting this value for  $\nu$  into the above equations, along with the typical density and modulus of elasticity values, will give typical wave speeds found in concrete. The modulus of elasticity of a concrete specimen, the compressive strength, and the appropriate wave speed of the concrete can be obtained. Equation 5 can be used as an example obtain a typical wave

P-wave speed for a concrete sample as follows:

Using:  $E=30 \times 10^9$  Pa,  $\rho = 2400$  kg/m<sup>3</sup>, and  $\nu = 0.18$

$$C_p = \sqrt{\frac{E(1-\nu)}{\rho(1+\nu)(1-2\nu)}} \quad C_p = \sqrt{\frac{30 \times 10^9 (1-0.18)}{2400(1+0.18)(1-2(0.18))}} = 3700 \text{ m/s}$$

As discussed above, 3700 m/s is an acceptable P-wave speed for concrete.

### Force-time function of impact

Stress waves can be produced by several different instruments. The ultrasonic pulse velocity method uses a stress wave transmitting piezoelectric transducer. The impact-echo method applies the collision of a steel sphere generating stress waves. The parameters that characterize the duration of the impact or contact time are sphere size, and the kinetic energy of the sphere at the point of impact. The variation of impact force with time is called the force-time function, accurately represented by a half sine curve (Sansalone & Streett 1997). The contact time duration between a small steel sphere and a concrete surface is relatively short, ranging from 30  $\mu$ s to 100+  $\mu$ s. Figure 2.30 illustrates the typical force-time relationship.

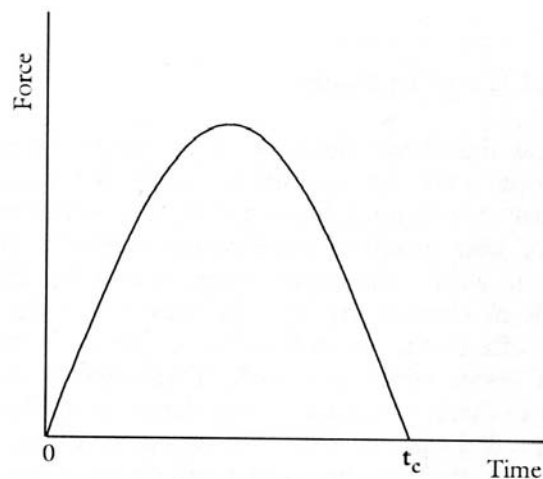


Figure 2.30: The typical force-time function for the elastic impact of a sphere on a solid (Sansalone & Streett 1997)

One result of the impact of a steel sphere on a concrete specimen is the transfer of kinetic energy from the sphere to the concrete. The energy transfer takes place in the form of particle displacements resulting in stress waves on the impacted solid. The maximum force is proportional to the kinetic energy of the moving sphere at impact, and the particle displacements are proportional to this force (Sansalone & Streett 1997). The time of contact, however, has a faint reliance on the kinetic energy of the sphere, being a linear function of sphere diameter.

The stress waves generated by the impact contain a wide distribution of frequencies. The frequency distribution is influenced by the force-time function of the collision. The objective of frequency analysis is to determine the dominant frequency components in the digital waveform. The optimum technique used to create the amplitude spectrum is the fast Fourier transform (FFT) technique. The FFT technique assumes that any waveform, no matter how complex, can be represented by a series of sine waves added together. The FFT displays the amplitudes of the various frequency components in the waveform. The amplitude spectrum obtained by the FFT contains half as many points as the time domain waveform. The maximum frequency in the spectrum is one-half the sampling rate. This shows the initial portion of the computed amplitude spectrum. Each of the peaks corresponds to one of the component sine curves (Carino 2001). Figure 2.31a illustrates a typical group of sine waves which is transformed into a typical frequency spectrum in Figure 2.31b.

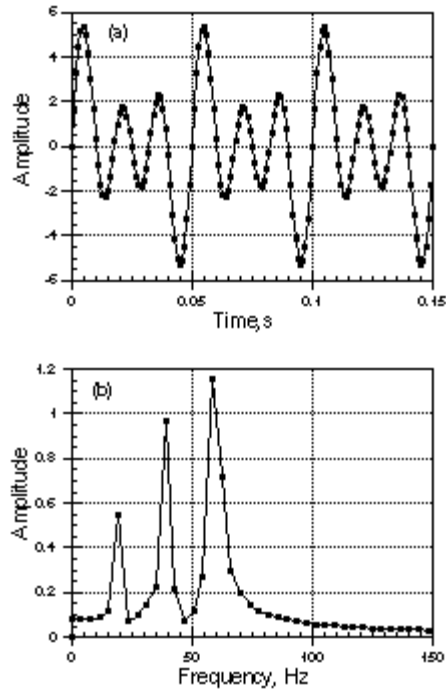


Figure 2.31: Example of frequency analysis using FFT: (a) represents the frequency distribution, (b) represents the corresponding amplitude spectrum (Carino 2001)

The linear relationship between time of contact and sphere diameter can be described as:

$$t_c = 0.0043D \quad (8)$$

(Sansalone & Streett 1997)

where  $D$  is the sphere diameter in meters and  $t_c$  is the contact time in seconds. For an impact using a sphere of a given diameter, a maximum frequency of useful energy is created. This relationship, like the sphere diameter and contact time relationship, can also be described as a linear function.

$$f_{\max} = \frac{291}{D} \quad (9)$$

(Sansalone & Streett 1997)

where  $f_{\max}$  is the maximum frequency of useful energy in hertz and  $D$  is the sphere diameter in meters.

The interesting concept behind Equation 9 is that maximum usable frequencies are smaller when larger diameter spheres produce impacts. However, larger spheres produce larger forces and larger maximum stress wave amplitudes. The contact time decreases with decreasing sphere diameter but the range of useful frequencies increases with a smaller diameter sphere. However, using smaller spheres increases the likelihood that the higher frequency stress will be scattered by the natural inhomogeneities inherent in concrete. In practice, it has been found that the smallest sphere useful in impact-echo testing has a diameter of approximately 3mm (Sansalone & Streett 1997).

### **Behavior of stress waves at material interfaces**

The term interface is defined as a surface forming a common boundary of two bodies, spaces, or phases. One of the most common interfaces people are familiar with is the oil-water interface. In material science, an interface is usually defined as a fringe between two materials which have different properties, such as density and phase. Other differences in material properties are acoustic properties (such as acoustic impedance). Acoustic impedance is defined as the material density multiplied by the materials stress wave velocity. When stress waves collide with material interfaces, portions of the waves are reflected and refracted. In obtaining the depth of a flawless concrete specimen, users assume stress waves are being reflected at the concrete/air interface as seen in Figure 2.32.

In the development of the impact echo method, the use of finite element models (FEMs) was prominent in the study of particle motion and stress wave propagation through a concrete medium. The use of FEMs permitted the developers of the impact-

echo technique to study waveforms at projected instantaneous phases in the wave's displacement. The model studies provided necessary information concerning the reflection of stress waves in a concrete media. Figure 2.33, illustrates the ray paths of typical P-wave propagation in a solid.

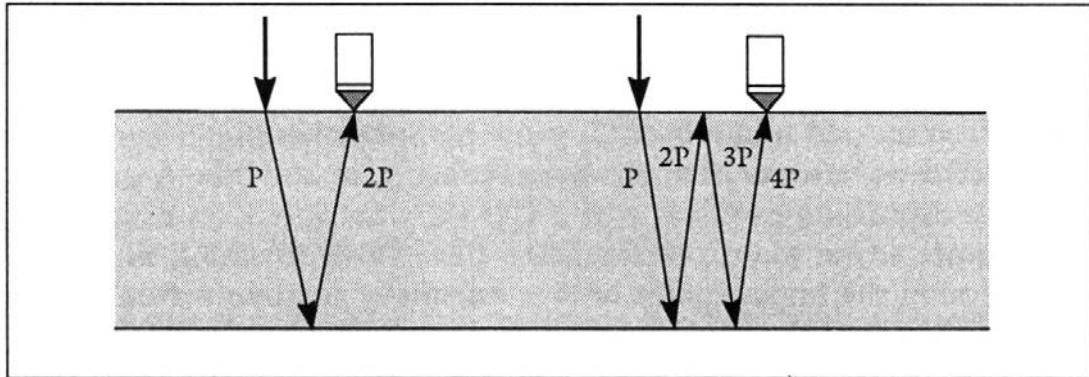


Figure 2.32: Plots of P, S and R-waves at various times after an impact: (a) 125  $\mu\text{s}$ , (b) 150  $\mu\text{s}$ , (c) 200  $\mu\text{s}$  and (d) 250  $\mu\text{s}$  (Sansalone & Streett 1997)

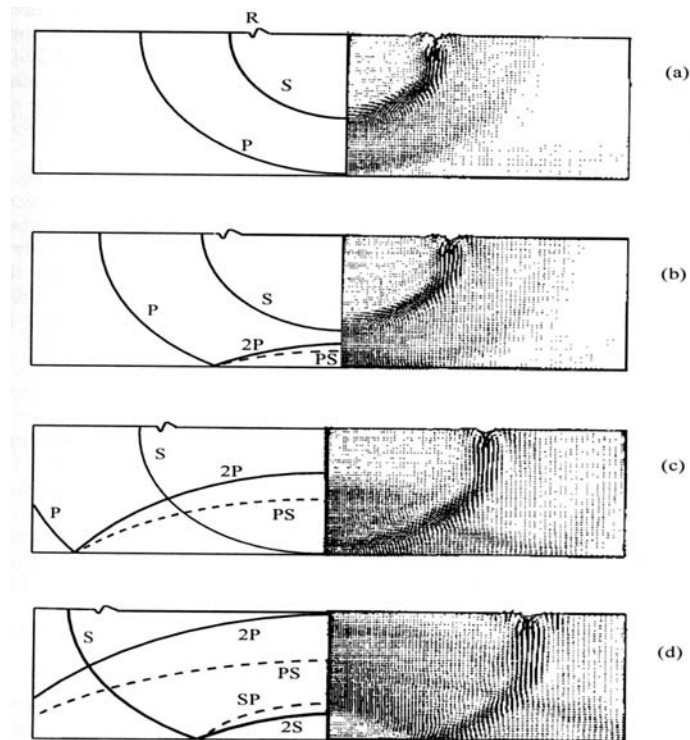


Figure 2.33: The ray path of typical P-wave propagation through a solid media (Sansalone & Streett 1997)

Stress wave behavior between interfaces of solids is more complicated than the stress wave behavior between a solid-gas interface. Upon collision with a solid-gas interface, most of the P-wave energy is reflected back into the solid media. However, in a stress wave collision with a solid-solid interface, the P-wave energy is partially reflected and partially refracted. The amount of energy that is allowed to pass through or refract the second solid medium depends upon its acoustic impedance. It is possible to get a coefficient of refraction if the acoustic impedance of the materials involved is known and the amplitude of the particle motion is obtained for the initial P-wave.

$$R = \frac{A_{\text{reflected}}}{A_i} = \frac{Z_2 - Z_1}{Z_2 + Z_1} \quad (10)$$

$$R = \frac{A_{\text{refracted}}}{A_i} = \frac{2Z_2}{Z_2 + Z_1} \quad (11)$$

(Sansalone & Streett 1997)

Where R is the coefficient of refraction,  $A_{\text{reflected}}$  &  $A_{\text{refracted}}$  are the reflected and refracted P-wave amplitudes;  $A_i$  is the amplitude of the initial P-wave;  $Z_1$  is the acoustic impedance of the initial medium; and  $Z_2$  is the acoustic impedance of the medium beyond the interface.

There are three basic relationships between  $Z_1$  and  $Z_2$ . The first relationship exists when  $Z_1$  is notably greater than  $Z_2$ . Due to this relationship, the  $Z_1/Z_2$  relationship is comparable to the solid-gas interface in which the P-wave is completely reflected and virtually no refraction takes place. This situation is common in the application because most defects in concrete are related to void space in the concrete matrix.

A second relationship between solid-solid interfaces is when the  $Z_2$  is much greater than  $Z_1$ . Consider  $Z_1$  to approach zero and consider Equation 11 above, then  $A_{\text{refracted}}$

approaches  $2A_i$ . When this condition exists, the amplitude of the wave is equal to that of the incident wave, while the amplitude of the refracted wave is twice that of the incident wave. There is no phase change in the reflected or refracted wave. In impact-echo testing, the no phase change case occurs, for example, when the first region is concrete and the second region is steel or rock, as the acoustic impedances of those materials are several times greater than that of concrete (Sansalone & Streett 1997).

The third relationship between solid-solid interfaces exists when  $Z_2$  is approximately equal to  $Z_1$ . When a value of 1 is used for both  $Z_1$  and  $Z_2$ ,  $A_{\text{reflected}}$  becomes zero and  $A_{\text{reflected}}$  becomes one. In this situation, most of the stress wave energy is transmitted through the interface to the second solid. This situation is possible when a concrete specimen is bonded to another concrete structure or a concrete structure has been properly patched.

Inserting  $Z_1$  and  $Z_2$ , into Equation 10 and  $Z_1$  is greater than  $Z_2$ , a negative value is obtained coefficient of friction “R”. The negative R value denotes a phase change in the stress wave at the point of reflection. Since impact induced P-waves are compression waves, a phase change indicates the waves will become tension waves upon reflection. This phenomenon is important to consider because when P-waves are reflected and  $Z_1$  is less than  $Z_2$ , as in a case when steel is the solid behind the interface, the reflected waves do not undergo phase change. Figure 2.34 below illustrates the phase changes that take place in stress waves upon reflection.

As seen in figure 2.34a illustrates the return of a tension wave in each reflection. In 2.34b, the return of a compression wave is alternated with the return of a tension wave for each stress wave reflection. The arrival of a tension wave causes an inward displacement

of the surface, while the arrival of a compression wave causes an outward displacement on the material surface. The reason stress waves do not change phase when reflected on a solid medium with a higher acoustic impedance is because the stress wave “bounces” off the second material and returns to the impact source. The “bouncing” takes place because materials with higher acoustic impedances have higher densities and the small surface displacements that usually take place at solid/gas interfaces, do not take place at boundaries more dense than the original medium.

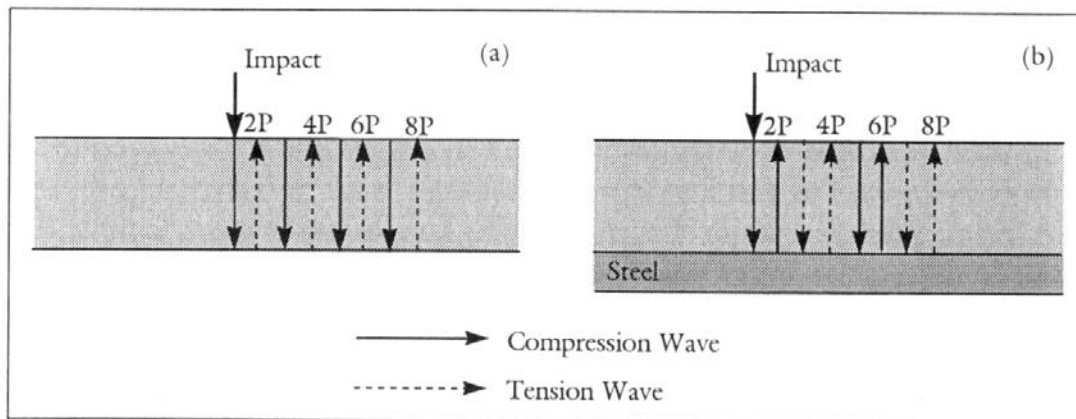


Figure 2.34: Impact echo ray paths (a) A phase change at both boundaries. (b) A phase change at upper boundary only (Sansalone & Streett 1997)

### Waveform analysis - idealized case

As stated in the introduction to stress waves section, such waves are the particle motion caused by the energy of an impact. When wavefronts reach the surface, the particle motion causes small displacements, which are detected by the receiving transducer. The transducer converts the surface displacement into a proportional voltage signal. The voltage signal becomes the primary output to the testing software. The output produced requires proper understanding of waveform analysis. For each test, the operator must properly interpret the waveform in order to ascertain the quality of the data obtained.

A common scenario in impact-echo testing is the testing of a solid plate with solid/gas interfaces at both concrete surfaces. As seen in Figure 2.35, the principle features of the idealized waveform detected by the transducer are those produced by the P-wave, which travels into the structure and undergoes multiple reflections between the two surfaces, and the R-wave, which travels outward across the surface (Sansalone & Streett 1997).

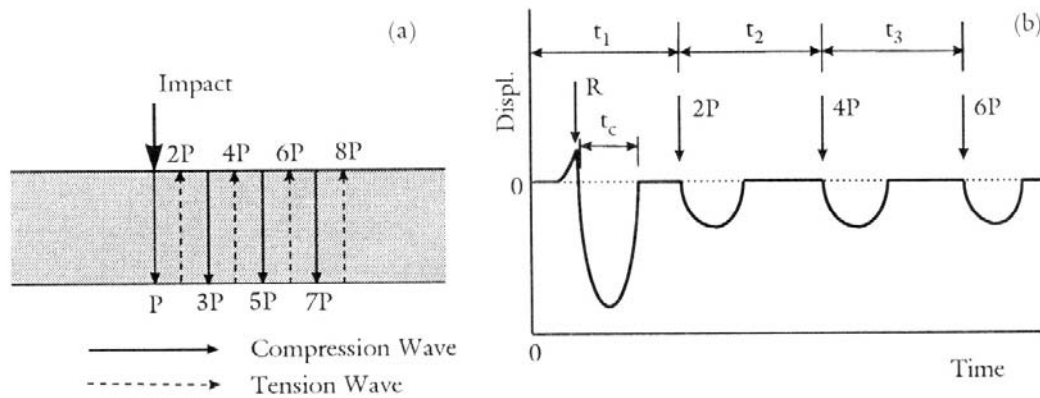


Figure 2.35: Schematic representations of (a) P-wave ray reflections and (b) the resulting idealized waveform (Sansalone & Streett 1997)

The typical elapsed time for the above waveform recorded is less than four milliseconds. As previously noted, R-waves propagate through a solid as surface waves and reflections of R-waves will not be recorded unless the distance between the receiving transducer and the horizontal solid-gas interface is less than the specimen depth. However, since the impact between the steel ball and the concrete specimen does not occur at a point directly below the transducer, the R-wave causes a negative displacement at the receiving transducer. As shown in the Figure 2.35, the amplitude of the R-wave is larger than any other feature in the wave spectrum. Figure 2.35 also illustrates that the time elapsed for the R-wave to return back to zero in the displacement spectrum is the time of contact " $\tau_c$ " of the impacting sphere. In this event, the point of the impacting

sphere is relatively far from the receiving transducer, the arrival of the P-wave reflection may occur before the arrival of the R-wave. To avoid this phenomenon, the operator must ensure that the impact point of the sphere is relatively close to the transducer. Since the P-wave and S-wave speeds are greater than the R-wave speed, there is a small displacement just prior to the arrival of the R-wave. This small displacement is due to the arrival of the P and S wavefronts.

The reflections of the P-wave with the solid-gas interface shown in Figure 2.35, illustrate the expected phase change. The arrival of the tension wave at the impacting surface causes a small inward displacement causing the wave reflections shown at times  $t_1$ ,  $t_2$  and  $t_3$ . The elapsed time  $t_1$ , between the impact and arrival of the 2P wave at the surface is the distance the wave has traveled, being twice the solid thickness. The P-wave arrivals at the upper surface cause displacements that are periodic in nature. This periodicity is the dominant feature of the waveform after the passage of the R-wave. The period of the waveform in Figure 2.35 is  $t_1$  and its frequency is  $1/t_1$ , the reciprocal of the period. This yields a simple relationship shown in Figure 2.33, which is at the heart of the impact-echo method (Sansalone & Streett 1997).

$$f = \frac{C_p}{2T} \quad (12)$$

(Sansalone & Streett 1997)

### **Waveform analysis - actual case**

The technique presented in the previous paragraph is an accurate description of waveform analysis, but it illustrates waveform circumstances under idealized conditions. One difference between the idealized case and the actual case is that the reactions of the transducer to the material displacements is caused by stress waves. As the stress waves

reflect due to the solid-gas interface, the receiving transducer experiences its own particle motions. This additional movement is referred to as “overshoot”. Overshoot causes the waveform displayed by the digital analysis software to have only the negative portion of each wave. This wave analysis software phenomenon is illustrated in Figure 2.36.

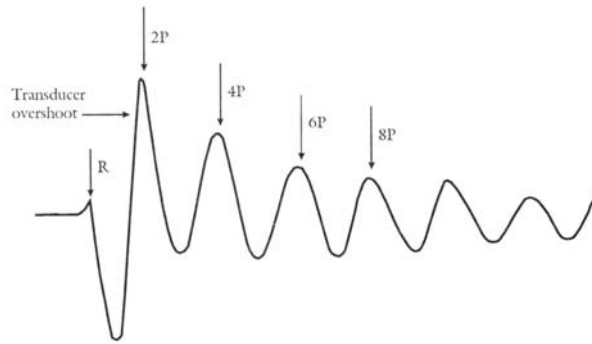


Figure 2.36: Actual waveform on an impact-echo test plate (Sansalone & Street 1997)

Figure 2.36 shows the actual waveform as it would be received and displayed by impact-echo software in field-testing. Another phenomenon that this figure illustrates is the decay of the spectral amplitude with the increasing number of wave reflections. This decay is a result of energy losses due to friction as the wave propagates within the solid matrix.

Through rigorous testing in the development of impact echo, it was observed that the frequencies obtained in laboratory testing of concrete specimens were not equal to the frequencies calculated in Equation 12. The use of finite element models and laboratory testing revealed a deviation of approximately 5% between the observed laboratory data and the expected results obtained by Equation 12. After considering the geometry of the specimen, the developers found that it was necessary to include a shape factor in the frequency equation. In the case of a solid plate, the characteristic dimension is the thickness  $T$ , and the shape factor  $\beta$  is 0.96 (Sansalone & Streett 1997).

$$f = \frac{\beta \cdot C_p}{2T} = \frac{0.96 \cdot C_p}{2T} \quad (13)$$

(Sansalone & Streett 1997)

### Field measurement of material stress wave speed

In field-testing, it is crucial to establish the wave speed of the solid before specimen dimensions and qualities are to be tested. The most common method for directly measuring the wave speed of a solid is through the use of two receiving transducers. The transducers are commonly placed in a spacer device, at a known fixed length from each other. Once the transducers are properly spaced and fixed to the concrete specimen, a single P-wave can be used to measure the wave speed of the concrete. Figure 2.37 illustrates the typical test set up behind the measurement of wave speed. Figure 2.38 is an example of a typical output obtained in acquisition of the wave speed.

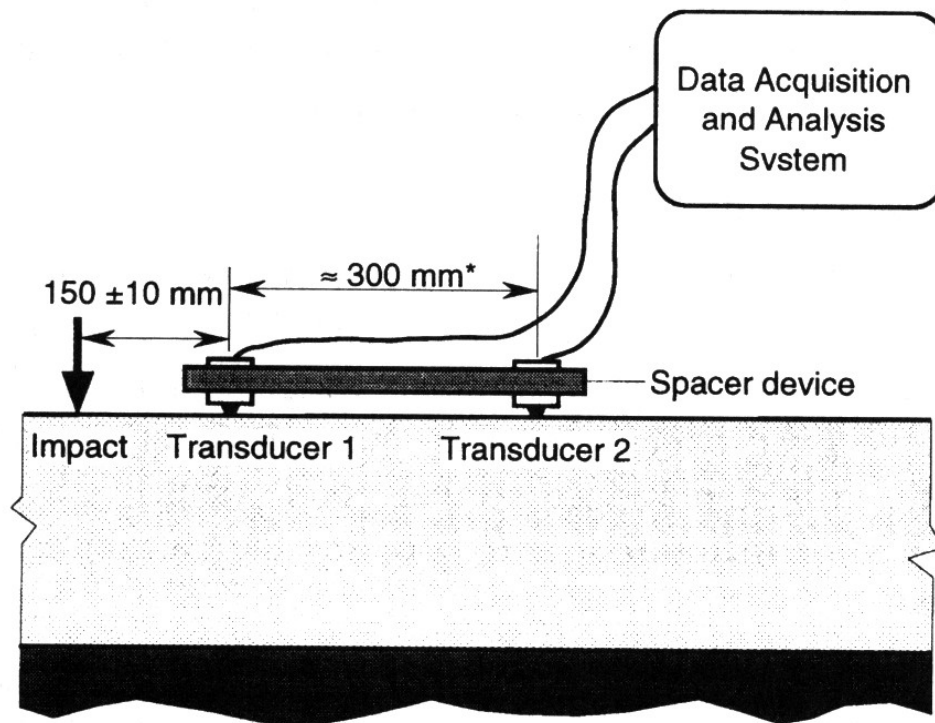


Figure 2.37: Schematic representation of the test set up for wave speed measurements (ASTMC 1383-R98a 2001)

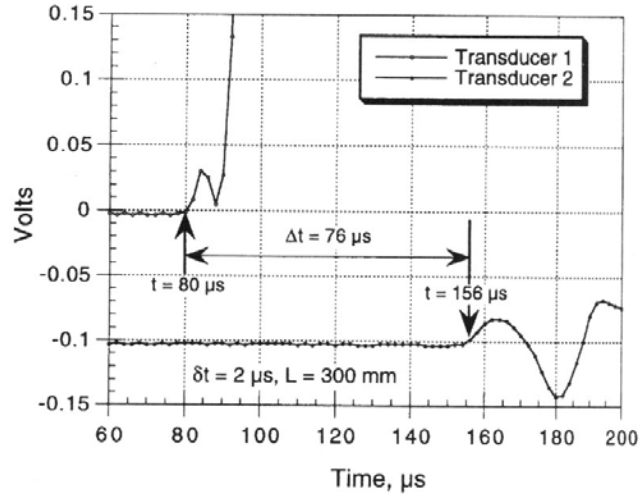


Figure 2.38: Example waveform obtained in wave speed measurements (ASTM 2001)

When the test is performed, the output would simply record the time at which the P-wave is received by each transducer. The wave speed would then be:

$$C_p = \frac{L}{t_2 - t_1} \quad (14)$$

(ASTM C1383 2001)

However, it is important to create the impact far enough from the initial transducer to allow for P-wave separation from the S and R-waves. This is the basis for having the minimum distance between the impact of the sphere and the first transducer set to  $\frac{1}{2}L$ . For the example of output illustrated in Figure 2.38, the results are  $t_2 = 156 \mu\text{s}$ ,  $t_1 = 80 \mu\text{s}$  and  $L=300 \text{ mm}$ . Using Equation 14, the wave velocity of the sample is obtained by the following:

$$C_p = \frac{300 \text{ mm}}{156 \mu\text{s} - 80 \mu\text{s}} = 3950 \text{ m/s}$$

Once the wave speed has been established for the concrete specimen, then testing for the specimen's thickness, concrete quality, flaw and anomaly detection may be performed.

### The effect of flaws on impact-echo response

Impact-echo was developed to nondestructively investigate concrete. One of the advantages of impact-echo testing is the versatile equipment and the relatively brief duration of the testing procedure. This allows inspectors to efficiently and accurately investigate structures and concrete specimens for condition assessment. The impact echo responses of materials can be classified according to the type, depth, and size of flaw.

For the purposes of impact-echo testing, a crack is defined as an interface or separation where the minimum opening is 0.08 mm or larger. Stress waves are able to propagate across voids that are smaller than 0.08 mm, hence there is not enough wave reflection to detect these smaller deficiencies. Since water has a coefficient of reflection of approximately 0.7, the majority of the stress wave energy at a solid-water interface is reflected and water filled voids can also be detected using the impact-echo method.

As the depth of a void from the surface increases, the smallest size that can be detected also increases. Based on analytical and laboratory studies, it has been suggested that if the lateral dimensions of a planar crack or void exceed  $1/3$  of its depth, the flaw depth can be measured. If the lateral dimensions exceed 1.5 times the flaw depth, the flaw behaves as an infinite boundary and the response is that of a plate with thickness equal to the flaw depth (Carino 2001). Figure 2.39 illustrates the relationship between crack depth and detectability.

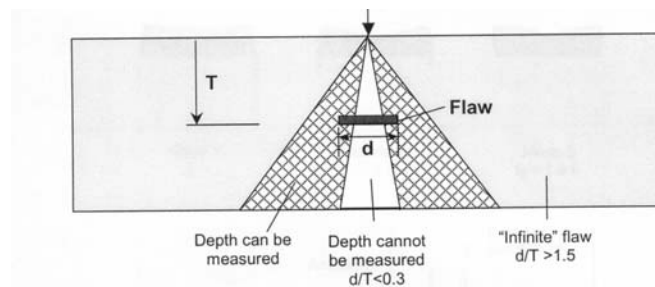


Figure 2.39: Illustration of the smallest detectable crack and its dependency on depth.

If the flaw is located entirely within the white area, the crack depth cannot be measured (Carino 2001) When larger cracks or voids are present, the impact-echo response will be essentially the same as if there was a solid/gas boundary at that interface. The test will produce results that represent the termination of the material at the depth of the flaw. A crack or void within a concrete structure forms a concrete/air interface. Laboratory experiments have shown that cracks with a minimum width (crack opening) of about 0.08mm (0.003 inches) cause almost total reflection of a P-wave. The responses from cracks and voids are similar, since stress waves are reflected from the first concrete/air interface encountered. Thus a crack at a depth  $d$  will give the same response as a void whose upper surface (nearest to the impact surface) is at the same depth (Figure 2.40).

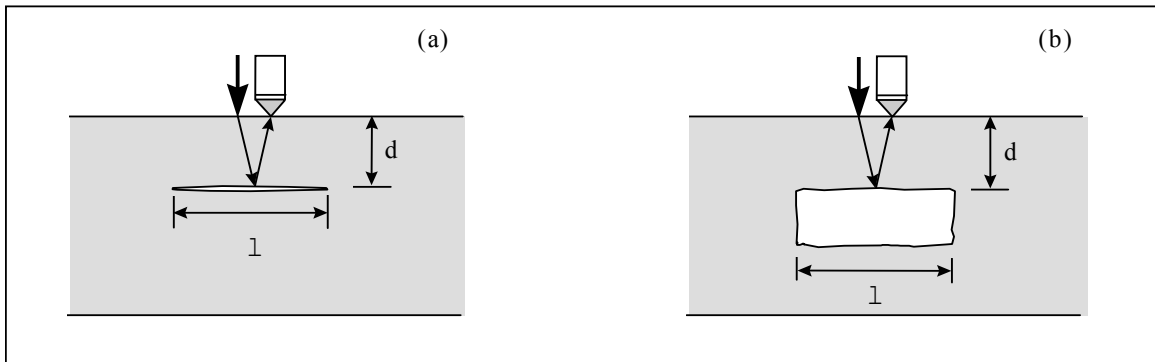


Figure 2.40: A crack at depth “ $d$ ” gives the same response as a void at that depth (Sansalone & Streett 1997)

In cases where the lateral dimensions of the crack are about equal or less than the depth of the crack, propagating stress waves are both reflected and refracted from the surface. Hence, they are diffracted around the edges of the crack (Sansalone & Streett 1997). For similar cases where more complicated waveforms exist, the frequency spectrums are affected accordingly.

## **Applications**

When properly used, the impact-echo method has achieved unparalleled success in locating flaws and defects in highway pavements, bridges, buildings, tunnels, dams, piers, sea walls and many other types of structures. It can also be used to measure the thickness of concrete slabs (pavements, floors, walls, etc.) with an accuracy of 3 percent or better. Impact-echo is not a "black-box" system that can perform blind tests on concrete and masonry structures and always tell what is inside. The method is used most successfully to identify and quantify suspected problems within a structure, in quality control applications (such as measuring the thickness of highway pavements) and in preventive maintenance programs (such as routine evaluation of bridge decks to detect delaminations). In each of these situations, impact-echo testing has a focused objective, such as locating cracks, voids or delaminations, determining the thickness of concrete slabs or checking a post-tensioned structure for voids in the grouted tendon ducts.

### **Determining the depth of surface-opening cracks**

A surface-opening crack is any crack that is visible at the surface. Such cracks can be perpendicular, inclined to the surface, or curved, as shown in Figure 2.41.

The two waveforms, labeled 1 and 2, in Figure 2.42(b), are the signals from transducers 1 and 2 in Figure 2.42(a). The arrival of the direct P-wave, a compression wave, at transducer 1 causes an upward surface displacement and a positive voltage (time  $t_1$ ), while the diffracted wave that first reaches transducer 2 is a tension wave, which causes a downward displacement and a sudden voltage drop (time  $t_2$ ). The elapsed time between  $t_1$  and  $t_2$ , the wave speed, and the known distances  $H_1$ ,  $H_2$  and  $H_3$ , are used to calculate the depth  $D$ .

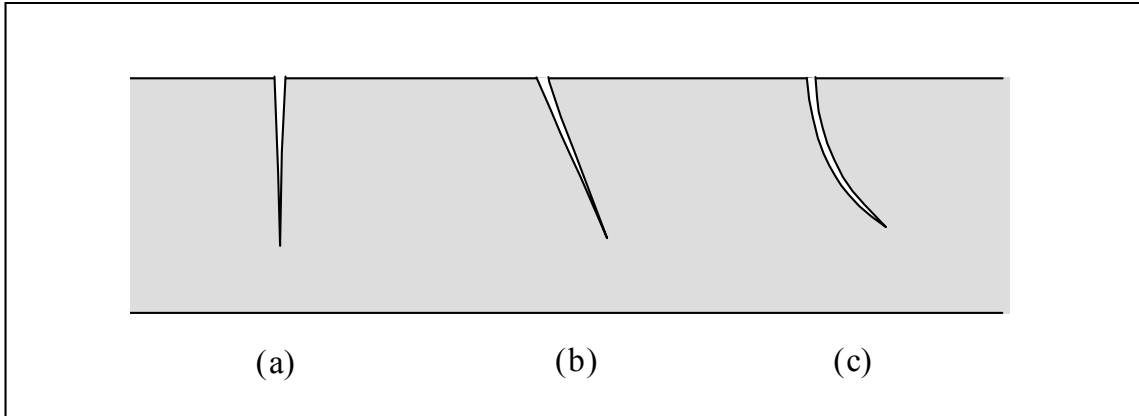


Figure 2.41: Surface-opening cracks: (a) perpendicular, (b) inclined, and (c) curved (Sansalone & Street 1997)

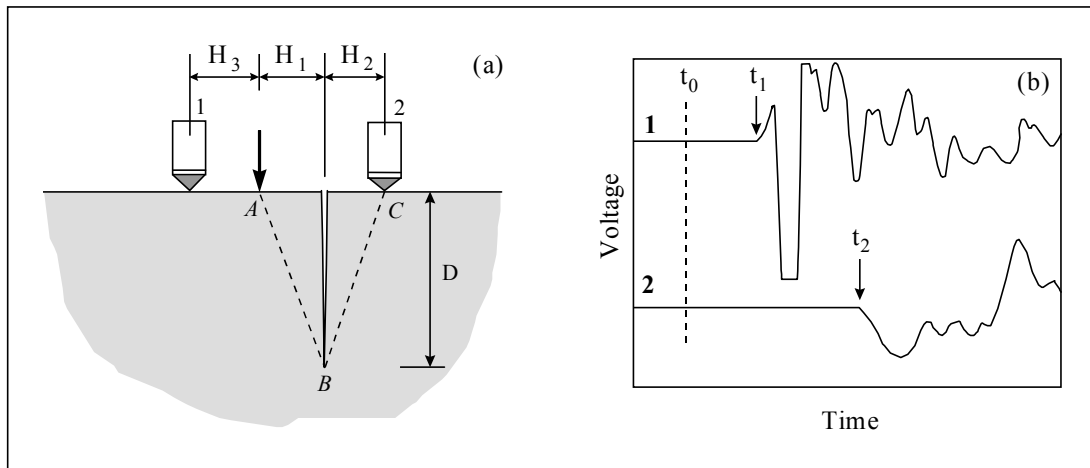


Figure 2.42: Measuring the depth of a surface-opening crack: (a) schematic of experimental test setup, and (b) sample waveforms (Sansalone & Street 1997)

### Voids under plates

Detecting voids under concrete plates is one of the simplest applications of the impact-echo method. It relies on the clear and easily recognizable difference between waveforms and spectra obtained from plates in contact with soil, on the one hand, and plates in contact with air (a void under the slab) on the other.

Figure 2.42 shows a typical set of results obtained from an impact-echo test on a concrete plate in contact with soil. The waveform shows periodic displacements caused

by P-wave reflections within the concrete plate, but because energy is lost to the soil each time a P-wave is incident on the concrete/soil interface, the amplitude of the displacements (indicated by the signal voltage) decays rapidly. The corresponding spectrum shows a single peak corresponding to the frequency of P-wave reflections from the concrete/soil interface. Note however, that the peak is somewhat rounded and is broader than those obtained from plates in contact with air. In Figure 2.43 only a few wave reflections were recorded before the signal decayed to an undetectable level.

For comparison, Figure 2.44 shows a typical result obtained from an impact-echo test on the same plate at a location where a void exists in the soil just below the plate. In this case P-wave reflections occur from a concrete/air interface at the bottom of the plate. Because virtually all of the wave energy is reflected at a concrete/air interface, surface displacements caused by the arrival of reflected P-waves decay more slowly compared to those reflected from a concrete/soil interface. The response is essentially the same as that obtained from a simple concrete plate in contact with air. The spectrum exhibits a very sharp, high amplitude peak corresponding to the P-wave thickness frequency. If the concrete slab is relatively thin (about 150mm or less) a lower frequency, lower amplitude peak, labeled  $f_{flex}$  in Figure 2.44(c), may also be present, as a result of flexural vibrations of the unsupported portion of the plate above the void. Flexural vibrations occur because the unsupported section above the void is restrained at its edges where it contacts the soil. The response is similar to that produced by an impact above a shallow delamination. However, because the thickness of the slab is relatively large, the amplitude of the flexural vibrations is smaller relative to the P-wave thickness response.

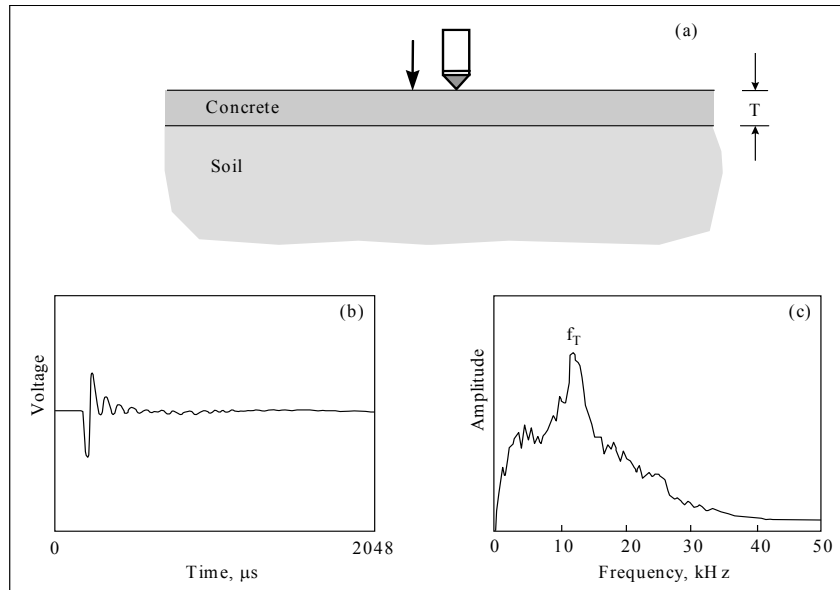


Figure 2.43: The impact-echo response of a concrete slab on soil subgrade: (a) cross-section, (b) waveform, and (c) spectrum (Sansalone & Streett, 1997)

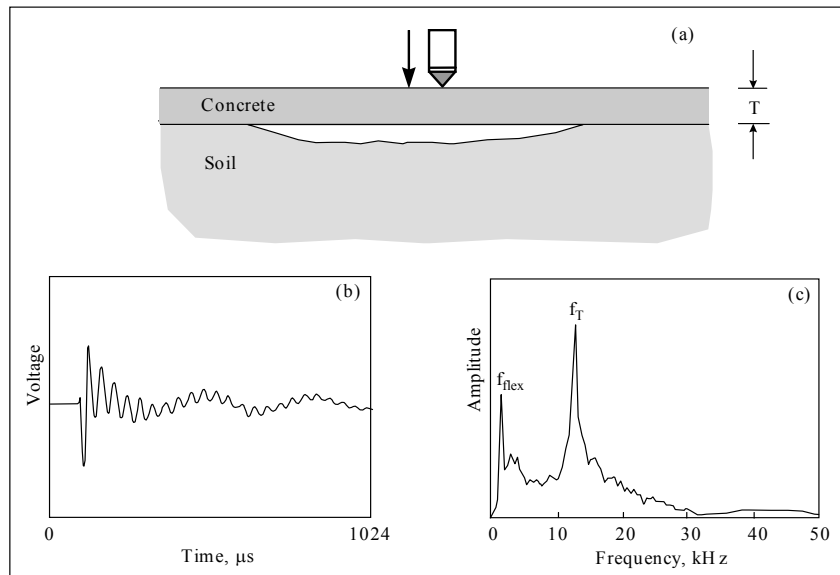


Figure 2.44: The impact-echo response obtained from a concrete slab at a location where a void exists in the soil subgrade: (a) cross-section; (b) waveform; and (c) spectrum (Sansalone & Streett, 1997)

### Steel reinforcing bars

Impact-echo is primarily used to locate flaws in, or thickness of, concrete structures.

Impact-echo may also be used to determine the location of steel reinforcing, though

magnetic or eddy current meters are better suited to this purpose. The acoustical impedance of steel is 5 times that of the concrete. If the sizes of reinforcement bars are known the impact-echo response can be estimated. If information is not known the reinforcing size can be estimated from a cover meter. Impact echo can be applied to evaluate the corrosion of reinforcing bars. The response is similar to solid plates, with single large amplitude peak P-wave thickness frequency. Waves travel around the corroding bar, instead of propagating through it, since the corrosion forms an acoustically soft layer around the bar. Short duration impacts result in peaks at higher frequencies, corresponding to reflections from the corroding surfaces. This method has been able to identify corrosion on reinforcement bars and has proven to be cost-efficient in identifying wall repair locations.

### **Voids in the tendon ducts of post-tensioned structures**

The impact-echo method can be used to detect voids in grouted tendon ducts in many, but not all, situations. The method's applicability depends on the geometry of a structure and the locations and arrangement of tendon ducts. Small voids in tendon ducts cannot be detected if the ratio of the size of the void to its depth beneath the surface is less than about 0.25. In addition, complicated arrangements of multiple ducts, such as often occur in the flanges of concrete I-beams, can preclude detection of voids in some or all of the ducts. In other cases, portions of structures can be successfully tested and information can be gained that permits an engineer to draw conclusions about the condition of the grouting along the length of the duct. The simplest case is that of post-tensioned ducts in a plate structure, such as a bridge deck or the web of a large girder, in which there is only one duct directly beneath the surface at any point. In all cases, the impact-echo method is restricted to situations where the walls of the ducts are metal

rather than plastic. Effective use of the impact-echo method for detecting voids in grouted tendon ducts requires knowledge of the location of the ducts within the structure. This information is typically obtained from plans and/or the use of magnetic or eddy-current cover meters to locate the centerlines of the metal ducts. Once the duct locations are known, impact-echo tests can be performed to search for voids.

### **Metal ducts**

Tendon ducts in post-tensioned structures are typically made of steel with a wall thickness of about 1mm (0.04 inches). The space not occupied by tendons inside the duct is (or should be) filled with grout, which has acoustic impedance similar to that of concrete. Because the wall thickness of a duct is small relative to the wavelengths of the stress waves used in impact-echo testing, and because a steel duct is a thin layer of higher acoustic impedance between two materials of lower acoustic impedance (concrete and grout), it is transparent to propagating stress waves. Therefore, the walls of thin metal ducts are not detected by impact-echo tests. (In contrast, plastic ducts have a lower acoustic impedance than concrete or grout, and they are not transparent, complicating attempts to detect voids within plastic ducts.)

### **Benefits to using impact-echo**

Applications of the IE method include quality control programs (such as measuring pavement thickness or assessing pile integrity), routine maintenance evaluations to detect cracks, voids, or delaminations in concrete slabs, delineating areas of damage and corrosion in walls, canals, and other concrete structures. Impact echo can be used to assess quality of bonding and condition of tunnel liners, the interface of a concrete overlay on a concrete slab, concrete with asphalt overlay, mineshaft and tunnel liner thickness.

Concrete pavements and structures can be tested in less time, and at lower cost, meaning more pavements and structures can be tested. No damage is done to the concrete and highway workers spend less time in temporary work zones, reducing the chance of injury and minimizing downtime for the traveling public. Impact-echo, according to ASTM, may substitute for core drilling to determine thickness of slabs, pavements, walks, or other plate structures.

### **Acoustic Emission**

Acoustic emission (AE) is defined as a transient elastic wave generated by the rapid release of energy within a material. These deformations can come from plastic deformation such as grain boundary slip, phase transformations, and crack growth. (Davis 1997). Unlike most nondestructive testing techniques, acoustic emission is completely passive in nature. In fact, acoustic emission cannot truly be considered nondestructive, since acoustic signals are only emitted if a permanent, nonreversible deformation occurs inside a material. As such, only nonreversible processes that are often linked to a gradually processing material degradation can be detected (Kaiser & Karbhari 2002). Acoustic emission is used to monitor cracking, slip between concrete and steel reinforcement, failure of strands in prestressing tendons, and fracture or debonding of fibers in fiber reinforced concrete.

### **Theory**

There are two types of acoustic emission signals: continuous signals and burst signals. A continuous emission is a sustained signal level, produced by rapidly occurring emission events such as plastic deformation. A burst emission is a discrete signal related to an individual emission event occurring in a material, such as a crack in concrete. An acoustic emission burst signal is shown in Figure 2.45.

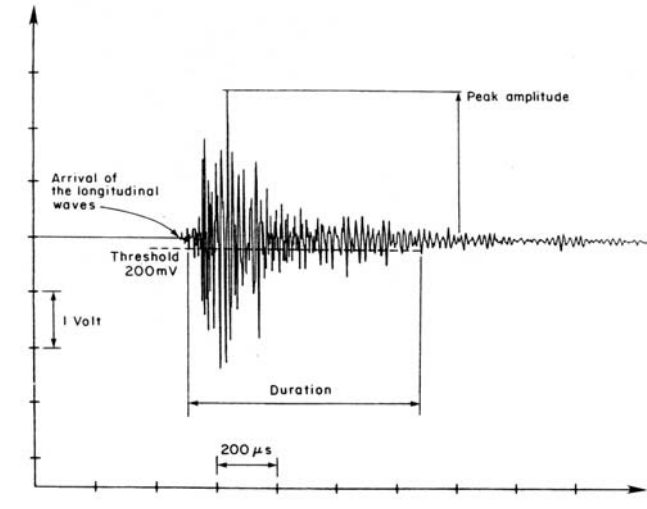


Figure 2.45: Burst acoustic emission signal with properties (Malhotra 1991)

The term “Acoustic emission signal” is often used interchangeably with acoustic emission. An AE signal is defined as the electrical signal received by the sensor in response to an acoustic wave propagating through the material. The emission is received by the sensor and transformed into a signal, then analyzed by acoustic emission instrumentation, resulting in information about the material that generated the emission.

An acoustic emission system setup is shown in Figure 2.46.

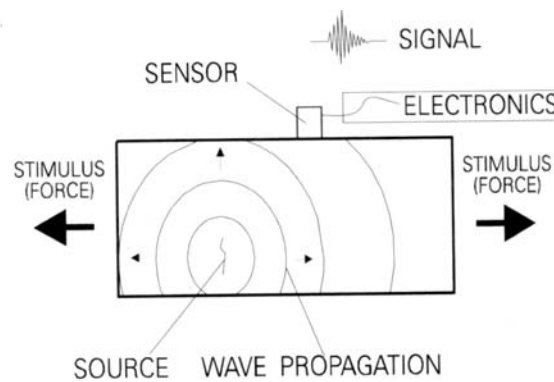


Figure 2.46: Acoustic emission process (Hellier 2001)

### Method development

Acoustic emission testing is used to obtain noise sounds produced by material deformation and fracture. Early terminology for acoustic emission testing was

“microseismic activity.” AE signals occur when micro or small fractures are detected within the material. The first documented observations of Acoustic Emission activities occurred in 1936 by two men, Forster and Scheil, who detected clicks occurring during the formation of martensite in high-nickel steel. In 1941, research by Obert, who used subaudible noise for prediction of rock bursts, noted that noise rate increased as a structure’s load increased. In 1950, Kaiser submitted a PhD thesis entitled “Results and Conclusions of Sound in Metallic Materials Under Tensile Stress” (Scott 1991).

Kaiser’s research is considered to be the beginning of acoustic emission as it is known today. In 1954 Schofield became aware of Kaiser’s early work, and initiated the first research program in the United States related to materials engineering applications of acoustic emission (Scott 1991).

During the early developmental testing for AE, several correlations were formed. Acoustic emission readings in materials of high toughness differed in amount and size from low toughness material. This was attributed to the differences in failure modes (Scott, 1991). Early acoustic emission testing signals were small and required a relatively calm environment for proper testing. With the use of an additional sensor, background noise could be isolated, which enabled testing to be carried out in a relatively noisy environment. The preliminary results of acoustic emission testing required massive data calculations due to the extensive numerical output the acoustic emission signals produced. This phenomenon distracted scientists, diverting too much of their attention to signal analysis instead of evaluation of the signal itself. Acoustic emission testing proved to be a highly sensitive indicator of crack formation and propagation.

Early use of acoustic emission testing proved to be valuable, but the first acoustic emission signals acquired contained large amounts of noise signals. This made it difficult as scientists were unable to develop AE as a quantitative technique. The material sensitivity and initial research results gave birth to a successful future for acoustic emission as a reliable nondestructive test.

### **Kaiser effect**

One of the most common uses of acoustic emission is in load testing of a structure or specimen. The generation of the acoustic emission signals usually requires the application of a stress to the test object. However, acoustic emissions were found not to occur in concrete that had been unloaded until the previously applied maximum stress was exceeded during reloading (Malhotra 1991). This phenomenon takes place for stress levels below 75 – 85% of ultimate strength and is found to be only temporary. Therefore, it cannot be used to determine the stress history of a structural specimen. Additional theory can be found in several references (Ohtsu et al. 2002; Hearn 1997; Tam & Weng 1995; Yuyama et al. 1992; Malhotra 1991; Scott 1991; Lew et al. 1988).

### **Equipment and instrumentation**

An acoustic emission system has the same basic configuration as seen in ultrasonic testing systems. The typical testing apparatus used for acoustic emission (shown in Figure 2.47 consists of the following:

- Transducer
- Receiver/Amplifier
- Signal Processors
- Transient Digitizers
- Display
- Calibration Block
- Coupling Agent

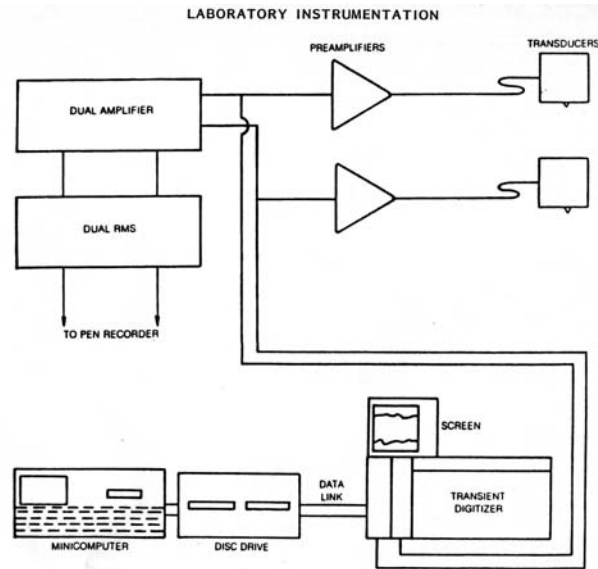


Figure 2.47: Basic setup of acoustic emission equipment (Miller 1985)

### Transducer

The acoustic emission transducer is more commonly referred to as a sensor. It is the most important part of the instrumentation. Sensors must be properly mounted to assure the proper configuration to attain the desired signal. Sensors are calibrated using test methods stated by societies. An array of different sensors is shown in Figure 2.48.



Figure 2.48: Various acoustic emission sensors (Miller 1985)

An important factor in acoustic monitoring is the location of sensors. For monitoring cases in which the location of a crack or deficiency is known, a single sensor

is sufficient for monitoring. However, for the detection of deficiencies in a two dimensional plane or three dimensional solid, the geometric configuration of the sensors is vital to the location of the deficiencies. ASTM Standard Guide for Mounting Piezoelectric Acoustic Emission Sensors specifies guidelines for mounting piezoelectric acoustic emission sensors. The performance of sensors relies heavily upon the methods and procedures used in mounting. Detection of acoustic emission signals requires both appropriate sensor–mounting fixtures and consistent sensor–mounting procedures (ASTM E-650-97).

### **Receiver/amplifier**

“Receiver” is the term applied to all of the circuit functions that amplify the weak signals and prevent loss in sensor activity. The receiver has four basic components: the preamplifier, the logarithmic amplifier, the rectifier and the low pass amplifier.

The function of the preamplifier is to ensure that any signal from the transducers arrives at the time measuring circuit. Since electrical outputs from the transducer are relatively small, signal amplification is necessary to overcome the resistance from the transducer cable, which can be relatively long. The function of the logarithmic amplifier is to process weak echo signals. Once the echo signals are amplified, the low pass filter processes the signals. After the signal has been processed by the receiver/amplifier, a useable signal can be transmitted to the display. Microprocessor-based systems have become more widely used in recent years. Such units perform single channel analysis, along with source location, for up to eight AE channels.

**Signal processors**

Signal processors are designed to allow data collection only on certain portions of a load cycle. Envelope processors attempt to filter out the high frequencies, leaving only the signal envelope to be counted. Logarithmic converters allow the output of the signal analyzer electronics to be plotted in logarithmic form. A unit allows combination of several preamplifier outputs so that several sensors can be monitored by one channel of electronics (Reese 1993).

**Transient digitizers**

Transient digitizers (also called transient recorders) are used to study individual AE burst signals. A signal is digitized in real time and then stored into memory. A transient digitizer is used in sequence with an oscilloscope or spectrum analyzer to display AE signals at visible speeds. Digital rates vary on transient digitizers. The fastest sampling rate becomes the limiting rate, with some instruments sampling up to 1 pulse/ns. Sampling rates can be modified for testing purposes. One advantage of transient digitizers is an additional mode of triggering, the pretriggering mode, where the input signal is continuously being digitized and the data fed into the memory (Reese 1993). This configuration allows a digitized picture of the signal to be displayed as received. More advanced digitizers allow recording of multiple signals simultaneously. The recording of more than one acoustic emission signal is shown in Figure 2.49.

**Display**

The signal received by acoustic emission test equipment is typically displayed digitally. The display uses an interval timer and a direct reading of display time on an x-y coordinate system. The x-axis displays the time trigger and the y-axis represents the mechanical energy received. The display units can also illustrate defect and anomaly

locations and sizes depending on the type of scan request by the user. Older acoustic emission systems used monitors to display received acoustic emission signals, however, most current acoustic emission systems use computer software and monitors to display results.

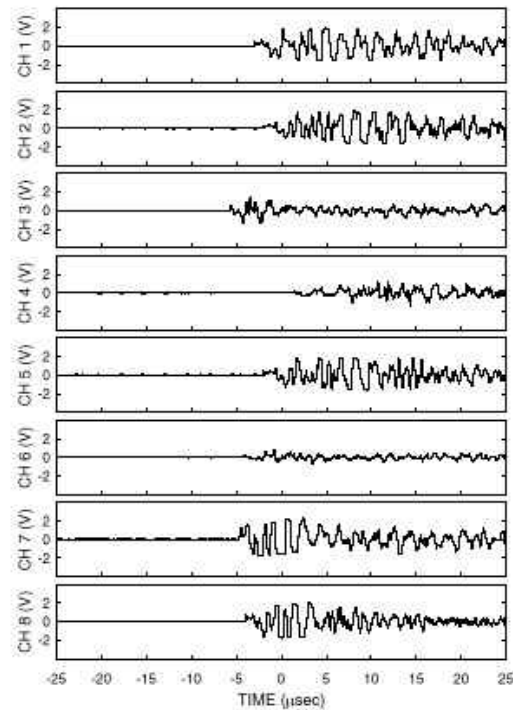


Figure 2.49: Transient recorder with multiple output acoustic emission signals (Sypeck 1996)

### Calibration block

ASTM states that annual calibration and verification of pressure transducers, AE sensors, preamplifiers (if applicable), signal processors, (particularly the signal processor time reference), and AE electronic simulators (waveform generators) should be performed. Equipment should conform to manufacturer's specifications. Instruments should be calibrated to National Institute for Standards and Technology (NIST) (ASTM E 1932-97). An AE electronic simulator, used in making evaluations, must have each channel respond with a peak amplitude reading within  $\pm 2\text{dBV}$  of the electronic

waveform output. (ASTM E 1932-97) Figure 2.50 is a photograph of a typical calibration block.

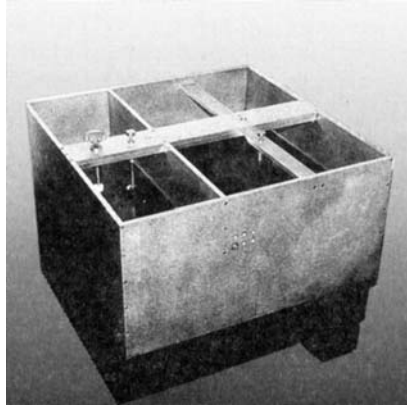


Figure 2.50. Acoustic emission calibration block

A system performance check should be done immediately before and after an acoustic emission examination. The preferred technique is the pencil lead break test. A description of the test procedure is described in ASTM E 750-98.

Acoustic emission signals are introduced into the structure and examined on an oscilloscope or with an AE system used in the test. If any doubt occurs in the sensor's response, it should be remounted. Three sources of the acoustic signal are the Hsu–pencil source, the gas–jet, and the electrical pulse to another sensor mounted on the structure. A description of the sources can be found in ASTM E-976. Two types of verification are periodic verification and post verification. ASTM defines periodic verification as the verification of the sensors periodically during the test. Post verification is defined as verifying the condition of the sensors to be in working condition at the end of the test.

### **Coupling agent**

A coupling agent is usually required to ensure the efficient transfer of mechanical energy between the tested material and the transducer. The purpose of placing the coupling material between the transducer and test specimen is to eliminate air between

the contact surfaces. Typical coupling agents are viscous liquids such as grease, petroleum jelly, and water-soluble jelly.

In acoustic emission testing it is common to bond the sensors to the test specimen. This setup is used for long term testing or monitoring of structures and specimens. When applying bonds, it is possible to damage the sensor or the surface of the structure during sensor removal.

### **Evaluation of acoustic emission activity**

Acoustic emission activity may be determined as the cumulative acoustic emission or as an event count. Analysis techniques should be uniform and repeatable. Techniques of evaluation include event counting, rise time, signal duration, frequency analysis and energy analysis. Field and laboratory evaluations include damage analysis and proof loading. The measurement of the acoustic emission count rate is one of the easiest and most applicable methods of analyzing acoustic emission data (Reese 1993). Acoustic emission count indicates the occurrence of acoustic emission and gives a rough estimate of the rate and amount of emission. The amplified signal is fed into an electronic counter. The counter output is often transformed by a digital-to-analog converter so that it can be plotted on a X-Y recorder (Reese 1993).

An event count will result in the number of burst emissions signals that are produced during an event. An acoustic emission event is defined as a detected acoustic emission burst. This means that an acoustic emission event describes the acoustic emission signal and not the acoustic emission. For the event count to be correct, the decay constants of the AE signals must be the same. A mixture of decay constants will often confuse the event-counting circuitry (Reese 1993).

For most experiments, the count or the energy per event will give about the same results (Reese, 1993). Acoustic emission bursts are larger when a loaded specimen is approaching failure. It is only when there is a change in either the damping factor or the frequency that the energy per event is the better parameter (Reese, 1993). The energy released per event will result in the amount of AE signals received.

### **Signal rise time**

The signal rise time can be defined as the interval between the time when the AE signal is first detectable above the noise level and the time when the peak amplitude occurs (Reese 1993). Rise depends on the distance between the acoustic emission source and the sensor. It can help to determine the type of damage mechanism.

### **Signal duration**

Signal duration is defined as the length of time that the burst emission signal is detectable. It is dependent upon the preamplifier noise level and detection of the signal. A trigger circuit is used to stop and start a separate counter that counts clock pulses. The signal duration is independent of the frequency content of the burst signal. The signal duration method is useful when repeating the same test. A change in either the average signal duration or the distribution of durations can indicate either a change in the signal path to the sensor or a change in the generating mechanism (Reese, 1993).

### **Sensor location**

Determination of the number of sensors required for the test, their placement strategy and location on the part to be monitored is needed. Placement of sensors on a concrete specimen during a fiber pull-out test is shown in Figure 2.51.

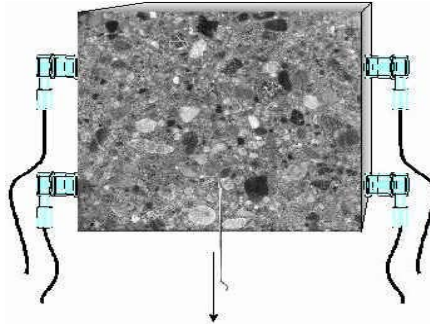


Figure 2.51: Placement of sensors on a concrete cube

A single sensor used near the expected source of AE is sufficient when background noise can be controlled or does not exist. When background noise is limited, the use of a single AE data sensor near the expected source plus guard sensors near any background source will suffice. ASTM defines a guard sensor as one whose primary function is the elimination of extraneous noise based on arrival sequences. The guard sensors will effectively block noises that emanate from a region closer to the guard sensors than to the AE data sensor. Another technique involves the placement of two or more sensors to perform spatial discrimination of background noise and allow AE events to occur. ASTM defines *spatial discrimination* as the process of using one or more guard and data sensors to eliminate extraneous noise. In situations where irrelevant noise cannot be controlled during testing and could be emanating from any and all directions, a multiple sensor location strategy should be considered. Using a linear or planar location strategy will allow for an accurate source location of the acoustic emission. Applications of spatial filtering and/or spatial discrimination will only allow data emanating from the region of interest to be processed as relevant AE data.

### **Applications of acoustic emission**

Acoustic emission has been used to determine the integrity of various materials, including metal and alloys, welds, forgings and castings. Acoustic emission has been

applied to concrete in an effort to nondestructively evaluate in situ concrete for load testing and structural monitoring.

### **Load testing**

The most successful application of acoustic emission is detecting the presence of discontinuities or cracks, and their location, in concrete specimens and structures. Perhaps the most researched application of acoustic emission testing has been used in the load testing of concrete structures and specimens. Since acoustic emission is a passive nondestructive testing technique, acoustic signals are only emitted if a permanent, nonreversible deformation occurs inside a material. Therefore, acoustic emission is extremely useful for detecting the formation of cracks and microcracks occurring in concrete structures.

Consideration of the load intensity in relation to the integrity of the test object results in the success of an acoustic emission examination. Applied load is defined by ASTM as the controlled or known force or stress that is applied to an object under test for the purpose of analyzing the object's reaction by means of acoustic emission monitoring of that stress. If the load is not of sufficient intensity, the tested object will not undergo sufficient stress and will not produce acoustic emissions. If the applied load is part of the monitoring process, a suitable time for acoustic emission examination is when process noise is low and the applied load at a maximum. Appropriate stress levels are used to excite the "latent defects" without damaging the object (ASTM E-1932-97).

A reinforced concrete slab under fatigue loading from the initial loading to final failure in the laboratory was compared to the acoustic emission monitoring of reinforced concrete slabs under traffic loading by comparing visual observations of cracking processes and acoustic emission source location (Yuyama et al. 1992). The experiment

concluded that, by comparing crack density history and acoustic emission activity history, cracking processes under fatigue loading can be predicted and evaluated by monitoring the acoustic emission signals. The research paper also revealed that the damaged area due to cracking can be roughly identified by the acoustic emission source location.

One valuable conclusion from laboratory testing is that the area of reinforced concrete near the initial emanation of acoustic emission signals will result in the cracking area during the final load. The fatigue process in reinforced concrete structures can be evaluated by periodically monitoring these structures under service loads (Yuyama et al. 1992).

A fundamental study was made of acoustic emissions generated in the joint of rigid frames of reinforced concrete under cyclic loading. The test concluded that different acoustic emission sources, such as tensile cracks or shear cracks, could be clearly discriminated by comparing the results of the visual observation and the crack width measurement (Yuyama et al. 1992).

Studies have been performed on fiber reinforced concrete specimens to observe the response of fiber reinforced concrete to loading. Based on the experiment, several conclusions can be drawn. The examination of acoustic emission activities and source location maps reveal that the microscopic fracture response recorded by acoustic emission monitoring is consistent with the macroscopic deformation of the material. Steel fibers are more efficient than PVA fibers in blunting microcrack nucleation (Li & Li 2000).

**Structural monitoring**

Most highway bridge inspection is performed via visual inspection. When deficiencies are observed, the action taken usually involves increased inspection of the defective area. Given that the rate of deterioration is usually unknown, the frequency of inspection is increased without a reasonable forecast of the behavior of the defect.

Acoustic emission testing utilizes the induced stress waves that are released when microstructural damage occurs. This passive NDT technique is commonly referred to as structural health monitoring.

At present, portable AE sensors are available for the continuous monitoring of known flaws. Research to date has provided a reasonable scientific base upon which to build an application of acoustic emission as part of a bridge management program (Sison et al. 1996). This technique could be best utilized by implementing a continuous monitoring system with an array of sensors on newly constructed bridges. The technology is available for instrumentation configured with portable data acquisition and transfer systems, making it possible for engineers to continuously monitor bridge condition. Engineers could use the information gained via AE systems to decrease the frequency of inspection on sound structures and monitor profound AE events to determine the need for essential inspections.

Other successful uses of AE have been applied to leak detection in tanks, pipelines, and conduits. It has also been used to monitor the integrity of dams and other mass concrete construction.

**Impulse Response**

The impulse response (IR) test has several applications relating to civil engineering and to the condition assessment of structures. Researchers originally developed it in the

1960's for evaluating the integrity of concrete drilled shafts. Engineers are less familiar with its widespread capabilities in relation to testing of reinforced concrete structural components such as floors, pavement slabs, bridge decks and other structures. The impulse response technique is similar to the impact-echo test method previously discussed in this chapter. Though the two methods are quite similar in theory, they differ in several respects, such as having different uses.

In essence, the IR method is a fast, coarse method of evaluating structures while the alternative methods are for more detailed investigations. The IR method is likened to a vague diagnosis made by a family doctor and subsequently referred to a medical specialist for further diagnosis.

### **Testing equipment**

The impulse response method uses a low-strain impact to propagate stress waves through an element. Most testing apparatuses are comprised of a one-kilogram sledgehammer with a load cell in the head. The hammer has a fifty-millimeter diameter double-sided head. One end is rubber-tipped for low stress level impacts, typically around 700 psi, while the other is aluminum-tipped for impacts that can reach stress levels of more than 7000 psi.

A structure's response to the impact is measured by a geophone. Both the geophone and the instrumented hammer are linked to a portable computer for data acquisition. Figure 2.52 is a photograph of a hammer and geophone. Figure 2.53 is a schematic of the typical equipment setup.

### **Principles of the impulse response method**

Most acoustic testing techniques are based on stress-wave propagation theory and monitor the behavior of such waves as they travel through a material. The impulse

response method differs from this approach; it instead measures the response of the tested material to the impact itself.



Figure 2.52: The instrumented sledgehammer and geophone used in the IR method (Davis 2003)

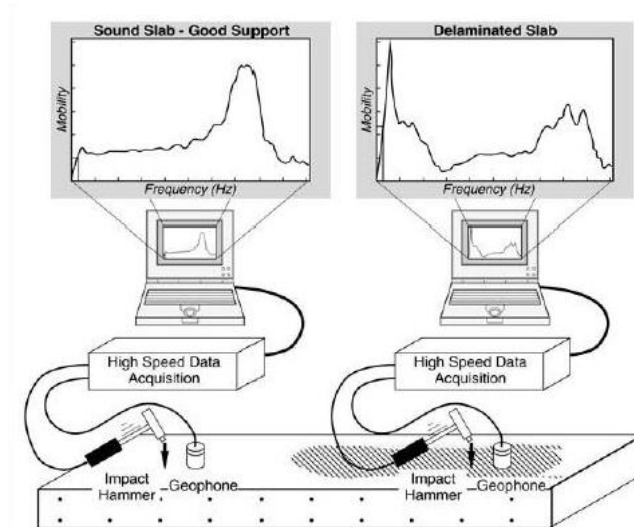


Figure 2.53: Schematic of the impulse response technique (Davis 2003)

Since the stress that is applied to a structure in the IR test is quite large, the structure responds to the impact in a bending mode over a relatively low frequency range (0 – 1000 Hz). This differs from structures being evaluated with the impact-echo method, which would respond to the generated stress waves in a reflective mode over a higher frequency range.

When testing a structure using the impulse response method, a geophone is placed upon the surface that is then struck with the instrumented sledgehammer. The geophone is usually attached to the surface of the concrete so that it can act in the same plane as the hammer blow. The time records for the hammer force and the velocity response from the transducer are received by the computer as voltage-time signals and then processed using the Fast Fourier Transform (FFT) algorithm. At that point, velocity and force spectra are generated, and the velocity spectrum is divided by the force spectrum, yielding a transfer function more commonly known as the mobility of the structure. A plot of mobility versus frequency can be generated. This plot represents velocity per unit force versus frequency and provides information regarding the condition of the structure being tested. Additional material properties that can be obtained include dynamic stiffness, mobility and damping, and the peak/mean mobility ratio.

### The transfer function

When an IR test is performed, the data gathered can be used to generate force and velocity spectra. The velocity spectrum is divided by the force spectrum to produce a transfer function more commonly referred to as the mobility of the structure. A theoretical impulse response spectrum is shown below in Figure 2.54.

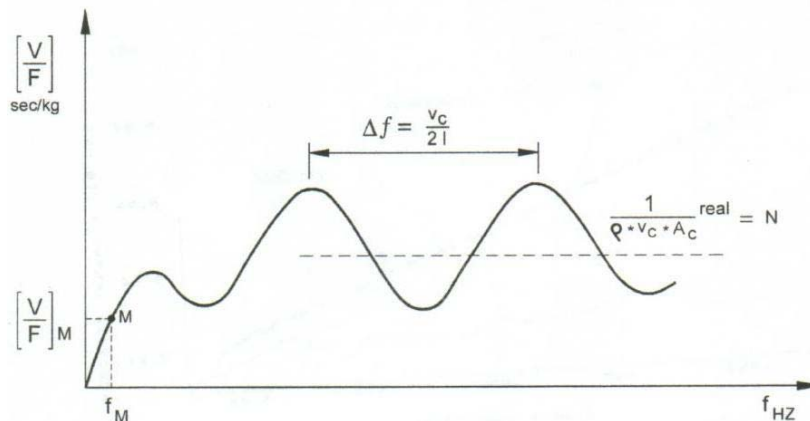


Figure 2.54: Theoretical impulse response mobility spectrum

The first portion of the transfer function is the dynamic stiffness portion (usually in the range of 0 – 100 Hz), which has a linear slope. This linear slope quantifies the flexibility of the area around the test point for a normalized force input. The dynamic stiffness of the material is the inverse of this flexibility.

The mobility of the structure being tested is the quotient of the velocity spectrum divided by the force spectrum, typically expressed in units of seconds per kilogram. The average mobility value over the frequency range of 100 - 1000 Hz is related to the thickness and the density of the specimen. Above a frequency level of approximately 100 Hz the measured mobility value oscillates around an average mobility value,  $N$ , which is a function of the specimen's thickness and its elastic properties. A reduction in thickness of the specimen correlates to an increase in average mobility. Figure 2.55 is a schematic of a typical mobility plot.

When a material is impacted, an elastic wave is generated. The decay of the spectral amplitude is due to the energy losses attributed to friction as the wave propagates through the solid matrix. When cracking, honeycombing or consolidation voids are present in the concrete, there will be an associated reduction in the damping and stability of the mobility plots over the frequency range that is evaluated.

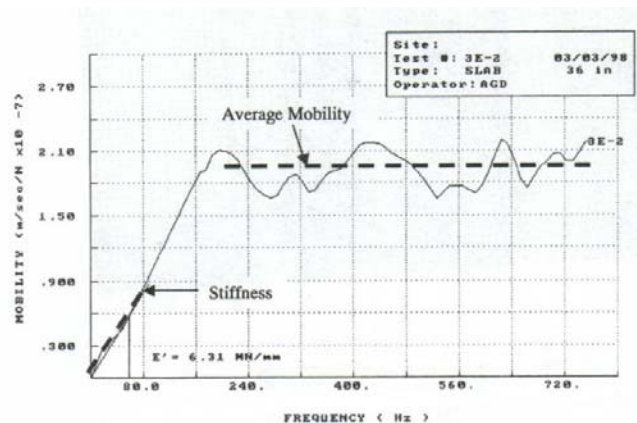


Figure 2.55: Typical mobility plot for sound concrete (Davis 2003)

### Peak/mean mobility ratio

When there is an area below a slab on grade that has been undermined, or there are debonding or delaminations present within a concrete sample, the response behavior of the uppermost layer controls the results of the IR test. There will be a noticeable increase in average mobility between the frequency range of 100 to 1000 Hz, and the dynamic stiffness will be considerably reduced. The ratio of this peak to the mean mobility is an indicator of loss of support below a slab on grade or the presence and degree of debonding within the sample. This concept is illustrated in Figure 2.56. Notice that the mobility of the concrete in the upper curve is considerably more than the mobility of the sound concrete shown in the lower curve.

The impulse response test is capable of detecting delaminations up to nine inches below the surface of a structure. Traditional methods, such as acoustic sounding, are able to detect concrete deficiencies up to approximately two to three inches below the surface. The impulse response method is able to test for delaminations through asphalt overlays when ambient temperatures are low enough to preserve relatively high asphalt stiffness. Figure 2.57 depicts typical mobility plots for sound and delaminated concrete.

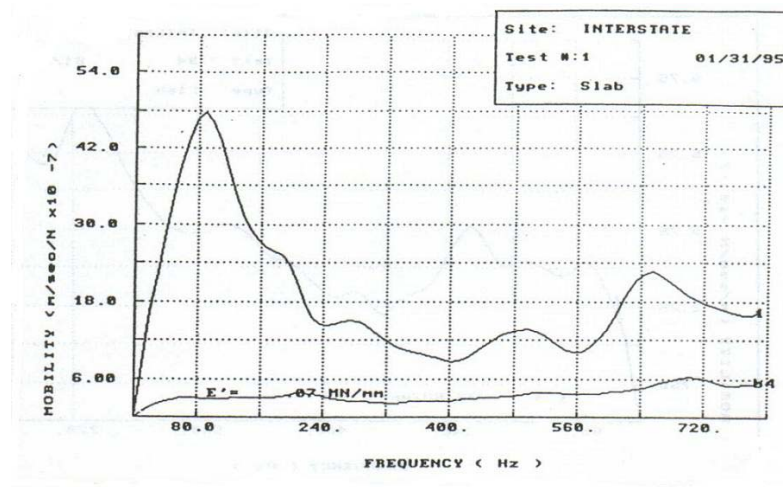


Figure 2.56: Mobility plots for sound and debonded concrete (Davis et al. 2001)

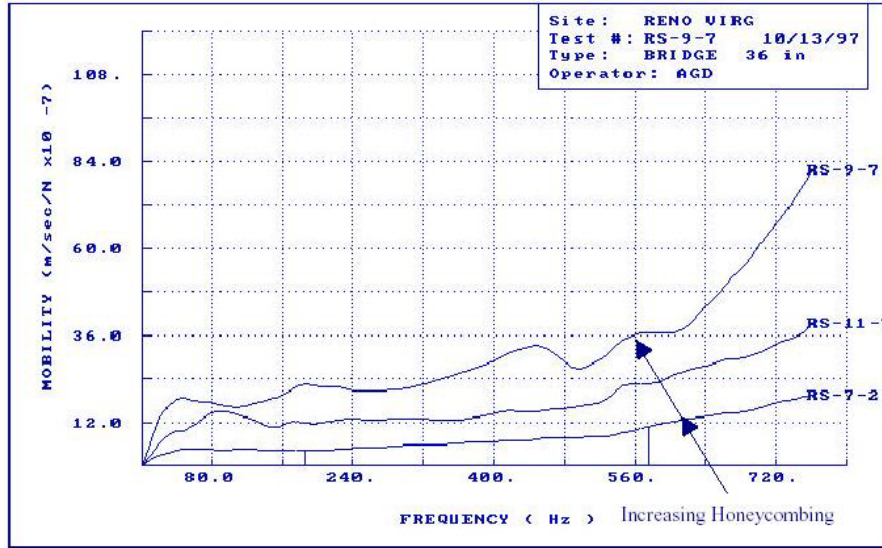


Figure 2.57: Mobility plots for sound and delaminated concrete (Davis et al. 2001)

### Further development for concrete applications

The inspection industry has focused on the practicality of this testing method, which has resulted in the development of more efficient testing procedures. Improvements have focused mainly on more rapid data acquisition and the storage of data from testing of large concrete surfaces, with computer extraction of the IR stiffness and mobility parameters for each test result. The time required for the impulse response method to perform the “family doctor” version of testing is approximately five percent of the time it would take for the impact-echo method to assess the same area.

In the early 1990's, the Federal Highways Administration (FHWA) published a report regarding the evaluation of bored concrete piles; the IR method was a less reliable test method than the cross-hole sonic logging method. Although the IR method has not been used in North America for evaluation of pile integrity, it is still applicable for material testing in other capacities.

## **Magnetic Methods**

Materials containing iron, nickel, cobalt, gadolinium and dysprosium have a high degree of magnetic alignment to each other and to themselves when they are magnetized. Therefore, they are called ferromagnetic materials. Other materials such as oxygen are faintly attracted or repelled by a magnetic field. These materials are referred to as paramagnetic materials. Diamagnetic materials have the magnetic equivalent of induced electric dipole moments, which are present in all substances. However, this is such a weak effect that its presence is masked in substances made of atoms that have a permanent fixed magnetic dipole moment.

The idea of using magnetic techniques for nondestructive testing and evaluation of ferromagnetic materials originated in 1905. In 1922, E.W Hoke was granted the first United States patent on a particular ferromagnetic inspection method. In recent history, this inspection technique has been used in the petroleum, aerospace and automotive industries, as well as in other industries that require quality control of ferromagnetic materials.

## **Magnetic fields**

A magnetic field is a volume of space containing energy that magnetizes a ferromagnetic material. The magnetic field is created by the introduction of electric current and perturbation outward in a radial pattern. Figure 2.58 is a schematic of a typical magnetic field induced by an electrical current. The density of the magnetic lines, referred to as the flux density, increases when the field strength and the magnetic permeability increase.

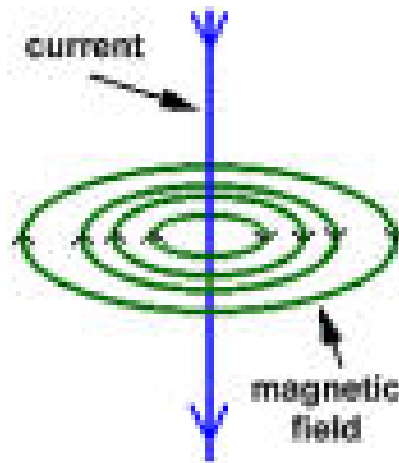


Figure 2.58: Schematic of a typical magnetic field induced by an electric current

### **Types of magnetizing energy**

Two sources of magnetizing energy used in magnetic testing are permanent magnets and electric currents. Permanent magnets usually consist of bar or horseshoe configurations. They are inexpensive methods of magnetization but are limited by a lack of control of field strength and the difficulty of removing strong permanent magnets from the tested specimens. The horseshoe type of magnet forms a uniform longitudinal field between the poles. It provides low levels of magnetization. Electric currents characterize the second category of magnetizing energy. Longitudinal or circular fields can be formed by the correct implementation of electric currents. Direct current (DC), alternating current (AC), and rectified alternating current are used to magnetize test materials. DC and rectified AC penetrate deeper into a material than AC, primarily due to a phenomenon called the “skin effect”. The skin effect is more defined in ferromagnetic materials than in nonmagnetic types of materials. Thus, DC or rectified AC is used when test requirements include the detection of deep flaws.

**Magnetization classifications**

The most common magnetization techniques are classified as direct or indirect. Direct magnetization involves the passage of an electric current through a material. Indirect magnetization is caused by an adjacent magnetic field, which is excited by current flow through a portion of the material.

**Magnetic flux leakage**

Magnetic flux leakage (MFL), formerly referred to as magnetic field perturbation testing (MFP), consists of subjecting a magnetically permeable material to a magnetic field. The field strength requirements depend on the permeability of the material and the sensitivity of the test probes.

The principles of magneto-statics demonstrate that when a homogeneous magnetically permeable material is immersed in a static, uniform, external magnetic field, the magnetic field within the material approaches the same magnitude as the magnetic field in which it is immersed. These perturbed fields are called leakage fields due to the “leakage” of magnetic flux out of the material and into the air. Leakage is caused by the reduction in cross-sectional area of the magnetic material due to the anomaly.

**Inspections using magnetic flux leakage techniques**

The preferred characteristic of the MFL technique is that mechanical contact with the test specimen is not necessary. In many cases, both the exciting coil and the sensing coil may be operated without directly contacting the material. This advantage has particular importance in the structural concrete industry. Another benefit of MFL is that it requires no specific surface preparation other than cleaning. This method is easily automated for high-speed, detailed testing. It is also useful for identifying surface cracks, near-surface inclusions, and nonmagnetic coating thickness on a permeable base, as well

as in monitoring physical and mechanical properties that cause changes in magnetic permeability. Sensitivity is limited by ambient noise and magnetic fields. The test specimen must be magnetically saturated, thereby limiting demagnetization concerns. The extreme sensitivity of the method has been utilized to detect surface cracks and subsurface inclusions on the order of 0.3 mm.

The magnetic flux leakage method has been applied to the determination of nonmagnetic coating thickness, the depth of case hardening, and the carbon content of a material. Another major application has been in testing steel bearing raceways and gear teeth. In its most refined form, MFL is one of the most sensitive methods for the detection of surface and near-surface cracks and flaws in ferromagnetic materials.

### **Electric current injection**

The Electric Current Injection (ECI) technique, also called the eddy current method, is an extension of the magnetic field perturbation method. It is used in materials that are electrically conductive but not magnetically permeable. ECI is classified as a non-particulate magnetic field method. The parameter sensed is the magnetic field perturbation near the surface of the test object. This testing method is carried out by inducing an electric current between two points of an electric current. Defects and flaws are obtained by recording the magnetic field signals in a manner similar to the MFP method.

### **Applications to concrete**

Currently, magnetic testing methods have no relevant use in the nondestructive testing of concrete itself. Concrete is nonmagnetic in nature, so the use of magnetic flux leakage for the detection of flaws and anomalies in concrete devoid of reinforcing steel is insignificant. However, the use of magnetic methods for the inspection of ferromagnetic

materials embedded within concrete structures has proven to be extremely valuable. Magnetic methods have been applied to detect defects in prestressing tendons and steel rebar within concrete structures. They have proven effective in the detection and location of embedded steel.

### Covermeter

The concrete covermeter, also referred to as the pacometer, was developed in 1951 in England. Since its original development, the covermeter has gone through several generations of revisions. Presently available, systems are reasonably priced for use in inspection. A photograph of a typical covermeter shown in Figure 2.59.



Figure 2.59: Covermeter used by the Civil Engineering Department at the University of Florida

The principle operation of the covermeter is based on ferromagnetic principles. The covermeter detects a bar by briefly magnetizing it, then registering the magnetic field as it tapers off. The typical configuration of the covermeter testing technique is depicted in Figure 2.60. The covermeter utilizes the eddy current method of magnetic testing. This method induces "eddy-currents" to flow around the circumference of the bar, producing a

magnetic field. The head of the device picks up the magnetic signal. Pulse techniques separate the received signal from the transmitted one. Therefore, no signal is produced in the absence of a metallic material. The strength of the induced magnetic field primarily depends on the depth of the ferromagnetic element beneath the probe and the size of the element being detected. The concrete industry primarily uses covermeters to detect the presence, size, and depth of rebars.



Figure 2.60. Typical configuration of covermeter testing apparatus

### **Applications of magnetic flux leakage**

Magnetic flux leakage has been effectively applied to the detection of deficiencies in steel members within concrete structures. The use of an array system has successfully identified ruptures of steel in prestressed tendons and rebar cracks in bridge decks (Krause et al. 2002).

Due to the extreme sensitivity of magnetic flux leakage sensors, the system is well suited for condition monitoring of the steel components in bridge decks. Slight changes in the metallic structure of embedded steel and tendons can be detected in order to monitor the onset of damage in the metallic components of bridge structures.

### **Ground Penetrating Radar**

The ground penetrating radar (GPR) method uses reflected waves to construct an image of the subsurface, in much the same way as seismic-reflection profiling. The source consists of a transmitter loop, which emits a short pulse of high-frequency (10 -

1000 MHz) electromagnetic energy into the ground. The reflection response is measured using a receiver loop, which is generally kept at a fixed distance from the transmitter. GPR is used in a variety of applications including soil stratigraphy, groundwater flow studies, mapping bedrock fractures, determining depth to the water table, and measuring the thickness of glaciers (Malhorta & Carino 1991).

### **Theory**

Both the GPR and ultrasonic pulse velocity techniques involve pulsing waves into a solid material. GPR differs from ultrasonics since it uses radar waves rather than stress waves. Radar waves and stress waves behave in a similar manner when introduced into a solid. GPR is governed by the reflection of the wavefronts in the host material in the same manner as the stress waves produced during impact-echo and ultrasonic testing. The basic theory behind GPR is analogous to the theory discussed in the impact echo section of this paper and will not be restated here.

In principle, the propagation of radar waves, or signals, is affected by the dielectric properties of the media, so that the attenuation and reflected components vary accordingly (Colla & Brunside 1998). Concrete is a low loss dielectric material, with the exception of any metal which may be present within the concrete. When an electromagnetic signal passes through a dielectric medium, the amplitude will be attenuated (Casas et al. 1996). The main parameter which controls the subsurface response is the dielectric constant,  $K^*$ , which is a dimensionless and complex number. The velocity at which radar signals propagate is given by:

$$v = \frac{c}{K^{1/2}} \quad (15) \text{ (Casas et al. 1996)}$$

where the speed of light  $c = 3 \times 10^8$  m/s, and  $K$  is the real part of  $K^*$ . Reflections occur when a radar pulse strikes a boundary where there is an abrupt change in the dielectric constant. The reflection coefficient, which represents the ratio of reflected-wave amplitude to the incident wave, is given by:

$$R = \frac{K_2^{1/2} - K_1^{1/2}}{K_1^{1/2} + K_2^{1/2}} \quad (16) \text{ (Casas et al. 1996)}$$

Equations 15 and 16 are the principle equations upon which the theory of GPR is based. The wave velocity and reflection coefficient of dissimilar materials within the same medium can be distinguished subsequent to signal processing.

### **Instrumentation**

The use of ground penetrating radar is fairly popular within the geological and geophysical fields throughout the world. Although GPR is becoming increasingly popular for the nondestructive testing of concrete structures, it is a highly specialized system. The primary components in a radar system are a waveform generator, an antenna, a signal processing unit and a display unit.

### **Generator**

Waveform generators are used to transmit a signal to the antenna. The signal can be a continuous or a pulsed excitation signal, which is then transmitted into the test material. Generators are capable of emitting varying or continuous frequencies of signals depending on the type of testing being performed.

### **Antenna**

Antennas for GPR radiate and receive electromagnetic waves. The GPR antenna performs basically the same functions as the “head” of the covermeter device. However, instead of using magnetic fields, it sends and receives an electromagnetic beam. The

beam is usually driven at 1 GHz for use in concrete and is much more focused than the excitation fields utilized in the covermeter device. The dipole antenna is most commonly used today. It is a contact based antenna that provides a diverging beam. Alternatively, the horn antenna employs a more focused beam and has found use in vehicle-mounted surveying of highway and bridge decks, where the antenna is usually located 30cm above the surface of inspection (Kaiser & Karbhari 2002).

### **Display**

Most of the GPR systems in service today employ a visual display that instantaneously produces an image of the scan. An oscilloscope produces the image after the antenna receives it. Internal discontinuities are produced by the reflected signal and are visualized through the use of grayscale or color. Figure 2.61 shows a typical GPR scan.

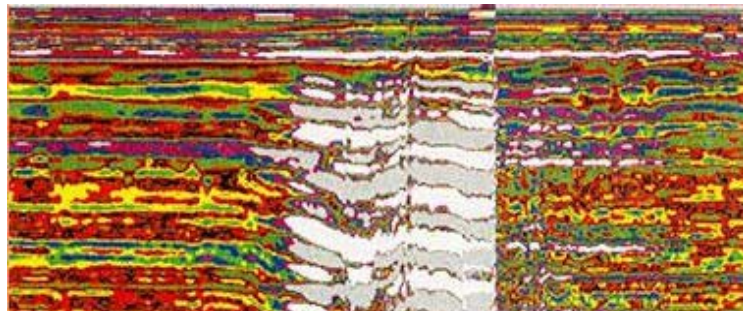


Figure 2.61: Typical display of a GPR Scan. The white portion denotes an anomaly

### **Applications**

GPR has been studied and applied to the nondestructive testing of materials for the past several decades. Several successful applications of GPR in the concrete industry include (Casas et al. 1996):

- the identification of reinforcing bars in concrete
- the identification of large cracks and voids in concrete

- concrete quality and appraisal
- duct location in post-tensioned bridges
- void identification in post-tensioned ducts

A logical classification for GPR would be to include it as a qualitative NDT technique that can effectively be used to aid in structural condition assessment and evaluation. Its performance in the rapid detection of anomalies embedded in concrete structures is an extremely valuable tool for inspectors, especially when identifying problems with post-tensioned ducts. The proper grouting of post-tensioned bridge structures has been a prevalent problem throughout the state of Florida for the past several decades. GPR offers an immediate inspection method that would enable owners of bridges to inspect the quality of post-tensioned structures before closing future contracts.

### **Resonant Frequency**

Powers originally developed the resonant frequency method in 1938. He discovered that the resonant frequency of a material can be matched with a harmonic tone produced by materials when tapped with a hammer (Malhorta & Carino 1991). Since then, the method has evolved and incorporated the use of electrical equipment for measurement.

### **Theory**

An important property of any elastic material is its natural frequency of vibration. A material's natural frequency of vibration can be related to its density and dynamic modulus of elasticity. Durability studies of concrete materials have been performed indirectly using resonant frequency as an indicator of strength and static modulus of elasticity. These relationships for resonant frequency were originally derived for homogenous and elastic materials. However, the method also applies to concrete

specimens if the specimens are large in relation to their constituent materials. (Malhorta & Carino 1991).

The study of physics has determined resonant frequencies for many shapes, including slender rods, cylinders, cubes, prisms and various other regular three-dimensional objects. Young's dynamic modulus of elasticity of a specimen can be calculated from the fundamental frequency of vibration of a specimen according to Equation 17 (Malhorta & Carino 1991).

$$E = \frac{4\pi^2 L^4 N^2 d}{m^4 k^2} \quad (17)$$

Where

E = Young's dynamic modulus of elasticity

d = density of the material

L = length of the specimen

N = fundamental flexural frequency

k = the radius of gyration about the bending axis

m = a constant (4.73)

### **Testing**

ASTM has created a standard test that covers measurement of the fundamental transverse, longitudinal and torsional resonant frequencies of concrete specimens for the purpose of calculating dynamic Young's Modulus of elasticity. (C-215-97, 2001) This test method calculates the resonant frequencies using two types of procedures, the forced resonance method or the impact resonance method.

The forced resonance method is more commonly used than the impact resonance method due to the ease of testing and interpretation of results. The forced vibration

method uses a vibration generator to induce vibration in the test specimen while the vibration pickup transducer is coupled to the specimen. The driving frequency is varied until the pickup signal reaches a peak voltage. The specimen's maximum response to the induced vibration occurs at the resonant frequency. Figure 2.62 illustrates the typical setup of a resonant frequency device. The vibration generator is coupled to the right side of the specimen while the pickup is coupled to the left.

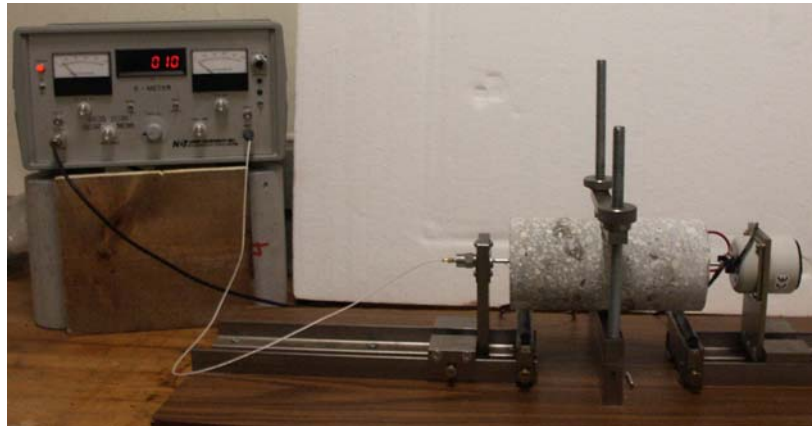


Figure 2.62: Typical forced resonant frequency setup

The impact resonance method is similar to the impact-echo and impulse response methods. The impact resonance method employs a small impactor to induce a stress wave into the specimen. However, the forced resonant frequency method uses a lightweight accelerometer to measure the output signal. The signal is then processed to isolate the fundamental frequency of vibration.

The standard test method is limited to the testing of laboratory specimens (i.e. cylinders or prisms), and at present there is no standardized method applying the use of resonant frequency to larger specimens or to specimens of irregular shape.

### **Limitations**

The resonant frequency method has been successfully applied to the nondestructive testing of laboratory specimens. The test is somewhat limited by a number of inherent

problems in the method. Resonant frequency testing is usually performed on test specimens to non-destructively calculate cylinder compressive strength. However, the test actually calculates the dynamic modulus of elasticity. Extensive laboratory testing has revealed that cylinder compressive strength and dynamic modulus of elasticity are not an exact correlation. Thus, when concrete strength is extrapolated from resonant frequency testing, two sources of error exist. The first source of error is experimental error, which can be fairly significant when performing the resonant frequency test. “Limited data are available on the reproducibility of the dynamic modulus of elasticity based on resonance tests” (Malhorta & Carino 1991, p155). The second source of error is the assumption that has to be made when converting dynamic modulus to compressive strength. Since the correlation between the two properties is not absolute, sources of error will be present in any modulus to strength conversion. Figure 2.63 graphically displays the experimental results obtained relating cylinder compressive strength with dynamic modulus of elasticity. The experimental data can be predicted within  $\pm 10\%$  assuming the results from a given resonant frequency test have zero error. In reality, converting dynamic elasticity to compressive strength would yield an uncertainty greater than  $\pm 10\%$ .

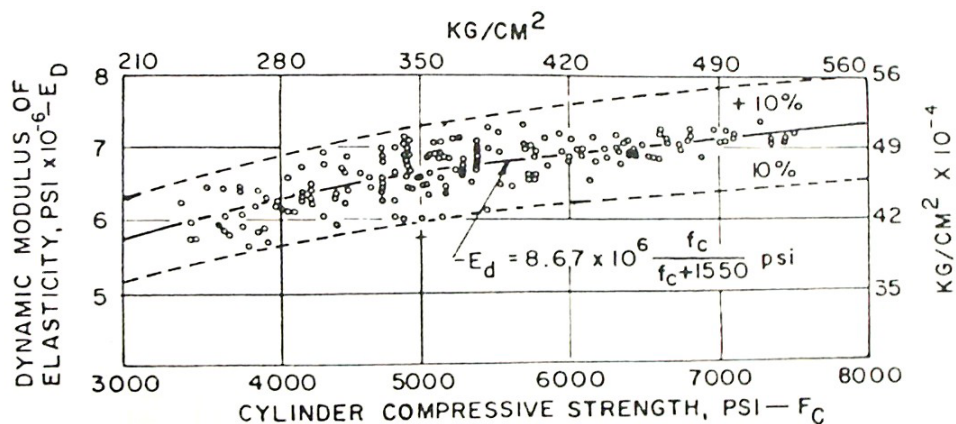


Figure 2.63: Dynamic modulus of elasticity vs. cylinder compressive strength (Malhorta & Carino 1991)

## **Applications**

Resonant frequency can be a useful tool for detecting material changes regardless of whether an actual dynamic modulus or compressive strength can be calculated.

Resonant frequency can be used to measure qualitative changes in a material property if used as a monitoring technique. The existence of structural damage in an engineering system leads to a modification of the modal parameters, one of which is resonant frequency.

It is possible to monitor a given complex structural element with shape parameters that prohibit an accurate calculation of geometric parameters such as radius of gyration or density. Complex structures are often too large or have immeasurable properties, such as the exact location of internal steel members, to extract relatively simple material properties that are easily calculated in the laboratory setting. However, when used as a quantitative technique resonant frequency can detect material changes between tests. A review of methods of damage detection using natural frequencies has shown that the approach is potentially practical for the routine integrity assessment of concrete structures (Salawu 1997). Using the natural frequency changes of a structure may not be useful for identifying the location and assessment of specific cracks and anomalies within a structure. The technique can detect changes in a structure or structural element, if an acceptable baseline is established at the time of construction.

## **Infrared Thermography**

Infrared thermography (IRT) is a non-destructive evaluation (NDE) technique that characterizes the properties of a material by monitoring its response to thermal loading. The term “*thermal loading*” is commonly used to describe the transfer of energy from a heat source to a solid object. This technique is currently being used on an array of

structures and materials ranging from carbon fiber reinforced polymers (CFRP) to human teeth. Due to this widespread applicability, the field of IRT has grown considerably in recent years. Recently, IR has been used for the nondestructive examination of concrete structures and structural repairs.

## Theory

The term “infrared” refers to a specific portion of the electromagnetic spectrum containing waves with frequencies just less than those of red visible light, *infrared* means less than red. Figure 2.64 illustrates the electromagnetic spectrum, depicting where infrared waves are classified.

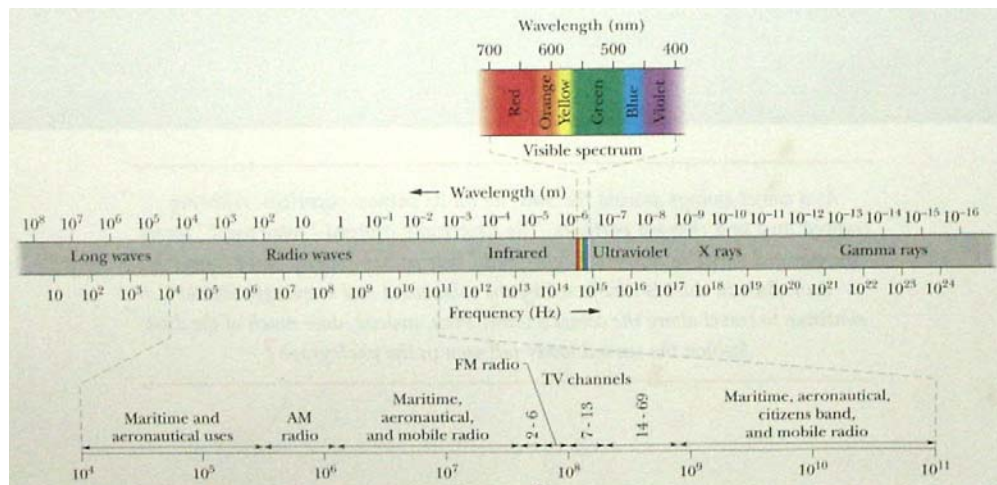


Figure 2.64: The electromagnetic spectrum (Halliday et al. 1997)

Sir Isaac Newton (1642-1727) was the first person to perform an experiment revealing the presence of IR waves. The relationship between visible light and heat had long been recognized, since sunlight had an obvious effect on the temperature of an object. The important observation in Newton’s experiment was that objects could still be heated if they were placed outside of the visible spectrum observed when a beam of light passes through a prism. Newton knew something was responsible for generating the heat, but it could not be observed with the naked eye (Maldague 2001).

The first person to formally quantify a thermal image was Max Planck. Planck's theory of radiation can be summarized as follows:

- All objects emit quantities of electromagnetic radiation
- Higher temperature objects emit greater quantities of radiation.
- The electromagnetic radiation emitted from a body consists of a "broadband" signal in that it contains radiation with a spectrum of wavelengths.

Since IR waves are essentially the same as visible light waves, it is important to understand how they interact with the surface being measured. For IR thermography images to contain the desired temperature data, it is important to distinguish between the radiation emitted from an object (which is related to its temperature) and radiation that is reflected off of the object from other sources. Emissivity ( $\epsilon$ ) is the quantity used to describe a particular surface's ability to absorb and emit radiation. For the case of a "blackbody", the emissivity is assumed to be 1. This means that all of the incident radiation falling on the surface is absorbed and results in an increase in temperature of the object. This increase in temperature then results in increased radiation by the object. For the case of a mirrored surface (a perfect reflector), the emissivity is assumed to be zero. This implies that none of the radiation being emitted by the surface was actually generated by the object.

Emissivities for common engineering materials are provided in Table 2.4. Note that materials with a low emissivity are not particularly well suited for inspection by IR thermography. However, it is possible to increase the emissivity of shiny objects by treating the surface with flat paint.

Another interesting phenomenon is the emissivity of glass. The relatively high value of 0.94 indicates that glass is essentially opaque to IR waves. As a result, an IR camera pointed at a glass window will provide temperature information for the glass

surface as opposed to the temperature of any visible objects on the other side. This phenomenon is of significant importance when considering which materials are suitable for use in IR camera lenses and associated optics.

Table 2.4: Emissivities of common engineering materials

Material	Emissivity
Steel	
Buffed	.16
Oxidized	.80
Concrete	.92
Graphite	.98
Wood	.95
Window Glass	.94

### IR thermography and material assessment

The fundamental concept behind using IR thermography as a non-destructive evaluation technique is that sound and unsound materials have different thermal conductivity properties. If a constant heat flux is applied to the surface of a uniform homogeneous material, the increase in temperature on the surface of the object should be uniform. If, however, the material is non-homogeneous, the temperature along the surface will vary (see Figure 2.65).

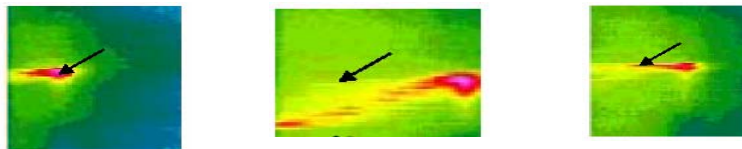


Figure 2.65: Typical thermograph revealing defects

### Passive thermography

The passive approach to IR thermography is simple and involves collecting temperature data from a scene without applying an external heat source. This method provides qualitative information about a situation and can be used to quickly determine if a problem exists. In the construction industry, passive IR thermography has been used

for many years to evaluate thermal insulation in buildings and moisture infiltration in roofs. Passive thermography is also used to detect delaminations in reinforced concrete bridge decks (ASTM D4788-88). The following sections contain detailed descriptions of each test standard and special considerations for each case are noted.

#### **ASTM D4788-88: delaminations in RC bridge decks**

In this test, a vehicle mounted IR imaging scanner is driven slowly over the bridge deck under consideration. If the evaluation is performed during daylight hours, the delaminated areas will appear as “hot spots”. During the evening time as the bridge is cooling down, the delaminated areas will appear “cooler” relative to the sound bridge deck. The IR scanner can also be incorporated with an electronic distance-measuring device so the resulting thermographs can be overlaid onto scaled CAD drawings. If any areas of concern appear in the thermographs, a more detailed inspection of the suspect area can be performed (usually by coring or ultrasonic evaluation).

For delaminations to be detected, there must be a minimum temperature difference of 0.5 °C between the delaminated area and sound areas. The test standard indicates that roughly three hours of direct sunshine is sufficient to develop this temperature differential.

It is also specified that the bridge deck should be dry for at least 24 hours prior to testing. Windy conditions should also be avoided and care must be taken when interpreting results in areas where shade may have influenced the surface temperature distribution.

Passive thermography is a non-destructive testing technique that provides qualitative information about a situation. Once potential problem areas have been

identified, further testing (usually destructive in nature) can be conducted in the suspect areas. The primary advantage of this technique is that large areas can be surveyed relatively quickly and without disruption to the users of a structure.

### **Active thermography**

In active thermography, heat is applied (by the inspector) to the surface of the object under investigation while an IR camera monitors the temperature variations on the surface. The advantage of active thermography over passive is that a quantitative analysis of the data collected can reveal important defect characteristics (size and depth). This type of IR thermography is not usually employed in civil engineering structures for overall NDE since the required energy inputs would be large. However, thermal input from the sun or a building's heating/cooling system and subsequent IR measurements is a form of active thermography.

Since IR thermography is only capable of monitoring the surface temperature of an object, the technique is usually limited to situations where defects are located near the surface. As defect depth increases and defect size decreases, assessment becomes more difficult. Active IR involves more elaborate test setups than are encountered in passive thermography. The required minimum resolvable temperature difference (MRTD) of IR camera equipment is smaller and heating of the specimen surface must be carefully controlled. As a result, most applications of active IR thermography are performed in a laboratory or well controlled manufacturing environment.

### **Equipment**

Scanning radiometers are devices capable of generating 320 x 240 pixel digital images containing the exact temperature data for each pixel. The precise temperature data is obtained by comparing the IR image signal to the signal generated by an internal

reference object. Depending on the data acquisition system employed, thermal images containing 76,800 unique temperature values can be obtained at a rate of 50 to 60 frames per second (see Figure 2.66).

### Applications

Current applications of IRT include the evaluation of concrete and composite structures for delaminations, coating thickness, and the integrity of coating-substrate bonds. With the increased use of advanced composites in civil engineering structures, IRT becomes a potential means of evaluating the quality of installation and long-term durability of the composite strengthening system.

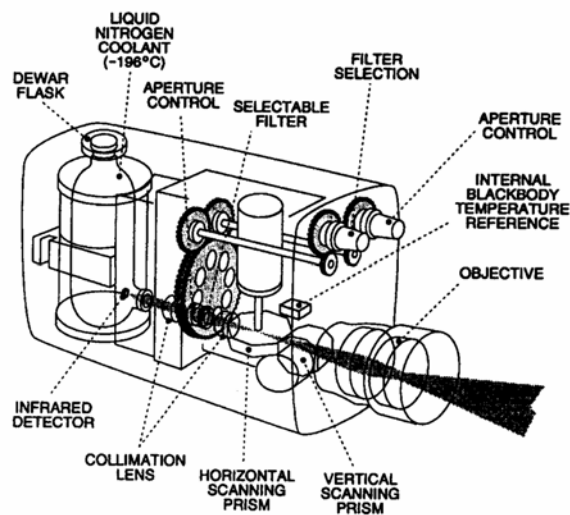


Figure 2.66: Schematic of a scanning radiometer IR camera (Maldague, 2001)

In an experiment performed at the University of Florida (Hamilton & Levar 2003), reinforced concrete beams were bonded with CFRP composites and tested to failure. During the test procedure, the beams were periodically IR inspected for initial bond quality and bond failure under load testing. The use of acoustic sounding to detect unbonded or disbonded CFRP laminates can leave as much as 25% of voids undetected. The use of IR thermography for the inspection of concrete structures strengthened with

CFRP laminates is the most efficient method of qualitative inspection for structures with this type of repair.

IRT was proven to be effective as a qualitative NDT technique for the inspection and repair of the concrete roof shell at the Seattle Kingdome prior to its demolition. “In 1992, ceiling tiles attached to the roof underside fell approximately 300ft onto the seating area prior to the venue opening for a baseball game. The safety problem initiated a major rehabilitation program for the concrete shell roof of the almost 25 year old structure” (Weil & Rowe 1998, p389). IRT was used as the primary NDT method to locate subsurface anomalies in the roof structure. Delaminated or voided areas of concrete will prevent solar energy from passing through the roof structure causing a “hot spot” to form when the roof is thermally loaded. Unbonded areas in concrete repaired with CFRP are detected in the same manner. Figure 2.67. provides an illustration of the effect that delaminations and voids in concrete have on the conduction of heat the through the roof structure.

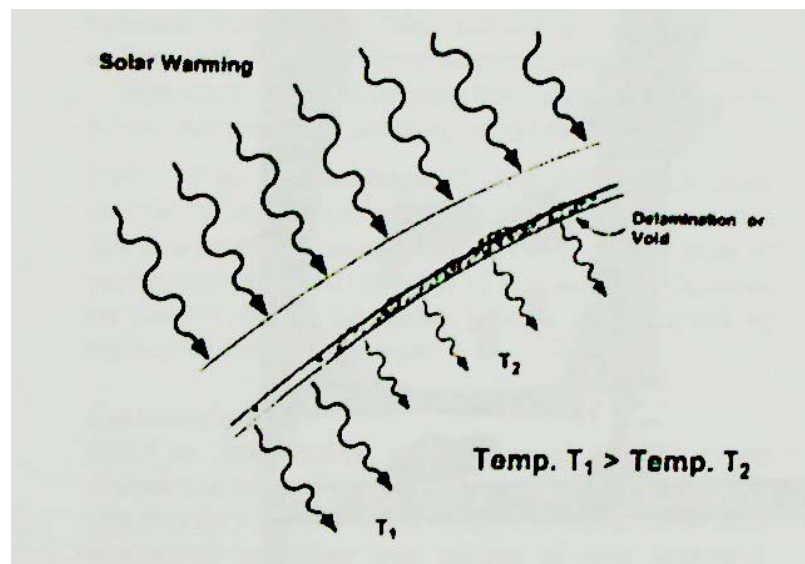


Figure 2.67 Schematic description of thermographic void detection process (Weil & Rowe 1998)

The inspectors were able to thermographically survey the entire roof structure, which was 360,000 ft<sup>2</sup> in area, in three days of testing using a single camera. Inspectors performed a more detailed inspection at each anomaly with sounding techniques and impact-echo for quantitative material analysis. Repairs to the roof shell were made according to test results and inspector recommendations.

### **Radioactive Testing**

Radioactive testing dates back to the discovery of X-rays by Ivan Pului and Wilhelm Roentgen in the late 1880's and 90's. While Pului published material relating to X-ray experiments in the "Notes" of the [Austrian] Imperial Academy of Sciences in 1883 several years before Roentgen's first publication on X-ray technology, Roentgen is credited as the discoverer of X-ray technology and won the 1901 Nobel Prize based on his achievements (Kulynak 2000).

The contributions by Marie and Pierre Curie are the most profound advances regarding radioactivity, a term they coined. The Curies discovered gamma rays in the late 1800's while working with several different elements including bismuth, barium and uranium. They discovered polonium and radium, and the experiments the Curies conducted with radium and its radioactive effects were presented in Marie's doctoral thesis in 1903. As a result, Marie won the Nobel Prize in 1903 (Hellier 2001).

### **Radiography**

A radiograph is a picture produced on a sensitive surface by a form of radiation other than visible light, typically an X-ray or a gamma ray. Radiography is the NDT technique that employs the use of radiographs for material inspection. X-rays are a form of electromagnetic radiation with a relatively short wavelength, about 1/10,000 the wavelength of visible light. Gamma rays are 1/1,000,000 that of visible light. It is this

extremely short wavelength that enables X-rays or gamma rays to penetrate through most materials (Reese 2003). Structural radiography is very similar to the X-ray technique people experience during a doctor's visit. The method involves a wave source, usually X-rays or radioisotopes, and a detector, which is most commonly photographic film. Figure 2.68 depicts a typical radiography setup.

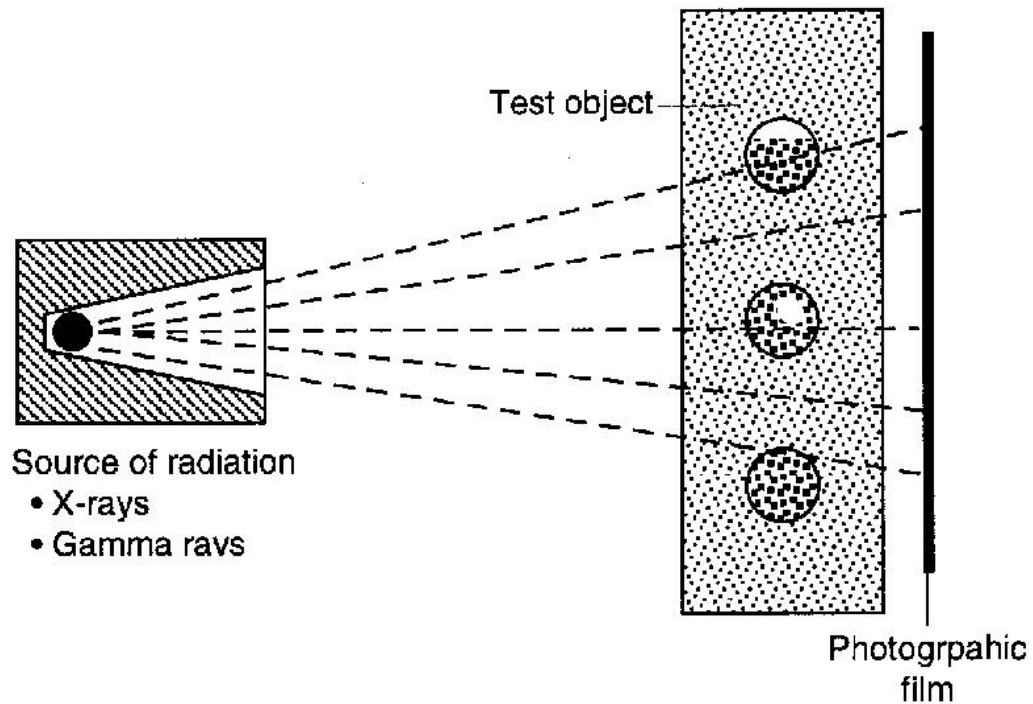


Figure 2.68: Radiography schematic (Lew et al. 1998)

A limitation of radiography as an NDT technique is that both sides of the material to be tested must be accessible for inspection. Therefore, structural elements like slabs and foundation walls are not typically accessible for testing with radiography. ASTM has developed a testing standard covering the practices to be employed in the radiographic examination of materials and components. The standard outlines a guide for the

production of neutron radiographs that possess consistent quality characteristics, as well as a guide for the applicability of radiography (ASTM E 748-02).

### **Radiometry**

Often the terms radiometry and radiography are used interchangeably despite the fact that the tests are different. While radiography produces a visible image, radiometry is more quantitative in nature and is used to ascertain material properties. While both NDT techniques implement the use of radiation energy to analyze material properties, some radiometry techniques require only one side of a material to perform testing. The backscatter mode and certain aspects of the direct transmission mode (for both radiometry techniques) can send and receive radiation signals from a single side of the material.

The direct transmission mode of radiometry uses the same principles as the radiography test, though the radioisotope source can be oriented in several configurations to enable personnel to perform surface testing of a material. The direct transmission mode of radiometry uses the same theory as radiography, the main difference being that the equipment is configured differently. The direct transmission mode of radiometry usually has one or two probes that penetrate into the test material. A radioisotope source emits pulses, which are received by the detector. The rate of arrival of the pulses is related to the density of the material. This technique is commonly used in geotechnical engineering for the rapid calculation of soil composition, water content and density. Figure 2.69a illustrates a direct radiometry configuration with an internal signal detector and external source. Figure 2.69b is a schematic of a direct radiometry device with both an external signal detector and source (Malhorta & Carino 1991).

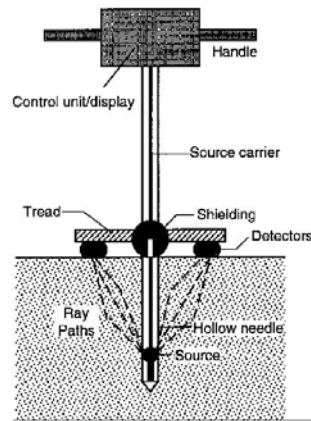


Figure 2.69a

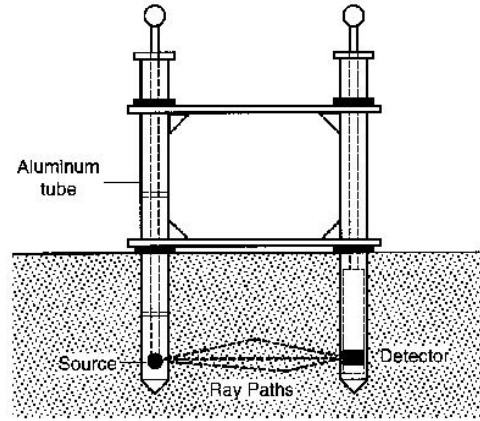


Figure 2.69b

Figure 2.69: Schematics of direct radiometry: (a) with an internal signal detector and external source, (b) with an external signal detector and source (Lew et al. 1998)

In the backscatter measurement of radiometry, the source and the detector are adjacent to each other, but are separated by a lead radiation shield. The backscatter method is basically the same test as direct transmission and measures the same material properties. The only difference between the two tests is equipment configuration. Figure 2.70 illustrates a backscatter radiometry configuration.

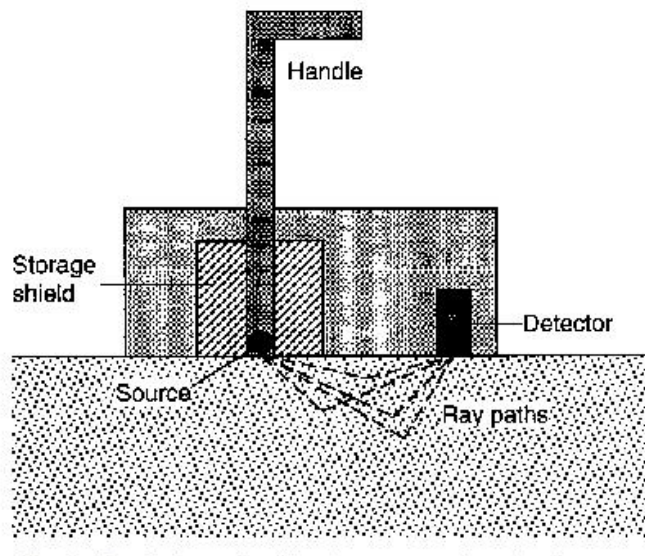


Figure 2.70: Schematic of backscatter radiometry (Lew et al. 1998)

## Applications

Radioactive methods have various applications in the nondestructive testing and monitoring of structures. Radiography may be the most powerful qualitative means of NDT since it offers inspectors a view of the internal structural elements unrivaled by any other nondestructive inspection technique. One example of the enhanced capabilities of radiography compared to any other NDT method is illustrated in Figures 2.71a and 2.71b.

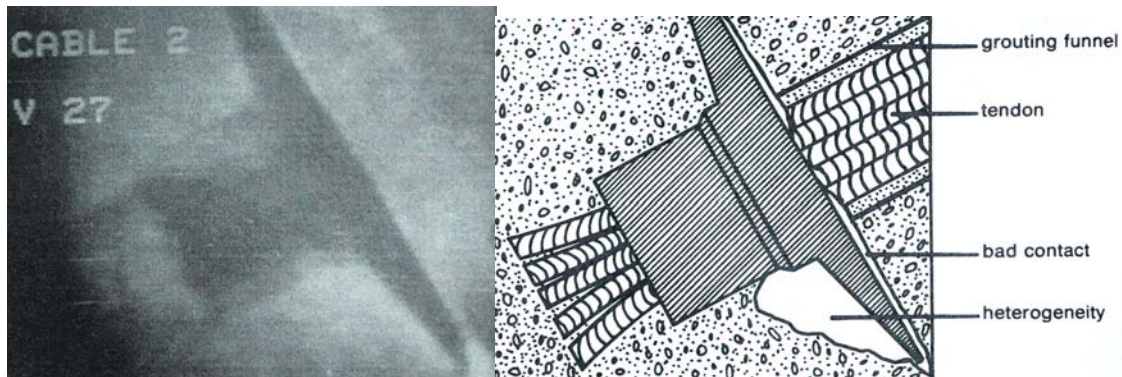


Figure 2.71a

Figure 2.71b

Figure 2.71: Image of prestressing cable anchorage in concrete (a) X-radioscopic image of a prestressing cable anchorage embedded in a concrete, (b) schematic and brief explanation of the radiographic image (Malhorta & Carino 1991)

Radiography can be applied to virtually any structural element in which two opposite sides are accessible. The method permits inspectors to assess every component on a visual basis, comparable to a medical doctor's ability to examine internal organs non-intrusively.

Radiometry has been successfully used to quantitatively determine properties of concrete such as density, porosity, water content and thickness. The techniques used for determining material properties and integrity using radiation waves is comparable to the techniques used in determining material properties via stress waves. However, stress waves are of a lower energy and less versatile for material inspection than radiation waves.

**Limitations**

Although radiation testing is among the most powerful methods used in nondestructive testing today, it has several limitations that prevent it from becoming the most widely used NDT technique. Radiation testing techniques are the most expensive of NDT methods available for the testing of concrete materials. The technique is so much more expensive than the other techniques in service today, that many inspectors don't consider it to be practical from a cost-benefit standpoint.

Radiation testing presents many safety concerns that are not easily addressed in the field. It is usually feasible to protect operating personnel while conducting testing. However, it is not always practical to use radiographic testing due to public safety concerns. An example of this problem was demonstrated by the FDOT in February of 2002. Before the removal of an abandoned bridge adjacent to the Ft. Lauderdale airport, the FDOT contracted several consultants to demonstrate the capabilities of different NDT systems on the bridge deck. Among the techniques demonstrated on the bridge were impact-echo testing, GPR, magnetic flux leakage and radiography. The radiographic method was the only method that required the bridge structure and the roadway beneath it to be completely free of personnel for testing, and that both roadways were completely closed to traffic. In most urban areas it is not feasible for such roadway closures since bridge structures are usually built in high traffic volume areas. The same types of problems arise when performing radiographic testing of buildings and building components.

### CHAPTER 3 SURVEY OF RELEVANT BRIDGE STRUCTURES IN FLORIDA

The National Bridge Inventory (NBI) covers 600,000 bridges on the nation's interstate highways, U.S. highways, state and county roads, and other routes of national significance. The NBI is maintained by the Federal Highway Administration using data provided by the state and local transportation departments (Bhide 2001). The FDOT's "Pontis" Bridge Management System (BMS) is the client run server application used to inventory the bridge structures for the state.

The majority of bridges in the state of Florida are constructed of concrete. These bridges are classified in the 25-50 year age range. Deterioration rate studies suggest that structures in this category deteriorate slowly during the first few decades of their design life (typically 50 years), followed by a rapid decline. (NBI 2003) If these predictions are correct, Florida, as well as the U.S. will incur extensive rehabilitation and reconstruction costs over the next two decades. The Department of Civil Engineering at University of Florida conducted a survey of bridge structures within the Pontis system in an attempt to categorize prevalent bridge deficiencies occurring throughout the state.

Currently, the FDOT's Pontis system has inventoried a total of 12,573 bridge structures sign structures. Of the 12,573 are bridge structures, 9,585 were constructed with concrete. The survey conducted by the University of Florida, inventoried and categorized relevant concrete bridge structures. In addition, personnel from the FDOT's State Maintenance Office, Materials Office and District Offices were interviewed to ascertain any prevalent problems within concrete bridges throughout the state.

### Definition of Sufficiency Rating

A bridge sufficiency rating is a numerical value assigned to a bridge structure subsequent to inspection, based on its condition. The major factors used to determine sufficiency rating are structural adequacy, serviceability and essentiality for public use. Therefore, the structural condition of a bridge and its sufficiency rating are not completely dependent upon each other. Figure 3.1: is a summary the factors used for calculating sufficiency rating.

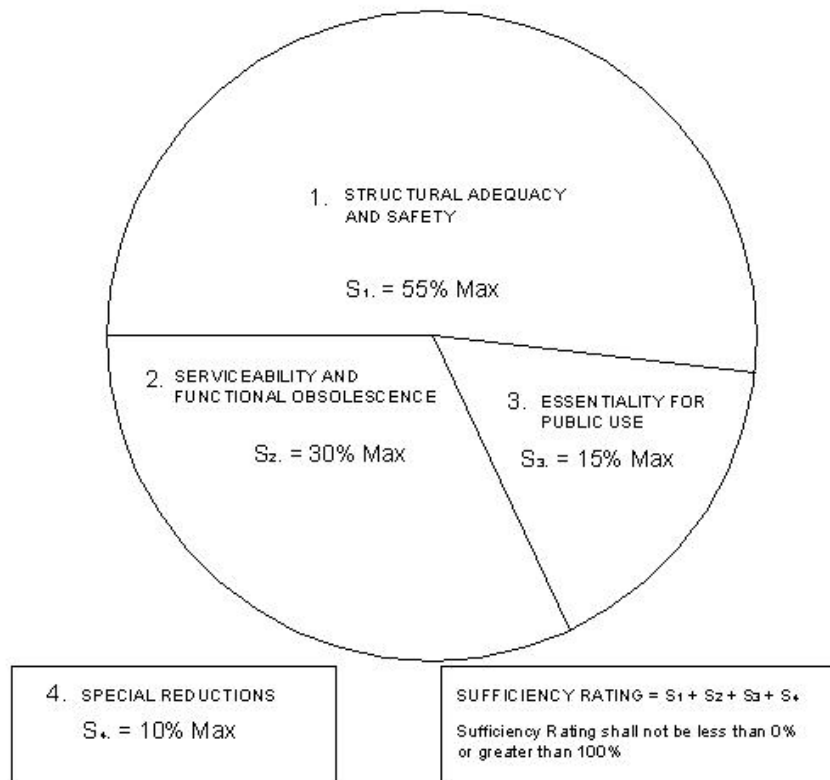


Figure 3.1: Summary of sufficiency rating factors (FHWA 1995)

Figure 3.1 illustrates the percentages of each factor used in the calculation of bridge sufficiency rating. Structural adequacy and safety comprise 55 percent of the total bridge rating. Since there are several components that affect a bridges sufficiency rating, it is not completely accurate to use the sufficiency rating as part of the methodology for a

materials or structural survey. Interviews with FDOT personnel confirmed that presently the sufficiency rating is the best way to query bridge structures based for structural deficiencies.

### **Methodology**

Originally, the purpose of the bridge survey was to identify prevalent bridge deficiencies that were typical among concrete structures throughout the state. However, the Pontis system is limited in its querying abilities and does not allow for specific problems, deficiencies, or inspector recommendations. Presently, the Pontis system can execute queries based on bridge ID number, structure name, name of the feature intersected, county, age, length and sufficiency rating. Another limitation of Pontis is that it lacks the ability to form more than one query at a time. Therefore, without printing, reading, and manually categorizing each of the 12,573 bridge reports, it was not possible to determine prevalent material or structural problems.

Pontis lacks the ability to make queries of specific bridge structure deficiencies. Therefore, the bridge queries were based solely on sufficiency rating. However, the structural condition of a bridge and its sufficiency rating are not completely dependent upon each other.

The Pontis system was used to query the bridges by sufficiency rating. A typical query is illustrated in Figure 3.2. Since the Pontis system cannot query by more than one item, all of the relevant bridges queried had to be categorized by hand. As an attempt to create a baseline of structure performance, the bridges were categorized by condition, age and feature intersected. All bridges that were 40 years of age and older with a sufficiency rating of 85 or above set the baseline for durable structures. All bridges 20 years or

younger with a sufficiency rating of 75 or below were considered to be less durable and should be monitored for material and structural problems.

Bridge ID	Feature Intersected	Dist	Cnty	Length (ft)	Built	Deck	Super	Sub	Culv	Suff Rate
034065	COCOHATCHEE CANAL	D1 - Bartow	(03)Collier	37	2002	N	N	N	8	100
080038	CR 578 COUNTY LINE RD	D8 - Turnpike	(08)Hernando	181	1999	9	9	8	N	100
100410	RAMP I75 NB TO SR582 WB	D7 - Tampa	(10)Hillsborough	148	1985	7	8	8	N	100
094043	PLATTS BRANCH	D1 - Bartow	(09)Highlands	57	1988	N	N	N	7	99.9
040012	HOG BAY CREEK	D1 - Bartow	(04)De Soto	43	1955	N	N	N	7	99.9
064094	OAK CREEK	D1 - Bartow	(06)Hardee	82	1990	7	7	7	N	99.9
064117	HORSE CREEK	D1 - Bartow	(06)Hardee	162	1998	7	7	7	N	99.9
094030	CATFISH CREEK	D1 - Bartow	(09)Highlands	37	1960	N	N	N	7	99.8
024047	APOPKA CANAL	D7 - Tampa	(02)Citrus	58	1987	7	7	7	N	99.8
050050	FISHEATING CRK OVERFLOW	D1 - Bartow	(05)Glades	252	1974	7	7	8	N	99.8
044038	HAMPTON BROOK	Central Office	(04)De Soto	25	1900	N	N	N	6	99.8
064097	OAK CREEK	D1 - Bartow	(06)Hardee	70	1990	7	7	7	N	99.8
010014	ALLIGATOR CREEK	D1 - Bartow	(01)Charlotte	49	1967	N	N	N	6	99.8
010097	BROAD CREEK	D1 - Bartow	(01)Charlotte	24	1981	N	N	N	7	99.8
024048	APOPKA CANAL	D7 - Tampa	(02)Citrus	72	1987	7	7	7	N	99.8
070062	GRANDMAS GROVE CREEK	D1 - Bartow	(07)Hendry	75	1999	8	8	8	N	99.7
094045	S.C.F.E. RAILROAD	D1 - Bartow	(09)Highlands	64	1999	8	8	8	N	99.7

Figure 3.2: The result of a typical bridge query by sufficiency rating

The FDOT uses visual inspection the primary method of gathering data that is imputed into the Pontis system. As discussed in Chapter 2 visual inspection is often subjective and is dependent upon ‘human factor’ that is often encountered during structural inspection. The susceptibility to human misinterpretation and the requirement for establishing a baseline for defects in general, especially under poor conditions, can lead to inconsistent identification of anomalies, resulting contradicting evaluations (Quaswari 2000).

Another limitation of using the Pontis system is that a bridge sufficiency rating is calculated by quantifying the results from visual inspections. Contradicting evaluations can alter a bridge sufficiency rating drastically. Interviews with FDOT personnel corroborated with the indication that discrepancies in evaluation ratings, as a result of

inconsistencies in visual inspection results affect the value bridge sufficiency rating when inputted into the Pontis system.

According to the FHWA's recording and coding guide for bridges, the deck, superstructure, and substructure are given a general condition code based on a scale of a 0-9, 0-code represents a bridge closed and a 9-code is superior to present desirable criteria. Rigorous attempts to classify data using the general condition codes were unsuccessful because the bridge sufficiency rating is dependent of the general condition code. Figure 3.3 shows examples of bridges that are approximately the same age, and the same structural code classifications but have different sufficiency ratings.

Feature Intersected	Cnty	Length (ft)	Built	Deck	Super	Sub	Culv	Suff Rate
LITTLE TROUT R/ER	(72)Duval	132	1939	7	7	7	N	99.5
SANTA FE RIVER	(26)Alachua	256	1994	7	7	7	N	99.5
MID-PRONG ST MARYS RIVER	(27)Baker	260	1992	7	7	7	N	99.5
SANTA FE RIVER	(26)Alachua	256	1994	7	7	7	N	99.5
PETERS CREEK	(71)Clay	193	1993	7	7	7	N	99.5
SANTA FE RIVER	(26)Alachua	256	1994	7	7	7	N	99.5
ST. JOHNS BLUF RD.	(72)Duval	220	1972	7	7	7	N	99.3
BLACK CREEK	(71)Clay	1,465	1973	7	7	7	N	99.3
LITTLE BLACK CREEK	(71)Clay	350	1985	7	7	7	N	99.2
BLACK CREEK	(71)Clay	1,465	1973	7	7	7	N	99.4
Canal	(73)Flagler	51	1949	7	7	7	N	61
Canal	(75)Orange	56	2003	7	7	7	N	60.8
JUMPER CREEK CANAL	(18)Sumter	100	1957	7	7	7	N	60.8
CANAL C-4	(75)Orange	80	1969	7	7	7	N	60.4
South Fork of New River	(86)Broward	410	1960	7	7	7	N	60.1
Sassagoula River	(75)Orange	90	1990	7	7	7	N	58.3
PANAMA CANAL	(86)Broward	40	1964	7	7	7	N	58
RIO ARAGON CANAL	(86)Broward	98	1968	7	7	7	N	58

Figure 3.3: Examples of Pontis codes vs. sufficiency ratings.

The inability of the Pontis system to sort and classify bridges with regard to structural or material integrity is the most limiting feature of the system. Due to the lack of such a feature, a statically significant data analysis based on structural sufficiency cannot be performed.

## Results

### Pontis Data Analysis

Currently the Pontis system has 12,573 bridge structures inventoried. However, the report published by the FHWA in 2002 has a total of 11,526 bridge structures inventoried. There are several reasons for the discrepancy between the current count and the 2002 published count

The first reason is that as new bridges are constructed on an annual basis, the number of bridges in the Pontis system will rise accordingly. Another reason for the inconsistency among the figures is that the NBI publishes the number of bridges that are completely constructed. While the Pontis system has an inventory of all bridges that are completely constructed, as well as bridges currently under construction. A third reason for the difference in numbers is due to errors in the inputs of the bridge data. The FDOT has downsized a large percentage of its staff. Private consultants are now performing the majority of the bridge inspection and data entering into to the Pontis system. Recently, there are instances in which bridges are mistakenly entered or duplicated within Pontis. For the purposes of this survey, we will use the numbers published from the 2002, NBI for overall quantities. However, the categorized figures were obtained through an analysis of data performed by the University of Florida.

Of the 11,526 bridge structures in the state, 9,585 were constructed with concrete. The concrete bridges were analyzed and 686 of them fit into the two durability categories previously stated. Of the 686 bridges, 202 bridges fit into the deficient new structure (DNS) category (i.e. 20 years or younger with a sufficiency rating of 75.0 or less). However, 41 of the DNS 202 bridges are made of concrete. The majority of the deficient bridges are steel or wood structures, accounting for 161 of the 202 bridges. Of the 41

DNS bridges made of concrete, 21 are functionally obsolete. Accordingly, 19 of the 21 DNS bridges, were functionally obsolete and had sufficiency ratings above 60.0. These 19 functionally obsolete bridges were considered to have a low deficiency rating based on the “S3” sufficiency rating input parameter from the equation in Figure 3.2. For the uses of this survey, they are considered to be structurally sufficient. Therefore, 22 of the 9,585 concrete bridges throughout the state can be classified as newly constructed and structurally deficient.

Over 90% of the concrete bridge structures within the state employ slab design and multi beam/girder design. Consequently, the 17 of the 22 newly constructed deficient bridges are slab and beam/girder design. Upon review of the individual bridge reports, it was found that the most prevalent deficiency in these structures is deterioration of the bridge deck. According to the FHWA’s recording and coding guide for bridges, the bridge deck average general code is 6.73 out of 10, for the 22 newly constructed deficient bridges (Where 7 is considered to be good condition and 6 is satisfactory condition.) Again, we see some inconsistency when trying to deduce a structural condition based on sufficiency rating.

### **Conclusions**

Subsequent to using the Pontis system for over a year, it is apparent that there is a need for more quality control regarding interpretation of structural deficiencies and disposition of the data within system. Private consultants rather than FDOT personnel performed most of the bridge inspections. As a result, consistency in the interpretations of bridge conditions is being compromised. It appears as though a more exact definition of conditions is needed to regain the necessary quality control of inspection reports.

The system appears to lack a protocol to maintain the consistency among units of physical properties (i.e. some reports use the English system of measurement, where others use SI units). Since the system lacks user consistency between such simple parameters, it is difficult to rely on the quality control of sufficiency ratings to draw any statistical conclusions based on the data within the system. Consequently, a statistical analysis was not performed on the bridge data within the Pontis system. Deductive arguments made from the data available would be insufficient to infer reliable conclusions.

Limitations of Pontis system include:

- The inability to process data sorts of more than one data field within the system for a single data query
- The inability to perform data sorts based on material type

The expansion of the Pontis system to include multiple data sorts would allow for more complicated data analyses to be undertaken. The addition of a sorting material based query would enable users to perform statistically significant data analysis on bridge structures based on material type.

As a result of our survey, it has been determined that 22 newly constructed concrete bridge structures were classified as deficient. Since 17 of the 22 deficient bridge structures are typical designs, they provide a good baseline for testing. Upon plan review, these bridges should be considered for condition monitoring. The use of several qualitative and quantitative NDT methods should be employed to further assess the material integrity of each bridge.

## CHAPTER 4 BRIDGE INSPECTIONS

### **Document Review**

As part of the bridge survey, the University of Florida conducted interviews with Mr. Charles Ishee and Mr. Ivan Lasa of the FDOT State Materials Office for the purpose of identifying prevalent bridge structure deficiencies that could be considered typical among concrete bridge structures throughout the state. The personnel interviews, in conjunction with the results from the bridge survey discussed in Chapter 2, were used to establish a sample of bridges to be surveyed and nondestructively tested.

The purpose of performing the bridge research conducted in Chapter 3 was to identify relevant structures through the Pontis BMS. The data gathered was originally to be used to identify bridges that contained typical deficiencies that warranted nondestructive testing and field inspection. Unfortunately, the Pontis system does not have the capacity to act as a stand alone system for these purposes. Therefore, it was essential to incorporate FDOT personnel interviews to establish a sample of bridges that were suitable for NDT testing and field inspection.

As a result of the survey and FDOT personnel interviews, the following bridges were visited:

- Bahia Honda Bridge
- Niles Channel Bridge
- Sebastian River Bridge
- Sebastian Inlet Bridge (Robert W. Graves Bridge)
- Wabasso Bridge

Each bridge was examined to locate typical deficiencies and to assess the overall quality of concrete used for construction.

### **NDT Methods Used for Inspection**

The literature review performed in Chapter 1 served as an evaluation of NDT technology currently available today. The NDT techniques most suitable for use in concrete materials inspection are: visual inspection, acoustic sounding, rebound hammer, impact-echo and ultrasonic pulse velocity. The penetration resistance methods and the breakoff test were considered suitable for material inspection but due to their partially destructive nature they were not permitted by the FDOT for use. Inspections were thus limited to non-intrusive testing techniques.

### **Bahia Honda Bridge**

#### **Site Information**

The Bahia Honda Bridge was constructed in 1972 and spans the big Spanish Channel waterway between Bahia Honda Key and Big Pine Key in Monroe County, Florida. The new bridge was built to replace the Old Bahia Honda Bridge, which was originally built in 1912 as part of the Flagler's Overseas Railroad. After the 1935 Labor Day Hurricane destroyed the railroad, a paved roadway was built on top of the steel trestles of the old bridge. The new bridge was built to replace the old bridge with a newer and wider double span crossing to increase traffic capacity.

#### **Procedures**

The evaluation began with a site visit by Mr. Christopher Ferraro and Dr. Andrew Boyd of the University of Florida, accompanied by Mr. Olen Hunter and Mr. Andrew Eiland of the FDOT, on May 20, 2003. During the visit the personnel observed the Bahia Honda bridge substructure and superstructure accessible from a boat provided by the

FDOT. The general condition of the bridge was observed and documented with photographs. No plans were available for review.

During the course of the fieldwork, the personnel performed materials testing on pile cap 55 and the accessible portion of its corresponding column. As part of the materials survey, the pile cap and the column were sounded, impact-echo tested, ultrasonically, and rebound hammer tested. (see Figures 4.1 and 4.2 for locations).

## **Results**

### **Site observations**

The bridge superstructure is composed of prestressed concrete girders resting on top of a concrete cap beams. The substructure is composed of concrete cylindrical columns with struts resting on top of pile caps. The submerged piles were not visible during the inspection. Refer to Figures 4.3 and 4.4 for photographs of the bridge structural elements.

The entire bridge structure was visually surveyed to get an overall appraisal of the structural integrity. The bridge girders showed little or no deterioration, though some locations of discoloration, efflorescence, and superficial cracking were noted. The concrete columns exhibited a range of deterioration levels. Few columns exhibited little or no deterioration. The majority of the columns displayed moderate to severe deterioration. Severe deficiencies such as large cracks, spalls, delaminations and section loss have been repaired. In spite of the extensive repair-work performed on the columns, some of the repairs have experienced deterioration and new deficiencies have developed since the columns were last maintained. The struts have gunite cover. The gunite is cracked and delaminated with random spalls throughout. The pile caps have experienced

the same types of deterioration as the columns. However, the majority of pile caps are in satisfactory condition whereas the majority of the columns are experiencing deficiencies.

Upon completion of the visual survey, it was decided that pile cap and column 55 exhibited typical deficiencies and had not yet been repaired, and thus were suitable for materials inspection. The crack observed on the column on pile cap 55 appears to be a typical deficiency observed throughout the bridge. However, most of the other columns observed had already undergone repairs in the same location, at the connection of the column, strut and pilecap.

### **NDT Analysis**

The column and pile cap were sounded, rebound hammer tested, impact-echo tested and ultrasonically tested in order to determine material quality. The tests were performed in accordance with relevant ASTM standards (ASTM C 805-97, ASTM C 597-97, ASTM C 1983-98a).

The column was tested using the sounding method, the ultrasonic pulse velocity meter and the impact-echo device. An ultrasonic pulse velocity meter was used to obtain a tomography of the column using through wavespeed of the material. The average through wavespeed was calculated to be 4530 m/s. Impact-echo was used to gather surface acoustic velocities. The average of the impact echo wavespeed was determined to be 3893 m/s. The column has two cracks on opposite sides of each other. Figures 4.5 and 4.6 consist of photographs of the cracks. Acoustic sounding adjacent to the crack revealed that the crack propagates inward. Ultrasonic tomography confirmed the orientation and crack depth. Figure 4.7 is a schematic of the calculated crack depth and orientation as a result of the acoustic and ultrasonic tomography testing. The impact echo device was also used to confirm obtained surface acoustic velocities using ASTM

C-1383a procedure B, which is described in the impact echo material thickness section of chapter 2. The through acoustic velocities were confirmed within acceptable tolerances.

The pile cap was tested using a rebound hammer, ultrasonic pulse velocity meter, and impact echo device. The average rebound number was determined to be 43.3, producing a corresponding strength value of approximately 5700 psi (Malhotra & Carino 1991). The average through wavespeed obtained using the pulse velocity meter was calculated to be 3676 m/s. The average impact-echo surface wavespeed was determined to be 3543 m/s. The impact echo device was also used to confirm surface wavespeeds obtained using ASTM C-1383a, as it was for the column, and again the average acoustic velocities were confirmed within acceptable tolerances.

### **Conclusions**

Previously published research has suggested that the quality of a concrete specimen is related to its wavespeed, with changes being proportional to changes in concrete strength. (Benedetti 1998, Neville 1996, Mindess et al. 2003, Lemming et al. 1996, Popovics et al. 1999, 2000, Popovics 2001, Gutra 2000, Lane 1998, Krautkramer 1990, Malhotra 1984, 1994, Malhotra & Carino 1991). Table 2.3 classifies concrete with wavespeeds in the range of 3500-4500 m/s as good quality. Though the quality of the concrete is most likely good in terms of compressive strength, the permeability of the concrete cannot be determined through the use of any NDT method to date. The deficiencies exhibited throughout the bridge structure appear to be a result of the rebar corrosion. Concrete exposed to seawater can be subjected to chemical attack including the chloride-induced corrosion of steel reinforcement (Neville 1996). Therefore, it is possible to have a structure undergo structural deterioration even with concrete of adequate strength.

The disparity between the through wavespeed and the surface wavespeed suggests that the column has sustained surface damage due to exposure. The through wavespeeds obtained with the impact echo were approximately 16% lower than those obtained by the ultrasonic pulse velocity method. There are several factors that contribute to this difference:

- An ultrasonic pulse is more likely to travel through the material with the fastest acoustic velocity. Large amounts of steel rebar within the column can distort the true acoustic velocity.
- The flow of traffic on the bridge can distort the through column signal.
- Circular columns can have different modes of frequency. Therefore, the response of circular columns can be complex.
- The frequency resolution is 32% of the total frequency, therefore producing a relatively large uncertainty in through wavespeed.

Although there was discrepancy between the ultrasonic wavespeed and the impact echo wavespeed, the differences were within acceptable tolerances. The disparities are most likely due to a combination of the reasons listed above. It is likely that the through acoustic velocities obtained with the ultrasonic pulse velocity meter are slightly high due to interactions with the rebar. As discussed in Chapter 2, the wave speed of a solid is dependent upon the material type. Therefore, it is possible for a combined effect to occur when measuring the time of travel of ultrasonic signals through composite materials. The pulse velocity method is dependent upon the time of travel of a pulse through the material from one transducer to the other. It is probable that any embedded steel will serve as a transport mechanism for the pulse within the concrete column. Since steel has a higher acoustic velocity, the resulting acoustic velocity for the column will be slightly higher than a concrete specimen without embedded steel.

Although the impact-echo through wavespeeds were calculated with relatively poor resolution, the impact echo testing method is used to confirm acoustic velocities through the use of frequency analysis and specimen geometry. Therefore any materials with higher acoustic velocity embedded within concrete typically do not affect the through wavespeed of an impact echo signal with a combined material effect. The impact echo method requires the analysis of a frequency spectrum to verify the acoustic velocity of a material. The impact echo section of chapter 2 discusses the analysis of frequency spectrums of impact echo testing.

With the data available, it is possible to conclude that the concrete material of the column is in good condition with some signs of distress. The crack in the column is most likely a torsional crack, which is due to loading or shifting of the structure. In marine environments, it is common for bridge columns to shift over time. However, the purpose of this survey was to examine the concrete material of the structure and not the structure itself.

The pile cap was found to be in relatively good condition. The surface wavespeed of the pile cap was slightly lower than the through wavespeed of the cap. The slight discrepancy between surface and through wavespeed is most likely a result of exposure. However, due to the small difference in wavespeeds, it can be concluded that exposure conditions have not distressed the concrete to a great extent. This is most likely due to the loading conditions on the pile cap, as they are not as likely to facilitate damage within.

The strength estimates produced by rebound hammer tests are, at most, reliable to within 25 percent (Malhotra & Carino 1991). The rebound hammer results verify the

concrete is in generally good condition. In conclusion, the concrete material of the pile cap is in good overall material condition.

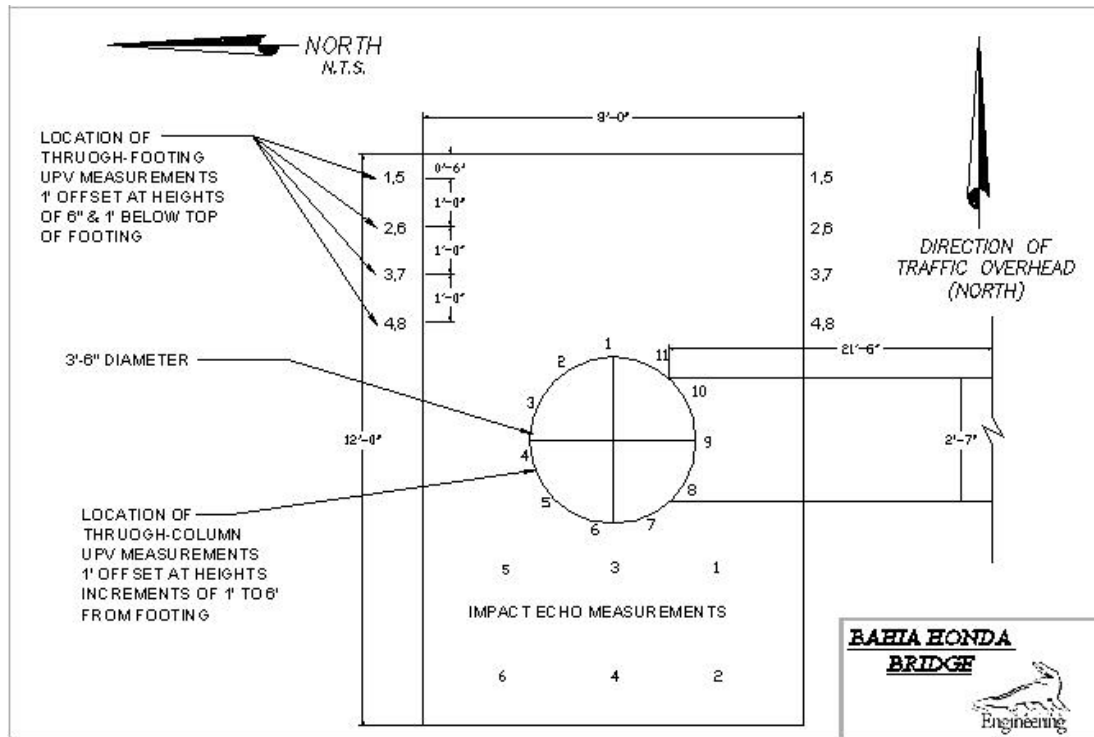


Figure 4.1: Plan view of Bahia Honda bridge pilecap and column 54

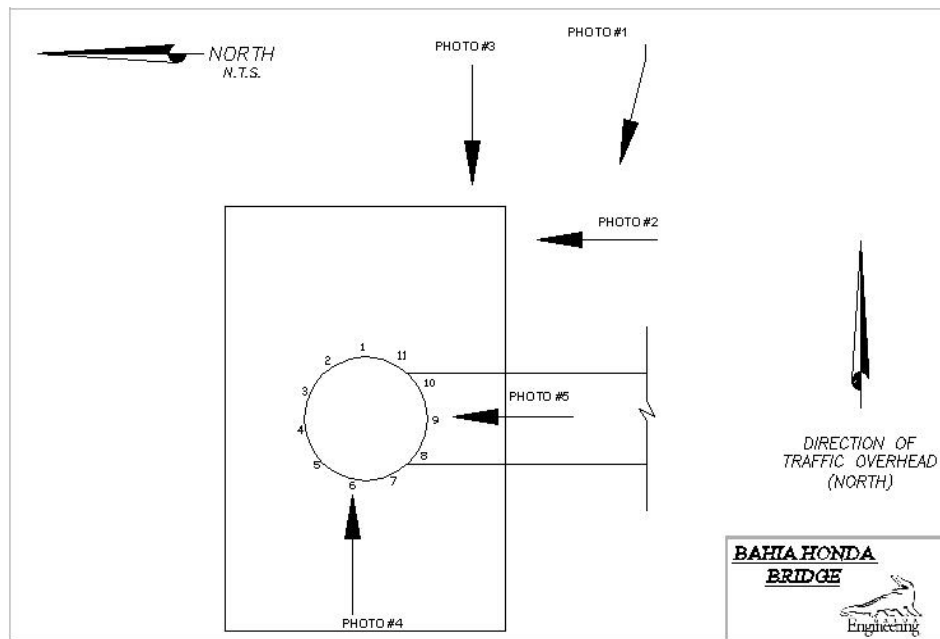


Figure 4.2: Photo location plan Bahia Honda bridge pile cap and column 54



Figure 4.3: View of bridge superstructure from water-level



Figure 4.4: View of footing



Figure 4.5: View of crack in column



Figure 4.6: View of crack in column. Efflorescence of the gunite topping on the strut can be seen in the background

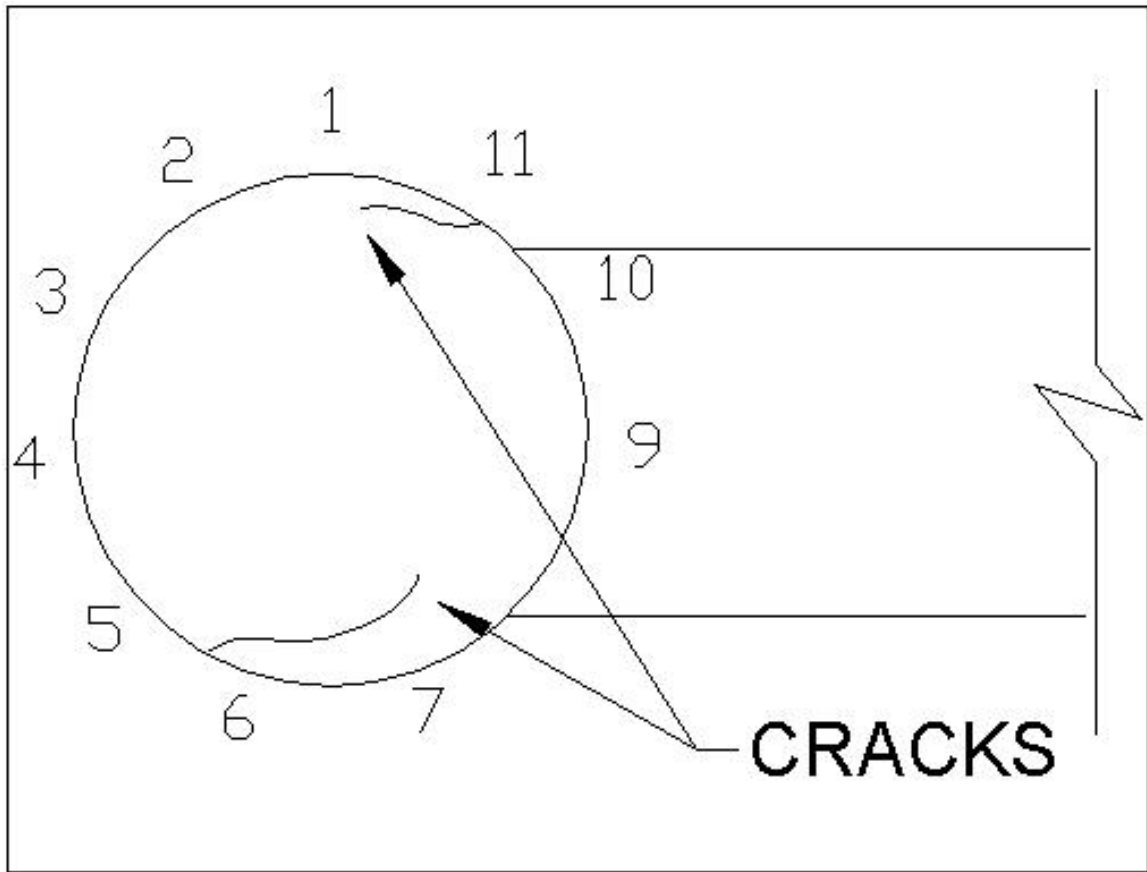


Figure 4.7: Plan view of crack orientation on column 54

### **Niles Channel Bridge**

#### **Site Information**

The Niles Channel Bridge was constructed in 1983. It spans the big Niles Channel Waterway between Summerland Key and Ramrod Key in Monroe County, Florida. Like the Bahia Honda Bridge, the Niles Channel Bridge replaced an older bridge which was originally built as part of the Flagler Overseas Railroad.

#### **Procedures**

The evaluation began with a site visit by Mr. Christopher Ferraro and Dr. Andrew Boyd of the University of Florida, accompanied by Mr. Olen Hunter and Mr. Andrew

Eiland of the FDOT, on May 21, 2003. During the visit, the personnel observed the Niles Channel bridge substructure and superstructure accessible from a boat provided by the FDOT. The general condition of the bridge was observed and documented with photographs. No plans were available for review.

During the course of the fieldwork, the personnel performed materials testing on Column Line 20. As part of the materials survey, the accessible portion of the column and strut were tested by means of sounding, impact-echo and ultrasonic pulse velocity. Locations of testing on Column Line 20 are depicted in Figure 4.8.

## **Results**

### **Site observations**

The bridge superstructure is composed of a prestressed concrete segmental box resting on girder concrete columns. The substructure is composed of concrete cylindrical columns with struts resting on top of cylindrical drill shafts. The submerged drill shafts were not visible during the inspection. Figures 4.9 and 4.10 contain photographs of the bridge structural elements.

The entire bridge structure was visually surveyed to obtain an overall appraisal of its structural integrity. The segmental box girder showed little or no deterioration, though there were some locations of discoloration, efflorescence, and superficial cracking. Some of the concrete columns were observed to have experienced delaminations and spalls and have been repaired. However, the majority of the columns displayed minor or no deterioration. Some of the struts exhibited little or no deterioration. However, the majority of the struts displayed moderate to severe deterioration. Severe deficiencies such as large cracks, spalls, delaminations and section loss have been repaired. In spite of the extensive repair-work performed on the struts, some of the repairs have experienced

deterioration and new deficiencies have developed since the columns were last maintained. Figure 4.11 is a photograph of a typical column strut repair, and new deficiency. The drill shafts showed little or no deterioration. There were some locations of discoloration, efflorescence, and superficial cracking.

Upon completion of the visual survey, it was decided that Column Line 20 exhibited typical deficiencies, yet had not been repaired. Thus, this column line was deemed suitable for materials inspection. The crack delamination of the concrete on the lower portion of Strut 20 appeared to be a prevalent deficiency observed throughout the bridge.

### **NDT Analysis**

The column and pile cap were tested by means of acoustic sounding, impact-echo, and ultrasonic pulse velocity in order to determine material quality. The tests were performed in accordance with relevant ASTM standards (ASTM C 597-97, ASTM C 1983-98a).

The columns were tested using the impact echo device. The average impact echo surface wavespeed for both columns was determined to be 3981 m/s. The impact echo device was used to confirm surface wavespeeds as it was for the Bahia Honda Bridge. The average impact echo through wavespeed was calculated to be 4083 m/s.

The strut was tested using the ultrasonic pulse velocity meter and the impact echo device. The ultrasonic pulse velocity meter was used to obtain a tomography of the strut using the through wavespeed of the material. The average through wavespeed obtained using the pulse velocity meter was calculated to be 4358 m/s. Acoustic sounding and ultrasonic tomography confirmed that the lower portion of the strut is cracked and delaminated. The average impact-echo surface wavespeed was determined to be 3930

m/s. The impact echo device was used to confirm obtained surface acoustic velocities as it was for the Bahia Honda Bridge. The average impact echo through wavespeed was calculated to be 4083 m/s.

### **Conclusions**

The data obtained from the nondestructive testing of the strut was similar to that obtained from the column of the Bahia Honda Bridge. The ultrasonic through wavespeeds taken from the strut were greater than the impact echo surface and through wavespeeds. The discrepancy between the ultrasonic pulse velocity data and the impact echo data can be attributed to the effects of the embedded steel on pulse velocity measurements. The slight disparity between the surface and through impact echo wavespeeds is consistent with the results from the Bahia Honda pile cap and most likely a result of exposure. However, due to the slight difference in wavespeeds, it can be concluded that exposure conditions have not distressed the concrete to a great extent. The lower portion of the strut was delaminated, most likely due to the corrosion of the embedded rebar. Figure 4.11 is a photograph of a typical deficiency of the strut. The deficiency is most likely a result of rebar exposure to chlorides, as the struts are partially submerged under severe weather conditions.

The columns on Line 20 were found to be in satisfactory condition with little or no signs of distress. The wavespeeds acquired from impact echo testing of column 20 indicate that the concrete is in good condition in that column. The overall condition of the structure was not determined for the purposes of this survey.

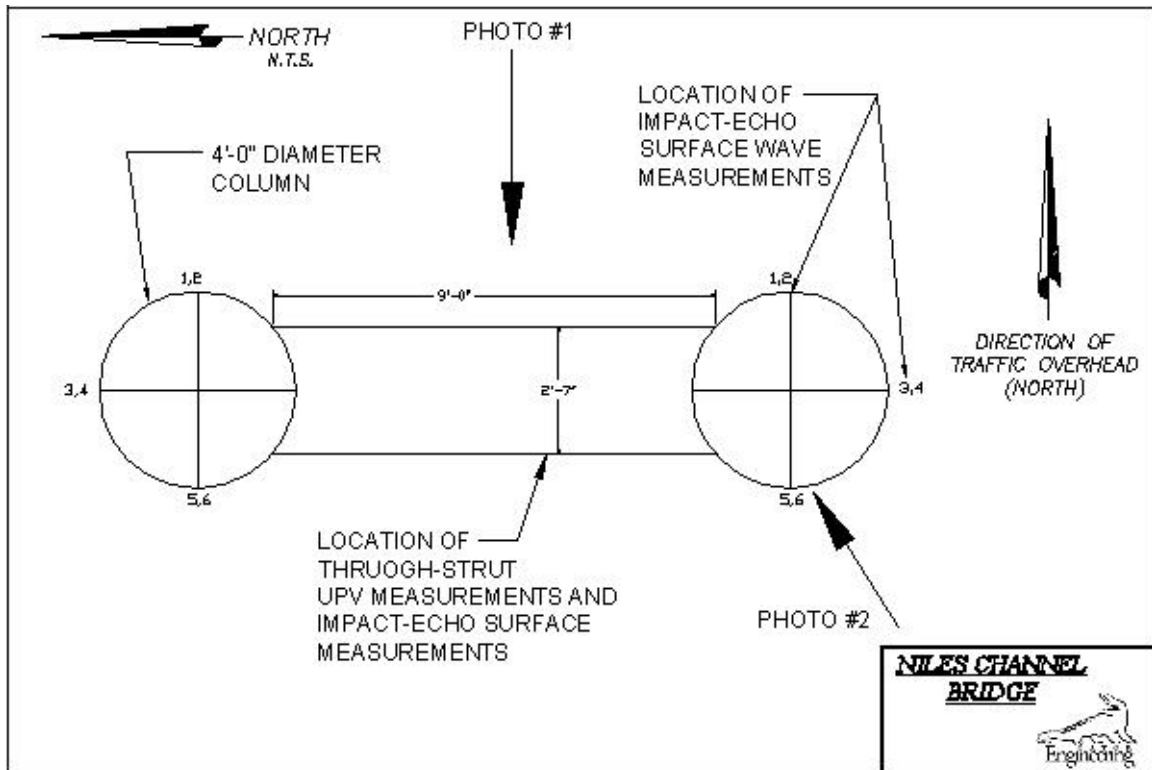


Figure 4.8: Plan view of Niles Channel Bridge column line 20



Figure 4.9: General view of Niles Channel Bridge underside, column line 20 in foreground



Figure 4.10: Impact-echo testing on bridge column



Figure 4.11: View of typical strut and column repair. Note spalls in strut underside

## **Sebastian River Bridge**

### **Site Information**

The Sebastian River Bridge was constructed in 1957, and spans the St. Sebastian River Waterway between Indian River County and Brevard County, Florida. The bridge was built to service an increased traffic flow on U.S. Highway 1, which is the only throughway from the State of Maine to the Florida Keys.

### **Procedures**

The evaluation began with a site visit by Mr. Christopher Ferraro of the University of Florida, accompanied by Mr. Ronald Ferraro, on June 12, 2003. During the visit the personnel observed the Sebastian River bridge substructure and superstructure accessible from a boat provided by the University of Florida. The general condition of the bridge was observed and documented with photographs. No plans were available for review.

During the course of the fieldwork, the personnel performed materials testing on Column Line 11. As part of the materials survey, the accessible portion of the column and strut were tested by means of sounding, rebound hammer, impact-echo, and ultrasonic pulse velocity meter. Locations of testing on Column Line 11 are depicted in Figure 4.12.

## **Results**

### **Site observations**

The bridge superstructure is composed of prestressed concrete girders resting on concrete cap beams. The substructure is composed of prestressed concrete piles with concrete pile jackets. The submerged drill shafts were not visible during the inspection. Figures 4.13 through 4.16 are photographs of the bridge structural elements.

The entire bridge structure was visually surveyed in order to obtain an overall appraisal of the structural integrity. The bridge girders showed little or no deterioration, though there are some locations of discoloration, efflorescence, and superficial cracking. The concrete columns were observed to have experienced a range of deterioration levels. Approximately 20 percent of the pile jackets were observed to have been replaced with non-structural fiberglass jackets filled with grout or epoxy. Severe cracks, spalls and delaminations were observed on the repaired pile jackets. Distress on the prestressed concrete columns was not observed. However, the prestressed column interiors were not visible.

Upon completion of the visual survey, it was decided that Column Line 11 exhibited a typical representation of the bridge superstructure. Of the five columns on this column line, three are intact. The other two columns have been previously repaired. Column 11-5 is an example of a column that has not been repaired, and Column 11-4 is an example of a typical repaired column. Figures 4.14 through 4.16 contain photographs of the columns. According to inspection reports the column repairs were performed approximately 12 years ago.

### **NDT Analysis**

Columns 11-4 and 11-5 were tested by means of sounding, rebound hammer, impact-echo, and ultrasonic pulse velocity meter in order to determine material quality. The tests were performed in accordance with relevant ASTM standards (ASTM C 805-97, ASTM C 597-97, ASTM C 1983-98a).

The pile jacket of Column 11-4 is composed of a mortar mix and was observed to be in poor condition. It appeared as though severe segregation of the constituents of the mortar took place prior to, or during placement. Severe cracking and delamination were

evident throughout. Figure 4-16 contains a photograph of a vertical crack, approximately 8 feet in length and approximately 0.07in wide, that was observed on the north side of the column. The column was acoustically sounded with a ball peen hammer to determine the presence of delaminations. As a result of the survey it was determined that approximately 50 percent of the pile jacket has delaminated from the pile. The extremely poor condition of the mortar resulted in large variances in the wavespeeds obtained with the impact echo device. Some impact echo tests did not produce data because the concrete permanently deformed upon impact. Therefore, data obtained from the impact echo was relatively unusable for analysis. The obtained surface wavespeeds ranged from 2400 m/s to 4000 m/s. Ultrasonic testing also produced data with a considerable range. Ten of the twenty UPV readings taken were above 3200m/s. A considerable range of through wavespeeds was produced by the UPV test.

Column 11-5 was observed to be in satisfactory condition. Acoustic sounding did not reveal any delaminations in the pile jacket. The average through wavespeed obtained using the pulse velocity meter was calculated to be 4354 m/s. The average impact-echo surface wavespeed was determined to be 4485 m/s. The data obtained using the impact echo through measurement did not verify the wavespeeds due to signal scatter, which was most likely produced by the presence of several material interfaces within the pile.

### **Conclusions**

The NDT data received from Column 11-4 revealed that the pile jacket is in poor condition. The severity of the deterioration combined with the relatively young age of the repairs indicates faulty repair work in the replacement of the pile jacket.

Column 11-5 was found to be in satisfactory condition with little or no sign of distress. The acoustic sounding, rebound hammer, impact echo and ultrasonic pulse

velocity data acquired from the column confirmed that the concrete is in good condition.

The impact-echo though wavespeeds could not be accurately obtained due to the interaction between the stress waves and several material interfaces within the pile.

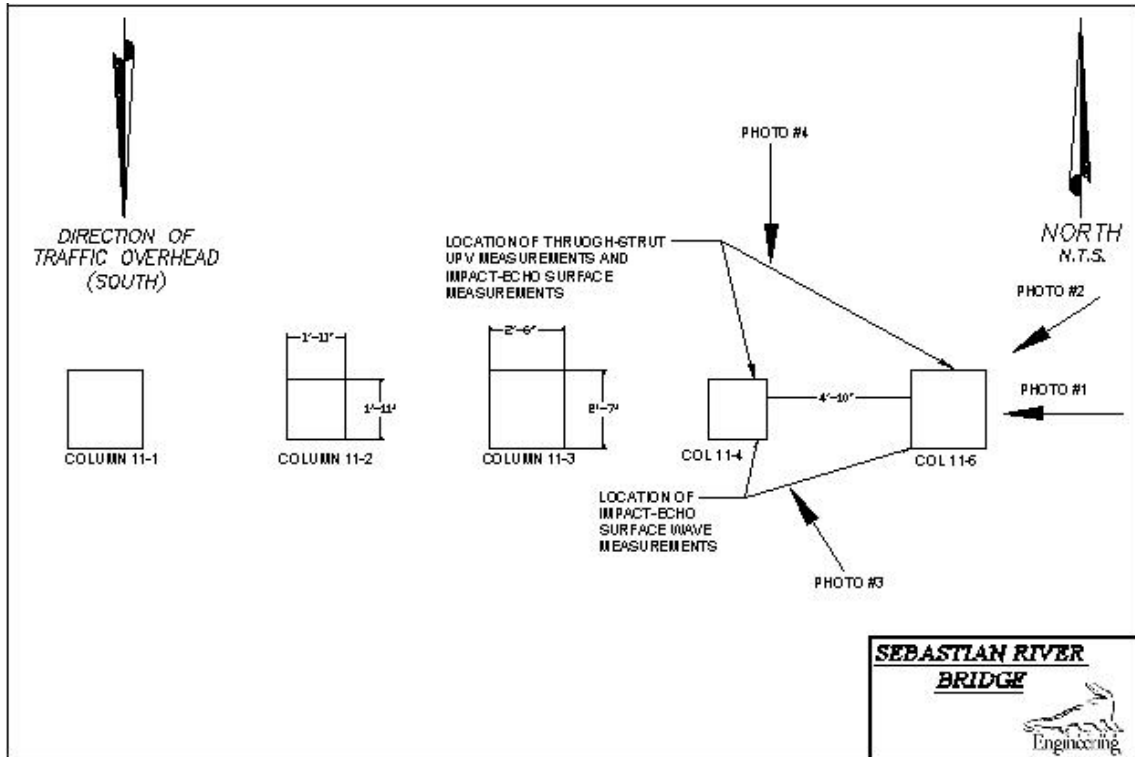


Figure 4.12: Plan view of Sebastian River Bridge column line 11



Figure 4.13: General view of Sebastian River Bridge



Figure 4.14: Column line 11 with column 11-5 in foreground



Figure 4.15: Column 11-4



Figure 4.16: Cracked and delaminated repair in column 11-4

## **Wabasso Bridge**

### **Site Information**

The Wabasso Bridge, constructed in 1970, spans the Indian River waterway in Indian River, Florida. This bridge serves as the easternmost segment of the Wabasso causeway. The bridge was built to service traffic flow on County Road 510, between Indian River Lagoon Scenic Highway (A1A) and U.S. Highway 1 in Indian River County, Florida.

### **Procedures**

The evaluation began with a site visit by Mr. Christopher Ferraro of the University of Florida accompanied by Mr. Ronald Ferraro on June 13, 2003. During the visit, they observed the bridge substructure and superstructure from a boat provided by the

University of Florida. The general condition of the bridge was observed and documented with photographs. No bridge plans were available for review.

During the course of the fieldwork, the personnel performed materials testing on Pier 5 and Pile Cap 5. As part of the materials survey, the accessible portion of the column and strut were tested by means of acoustic sounding, rebound hammer, and impact-echo. Figure 4.17 depicts testing locations on the Wabasso Bridge.

## **Results**

### **Site observations**

The Wabasso Bridge superstructure is composed of prestressed concrete girders. The substructure is composed of concrete hammerhead piers with a concrete pile cap. The submerged piles were not visible during the inspection. Figures 4.18 and 4.19 contain photographs of the bridge's structural elements.

The bridge superstructure and substructure were visually surveyed to get an overall appraisal of the structural integrity. The bridge girders showed little or no deterioration. There were some areas of discoloration, efflorescence, and superficial cracking. The concrete piers showed little or no evidence of deterioration. The accessible portions of concrete pile caps revealed that crushed seashell was used as a constituent in the concrete mix, as shown in Figure 4.20. The pile caps were observed to be in good condition with little or no signs of distress.

### **NDT Analysis**

Pier 5 and Pile Cap 5 were tested by means of acoustic sounding, rebound hammer, and impact-echo in order to determine material quality. The tests were performed in accordance with relevant ASTM standards (ASTM C 805-97, ASTM C 1983-98a).

The average surface wavespeed for Pier 5, obtained by the impact echo device, was 3157 m/s. Through wavespeeds were confirmed within acceptable tolerances, using the impact echo device. The average rebound number was determined to be 58.5. The corresponding strength value, extrapolated from the best-fit equations (Malhotra & Carino 1991), was approximately 11,000 psi.

The average surface wavespeed for pile cap 5, obtained by the impact echo device, was measured to be 2515 m/s. The through wavespeeds were confirmed within acceptable tolerances, using the impact echo device. The average rebound number was determined to be 46.25. The corresponding strength value, extrapolated from the best-fit equations (Malhotra & Carino 1991), was approximately 8,100 psi.

No material defects on any of the accessible structural components were revealed as a result of acoustic sounding.

### **Conclusions**

The NDT data collected from the bridge elements appear to contain some conflicting values. The data obtained from the rebound hammer indicate that the concrete elements are in good condition, whereas the data obtained from the impact echo device suggest that the concrete elements show signs of distress. The aggregate used in the mix design, which was observed to contain crushed seashell, most probably caused this disparity between surface hardness measurements versus wavespeed measurements.

Crushed seashell or calcium carbonate is less dense and more porous than conventional coarse aggregates used for concrete production. As discussed in Chapter 2, density and porosity are two properties of a solid that can reduce its acoustic impedance or wavespeed. The use of crushed seashell in the structural components resulted in low

wavespeeds. However, the low wavespeeds calculated for the concrete components does not correlate to distress of the actual structure.

The large values obtained using the rebound hammer appear to suggest that the material is in good condition. Rebound values corresponding to strengths of 11,000 and 8,000 psi are extremely high. One possible reason for the high rebound hammer values could be due to the carbonation of the concrete surface. Surface carbonation can result in rebound numbers 50% higher than those obtained on an uncarbonated surface (Malhotra & Carino 1991). Carbonation of concrete is promoted in environments where the relative humidity is maintained between 50 and 75 percent (ACI 201.2R92). Consequently, it is unlikely that carbonation is taking place on the surface of the bridge because the average relative humidity exceeds 85 percent approximately 11 months of each year (NOAA 2003).

The most probable cause of the high rebound number values is the material constituents in the concrete mix design. Research has revealed that the type of aggregate and cement can significantly affect rebound hammer readings (Malhotra & Carino 1991). Due to the angularity of seashells, it is common to require additional cement in a concrete mix to increase workability (Neville 1996). At present, there is no research available that correlates compressive strength with concrete containing crushed seashells as aggregate. Unfortunately, the mix design is not available for review and the uncertainties within the exact mix design prohibit specific material based conclusions.

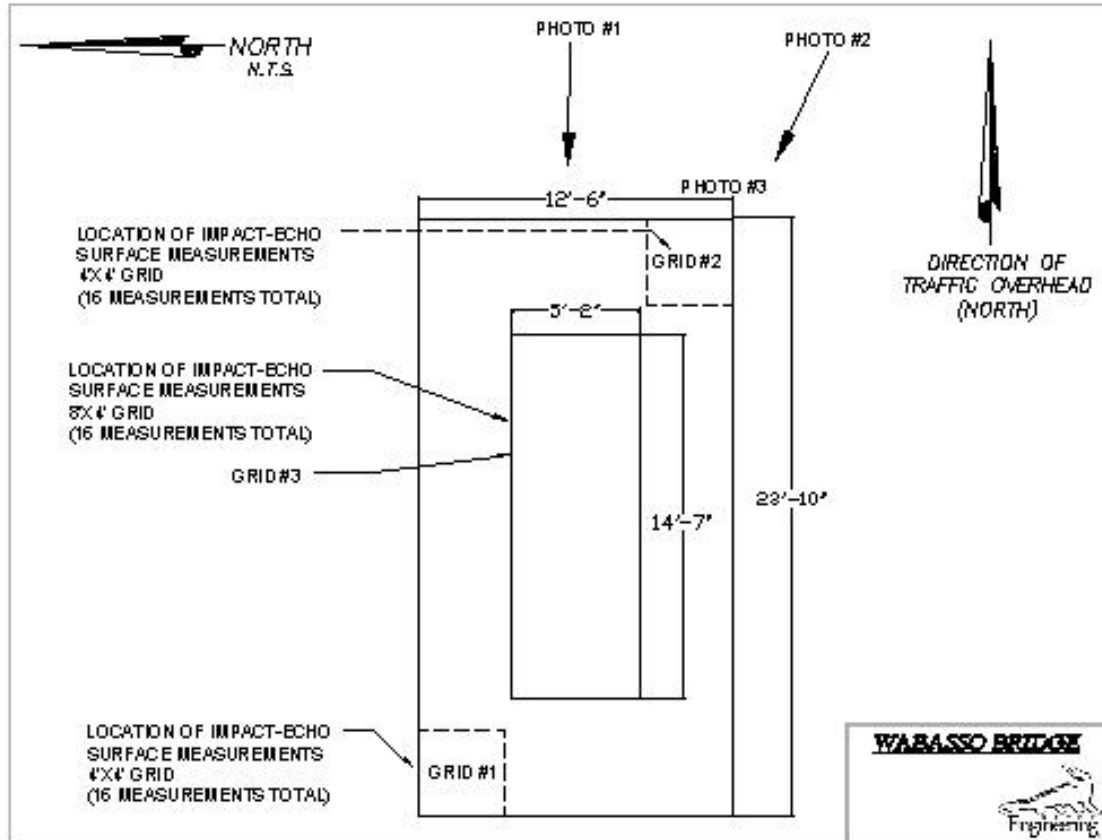


Figure 4.17: Plan view of Wabasso Bridge column



Figure 4.18: General view of Wabasso Bridge



Figure 4.19: Column / pilecap 5

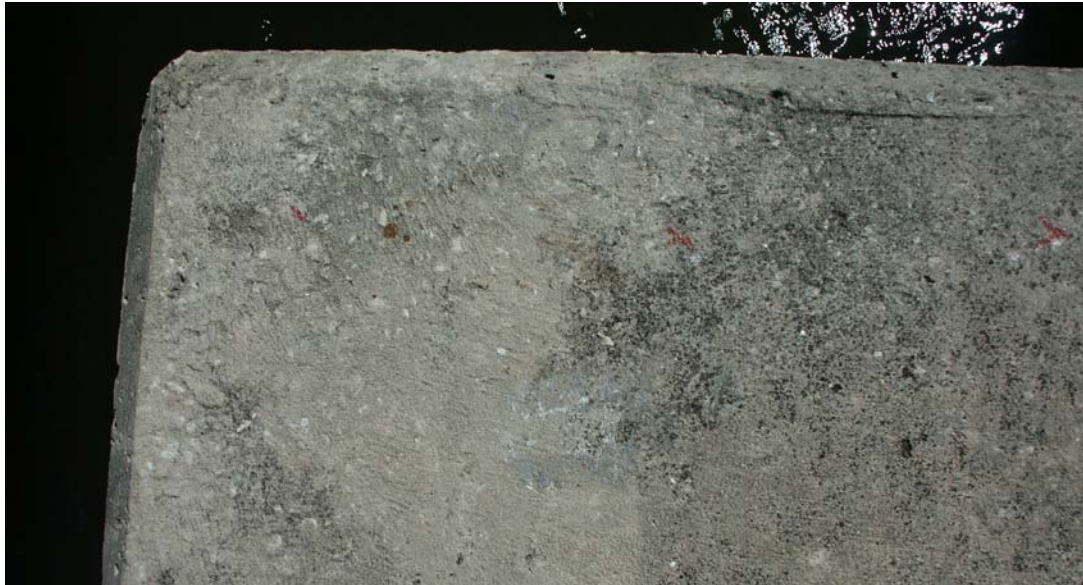


Figure 4.20: Close-up of exposed seashell aggregate on pile cap 5

### **Sebastian Inlet Bridge**

#### **Site Information**

In 1886, the first inlet (Gibson's cut) was dug by hand approximately 3 miles south of the present day inlet. In 1924, the Sebastian Inlet was opened at its current location. Between 1924 and 1941 the Inlet opened and closed several times due to the shifting

sands caused by storms. For safety reasons, it was left closed during World War II, then permanently blasted open in 1947.

The Sebastian Inlet Bridge, also known as the Robert W. Graves Bridge was completed in 1967. The 1,548 foot long bridge spans the inlet and is part of the Indian River Lagoon Scenic Highway (A1A). The waterway serves as part of the borderline between Indian River County and Brevard County, Florida.

### **Procedures**

The evaluation began with an interview of Mr. Ivan Lasa on June 10, 2003 by Mr. Christopher Ferraro. Mr. Lasa reported that the bridge had recently undergone repair work, including the rehabilitation of deficiencies in the bridge superstructure and substructure. Portions of the bridge, including the columns, were painted as part of the repair work.

Mr. Christopher Ferraro of the University of Florida, accompanied by Mr. Ronald Ferraro, performed site visits on June 14 and 15 of 2003. During the site visit, they accessed by foot and observed the bridge substructure and superstructure. The general condition of the bridge was observed and documented with photographs. No plans were available for review.

During the course of the fieldwork, the personnel performed materials testing on Pile Cap 12 and Pile Cap 16, as well as the accessible portion of Column 12. As part of the survey, portions of elements were tested by means of acoustic sounding, ultrasonic pulse velocity, impact-echo, and rebound hammer. Figure 4.21 depicts locations of testing on the Sebastian Inlet Bridge.

## **Results**

### **Site observations**

The bridge superstructure is composed of prestressed concrete girders resting on concrete cap beams. The substructure is composed of concrete cylindrical columns with struts resting on pile caps. The submerged piles were not visible during the inspection. Figures 4.22 and 4.23 contain photographs of the bridge's structural elements.

The entire bridge structure was visually surveyed to get an overall appraisal of the structural integrity. The bridge girders showed little or no deterioration, although there were some areas of discoloration, efflorescence, and superficial cracking. The concrete columns showed little or no evidence of deterioration. The pile caps were observed to be in good condition with little or no sign of distress.

### **NDT Analysis**

Pile Cap 12 and Pile Cap 16 were tested by means of sounding, rebound hammer, and impact-echo in order to determine material quality. The tests were performed in accordance with relevant ASTM standards (ASTM C 805-97, ASTM C 597-97, ASTM C 1983-98a).

The column was tested using the sounding method and the ultrasonic pulse velocity meter. The ultrasonic pulse velocity meter was used to obtain a tomography of the column using through wavespeeds of the material. The average through wavespeed was calculated to be 3675 m/s. The column has two cracks on opposite sides of each other. The cracks were not visible due to recent repairs performed on the surface of the column. Ultrasonic tomography confirmed the orientation and depth of the crack. Figure 4.24 is a schematic of the calculated crack depth and orientation as a result of the acoustic and ultrasonic tomography testing.

The pile caps were tested using the sounding method, the rebound hammer, and the impact-echo device. The average surface wavespeed obtained by the impact echo device was measured to be 3622 m/s. The through wavespeeds were confirmed using the impact echo device within acceptable tolerances. The average rebound number was determined to be 47.22, corresponding to a strength value of approximately 8,500 psi, extrapolated from the best-fit equations (Malhotra & Carino 1991).

No material defects on any of the accessible structural components were revealed as a result of acoustic sounding.

### **Conclusions**

With the data available, it is possible to conclude that the concrete material on the column is in good condition, with some signs of distress. The cracks in the column are most likely torsional cracks, which are due to loading or shifting of the structure. The crack found on the Bahia Honda bridge structure was of the same orientation as the strut. It is possible that results of the NDT testing revealed a design flaw in the column-strut connection for bridges of this type. However, further testing is needed to confirm this hypothesis. The purpose of this survey was to examine the concrete material on the structure and not the structure itself.

The NDT data recorded from the bridge elements appear to have some conflicting values. The data received from the rebound hammer indicate that the concrete elements are in good condition, whereas the data obtained from the impact echo device suggest the concrete elements show signs of distress. The aggregate used in the mix design is the most probable cause of the disparity between surface hardness measurements and wavespeed measurements. The same circumstances were encountered in the analysis of the NDT data at the Wabasso Bridge. It is possible that the same mix design was used on

the pile caps at the Sebastian Inlet Bridge and the Wabasso Bridge given their construction was within the same time period and the bridges are located in relatively close proximity of each other.

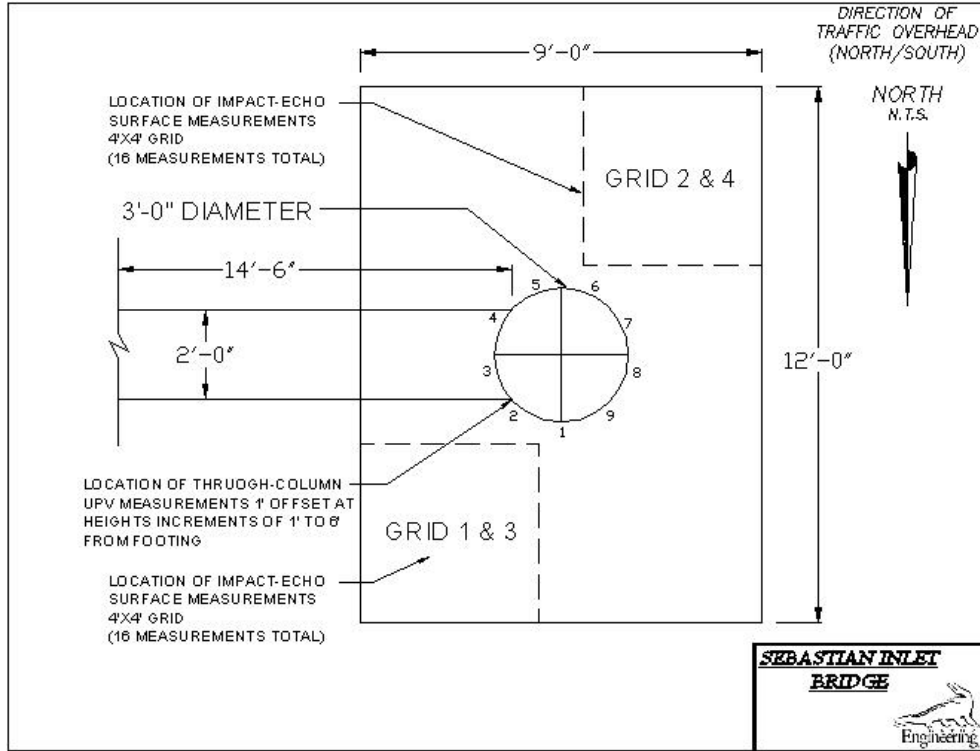


Figure 4.21: Plan view of column / pile cap of Sebastian Inlet Bridge



Figure 4.22: General view of Sebastian Inlet Bridge underside. Column line 7 in foreground adjacent to stairs



Figure 4.23: Column line 6

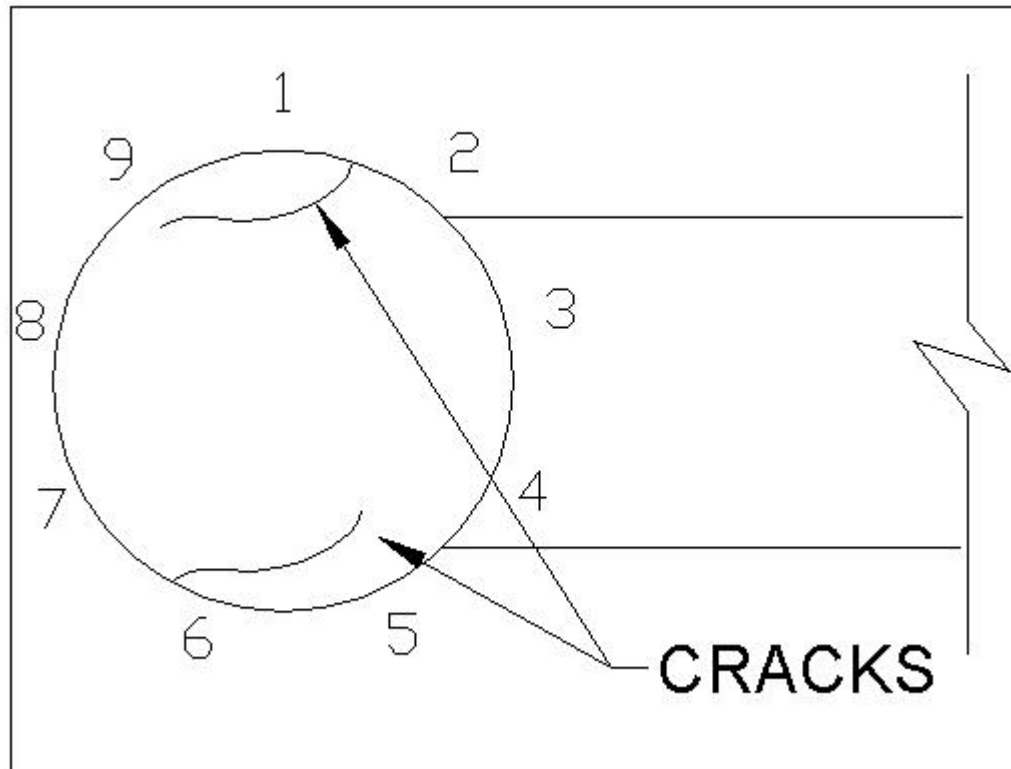


Figure 4.24: Plan view of crack orientation on column 12

## CHAPTER 5 NONDESTRUCTIVE LABORATORY SPECIMEN TESTING

Concrete is among the most complex materials used in construction today. It is a mixture of Portland cement, mineral aggregates, water, air, and often includes chemical and mineral admixtures. Unlike other materials used in construction, concrete is usually designed specifically for a particular project using locally available materials (Mindess et al. 2003). Therefore, it is common for the physical properties of concrete within a particular structure or even a structural element to differ. The internal structure of concrete is more complex than any other construction material (Popovics 2001) because:

- Hardened cement paste is a multiphase material.
- Mineral aggregate is a porous composite material which has varying material properties depending on type.
- The interface between the cement paste and the aggregates has unique properties.

Thus, concrete can be aptly considered as a composite of composites, heterogeneous at both the microscopic and macroscopic levels (Popovics 2001, p 125). Therefore it is difficult to precisely determine the physical properties of any one specific concrete specimen without knowledge of its components.

### **Prior Research**

Research has been conducted using stress wave propagation methods such as the ultrasonic pulse velocity method and the impact echo method to correlate stress wave velocity with concrete strength. The research has shown that many factors can influence the strength and the wave velocity of concrete, such as porosity, age, and composition. However, the factors that influence wave velocity do not influence strength in the same way or to the same extent. In an attempt to develop empirical equations, experiments

have been conducted to establish a strength/wave velocity relationship of concrete (Pessiki & Carino 1988, Popovics 2001, Qaswari 2000). Literature suggests that Young's modulus of elasticity can be obtained through the use of resonant frequency.

### Methodology

The purpose of performing nondestructive laboratory testing on concrete cylinders was to establish correlations between stress wave velocity, longitudinal resonant frequency and compressive strength change over time. The other objective of the research was to evaluate the variation in NDT data related to mixture design.

### Procedure

Two separate groups of concrete cylinders were created for this study. The proportions given in Table 5.1 were used in an attempt to reproduce actual mix designs used in residential concrete footings and foundations. Larger specimens were cast from the same batches as the cylinders to ensure consistency of the concrete used for each design.

Table 5.1: Mixture proportions for NDT and strength tests.

<b>Mix Design</b> <b>Volume = 1 m<sup>3</sup></b>	<b>A</b> <b>0.45 w/cm</b>	<b>B</b> <b>0.65 w/cm</b>
<b>Cement</b>	507.7	350.3
<b>Water</b>	228.6	228.6
less M/C sand	0.0	0.0
less M/C aggregate	0.0	0.0
Total	228.6	228.6
<b>Sand</b>	855.1	985.7
plus M/C sand	0.0	0.0
Total sand	855.1	985.7
<b>Aggregate</b>	733.4	626.5
plus M/C aggregate	0.0	
Total aggregate	733.4	626.5
<b>Admixtures</b>		
Superplasticizer (Adva 100)	0.8	0.0
<b>Total</b>	<b>2324.8</b>	<b>2191.2</b>

Casting of the concrete specimens took place at the Florida Department of Transportation State Materials Office. After casting, the cylinders were transported to the University of Florida for curing and testing. The samples were cured in limewater bath until preparation and testing. The testing regimen consisted of testing three cylinders per day, at ages of one, two, three, seven, 14, 21, 28, 42, and 56 days. The cylinders were kept in limewater until the predetermined age of testing. All nondestructive testing and destructive testing was performed within a 6 hour period after removal of the specimens from the bath to ensure complete saturation of the specimen.

The preparation of cylinders included grinding of the ends to create a planar surface in accordance with ASTM C-39-01.

Nondestructive testing was carried out using a NDT James Instruments ultrasonic pulse velocity meter, and a Germann Instruments Docter-1000 impact echo device. Each of the tests was performed in accordance with the relative ASTM standard (ASTM C597-97, ASTM C1383-98a).

The ultrasonic pulse velocity meter was used to obtain through wave velocities for the concrete cylinders. As described in Chapter 2, travel times and cylinder lengths were recorded for each cylinder. Figure 5.1 contains a photograph of the ultrasonic pulse velocity experimental setup.



Figure 5.1: Ultrasonic pulse velocity experimental setup.

Longitudinal resonant frequency testing was also determined for each of the cylinders. The test method, described in Chapter 2, was performed and the results recorded. Figure 5.2 contains a photograph of the torsional resonant frequency experimental setup.

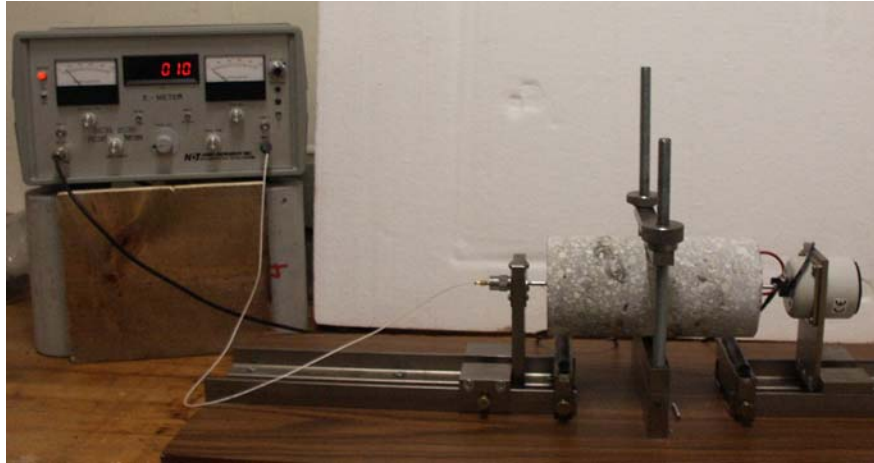


Figure 5.2: Resonant frequency experimental setup

The impact echo device was used to obtain through wavespeeds for the cylinders. As described in Chapter 2, the frequency spectrums and cylinder lengths were recorded for each cylinder. Figure 5.3 contains a photograph of the impact echo experimental setup.

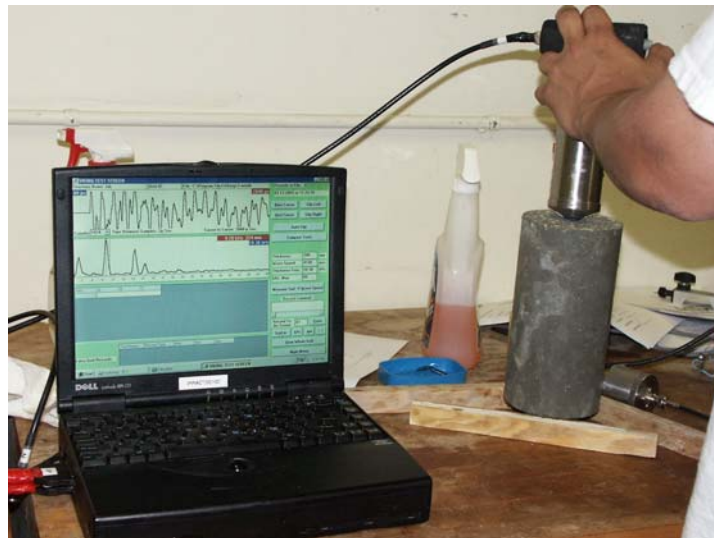


Figure 5.3: Impact echo experimental setup

Upon completion of the nondestructive testing on the cylinders, their ultimate compressive strength was determined in accordance with ASTM C39-01.

### Results and Discussion

Relationships were developed between wave velocity and compressive strength. The wavespeeds were obtained with the ultrasonic pulse velocity meter, then confirmed with the use of the impact echo device. The impact echo method provides a resulting wave spectrum of the tested material identifying possible defects in the specimen. This can facilitate a reduction in the specimen's ultimate strength. Defect detection within specimens can aid users in rationalizing the existence of outlying data points based on material consistency. Figure 5.4 shows the relationship between the compressive strength and wave velocity for Mixtures A and B.

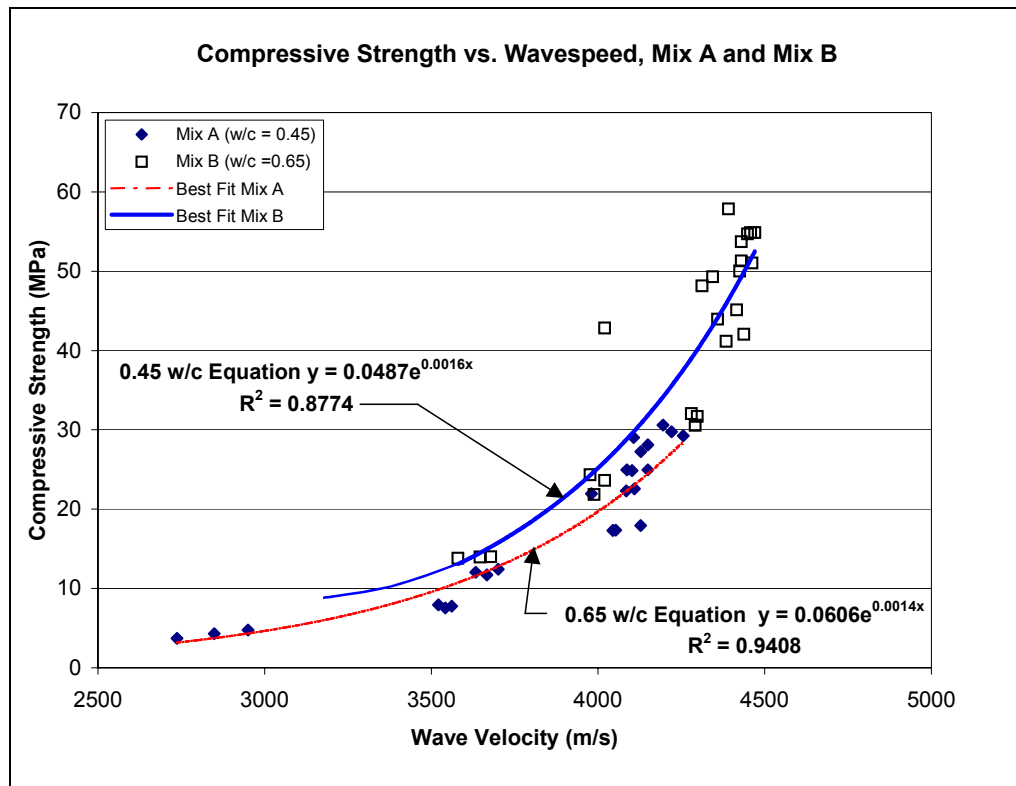


Figure 5.4: Compressive strength vs. wave velocity for Mixtures A and B

The results indicate that differences in mixture design create differences in the strength versus wave velocity relationship. The data shows that the Mixture B, with a higher water to cement ratio, produced samples with lower compressive strengths than Mixture A (as expected). The concrete in Mixture B produced lower wave velocities than Mixture A as well. Pessiki & Carino 1988, suggests that the water to cement ratio does not affect the compressive strength and wave velocity relationship. However, the data obtained in this experiment and an experiment performed by Yan et al. 2003 suggest otherwise.

However, the proportion of coarse to fine aggregate varied between the mixtures. It is possible that the difference in wave velocities between Mixture A and Mixture B can be attributed to the change in proportion of coarse aggregate to fine aggregate between the mixes. Presently, no research is available regarding the relationship between the compressive strength and wave velocity of mixtures, and the effect of coarse to fine aggregate proportion on wave velocity. Therefore, further testing is needed to determine what effect this proportion has on wave velocity.

As indicated by the results, the wave velocity verses compressive strength relationship increases in a relative trend. The results were compared with the equations developed by Pessiki & Carino 1988, Qaswari 2000 and Yan et al. 2002. The estimated compressive strength based on the experimental equations, using the wave velocities obtained in the lab wave velocity equations differed from the actual compressive strengths by an average of approximately 35 percent. However, the general trend of the data appears to correlate to the Equation 1 presented by Pessiki.

$$f'_c = a \left( \frac{C_p}{n+1} \right)^b \quad (1)$$

Where:  $f'_c$  is compressive strength (MPa);  $C_p$  is wave velocity;  $a$ ,  $b$  and  $n$  are constants.

The equation used by Qaswari to relate compressive strength to wavespeed is a linear equation. Figure 5.5 relates the strength and wave velocity for the experimental data from Mixture A to equations used by Pessiki & Carino and Qaswari. The experimental wave velocity data for Mixture A was used to calculate the predicted trends in Figure 5.5.

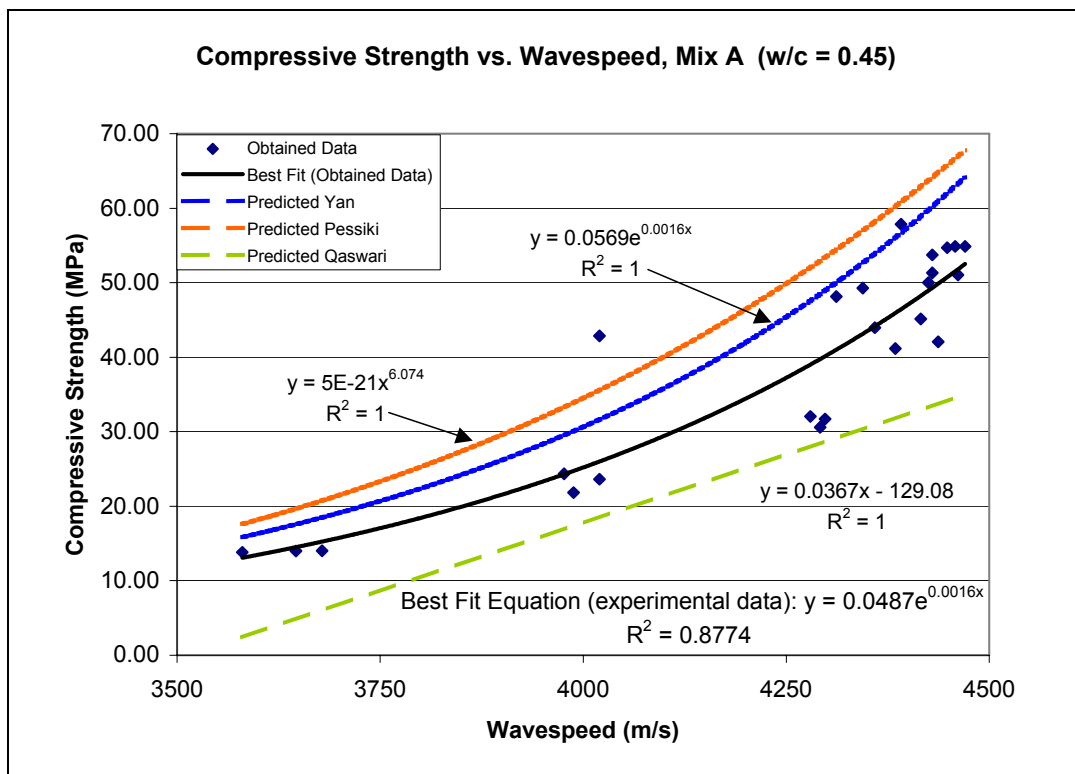


Figure 5.5: Results from compressive strength vs. wave velocity results for Mixture A  
The use of a power equation properly correlates the early strength verses

wavespeed of concrete when the wavespeeds are relatively low. The equation presented by Qaswari is a linear equation that intercepts the compressive strength/axis at 3515 m/s.

The equation obtained by Yan et al., Pessiki & Carino and the experimental data are

power functions as they intercept the strength/axis at 0 m/s. Consequently, using this equation to predict strengths of early age is inappropriate.

The concrete mixture designs used in the experiment performed by Pessiki contained different proportions of cement, aggregates, and water than Mixtures A and B used in this experiment. As stated earlier in this chapter, differences within the material properties of the concrete constituents will usually result in variability within the compressive strengths and wavespeeds of concrete.

The experimental results plotted in Figure 5.4 are within acceptable tolerances with the exception of one data point. The outlying data point had a compressive strength of 42.84 MPa and a corresponding wavespeed of 4020 m/s. The use of the impact echo device provided an alternate method for obtaining wave speeds. The graph shown in Figure 5.5 is the resulting frequency spectrum of the outlying data point. Figure 5.6 is the frequency spectrum of a typical data point.

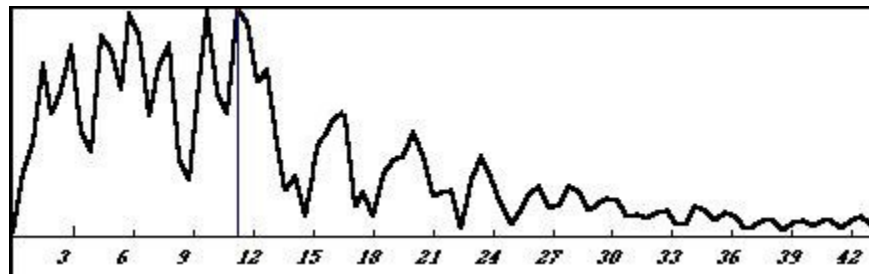


Figure 5.5: Frequency spectrum of outlying data point.

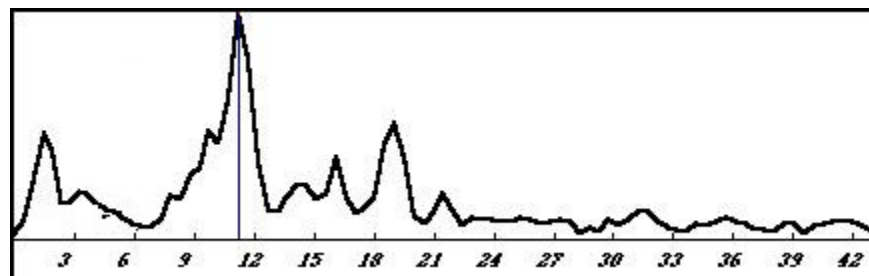


Figure 5.6: Frequency spectrum of typical impact echo data point.

The impact echo section of Chapter 2 describes the results of frequency spectrums. The frequency spectrum shown in Figure 5.6 is a spectrum typical for concrete with numerous voids and cracks. A slower calculated wave velocity using the ultrasonic pulse velocity for a concrete sample would be expected for a heavily voided concrete specimen. As discussed in the ultrasonic pulse velocity portion of Chapter 2, the travel path for a given wave in a voided concrete specimen is longer than in a specimen without voids. Therefore, improper preparation of the concrete sample is most likely the reason for the outlying data point.

Resonant frequency analysis has been performed with concrete specimens to develop relationships between compressive strength and longitudinal resonant frequency. Literature has suggested that Young's modulus of elasticity can be obtained through the use of resonant frequency (Malhotra & Carino 1991). The resonant frequency section of Chapter 2 discussed some of the limitations of the resonant frequency test. Lack of reproducibility of the test results is one such limitation. Figure 5.7 shows the relationship between the compressive strength and resonant frequency for Mixtures A and B.

Figure 5.7 shows the compressive strength versus resonant frequency for concrete specimens. This is similar to the data obtained from the compressive strength versus wave velocity relationship. The results show that differences in mixture design create differences in the strength versus resonant frequency relationship. The data shows that Mixture B, with a higher water to cement ratio, produced samples with lower compressive strengths than Mixture A (as expected). The concrete in Mixture B produced lower resonant frequencies than Mixture A as well.

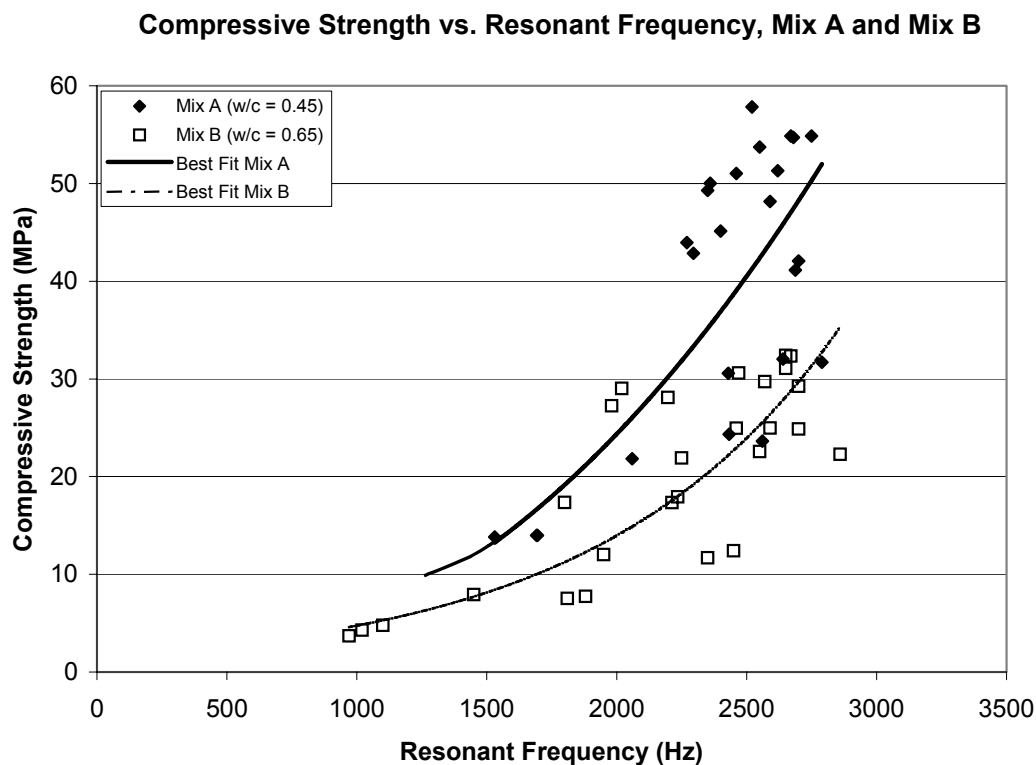


Figure 5.7: Compressive strength vs. resonant frequency for Mixtures A and B

The results did not produce reliable data for the purposes of predicting compressive strength. Most of the cylinders tested produced resonant frequencies in the 2000 to 2600 Hz range, but the corresponding compressive strengths ranged from 12 to 58 MPa.

Table 5.2: Compressive strength vs. resonant frequency of concrete samples.

Compressive Strength (MPa)	Resonant Frequency (Hz)
24.85	2700
24.97	2590
28.10	2197
29.04	2020
27.26	1980
29.25	2700

Table 5.2 shows the distribution of the data. Note that the resonant frequency vs. compressive strength does not follow a particular pattern for the data provided. Thus,

using resonant frequency for predicting the strength of concrete cylinders was not proven to be a viable NDT technique.

A significant relationship was not produced from the data due to the extreme variation of the data points. However, the resonant frequency test was useful for establishing a general trend in the data, and was useful in determining early strength gain in the cylinders. The data grouping at lower ages and compressive strengths experienced less variability than those of higher ages and compressive strengths.

### **Conclusions**

The results of these studies have demonstrated that the ultrasonic pulse velocity technique is a practical method for monitoring the strength of concrete samples. The results of the resonant frequency studies demonstrated that the technique shows some validity for monitoring the strength of early age concrete samples.

The objective of the study was to relate the ultrasonic pulse velocity and resonant frequency to the strength of concrete samples. Presently, there is no acceptable method for the nondestructive determination of concrete strength (Popovics 2001). However, the use of the nondestructive testing methods can successfully monitor the changes within concrete samples in relation to strength increase.

Although the resonant frequency experiment produced less conclusive results than the ultrasonic pulse velocity tests for predicting the strength of concrete cylinders, the technique did produce a general trend for resonant frequency and compressive strength and did show some promise as to the early age testing of concrete for compressive strength. The experiment did have value, as it is a secondary test for the nondestructive testing of concrete samples. Perhaps the value of the resonant frequency technique, is that it can easily be implemented into a laboratory which specializes in NDT. The laboratory

test equipment is relatively inexpensive and quick to implement. From a labor standpoint, the use of the technique is advantageous.

The use of ultrasonic pulse velocity has potential to determine in place strength of concrete materials. However, to achieve an accurate strength verses wave velocity relationship, experiments have to be performed on specific concrete mixture designs in order to create a valid correlation. Presently there is not enough research available correlating ultrasonic wave velocity and concrete mix design.

Most of the research that has been applied to the nondestructive testing of concrete has focused on the abilities and improvement of the method itself. As the applications of NDT methods become more complex, research needs to focus on the interactions of NDT techniques with the concrete material.

Further investigation should be conducted using varying ingredients with varying concrete mixture designs. Additional research may result in a family of curves similar to those produced by this experiment.

## CHAPTER 6 LABORATORY SIMULATION OF DAMAGE OBSERVED IN THE FIELD

This experiment was designed to differentiate between the effects that certain solutions have on field-size samples of concrete when exposed over periods of time. Solid salts do not attack concrete but, when present in solution, can react with the hydrated cement paste. Particularly common are the sulfates of sodium, potassium, magnesium and calcium, which can occur in soil, groundwater or seawater (Neville 1996). The reaction between the salt solution and hydrated cement paste can lead to several material problems with the concrete such as:

- Expansion and cracking
- Strength and mass loss
- Leaching of hydrated cement paste components

The primary objective of this experiment was to observe the effect of concrete exposure to a sulfate solution on ultrasonic wave velocity. Another objective of the experiment was to correlate the effects of such exposure to the physical properties of the concrete and the corresponding NDT data.

### **Prior Research**

Research has been conducted using stress wave propagation methods such as the ultrasonic pulse velocity method and the impact echo method to correlate the stress wave velocity and strength of concrete. Currently there is no research available on the effect of laboratory damage within concrete specimens relative to changes in stress wave velocity. However, concrete samples in field studies suggest that the wave velocity of concrete samples decreases with increasing damage. Despite this, the quantification of the two

parameters has been prevented by the lack of controlled experiments involving continuous laboratory monitoring.

### **Methodology**

While it is known that sulfates tend to reduce wavespeed in concrete when specimens are exposed over time, the exact effect is unknown. Concrete specimens were cast and placed in solutions to observe changes in the material properties.

One set of specimens was partially submersed in sulfate solution to simulate the effect of a harsh environment and its effects on concrete specimens over time. A different set of specimens was concurrently partially submersed in limewater solution to simulate the effect of a control group. Partial submersion was used in an attempt to more closely duplicate field conditions, where complete immersion is rare. By exposing the upper portion of the block to air, an evaporation cycles is created as the surrounding solution is drawn into the bottom portion of the block, migrates upward toward the exposed surface, and then evaporates. This cycle greatly accelerates the ingress of sulfates into the concrete due to the pressure head developed.

### **Procedure**

Two separate groups of concrete specimens were created for this study. The concrete mixture proportions seen in Table 6.1 were used in an attempt to reproduce actual mixture designs used to construct concrete footings and foundations. The larger specimens were cast from the same batches as the cylinders in order to ensure consistency of the concrete used for each design.

Table 6.1: Mixture proportions for NDT and strength tests

<b>Mix Design</b> Volume = 1 m <sup>3</sup>	<b>A</b> 0.45 w/cm	<b>B</b> 0.65 w/cm
<b>Cement</b>	507.7	350.3
<b>Water</b>	228.6	228.6
less M/C sand	0.0	0.0
less M/C aggregate	0.0	0.0
Total	228.6	228.6
<b>Sand</b>	855.1	985.7
plus M/C sand	0.0	0.0
Total sand	855.1	985.7
<b>Aggregate</b>	733.4	626.5
plus M/C aggregate	0.0	0.0
Total aggregate	733.4	626.5
<b>Admixtures</b>		
Superplasticizer (Adva 100)	0.8	0.0
<b>Total</b>	<b>2324.8</b>	<b>2191.2</b>



Figure 6.1: Setup of laboratory experiment

Casting of the concrete specimens took place at the Florida Department of Transportation State Materials Office. As depicted in Figure 6.1, the sample dimensions were 900mm in length by 480mm in height by 245 mm in width. These dimensions varied little between blocks.

After casting, the specimens were transported to the University of Florida for exposure and monitoring. Two concrete samples from each mixture design A and B (4 samples total) were exposed to a 5 percent sulfate solution for a period of 90 days. Two additional samples from each mixture design (4 samples total) were exposed to a limewater solution for a period of 90 days. Exposure consisted of partial submersion in a bath to a depth of 150mm, approximately 1/3 of the total height of the concrete samples. Laboratory temperature was maintained at 22°C.

The testing regimen consisted of regular nondestructive evaluation of the concrete samples at ages of 1 day, and 1, 2, 3, 4, 6, 8, 10, 12, and 13 weeks. The samples were removed from their respective solutions at the age of 90 days. Nondestructive testing was carried out using a James Instruments V-meter Model, ultrasonic pulse velocity meter, and a Germann Instruments Docter-1000 impact echo device. Each of the tests was performed in accordance with the relative ASTM standard (ASTM C597-97, ASTM C1383-98a). Figures 6.2 and 6.3 contain photographs of ultrasonic and impact echo testing on the specimens.

The weekly ultrasonic tests consisted of 15 measurements per specimen. Through width measurements were taken at heights of 75 mm (which corresponded to the mid height of the saturated zone), 240 mm (which was just above the immersion line) and 405 mm (well above the immersion line). Four measurements were made at each height.

The other 3 measurements consisted of through length measurements at the same height intervals stated above. The four through wave velocity measurements at each height were averaged to provide a weekly average wave velocity for that height.



Figure 6.2: Ultrasonic pulse velocity testing on specimen

The weekly impact echo tests consisted of 6 surface wave measurements per specimen. Two measurements were taken at each of three height intervals in order to compare surface wave velocity measurements with through wave velocity measurements. The two surface wave velocities obtained at each height were averaged to provide a weekly value for each height.



Figure 6.3: Impact-echo testing on specimen

Upon completion of the exposure period (90 days), the blocks were removed from their respective solutions and cored. The resulting cores were then trimmed to obtain standard 101mm x 202 mm (4"x 8") cores. These cores were then nondestructively tested with the ultrasonic pulse velocity meter in accordance with ASTM standard C597-97.

Upon the completion of the nondestructive testing on the cylinders they were submerged in a limewater bath for a period of 7 days in order to establish full saturation. Half of the cylinders were tested for compressive strength (in accordance with ASTM C39-01) while the other half were tested in splitting tension (in accordance with ASTM C496-96).

### **Results and Discussion**

Relationships were developed between through wave velocity and surface wave velocity over time. Figures 6.4 and 6.5 are graphical representations of the data obtained for two of the blocks for Mixture A with a water/cement ratio of 0.45

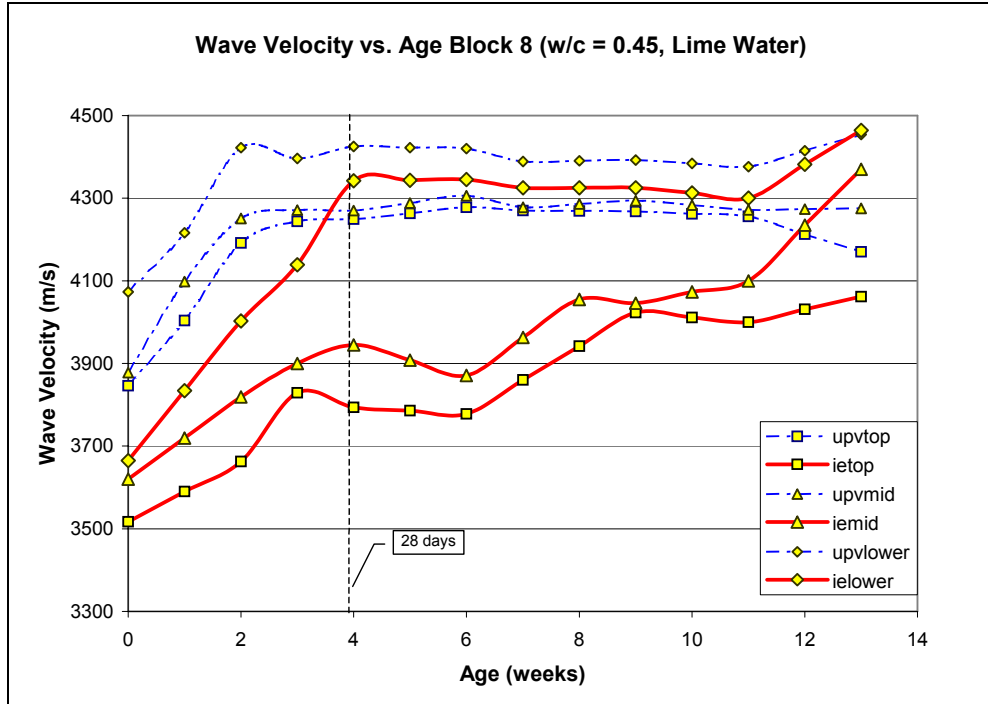


Figure 6.4: Wave velocity vs. age for a sample from Mixture A exposed to limewater.

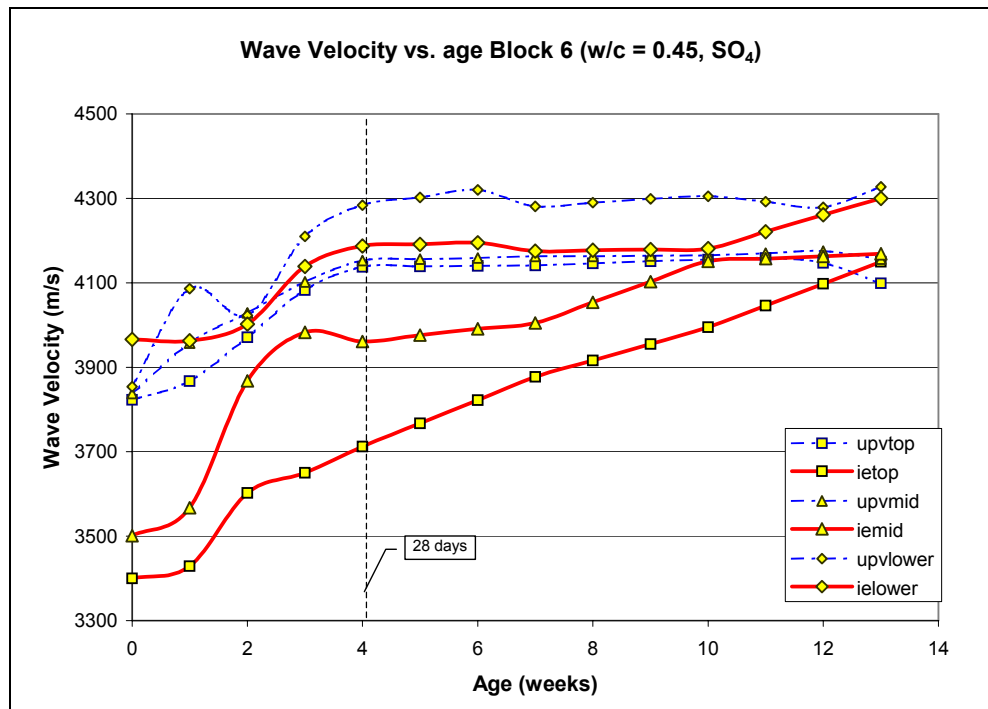


Figure 6.5: Wave velocity vs. age for a sample from Mixture A exposed to sulfate solution.

Figures 6.4 and 6.5 are graphical representations of the average wave velocities per specimen height level for each exposure condition for Mixture A. In the legend, lines names beginning with 'ie' refer to surface wave velocity readings obtained with the impact echo technique. Those beginning with 'upv' represent through wave readings measured with the ultrasonic pulse velocity meter. The figure indicates that the lower wave velocities occur at higher heights on the block. This is to be expected due to segregation during casting. As large samples of concrete are poured, the larger aggregates and denser materials within the matrix tend to migrate toward the bottom, whereas the water and less dense materials tend to migrate toward the top. As stated in Chapter 2, denser materials tend to have higher wave velocities.

Figures 6.4 and 6.5 illustrate a trend appearing in the wave velocity related to height level for the concrete sample. It appears as though the portion of the concrete sample that was constantly immersed in either solution tends to have a more rapid gain in wave velocity for both surface and through wave velocities (ielower, upvlower). This can be attributed to the curing of the lower portion of the sample, as it was constantly immersed in the solution. "In order to obtain good quality concrete, the placing of an appropriate mix must be followed by curing in a suitable environment during the early stages of hardening: (Neville 1996 p. 318). It is likely that the development of higher surface wave velocities in the lower portion of the specimen is due to superior curing.

Permeability variations within the concrete is the most probable explanation for the curing effect not being as prominent for the through wave velocities. The improvement due to curing is a near surface effect that has a continuously decreasing influence relative to distance from the surface.

However, it is possible that that some of the curing effects did permeate upward through the sample. Concrete samples that are kept continuously in air tend to lose strength over time (Neville 1996). At week 12, we see that the through wave velocities at the top levels tend to drop off, whereas the mid-level wave velocities tend to maintain a constant wave velocity. The cause is most likely due to some saturation of the middle portion of the sample, whereas the water did not migrate into the upper portion of the block, instead evaporating out of the vertical surfaces. Therefore, it is likely that little or no curing took place at the upper portions of the specimens.

Evidence of the evaporation cycle was seen in the samples exposed to the sulfate solution. Salt crystals formed in a region approximately 75 mm above immersion line. These crystals were a result of the evaporation of sulfate solution from the surface of the blocks. A similar effect was observed on the blocks exposed to lime water, as the evaporation cycle resulted in the formation of a lime precipitate on the surface of the block. The region containing the lime precipitate was roughly in the same place as the region observed on the samples exposed to sulfate solution.

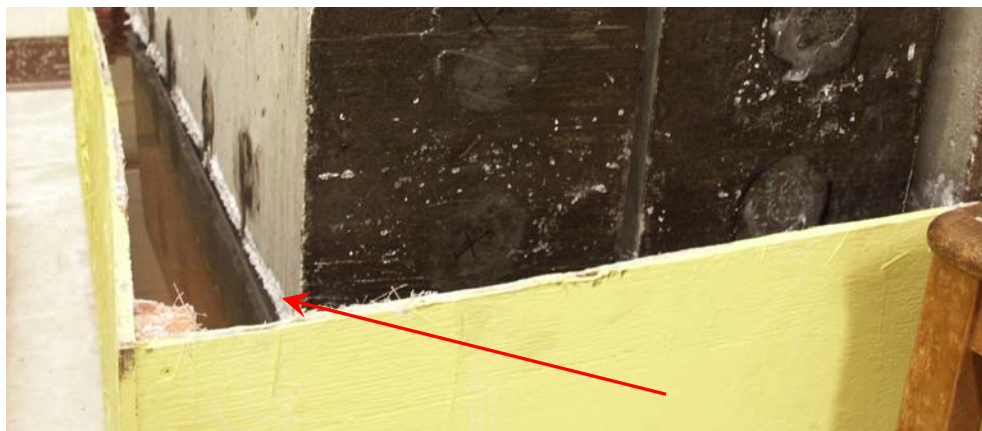


Figure 6.6: Close up view of a sample exposed to sulfate solution. The arrow denotes the area of precipitated salt crystals.

Relationships were developed between through wave velocity and surface wave velocity over time. Figures 6.7 and 6.8 are graphical representations of the data obtained for two of the blocks for Mixture B with a water/cement ratio of 0.65.

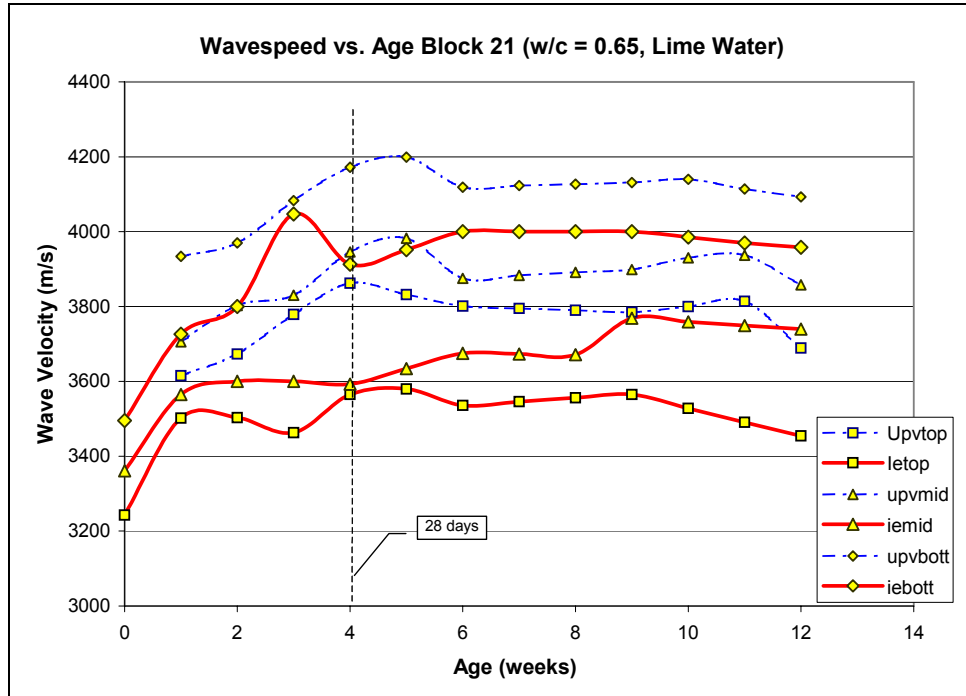


Figure 6.7: Wave velocity vs. age for a sample from Mixture B exposed to limewater

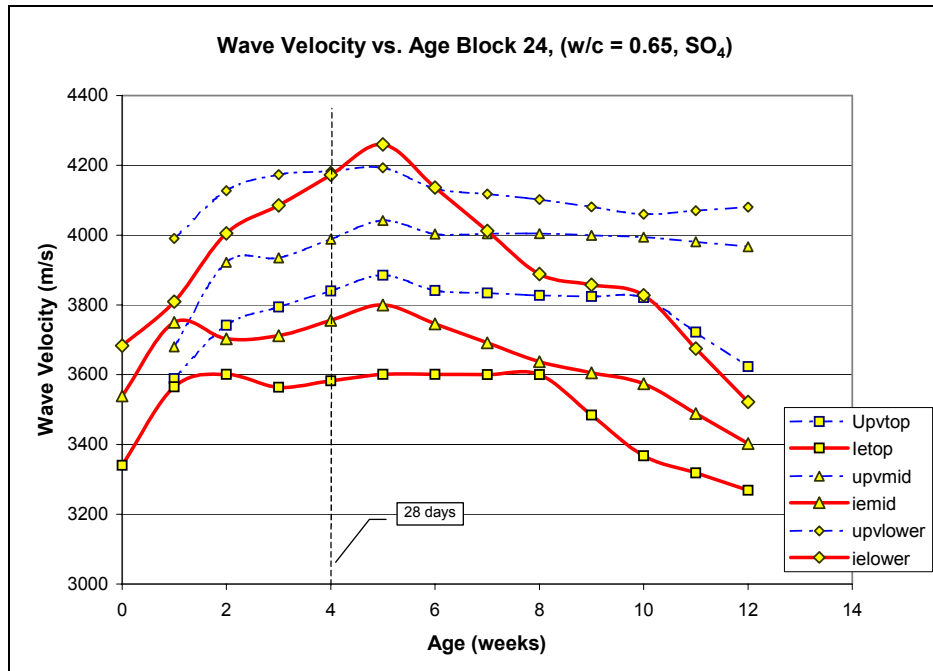


Figure 6.8: Wave velocity vs. age for a sample from Mixture B exposed to sulfate solution

Figures 6.7 and 6.8 are graphical representations of the average wave velocities per specimen height level for each exposure condition for Mixture B. Similar to the results obtained for Mixture A, the lower wave velocities occurred at higher heights on the block. Again, this is due to segregation or migration of the constituents toward the bottom of the concrete specimens during casting.

Figures 6.7 and 6.8 illustrate that the trend developed for wave velocity versus height level for Mixture B was similar to that for Mixture A. It appears as though the portion of the concrete sample that was constantly immersed in either solution tends to have a more rapid gain in wave velocity for both surface and through wave velocities (i.e., lower, up lower). Similar to the effects seen for Mixture A, the week 12 through wave velocities on the top levels for Mixture B tend to decrease compared to previous values, and the mid-level wave velocities tend to remain constant. Again, the cause is most likely due to some saturation of the middle portion of the sample, and no transport of water to the upper portion of the sample.

Results obtained for the samples exposed to limewater exhibited several differences. Mixture A and Mixture B differ in the decay rate of the wavespeeds in the later weeks. Block 21 (from Mixture B) experienced a profound decline in the top-level wavespeeds after week 10. Similar to block 8 (from Mixture A), this is most likely due to the lack of curing in the top portion of the specimen. The larger decay of top-level wavespeeds in Block 21 is most likely due to the higher water/cement ratio. The hydration of the concrete was curtailed because water loss was not prevented in the upper portion of the sample. As discussed in Chapter 5, concretes with lower water/cement ratios are less permeable; Therefore, the samples in Mixture A (0.45 w/c) did not

experience as much water loss as the samples in Mixture B (0.65 w/c), even though the upper levels in each specimen were continuously exposed to air.

Figure 6.8 illustrates that the surface wave velocities for block 24 decayed after week 6. The portion of the block that was submersed in the sulfate solution exhibited a decay of nearly 15 percent. By comparison, the same portion of the block that was exposed to lime water exhibited a negligible decay of wave velocity. However, the upper level of block 24 experienced the same decay in wave velocity as the upper level of block 21. Therefore, it can be concluded that the decay in wave velocity in the lower level of the blocks exposed to sulfate solution is due to the onset of damage caused by sulfate attack.

### **Conclusions**

The results of these studies have demonstrated that there are significant differences between the surface wave velocities and through wave velocities of large-scale concrete samples under different exposure conditions. The study also revealed that it is possible to detect the onset of damage due to sulfate attack on concrete specimens.

The study confirmed that the water / cement ratio does have a dramatic effect on the flow properties within concrete samples which, in turn, has an effect on the durability of the concrete.

Most of the research that has been applied to the nondestructive testing of concrete has focused on the ability and improvement of the method itself. As the applications of NDT methods become more complex it will be necessary for research needs to focus on the interactions of NDT techniques with the concrete material. Further investigation should be conducted using varying ingredients with varying concrete mixture designs as well as varied exposure times to curing solutions and salt solutions.

APPENDIX A  
SUMMARY OF PONTIS RESULTS

UF ID Number	Type	Year	Rating	Length (m)	Inventory List
1	Prestr/String	1961	87.2	171	
2	Slab	1935	98.4	20	
3	Slab	1955	86.9	23	
4	Slab	1950	88.0	14	
5	Slab	1950	88.0	18	
6	Slab	1955	94.8	32	
7	Slab	1960	95.9	18	
8	Slab	1962	91.7	23	
9	Slab	1962	91.7	23	
10	Prestr/Slab	1962	90.8	41	Posted/Closed
11	Prestr/Slab	1962	90.8	31	
12	Prestr/Slab	2001	66.5	28	Func Obs
13	Prestr/String	1961	88.4	85	
14	Slab	1948	92.5	12	
15	Slab	1948	91.5	16	
16	Prestr/Slab	1958	85.2	52	Posted/Closed
17	Prestr/Slab	1955	89.5	29	Posted/Closed
18	Prestr/String	1961	97.4	37	
19	Slab	1944	99.5	59	
20	Slab	1961	85.3	22	Posted/Closed
21	Prestr/String	1960	91.8	30	
22	Slab	1948	86.0	32	
23	Prestr/Slab	1982	69.6	46	
24	Prestr/Slab	1950	92.2	11	
25	Prestr/Slab	1920	97.2	22	
26	Prestr/Slab	1985	73.6	16	
27	Prestr/Slab	1960	87.0	12	
28	Prestr/Slab	1960	85.4	12	
29	Prestr/Slab	1997	72.2	18	
30	Prestr/String	1992	74.5	102	
31	Slab	1960	87.3	14	Posted/Closed
32	Prestr/ChBeam	1950	92.3	9	Posted/Closed
33	Prestr/ChBeam	1960	94.3	6	
34	Prestr/ChBeam	1960	96.8	6	Posted/Closed
35	Prestr/ChBeam	1960	96.8	6	
36	Prestr/ChBeam	1960	87.9	24	Posted/Closed
37	Prestr/ChBeam	1960	96.8	18	
38	Prestr/ChBeam	1960	96.8	18	Posted/Closed
39	Prestr/ChBeam	1960	91.4	15	
40	Prestr/ChBeam	1960	96.9	12	

UF ID Number	Type	Year	Rating	Length (m)	Inventory List
41	Prestr/ChBeam	1955	97.0	13	
42	Prestr/Teebeam	1950	85.0	21	Posted/Closed
43	Prestr/ChBeam	1960	88.0	13	Posted/Closed
44	Slab	1958	90.4	37	
45	Prestr/String	1955	85.8	10	
46	Prestr/String	1958	90.0	16	
47	Prestr/ChBeam	1957	88.5	7	
48	Prestr/Slab	1982	72.5	66	Func Obs
49	Tee Beam	1937	89.7	10	
50	Prestr/ChBeam	1960	86.5	9	
51	Slab	1947	89.1	14	
52	Slab	1947	89.2	9	
53	Slab	1947	89.3	9	
54	Slab	1947	89.4	32	
55	Slab	1947	86.1	19	
56	String-Gir	1963	85.5	82	Func Obs
57	Prestr/String-Gir	1963	90.9	80	
58	Prestr/String-Gir	1963	91.1	37	Func Obs
59	Prestr/String-Gir	2002	36.5	112	
60	Slab	1961	88	31	
61	prestr slab	1962	88.5	46	
62	prestr slab	1962	89.5	73	
63	Prestr/String-Gir	1961	97	44	
64	Slab	1983	49	8	Func Obs
65	Prestr/String-Gir	1962	90.9	91	
66	Prestr/String-Gir	1962	91.1	54	
67	Prestr/String-Gir	1962	87.6	90	
68	Prestr/String-Gir	1962	86.3	54	func Obs
69	Prestr/String-Gir	1962	89.2	52	
70	Prestr/String-Gir	1962	91.5	102	
71	Prestr/String-Gir	1963	86	110	
72	Slab	1987	37.1	18	Posted/Closed
73	Slab	1987	54.1	14	Posted/Closed
74	Slab	1986	50.2	37	Posted/Closed
75	Slab	1987	55.9	9	Posted/Closed
76	Steel String-Gir	1940	86.1	18	
77	Steel String-Gir	1940	86.1	31	
78	Steel String-Gir	1940	86.1	31	
79	Steel String-Gir	1940	86.3	31	
80	prestr slab	1963	88.4	82	Func Obs

UF ID Number	Type	Year	Rating	Length (m)	Inventory List
81	prestr slab	1963	87.4	55	Func Obs
82	Tee Beam	1946	88.4	55	Func Obs
83	Tee Beam	1946	87.4	23	Func Obs
84	Slab	1948	85.1	23	Func Obs
85	Prestr/String-Gir	1961	88.1	69	
86	Tee Beam	1963	88	30	
87	Prestr/String-Gir	1959	86	110	
88	Wood String-Gir	1988	56.2	16	
89	Wood String-Gir	1989	45.7	21	Func Obs
90	Wood String-Gir	1995	53.9	13	Posted/Closed
91	Wood String-Gir	1996	49	13	Posted/Closed
92	Wood String-Gir	1996	58.8	23	Posted/Closed
93	Steel Cont-Gir	1940	88	37	Posted/Closed
94	Wood String-Gir	1996	55.6	24	
95	Tee Beam	2000	75	46	
96	Steel String-Gir	1952	85.2	96	
97	Slab	1984	52.5	27	
98	Slab	1987	45.8	23	Posted/Closed
99	Wood String-Gir	1989	49.6	9	Posted/Closed
100	Steel Spread Box	1994	20.8	16	Posted/Closed
101	Wood String-Gir	1997	72.7	18	
102	Wood String-Gir	1997	72.7	22	
103	Slab	1942	87.1	55	
104	Slab	1942	87.1	55	Func Obs
105	Slab	1942	88.2	55	Func Obs
106	Slab	1942	87	46	
107	Prestr/String-Gir	1986	68	121	Func Obs
108	Prestr/String-Gir	1986	68	121	Func Obs
109	Steel String-Gir	1994	49.5	16	
110	Tee Beam	1922	91.3	10	
111	prestr slab	1960	90.6	11	
112	Prestr/String-Gir	1961	88	43	
113	Prestr/String-Gir	1959	87.2	80	
114	Prestr/String-Gir	1961	89.2	138	
115	Tee Beam	1952	90.2	60	
116	Prestr/String-Gir	1961	86.8	42	
117	Prestr/String-Gir	1960	90.8	138	
118	Prestr/String-Gir	1962	90.6	67	Func Obs
119	Mult Box Beam	1961	88	166	
120	Prestr/String-Gir	1961	86.7	44	

UF ID Number	Type	Year	Rating	Length (m)	Inventory List
121	Prestr/String-Gir	1959	85	55	Func Obs
122	Prestr/String-Gir	1957	87.7	42	Func Obs
123	Prestr/String-Gir	1959	90.9	38	Func Obs
124	Prestr/String-Gir	1958	85	46	
125	Prestr/String-Gir	1959	85	65	
126	Prestr/String-Gir	1959	89.5	37	
127	Prestr/String-Gir	1959	90.6	11	Func Obs
128	Prestr/String-Gir	1959	90.6	49	
129	Prestr/String-Gir	1960	88.9	40	
130	Prestr/String-Gir	1959	87.8	27	
131	Prestr/String-Gir	1959	89.2	20	
132	Prestr/String-Gir	1959	90.5	37	
133	Steel String-Gir	1967	85.7	1	
134	Tee Beam	1925	86.6	13	
135	prestr slab	1924	90.6	19	
136	prestr slab	1926	86.7	59	
137	prestr slab	1957	90.8	18	
138	prestr slab	1960	89.6	51	
139	prestr slab	1955	90.8	37	
140	Wood Truss	1986	72.1	46	
141	Wood Truss	1996	0	45	
142	Arch Deck	1940	91.5	9	
143	Steel String-Gir	1990	38.4	12	Func Obs
144	Steel String-Gir	1991	37.4	12	Posted/Closed
145	Slab	1991	75	18	
146	Wood/String-Gir	1993	25.9	9	
147	Prestr/String-Gir	2002	40	432	
148	Wood Slab	1991	71.5	9	Func Obs
149	Wood Truss	1986	57.2	31	
150	Slab	1957	92.5	37	
151	Prestr/String-Gir	1960	98.8	69	
152	Prestr/String-Gir	1963	91.8	53	Func Obs
153	Prestr/String-Gir	1963	96.9	37	
154	Prestr/String-Gir	1963	92	83	
155	Prestr/String-Gir	1963	92.9	53	Func Obs
156	Prestr/String-Gir	1963	94.9	37	
157	Prestr/String-Gir	1963	95.9	83	
158	Prestr/String-Gir	1960	98.8	80	
159	Prestr/String-Gir	1963	98	69	
160	Prestr/String-Gir	1960	97.4	93	

UF ID Number	Type	Year	Rating	Length (m)	Inventory List
161	Prestr/String-Gir	1960	96	54	
162	Prestr/String-Gir	1960	96.6	71	
163	Prestr/String-Gir	1962	92.9	68	
164	Prestr/String-Gir	1962	92.9	68	
165	Prestr/String-Gir	1961	97.0	44	
166	Prestr/String-Gir	1960	97.4	93	
167	Prestr/String-Gir	1960	96	54	
168	Prestr/String-Gir	1960	96.6	71	
169	Prestr/String-Gir	1962	96.5	42	
170	Prestr/String-Gir	1962	94.5	42	
171	Slab	1941	98	19	
172	Slab	1941	98	28	
173	Slab	1942	95.9	46	
174	Steel String-Gir	1958	93.7	159	
175	Prestr/String-Gir	1962	97	63	
176	Prestr/String-Gir	1962	92.6	94	
177	Prestr/String-Gir	1962	98	92	
178	Prestr/String-Gir	1963	96	58	
179	Prestr/String-Gir	1962	96	68	
180	Prestr/String-Gir	1962	98	92	
181	Prestr/String-Gir	1962	97.2	63	
182	Prestr/String-Gir	1962	93.1	54	
183	Prestr/String-Gir	1962	96.2	54	
184	Prestr/String-Gir	1962	96.6	102	
185	Prestr/String-Gir	1962	92.1	48	
186	Prestr/String-Gir	1962	96.6	38	
187	Prestr/String-Gir	1962	96.6	38	
188	Prestr/String-Gir	1962	95.8	48	
189	Prestr/String-Gir	1963	96	58	
190	Prestr/String-Gir	1963	97.1	110	
191	Prestr Slab	1963	98.9	23	
192	Prestr Slab	1963	98.9	27	
193	Prestr Slab	1963	98.9	23	
194	Prestr Slab	1962	98.9	27	
195	Prestr Slab	1962	98.9	41	
196	Prestr Slab	1963	98.9	46	
197	Prestr Slab	1963	98.9	31	
198	Prestr Slab	1963	98.9	31	Func Obs
199	Prestr Slab	1962	98.9	31	
200	Prestr Slab	1962	98.9	23	

UF ID Number	Type	Year	Rating	Length (m)	Inventory List
201	Prestr Slab	1963	98.9	23	
202	Prestr/String-Gir	1962	97.3	52	
203	Prestr/String-Gir	1962	95.3	117	
204	Prestr/String-Gir	1962	97.3	79	
205	Prestr/String-Gir	1961	97.4	46	
206	Prestr/String-Gir	1962	97.2	116	
207	Prestr/String-Gir	1962	97.3	79	
208	Prestr/String-Gir	1961	97.4	46	
209	Prestr/String-Gir	1962	97.2	52	
210	Prestr/String-Gir	1962	97.3	85	
211	Prestr/String-Gir	1962	97.3	76	
212	Prestr/String-Gir	1962	92.3	85	
213	Prestr/String-Gir	1962	97.4	104	
214	Prestr/String-Gir	1961	99.8	50	
215	Steel String-Gir	1931	97.8	8	
216	Tee Beam	1924	93.2	55	
217	Tee Beam	1939	95.5	60	
218	Tee Beam	1939	99.5	40	
219	Steel String-Gir	1947	97	108	
220	Prestr/String-Gir	1961	100	42	
221	Prestr/String-Gir	1961	96	45	
222	Prestr/String-Gir	1961	99	43	
223	Prestr/String-Gir	1959	94.7	26	
224	Steel String-Gir	1958	95.9	34	
225	Steel String-Gir	1958	94.3	51	
226	Prestr/String-Gir	1961	94.8	60	
227	Prestr Slab	1961	92.4	27	
228	Steel String-Gir	1957	92.4	42	
229	Prestr/String-Gir	1959	95	37	
230	Prestr/String-Gir	1959	95	96	
231	Prestr/String-Gir	1959	95	46	
232	Prestr/String-Gir	1959	94	41	Func Obs
233	Prestr/String-Gir	1957	97	37	
234	Prestr/String-Gir	1959	97	60	
235	Prestr/String-Gir	1960	98	43	
236	Prestr/String-Gir	1960	94.9	43	
237	Cont Slab	1960	96.6	46	
238	Prestr/String-Gir	1960	93.3	58	
239	Steel String-Gir	1961	93.9	116	
240	Prestr/String-Gir	1960	95	42	

UF ID Number	Type	Year	Rating	Length (m)	Inventory List
241	Cont Slab	1960	97	46	
242	Prestr/String-Gir	1960	94.7	41	Func Obs
243	Cont Slab	1960	97	46	
244	Steel String-Gir	1957	91.9	42	
245	Prestr/String-Gir	1959	93	27	
246	Prestr/String-Gir	1959	93	27	
247	Prestr/String-Gir	1959	94.7	37	
248	Prestr/String-Gir	1959	97	60	
249	Prestr/String-Gir	1960	98	43	
250	Prestr/String-Gir	1960	95	40	
251	Prestr/String-Gir	1960	96.8	55	
252	Prestr/String-Gir	1960	91.8	56	
253	Prestr/String-Gir	1960	93.8	43	
254	Prestr Slab	1960	96.6	46	
255	Prestr/String-Gir	1960	93.3	58	
256	Prestr/String-Gir	1961	92.9	116	
257	Prestr/String-Gir	1960	95	42	
258	Prestr/String-Gir	1960	94.7	41	
259	Prestr/String-Gir	1958	97.1	60	
260	Prestr Slab	1957	97.1	34	
261	Prestr Slab	1956	96.3	66	
262	Cont Slab	1960	98.8	40	
263	Tee Beam	1940	96.2	8	
264	Prestr Tee Beam	1950	96.4	14	
265	Prest Chann Beam	1959	94.4	27	
266	Prest Chann Beam	1952	95.4	18	
267	Prest Chann Beam	1955	97.7	18	
268	Prestr Slab	1956	94.5	18	
269	Prest Chann Beam	1955	96.4	18	
270	Prest Chann Beam	1961	97.9	28	
271	Prest Chann Beam	1955	95	38	
272	Prest Chann Beam	1958	93.6	27	
273	Prestr Slab	1960	99.8	13	
274	Slab	1956	99.7	37	
275	Slab	1956	99.7	31	
276	Slab	1956	99.8	37	
277	Prestr Slab	1931	97.9	40	
278	Slab	1922	96	13	
279	Prestr/String-Gir	1965	96	64	
280	Prestr/String-Gir	1958	97.3	736	

UF ID Number	Type	Year	Rating	Length (m)	Inventory List
281	Wood	1984	58.6	7	Func Obs
282	Steel Truss	1997	44	12	Str Def
283	Steel Truss	1997	47	12	Str Def
284	Steel Truss	2001	19.7	18	
285	Steel String-Gird	1994	51.8	20	Str Def
286	Steel Spread Box	1999	38.1	14	
287	Wood/String	1984	56.5	13	Func Obs
288	Wood/String	1984	48.7	13	Func Obs
289	Wood/String	1984	47.7	8	Func Obs
290	Wood/String	1989	51.1	8	Func Obs
291	Wood/String	1986	52.8	8	Func Obs
292	Wood/String	1994	25.9	8	Func Obs
293	Wood/String	1983	43.8	8	Func Obs
294	Wood/String	1994	35.7	7	Func Obs
295	Wood/String	1994	52.9	8	Str Def
296	Wood/String	1994	50.8	8	Str Def
297	Wood/String	2003	40.9	9	Str Def
298	Wood/String	2003	37.9	8	Func Obs
299	Wood/String	1989	50.8	8	Func Obs
300	Wood/String	1991	48.6	8	Func Obs
301	Wood/String	1991	54.2	15	Func Obs
302	Wood/String	1991	56.3	12	Func Obs
303	Wood/String	1991	55.2	8	Func Obs
304	Wood/String	1991	55.2	14	Func Obs
305	Wood/String	1991	54.2	7	Func Obs
306	Wood/String	1995	45.3	7	Func Obs
307	Wood/String	1996	42.9	9	Func Obs
308	Steel String	1996	74.9	53	
309	Wood/String	1987	43.9	17	Func Obs
310	Wood/String	1984	38.9	27	Str Def
311	Wood/String	1984	55.5	7	Posted/Closed
312	Wood/String	1987	44.4	7	Posted/Closed
313	Wood/String	1986	39	7	Str Def
314	Wood/String	1994	57.5	7	Str Def
315	Wood/String-	1986	57.9	22	Str Def
316	Wood/String	1986	55	9	Str Def
317	Wood/String	1985	57.3	36	Str Def
318	Wood/String	1989	38	17	Str Def
319	Wood/String	1990	54.6	21	Str Def
320	Wood/String	1990	50.1	10	Str Def

UF ID Number	Type	Year	Rating	Length (m)	Inventory List
321	Wood/String	1990	54.2	18	Str Def
322	Wood/String	1991	55.8	13	Str Def
323	Wood/String	1991	37.5	13	Str Def
324	Wood/String	1994	35.6	8	Posted/Closed
325	Steel String	1985	52.1	60	Posted/Closed
326	Steel String	1985	57.2	124	Posted/Closed
327	String-Gird	1985	58.8	55	Str Def
328	Wood/String	1985	31.2	13.0	Str Def
329	Wood/String	1990	53.6	7	
330	Steel Spread Box	1997	56.5	20	Fract/Crit
331	Wood/String	1999	40	7	Posted/Closed
332	Wood/String	2001	52.4	18	Posted/Closed
333	Wood/String	2002	55.3	10	Posted/Closed
334	Wood/String	2002	54.7	8	Posted/Closed
335	Wood/String	1986	53.1	24	Posted/Closed
336	Wood/String	1986	55.9	22	Posted/Closed
337	Wood/String	1987	39.9	12	Posted/Closed
338	Wood/String	1987	53.4	32	Posted/Closed
339	Wood/String	1985	47.3	17	Posted/Closed
340	Wood/String	1988	30.9	13	Posted/Closed
341	Wood/String	1984	55	9	Func Obs
342	Wood/String	1984	40	10	Str Def
343	Wood/String	1990	42.2	26	Str Def
344	Wood/String	2002	30.7	9	Func Obs
345	Slab	1962	91.8	7	
346	Slab	1962	91.8	30	
347	Slab	1951	85	36	
348	Steel String-Gird	1951	96.6	84	
349	Steel String-Gird	1949	89.4	69	
350	Steel String-Gird	1949	90.6	92	
351	Slab	1957	86.6	23	
352	Slab	1957	87.3	439	
353	Steel Cont-Gird	1934	85.9	26	
354	Steel Cont-Gird	1949	85.6	61	
355	Slab	1939	96.8	20	
356	Prestr/String-Gird	1958	99.8	44	
357	Prestr/String-Gird	1958	98.8	66	
358	Prestr/String-Gird	1961	85	86	
359	Prestr/String-Gird	1961	96	57	
360	Prestr/String-Gird	1961	90	86	

UF ID Number	Type	Year	Rating	Length (m)	Inventory List
361	Prestr/String-Gird	1961	86.6	57	
362	Prestr/String-Gird	1962	91.5	80	Func Obs
363	Tee Beam	1955	87.8	53	
364	Prestr/String-Gird	1960	85.2	268	
365	Slab	1961	90.9	27	
366	Wood/String	1989	70.9	46	Posted/Closed
367	Steel Truss	1997	74	6	Fract/Crit
368	Steel Truss	1997	74	6	Fract/Crit
369	Steel Truss	1997	74	27	Fract/Crit
370	Steel Truss	1997	74	9	Fract/Crit
371	Steel Truss	2001	71	64	Fract/Crit
372	Steel Truss	2001	71	43	Fract/Crit
373	Steel Truss	2001	71	12	Fract/Crit
374	Steel Truss	2001	71	6	Fract/Crit
375	Steel Truss	2001	71	6	Fract/Crit
376	Steel Truss	2001	71	6	Fract/Crit
377	Steel Truss	2001	71	6	Fract/Crit
378	Steel Truss	2001	71	6	Fract/Crit
379	Steel Truss	2001	71	9	Fract/Crit
380	Steel Truss	2001	71	6	Fract/Crit
381	Steel Truss	2001	71	15	Fract/Crit
382	Steel Truss	2001	71	12	Fract/Crit
383	Steel Truss	2001	71	6	Fract/Crit
384	Steel Truss	2001	71	9	Fract/Crit
385	Steel Truss	2001	71	9	Fract/Crit
386	Steel Truss	2001	71	9	Fract/Crit
387	Steel Truss	2001	71	9	Fract/Crit
388	Steel Truss	2001	71	9	Func Obs
389	Steel Truss	1999	62	9	Fract/Crit
390	Steel String-Gird	1960	97	9	
391	Steel Truss	1996	74.9	46	Fract/Crit
392	Slab	1961	89.7	14	
393	Steel Truss	1950	86.5	34	
394	Wood/String	1988	66.6	12	Posted/Closed
395	Wood/String	1989	69.7	9	Posted/Closed
396	Wood/String	1989	64.5	19	Posted/Closed
397	Steel Spread Box	1993	61.8	21	Fract/Crit
398	Steel Gird/Flow	1993	73.4	21	Fract/Crit
399	Tee Beam	1950	88.6	50	
400	Tee Beam	1955	99.8	141	

UF ID Number	Type	Year	Rating	Length (m)	Inventory List
401	Tee Beam	1955	99.8	50	
402	Slab	1992	60.1	14	
403	Wood/String	1994	65.2	17	
404	Wood/String	1994	65.2	8	
405	Wood/String	2000	71.6	16	
406	Wood/String	2002	68.7	12	
407	Wood/String	2002	74.3	8	
408	Steel Gird	1959	93.8	499	
409	Wood/String	1991	63.4	17	Posted/Closed
410	Wood/String	1947	85.6	15	
411	Channel Beam	1962	86.1	10	Func Obs
412	Channel Beam	1954	100	7	
413	Prestr/String-Gird	1951	86.1	93	Func Obs
414	Steel Truss	2000	74.9	64	Fract/Crit
415	Steel Truss	2000	74.9	19	Fract/Crit
416	Slab	1961	92.4	127	Fract/Crit
417	Tee Beam	1954	95.9	120	
418	Slab	1947	91	9	
419	Slab	1958	93.9	30	Func Obs
420	Slab	1929	92	9	
421	Steel Spread Box	1996	72.7	21	Fract/Crit
422	Steel Spread Box	1996	72.7	14	Fract/Crit
423	Steel Spread Box	1996	70.7	14	Fract/Crit
424	Steel Spread Box	1996	70.7	21	Fract/Crit
425	Steel Spread Box	1996	70.7	21	Fract/Crit
426	Steel Spread Box	1996	70.7	21	Fract/Crit
427	Steel Spread Box	2001	71	18	Fract/Crit
428	Prestr/String-Gird	1962	97.6	466	
429	Prestr/String-Gird	1958	85.7	443	
430	Seg Box Gird	1993	72.3	5871	Posted/Closed
431	Steel Truss	2002	60.6	18	Func Obs
432	Steel Truss	2002	67.7	9	Func Obs
433	Wood/String	1935	88.8	23	
434	Wood/String	1984	72.1	24	Str Def
435	Wood/String	1983	62.8	14	Func Obs
436	Wood/String	1989	74.2	18	
437	Tee Beam	1951	89.1	121	
438	Tee Beam	1949	92.2	101	
439	Tee Beam	1953	97.2	423	
440	Tee Beam	1953	87.5	332	

UF ID Number	Type	Year	Rating	Length (m)	Inventory List
441	Tee Beam	1951	88.5	91	
442	Prestr/String-Gird	1962	99	66	
443	Wood	1988	74.8	17	Posted/Closed
444	Wood/String	1991	67.2	7	
445	Steel String	1960	96	19	
446	Prestr Slab	1960	96	9	
447	Steel String-Gird	1960	88.2	18	
448	Wood/String	1987	68.6	7	Posted/Closed
449	Wood/String	1987	68.3	17	
450	Wood/String	1988	60	23	Func Obs
451	Wood/String	1988	68.4	13	
452	Wood/String	1989	65.2	26	Posted/Closed
453	Wood/String	1989	66.5	13	Posted/Closed
454	Wood/String	1990	73	20	Posted/Closed
455	Wood/String	1992	64.7	22	Posted/Closed
456	Wood/String	1993	71.6	13	Posted/Closed
457	Wood/String	1992	68.8	13	Posted/Closed
458	Steel String-Gird	1960	95	9	
459	Steel Spread Box	1994	65.6	13	Fract/Crit
460	Slab	1963	90.7	31	Posted/Closed
461	Wood/String	1985	60.7	6	Func Obs
462	Wood/String	1985	71.2	8	Posted/Closed
463	Wood/String	1988	59.2	15	Posted/Closed
464	Wood/String	1990	60.2	11	Posted/Closed
465	Wood/String	1992	71.2	15	Str Def
466	Wood/String	1994	71.4	22	Str Def
467	Wood/String	1994	72.2	14	Str Def
468	Wood/String	1995	66.7	12	Str Def
469	Wood/String	1996	63.8	13	Str Def
470	Wood/String	1999	59.7	10	Str Def
471	Wood/String	2002	59.1	20	Str Def
472	Wood/String	1960	85.1	6	Str Def
473	Tee Beam	1953	89.5	141	Str Def
474	Tee Beam	1952	91.6	131	
475	Slab	1994	70.2	8	
476	Steel String-Gird	1930	91.6	31	
477	Slab	1963	93.5	24	
478	Prestr/String-Gird	1963	91.6	44	
479	Prestr/Slab	1954	99.8	36	
480	Prestr/Slab	1954	99.6	36	

UF ID Number	Type	Year	Rating	Length (m)	Inventory List
481	Prestr/Slab	1961	97.2	49	
482	Tee Beam	1956	85	50	
483	Slab	1949	87	24	
484	Tee Beam	1957	87.7	23	
485	Prestr/String-Gird	1962	91.5	45	
486	Prestr/Slab	1962	98.1	46	
487	Prestr/Slab	1963	88.7	46	
488	Prestr/String-Gird	1962	91.5	45	
489	Slab	1957	92.7	8	
490	Prestr/Slab	1954	99.8	36	
491	Slab	1963	91.3	21	
492	Slab	1957	85.1	7	
493	Slab	1993	71.3	11	
494	Prestr/String-Gird	1995	0		
495	Slab	1963	85.4	23	
496	Slab	1962	94.2	18	
497	Steel String-Gird	1956	98.5	60	
498	Steel String-Gird	1956	98.5	60	
499	Prestr/Seg Box Gird	2001	74	909	Func Obs
500	Slab	1958	99.3	18	
501	Prestr/String-Gird	1995	0	173	
502	Prestr/Slab	1963	96.5	47	
503	Prestr/Slab	1959	94.5	32	
504	Prestr/Slab	1954	91.7	27	
505	Slab	1957	92.7	37	
506	Wood/String	1985	23.6	13	Str Def
507	Slab	1959	86	14	
508	Prestr/Slab	1961	91.9	14	
509	Prestr/Slab	1989	71.4	32	
510	Wood/String	1989	39.8	19	Str Def
511	Prestr/Slab	1962	93.5	18	
512	Prestr/Slab	1988	73.2	37.0	
513	Prestr/Slab	1988	74.4	37	
514	Slab	1990	73.1	34	
515	Slab	1990	71.1	34	
516	Slab	1962	89.7	18	Posted/Closed
517	Slab	1962	85.6	31	Posted/Closed
518	Slab	1962	88.6	31	Posted/Closed
519	Slab	1963	95.9	8	
520	Slab	1963	95.9	8	

UF ID Number	Type	Year	Rating	Length (m)	Inventory List
521	Tee Beam	1948	91	81	
522	Slab	1961	87.4	49	
523	Prestr/Slab	1963	94.2	54	
524	Prestr/Slab	1962	89.3	68	Str Def
525	Steel String-Gird	1957	87.6	153	
526	Arch Deck	1925	97	14	
527	Slab	1961	93	14	
528	Slab	1961	91.3	14	
529	Slab	1961	92.4	14	
530	Slab	1961	94.6	14	
531	Prestr/Slab	1958	94.4	61	
532	Slab	1952	87.5	46	
533	Slab	1960	92.9	37	
534	Prestr/Slab-Gird	1961	97.4	62	
535	Prestr/Slab-Gird	1998	18.4	8	Posted/Closed
536	Prestr/Slab	1959	89.4	101	
537	Prestr/Slab	1993	0	76	
538	Prestr/ChBeam	1963	93.8	13	
539	Prestr/String-Gird	1959	91.6	53	
540	Tee Beam	1927	90.7	46	
541	Prestr/Slab	1962	90.6	27	
542	Steel String-Gird	2002	0	56	
543	Steel String-Gird	2002	0	14	
544	Prestr/Slab	1963	96	44	
545	Prestr/Slab	1960	88.3	9	Posted/Closed
546	Prestr	1991	0	68	
547	Slab	1983	44.2	55	Func Obs
548	Slab	1939	91.3	9	
549	Prestr/Slab	1937	93.6	27	
550	Prestr/Slab	1937	93.6	27	
551	Prestr/Slab	1960	92.8	48	
552	Prestr/String-Gird	1959	89.2	94	
553	Prestr/String-Gird	1959	90.7	94	
554	Prestr/String-Gird	1958	95.6	66	
555	Prestr/String-Gird	1961	85.5	456	Func Obs
556	Prestr/String-Gird	1963	92.2	85	Func Obs
557	Prestr/String-Gird	1963	88.1	48	
558	Prestr/String-Gird	1963	88.1	48	Func Obs
559	Prestr/String-Gird	1963	85.9	74	Func Obs
560	Prestr/String-Gird	1960	89.6	27	

UF ID Number	Type	Year	Rating	Length (m)	Inventory List
561	Prestr/String-Gird	1960	91.7	48	
562	Prestr/String-Gird	1960	91.4	49	
563	Prestr/String-Gird	1960	86.1	65	
564	Prestr/String-Gird	1960	93.1	57	
565	Prestr/String-Gird	1959	90.7	73	
566	Prestr/String-Gird	1959	92.3	59	
567	Prestr/String-Gird	1963	97.6	91	
568	Steel String-Gird	1961	97.1	82	
569	Prestr/String-Gird	1960	92.9	46	
570	Prestr/String-Gird	1960	90.3	47	
571	Prestr/String-Gird	1960	91.3	123	
572	Prestr/String-Gird	1960	92.2	58	
573	Prestr/String-Gird	1959	91.8	51	
574	Prestr/String-Gird	1959	93.3	60	
575	Prestr/String-Gird	1963	92.1	85	
576	Prestr/String-Gird	1963	92.2	44	
577	Prestr/ChBeam	1961	88.4	24.0	
578	Prestr/ChBeam	1961	86	16	
579	Prestr/ChBeam	1961	86	16	
580	Prestr/Slab	1988	70.2	15	Func Obs
581	Tee Beam	1942	88.7	9	
582	Prestr/String-Gird	1963	91.3	69	
583	Prestr/String-Gird	1991	74.1	81	Func Obs
584	Prestr/Slab	1984	71.7	13	Func Obs
585	Slab	1989	68.5	12	
586	Prestr/Slab	2003	60.8	17	
587	Prestr/Slab	1990	58.3	27	Func Obs
588	Steel Truss	1998	0	234	
589	Tee Beam	1935	95.9	19	
590	Prestr/String-Gird	1963	95	45	Func Obs
591	Prestr/String-Gird	1963	85.9	87	
592	Prestr/String-Gird	1963	91.2	74	
593	Prestr/String-Gird	1963	95.1	45	
594	Prestr/Slab	1988	66	41	
595	Tee Beam	1931	93.3	12	
596	Slab	1957	90.2	37	
597	Slab	1957	88	25	
598	Slab	1957	85	49	
599	Prestr/String-Gird	1959	93.9	46	
600	Prestr/String-Gird	1959	93.2	100	

UF ID Number	Type	Year	Rating	Length (m)	Inventory List
601	Prestr/String-Gird	1998	20.3	9	Func Obs
602	Prestr/String-Gird	1959	89.4	46	
603	Prestr/ChBeam	1962	89.5	16	
604	Wood/String	1983	54.1	17	Posted/Closed
605	Prestr/String-Gird	1960	95.4	54	
606	Prestr/String-Gird	1960	93.9	101	
607	Prestr/ChBeam	1963	89.9	15	
608	Slab	1956	86.8	41	
609	Prestr/String-Gird	1995	64.6	50	
610	PreStr Slab	1962	33	89.7	Fun Obs
611	PreStr-Str Gir	1960	58	90.2	Fun Obs
612	Slab	1956	46	86.0	
613	PreStr Slab	1960	28	87.7	
614	Slab	1951	31	89.5	
615	Str - Gir	1954	37	87.5	
616	Tee Beam	1948	40	98.0	
617	Tee Beam	1948	40	85.0	
618	Slab	1959	27	95.3	
619	PreStr-Str Gir	1961	30	99.0	
620	Slab	1960	36	88.1	
621	Slab	1960	38	90.0	
622	Slab	1960	37	87.7	
623	Slab	1959	27	95.1	
624	PreStr-Str Gir	1960	40	88.0	
625	PreStr-Str Gir	1961	54	95.4	
626	PreStr-Str Gir	1959	347	85.0	
627	PreStr-Str Gir	1961	57	88.6	Fun Obs
628	PreStr-Str Gir	1961	42	88.0	Fun Obs
629	PreStr-Str Gir	1961	343	88.0	
630	PreStr Slab	1961	56	96.1	
631	Slab	1959	44	95.5	
632	Slab	1959	40	95.1	
633	Slab	1961	48	87.6	
634	PreStr Slab	1958	21	85.7	
635	Type	Year		Rating	
636	PreStr Slab	1956	24	85.5	
637	PreStr-Str Gir	1959	49	86.9	
638	Arch Deck	1956	17	95.2	
639	Slab	1951	77	92.6	
640	PreStr-Str Gir	1996	748	61.9	Fun Obs

UF ID Number	Type	Year	Rating	Length (m)	Inventory List
641	PreStr-Str Gir	1995	748	60.7	Fun Obs
642	Slab	1960	8	86.2	
643	Slab	1960	21	97.0	
644	PreStr-Str Gir	1959	121	93.3	
645	Slab	1960	90	87.1	
646	Tee Beam	1960	40	97.0	
647	PreStr Slab	1962	79	98.5	
648	PreStr Slab	1960	91	93.0	
649	PreStr Slab	1960	25	92.4	
650	Slab	1950	22	88.9	
651	Seg-Box Gir	1991	2521	62	
652	Slab	1988	613	74.0	
653	Slab	2000	61	33.7	Fun Obs
654	Tee Beam	1956	139	96.4	
655	PreStr-Box Gir	1982	4923	73.0	
656	PreStr-Box Gir	1983		72.0	
657	Tee Beem	1922	94.9	31	
658	Prestr/Channel	1961	90.4	41	
659	Prestr/Channel	1963	86.5	24	
660	Stringer Girder	1962	99.4	190	
661	Prestr/Channel	1960	85.4	26	
662	Prestr/Channel	1982	52.8	45	Deficient List
663	Tee Beem	1982	93.1	20	
664	Prestr/Girder	1982	95.8	83	Deficient List
665	Prestr/Girder	1982	95.8	83	Deficient List
666	Prestr/String	1981	93.2	474	Deficient List
667	Cont.Girder	1997	97.3	4226	Deficient List
668	Prestr/String	1988	66.1	100	
669	Prestr/Channel	1960	90.2	9	
670	Prestr/Slab	1982	76.8	11	Deficient List
671	Culvert	1957	98.6	8	
672	Conc Slab	1941	85.7	14	
673	Tee Beem	1926	85.7	13	
674	Stayed Girder	1986	63.9	6668	Deficient List
675	Cont.Girder	1991	89	4846	Deficient List
676	Prestr/Slab	1958	91.6	10	Closed/Posted
677	Conc Slab	1928	89.5	66	
678	Prestr/Girder	1956	99	79	
679	Prestr/Girder	1957	99.8	78	
680	Prestr/Girder	1922	93.8	64	
681	Prestr/Girder	1962	92	41	
682	Prestr/Girder	1961	91.9	58	Func/Obs
683	Prestr/Girder	1959	89.5	58	
684	Steel Girder	1952	89.3	65	
685	Prestr/Girder	1962	89	41	
686	Steel Girder	1957	87.7	165	Fracture Crit.
687	Prestr/Girder	1962	86.1	44	Func/Obs

APPENDIX B  
SUMMARY OF DEFICIENT BRIDGES

UF ID Number	Year	Rating	Deck	SuperS	SubS	Channel	Type
609	1995	64.6	7	8	8	8	prestressed str-girder
26	1985	73.6	7	7	7	7	prestressed slab
30	1992	74.5	7	7	7	7	prestressed str-girder
29	1997	89.2	7	7	7	7	prestressed slab
73	1987	54	6	6	6	6	slab
74	1986	50.2	6	6	6	6	slab
75	1987	62.1	6	6	6	6	slab
97	1984	52.7	6	6	6	7	slab
98	1987	45.8	5	5	6	7	slab
145	1991	75	6	6	6	6	slab
475	1994	70.2	8	8	8	8	slab
512	1988	73.2	7	7	7	7	prestressed slab
513	1988	74.4	7	7	7	7	prestressed slab
514	1990	73.1	7	7	7	7	slab
515	1990	71.1	7	7	7	7	slab
652	1988	79	7	7	7	7	slab
655	1982	73	7	6	7	8	prestressed str-girder
656	1983	72	7	6	6	9	prestressed str-girder
651	1991	62	8	8	8	8	continuous box girder
668	1988	66.1	7	7	7	7	prestressed str-girder
	1982	51.8	7	6	7	7	Channel Beam
674	1986	63.9	6	6	5	7	Continuous stayed girder

APPENDIX C  
NDT DATA AND RESULTS FROM BRIDGE TESTING

Data Sheet for Bahia Honda Bridge

Date: 5/20/2003

Location: Column Tomography Row A (Top Row)

Point #	UPV Time ( $\mu$ s)	Distance (ft)	UPV Wavespeed (m/s)
1-5	247.4	43.66	4482.47
1-6	268.5	47.51	4494.43
1-7	268.4	47.51	4496.10
1-8	247.0	43.66	4489.73
2-6	247.2	43.66	4486.10
2-7	267.8	47.51	4506.18
2-8	268.5	47.51	4494.43
2-9	245.9	43.66	4509.82
3-7	246.8	43.66	4493.37
3-8	267.6	47.51	4509.54
3-9	267.1	47.51	4517.99
3-10	246.4	43.66	4500.67
4-8	247.2	43.66	4486.10
4-9	265.0	47.51	4553.79
4-10	266.3	47.51	4531.56
4-11	246.0	43.66	4507.98
5-9	242.1	43.66	4580.60
5-10	266.1	47.51	4534.96
5-11	267.9	47.51	4504.49
6-10	244.8	43.66	4530.08
6-11	268.4	47.51	4496.10
7-11	248.3	43.66	4466.23

Data Sheet for Bahia Honda Bridge

Date: 5/20/2003

Location: Column Tomography Row B

Point #	UPV Time ( $\mu$ s)	Distance (in)	UPV Wavespeed (m/s)
1-5	249.6	43.66	4442.96
1-6	269.1	47.51	4484.41
1-7	316.4	47.51	3814.01
1-8	245.7	43.66	4513.49
2-6	247.1	43.66	4487.92
2-7	316	47.51	3818.84
2-8	267.4	47.51	4512.92
2-9	245.8	43.66	4511.65
3-7	299	43.66	3708.91
3-8	265.3	47.51	4548.64
3-9	265.4	47.51	4546.93
3-10	245.4	43.66	4519.01
4-8	242.2	43.66	4578.71
4-9	261.5	47.51	4614.74
4-10	265.7	47.51	4541.79
4-11	246.5	43.66	4498.84
5-9	240.5	43.66	4611.08
5-10	266.6	47.51	4526.46
5-11	267.2	47.51	4516.29
6-10	240.5	43.66	4611.08
6-11	266.2	47.51	4533.26
7-11	290	43.66	3824.01

## Data Sheet for Bahia Honda Bridge

Date: 5/20/2003

## Column Tomography Row C

Point #	UPV Time ( $\mu$ s)	Distance (ft)	UPV Wavespeed (m/s)
1-5	246.5	43.66	4498.84
1-6	265.5/359.1	47.51	#VALUE!
1-7	267.5	47.51	4511.23
1-8	266	43.66	4169.04
2-6	242.1/302.2	43.66	#VALUE!
2-7	264.3	47.51	4565.85
2-8	266.2	47.51	4533.26
2-9	250.9	43.66	4419.94
3-7	239.8	43.66	4624.54
3-8	267.1	47.51	4517.99
3-9	271.1	47.51	4451.32
3-10	249.9	43.66	4437.63
4-8	242.3	43.66	4576.82
4-9	266	47.51	4536.67
4-10	268.9	47.51	4487.74
4-11	357.5	43.66	3102.00
5-9	239.1	43.66	4638.08
5-10	265	47.51	4553.79
5-11	345.9	47.51	3488.74
6-10	240.1/511.7	43.66	#VALUE!
6-11	357.7/546.7	47.51	#VALUE!
7-11	360.3	43.66	3077.89

## Data Sheet for Bahia Honda Bridge

Date: 5/20/2003

## Column Tomography Row D

Point #	UPV Time ( $\mu$ s)	Distance (ft)	UPV Wavespeed (m/s)
1-5	244.5	43.66	4535.64
1-6	265.2	47.51	4550.35
1-7	323.3	47.51	3732.61
1-8		43.66	
2-6	243.9	43.66	4546.80
2-7	351.9	47.51	3429.25
2-8		47.51	
2-9		43.66	
3-7	377.3	43.66	2939.21
3-8		47.51	
3-9		47.51	
3-10		43.66	
4-8		43.66	
4-9		47.51	
4-10		47.51	
4-11	325.3	43.66	3409.05
5-9		43.66	
5-10		47.51	
5-11		47.51	
6-10		43.66	
6-11		47.51	
7-11		43.66	

## Data Sheet for Bahia Honda Bridge

Date: 5/20/2003

## Column Tomography Row E

Point #	UPV Time ( $\mu$ s)	Distance (ft)	UPV Wavespeed (m/s)
1-5	240.5	43.66	4611.08
1-6	258.0	47.51	4677.34
1-7	264.0	47.51	4571.04
1-8		43.66	
2-6	240.2	43.66	4616.84
2-7	261.6	47.51	4612.97
2-8		47.51	
2-9		43.66	
3-7	235.8	43.66	4702.99
3-8		47.51	
3-9		47.51	
3-10		43.66	
4-8		43.66	
4-9		47.51	
4-10		47.51	
4-11		43.66	
5-9		43.66	
5-10		47.51	
5-11		47.51	
6-10		43.66	
6-11		47.51	
7-11		43.66	

## Data Sheet for Bahia Honda Bridge

Date: 5/20/2003

## Column Tomography Row F (Bottom Row)

Point #	UPV Time ( $\mu$ s)	Distance (ft)	IE Wavespeed (m/s)
1-5	235.9	43.66	4700.99
1-6	258.6	47.51	4666.49
1-7	261.0	47.51	4623.58
1-8		43.66	
2-6	235.7	43.66	4704.98
2-7	260.3	47.51	4636.01
2-8		47.51	
2-9		43.66	
3-7	233.9	43.66	4741.19
3-8		47.51	
3-9		47.51	
3-10		43.66	
4-8		43.66	
4-9		47.51	
4-10		47.51	
4-11	280.3	43.66	3956.35
5-9		43.66	
5-10		47.51	
5-11	263.0	47.51	4588.42
6-10		43.66	
6-11	262.6	47.51	4595.41
7-11	242.4	43.66	4574.93

Data Sheet for Bridge TestingDate: 5/20/2003Bahia Honda BridgeImpact Echo Column Data

Point #	IE Wavespeed (m/s)	IE Wavespeed (m/s)
	Row B	Row E
1	3711	3789
2	3583	4000
3	3673	3893
4	3812	4261
5	3602	3831
6	3916	4001
7	4187	3801
8	4188	4100
9	3851	
10	4092	
11	3750	3800

Data Sheet for Bridge TestingDate: 5/20/2003Bahia Honda BridgeImpact Echo Pile Cap Data

Point #	Distance (ft)	IE Wavespeed (m/s)
1	1.5	3514
2	1.5	3788
3	4.0	3279
4	4.0	3770
5	6.5	3445
6	6.5	3463

Data Sheet for Bridge TestingDate: 5/20/2003Bahia Honda BridgeUltrasonic Pile Cap Data

Point #	UPV Time ( $\mu$ s)	Distance (in)	IE Wavespeed (m/s)
1	647.3	96	3767.03
2	664.2	96	3671.18
3	661.7	96	3685.05
4	668.5	96	3647.57
5	624	96	3907.69
6	662.4	96	3681.16
7	723.1	96	3372.15
8	662.7	96	3679.49

## Data Sheet for Bridge Testing

Date: 5/20/2003

Bahia Honda Bridge

Ultrasonic Tomographic Crack Data from Column

## Row B

Point #	UPV Time ( $\mu$ s)	Distance (in)	Length Traveled (in)
1-7	316.4	47.51	54.06
2-7	316	47.51	53.99
3-7	299	43.66	51.09
7-11	290	43.66	49.55

## Row C

Point #	UPV Time ( $\mu$ s)	Distance (in)	Length Traveled (in)
1-6	265.5/359.1	47.51	61.36
2-6	242.1/302.2	43.66	51.64
6-10	240.1/511.7	43.66	87.43
6-11	357.7/546.7	47.51	93.41
7-11	360.3	43.66	61.56

## Row D

Point #	UPV Time ( $\mu$ s)	Distance (in)	Length Traveled (in)
2-7	351.9	47.51	60.13
3-7	377.3	43.66	64.47
4-11	325.3	43.66	55.58

## Data Sheet for Niles Channel Bridge

Date 5/20/2003

## Column Tomography Using Ultrasonic Pulse Velocity

Point #	UPV Time ( $\mu$ s)	Distance (in)	UPV Wavespeed (m/s)	IE Wavespeed (m/s)
S1	148.4	26	4450.13	4001
S2	150.5	26	4388.04	3840
S3	151.4	26	4361.96	3911
S4	159.6	26	4137.84	3892
S5	151	26	4373.51	4175
S6	151.1	26	4370.62	4001
S7	151.6	26	4356.20	3944
S8	151.8	26	4350.46	4056
S9	154.7	26	4268.91	3608
S10	149.2	26	4426.27	4001
S11	150.1	26	4399.73	3827
S12	150.4	26	4390.96	3998
S13	151.2	26	4367.72	3894
S14	304.4	26	2169.51	4298
S15	149.8	26	4408.54	3839
S16	153.2	26	4310.70	3842
S17	150.7	26	4382.22	3617
S18	332.2	26	1987.96	3998
S19	331.8	26	1990.36	3944
S20	325	26	2032.00	N/A

## Data Sheet for Niles Channel Bridge

Date 5/20/2003

## Surface wave velocities using impact echo

Point #	IE Wavespeed (m/s)
N Col 1	3841.00
N Col 2	4058.00
N Col 3	3601.00
N Col 4	4113.00
N Col 5	3759.00
N Col 6	3998.00
S Col 1	4000.00
S Col 2	4090.00
S Col 3	4014.00
S Col 4	4068.00
S Col 5	4056.00
S Col 6	4000.00

## Data Sheet for Bridge Testing, Sebastian River Bridge

Date: 6/12/2003

NDT Data from Column 11-4 North to South

Point #	UPV Time (ms)	UPV Wavespeed (m/s)	IE Wavespeed (m/s)	Hammer #
S1	592	986.8	4000.0	
S2	180.6	3234.8		52
S3	174.9	3340.2	difficulty/thru wave	44
S4	136.8	4270.5		
S5	802	728.4	N/A	
S6	345.2	1692.4		48
S7	226	2585.0		48
S8	136.7	4273.6		
S9	254	2300.0	2436.0	
S10	548/1600	#REF!		42
S11	175.5	3328.8		52
S12	132.2	4419.1		
S13	596	980.2		
S14	608	960.9	2535.0	38
S15	408	1431.9		49
S16	132.6	4405.7		
S17	144.8	4034.5		
S18	138.3	4224.2		
S19	438	1333.8		34
S20	132.8	4399.1		42

## Data Sheet for Bridge Testing, Sebastian River Bridge

Date: 6/12/2003

NDT Data from Column 11-4 East to West

Point #	UPV Time (ms)	UPV Wavespeed (m/s)	Hammer #
W1	351	1664.4	
W2	420	1391.0	52
W3	248	2355.6	52
W4	139.2	4196.8	
W5	356	1641.0	
W6	309	1890.6	49
W7	265	2204.5	51
W8	306	1909.2	
W9	219	2667.6	
W10	449	1301.1	53
W11	345	1693.3	50
W12	335	1743.9	
W13	934	625.5	
W14	273	2139.9	40
W15	753	775.8	44
W16	446	1309.9	
W17	407	1435.4	
W18	251	2327.5	
W19	146.9	3976.9	46
W20	248	2355.6	44

## Data Sheet for Bridge Testing, Sebastian River Bridge

Date: 6/12/2003

## NDT Data from Column 11-5 North to South

Point #	UPV Time (ms)	UPV Wavespeed (m/s)	IE Wavespeed (m/s)	Hammer #
S1	176.4	4463.7		
S2	182	4326.4	3979	52
S3	183.6	4288.7		55
S4	178.8	4403.8		
S5	173.6	4535.7	4366	
S6	183	4302.7		54
S7	184.3	4272.4		54
S8	174.4	4514.9		
S9	174.4	4514.9		
S10	184.1	4277.0	5296	54
S11	183.2	4298.0		50
S12	174.6	4509.7		
S13	166.1	4740.5		
S14	180.2	4369.6	3600	54
S15	179.1	4396.4		56
S16	174.1	4522.7		
S17	173.3	4543.6		
S18	177.6	4433.6		54
S19	173.6	4535.7		45
S20	172.6	4562.0	4298	

## Data Sheet for Bridge Testing, Sebastian River Bridge

Date: 6/12/2003

## NDT Data from Column 11-5 East to West

Point #	UPV Time (ms)	UPV Wavespeed (m/s)	Hammer #
W1	174.1	4376.8	
W2	183.2	4159.4	56
W3	184.3	4134.6	54
W4	177.1	4302.7	
W5	176.8	4310.0	
W6	186.3	4090.2	51
W7	182.8	4168.5	54
W8	176.8	4310.0	
W9	175.1	4351.8	
W10	186.8	4079.2	51
W11	186.2	4092.4	32
W12	175.7	4336.9	
W13	173.3	4397.0	
W14	182.4	4177.6	54
W15	180.2	4228.6	53
W16	172.1	4427.7	
W17	169.9	4485.0	
W18	174.5	4366.8	52
W19	176.2	4324.6	54
W20			

## Data Sheet for Bridge Testing, Wabasso Bridge

Date: 6/13/2003

## NDT Data Pile Cap 5 Grid #1

Point #	IE Wavespeed (m/s)	Hammer #
1-1	2647	45
1-2	2536	46
1-3	2405	45
1-4	2419	35
2-1	2342	40
2-2	2250	40
2-3	2233	46
2-4	2307	48
3-1	2500	52
3-2	2028	48
3-3	2229	48
3-4	2199	48
4-1	2267	42
4-2	2312	39
4-3	2368	47
4-4	2950	48

## Data Sheet for Bridge Testing, Wabasso Bridge

Date: 6/13/2003

## NDT Data Pile Cap 5 Grid #2

Point #	IE Wavespeed (m/s)	Hammer #
1-1	2338	46
1-2	2369	49
1-3	2275	46
1-4	2466	46
2-1	2951	49
2-2	2535	41
2-3	2774	50
2-4	2250	48
3-1	3052	49
3-2	2400	52
3-3	2360	49
3-4	2770	50
4-1	2500	50
4-2	2743	47
4-3	2902	52
4-4	2686	48

Data Sheet for Bridge Testing, Wabasso BridgeDate: 6/13/2003

## NDT Data Column 5 Grid #3

Point #	IE Wavespeed (m/s)	Hammer #
1-1	2465	54
1-2	2916	62
1-3	2441	62
1-4	2457	60
2-1	3214	54
2-2	3117	58
2-3	3477	60
2-4	3326	62
3-1	3159	64
3-2	3600	58
3-3	2608	64
3-4	3829	58
4-1	3157	58
4-2	3601	58
4-3	3611	53
4-4	3529	55

## Data Sheet for Bridge Testing

Date: 6/14/2003

Sebastian Inlet Bridge

NDT Data Pilecap #12 Grid 1

Point #	IE Wavespeed (m/s)	Hammer #
1-1	2697	48
1-2	3829	44
1-3	3274	38
1-4	3808	50
2-1	2687	44
2-2	3831	42
2-3	3808	43
2-4	3751	50
3-1	3529	46
3-2	4000	48
3-3	3333	46
3-4	4000	46
4-1	3810	46
4-2	3894	50
4-3	3829	56
4-4	3764	49

## Data Sheet for Bridge Testing

Date: 6/14/2003

Sebastian Inlet Bridge

NDT Data Pilecap #16 Grid 3

Point #	IE Wavespeed (m/s)	Hammer #
1-1	3421	44
1-2	3573	44
1-3	3729	52
1-4	3991	42
2-1	3399	40
2-2	3253	52
2-3	3751	50
2-4	3908	52
3-1	4023	44
3-2	3821	45
3-3	3753	47
3-4	4120	46
4-1	3406	43
4-2	3329	43
4-3	3501	52
4-4	3299	52

## Data Sheet for Bridge Testing

Date: 6/14/2003

Sebastian Inlet Bridge

NDT Data Pilecap #12 Grid 2

Point #	IE Wavespeed (m/s)	Hammer #
1-1	3231	44
1-2	3461	46
1-3	3758	48
1-4	3907	47
2-1	3300	44
2-2	4032	44
2-3	3971	46
2-4	3763	46
3-1	3333	47
3-2	3821	52
3-3	3653	46
3-4	2781	47
4-1	3521	48
4-2	3675	48
4-3	3803	47
4-4	3731	45

## Data Sheet for Bridge Testing

Date: 6/14/2003

Sebastian Inlet Bridge

NDT Data Pilecap #12 Grid 1

Point #	IE Wavespeed (m/s)	Hammer #
1-1		50
1-2		48
1-3		50
1-4		52
2-1		54
2-2		55
2-3		52
2-4		50
3-1		53
3-2		50
3-3		48
3-4		46
4-1		50
4-2		54
4-3		54
4-4		52

## Data Sheet for Bridge Testing

Date: 6/14/2003

Sebastian Inlet Bridge

Column Tomography Data

Point #	UPV Time (ms)					
	Row A	Row B	Row C	Row D	Row E	Row F
1-5	246.7	231.2	515.8	424.6	552.0	401.0
1-6	251.8	241.5	449.3	481.6	646.9	740.0
1-7	228.8	217.9	341.6	343.7	820.2	402.5
2-6	248.4	237.7	239.8	234.8	454.0	616.0
2-7	251.7	241.6	293.5	242.6	399.6	427.9
2-8	231.5	212.8				
3-7	243.9	237.6				
3-8	255.6	241.7				
3-9	233.6	249.8				
4-8	249.1	239.2				
4-9	252.6	238.9				
4-1	211.9	192.8	436.3	251.9	382.0	294.9
5-9	249.5	236.4				
5-2	215.6	201.0				
3-6	213.8	204.7	294.5	199.5	320.0	457.3

## Data Sheet for Bridge Testing

Date: 6/14/2003

Sebastian Inlet Bridge

Column Tomography Calculations

Point #	UPV Time (ms)	Wavespeed (m/s)	UPV Time (ms)	Wavespeed (m/s)	UPV Time (ms)	Wavespeed (m/s)
	Row A		Row B		Row C	
1-5	246.7	3649.898662	231.2	3894.593426	515.8	1745.696006
1-6	251.8	3575.972994	241.5	3728.488613	449.3	2004.073002
1-7	228.8	3460.305944	217.9	3633.400642	341.6	2317.675644
2-6	248.4	3624.919485	237.7	3788.094236	239.8	3754.920767
2-7	251.7	3577.393723	241.6	3726.945364	293.5	3067.9046
2-8	231.5	3419.948164	212.8	3720.479323		
3-7	243.9	3691.799918	237.6	3789.688552		
3-8	255.6	3522.809077	241.7	3725.403393		
3-9	233.6	3389.203767	249.8	3169.407526		
4-8	249.1	3614.733039	239.2	3764.339465		
4-9	252.6	3564.647664	238.9	3769.066555		
4-1	211.9	3736.281265	192.8	4106.421162	436.3	1814.618382
5-9	249.5	3608.937876	236.4	3808.92555		
5-2	215.6	3672.16141	201.0	3938.895522		
3-6	213.8	3703.077643	204.7	3867.699072	294.5	2688.34635

APPENDIX D  
LABORATORY DATA OF CYLINDER SPECIMENS

Raw Data for Cylinder Samples w/c ratio = 0.45

Load (N)	Compressive Strength (Mpa)	UPV Time ( $\mu$ s)	Impact Echo Wave Speed (m/s)	Resonant Frequency (Hz)	Age
112095.2	13.83	56.7	3580.2	1530	1 day
113420.8	13.99	55.4	3646.2	1695	
113563.1	14.01	54.1	3678.4	1692	
177003.6	21.83	50.9	3988.2	2060	3 days
191576	23.63	49.5	4020.2	2561	
197309.8	24.34	50.8	3976.4	2433	
259776.2	32.04	47.2	4279.7	2640	7days
247988.4	30.59	46.6	4291.8	2430	
256929.3	31.69	47.0	4297.9	2790	
341054.1	42.07	45.3	4437.1	2700	14days
333678.9	41.16	46.3	4384.4	2687	
347357.2	42.84	50.0	4020.0	2295	
390424.9	48.16	46.5	4311.8	2590	21days
356467.2	43.97	46.8	4359.0	2270	
399623.8	49.29	46.5	4344.1	2350	
413720.2	51.03	45.5	4461.5	2460	28 days
405508.8	50.02	46.1	4425.2	2360	
365817.3	45.12	46.2	4415.6	2400	
444822.2	54.86	45.3	4470.2	2670	45days
444822.2	54.86	45.2	4458.0	2750	
443554.5	54.71	45.3	4448.1	2680	
416020	51.31	45.6	4429.8	2620	60 days
435698.9	53.74	45.6	4429.8	2550	
469002.7	58	46.0	4391.3	2520	

Calculations for Predicted Strength Data Using obtained  
Laboratory Data Mixture A (w/c = 0.45)

Wave Velocity Observed (km/s)	Predicted Strength (MPa) by Author			Actual Compressive Strength (Mpa)
	Yan	Qaswari	Pessiki	
3.580	15.84	2.39	18.03	13.83
3.646	17.57	4.81	19.91	13.99
3.678	18.48	5.99	20.90	14.01
3.988	30.08	17.37	33.28	21.83
4.020	31.63	18.54	34.92	23.63
3.976	29.53	16.94	32.70	24.34
4.280	47.56	28.07	51.53	32.04
4.292	48.48	28.52	52.48	30.59
4.298	48.94	28.74	52.96	31.69
4.437	60.92	33.85	65.24	42.07
4.384	56.08	31.92	60.29	41.16
4.020	31.62	18.54	34.91	42.84
4.312	50.03	29.25	54.08	48.16
4.359	53.88	30.98	58.04	43.97
4.344	52.63	30.44	56.76	49.29
4.462	63.30	34.75	67.67	51.03
4.425	59.79	33.41	64.09	50.02
4.416	58.89	33.06	63.17	45.12
4.470	64.17	35.07	68.56	54.86
4.458	62.95	34.62	67.31	54.86
4.448	61.98	34.26	66.33	54.71
4.430	60.23	33.59	64.53	51.31
4.430	60.23	33.59	64.53	53.74
4.391	56.69	32.17	60.92	57.85

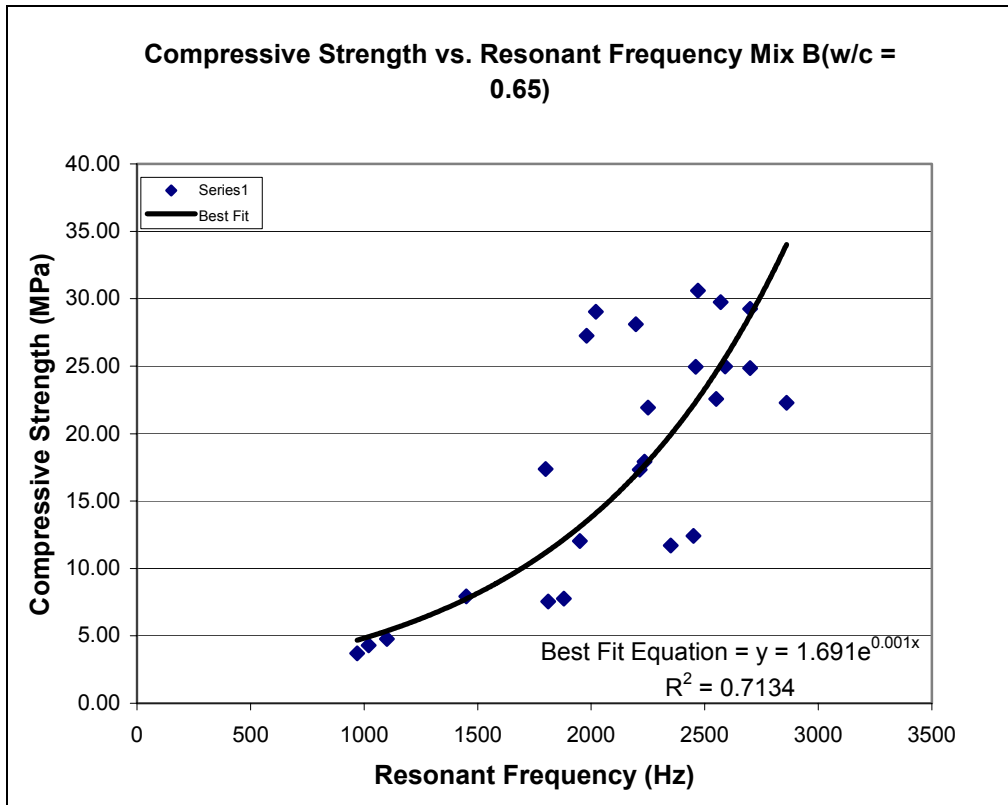
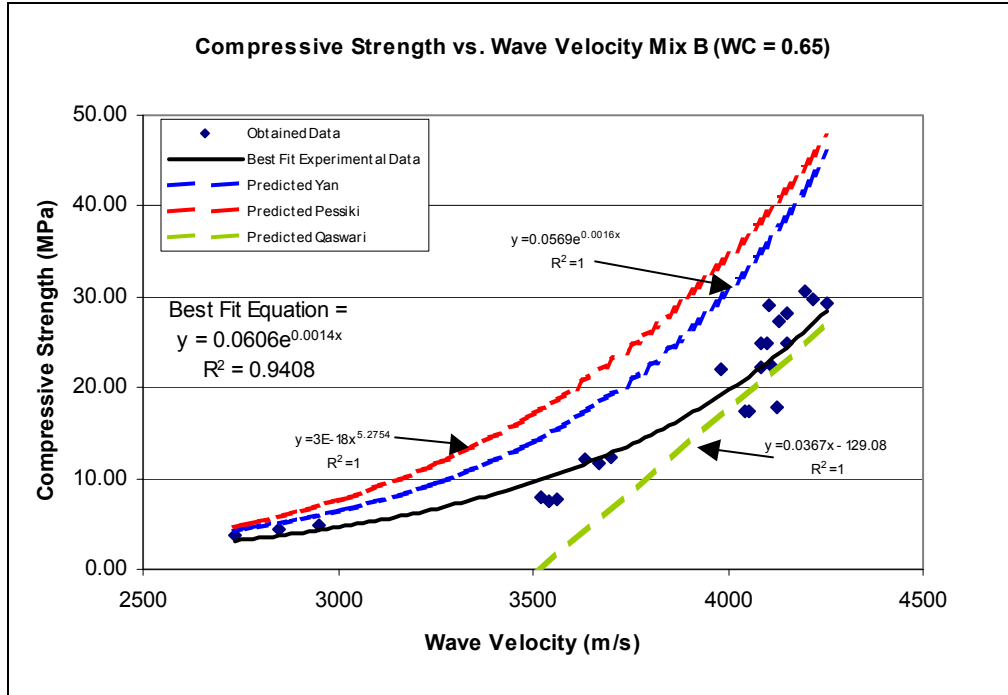


Raw Data for Cylinder Samples w/c ratio = 0.65

Load (N)	Compressive Strength (Mpa)	UPV Time (ms)	Impact Echo Wave Speed (m/s)	Resonant Frequency (Hz)	Age
38655	4.77	67.8	2949.9	1100	1 day
34874.1	4.30	70.2	2849.0	1020	
29981	3.70	73.8	2737.1	970	
64321.3	7.93	56.8	3521.1	1450	2 day
61163.1	7.54	55.9	3542.0	1810	
62897.9	7.76	57.0	3561.4	1880	
94871.7	11.70	54.0	3666.7	2350	3day
100668	12.42	53.5	3700.9	2450	
97620.7	12.04	54.5	3633.0	1950	
145372	17.93	48.7	4127.3	2235	7day
140537	17.33	50.2	4043.8	2213	
140804	17.37	49.6	4052.4	1800	
177809	21.93	51.0	3980.4	2250	14day
182978	22.57	49.4	4109.3	2550	
180767	22.30	49.7	4084.5	2860	
201553	24.86	49.0	4102.0	2700	21 Day
202510	24.98	48.2	4149.4	2590	
202274	24.95	48.7	4086.2	2460	
227807	28.10	48.2	4149.4	2197	28 day
235422	29.04	48.7	4106.8	2020	
220997	27.26	48.2	4128.6	1980	
241125	29.74	48.1	4220.4	2570	42 day
248024	30.59	47.2	4194.9	2470	
237184	29.25	47.0	4255.3	2700	
262690	32.40	47.4	4219.4	2650	56 day
252085	31.09	48.5	4164.9	2650	
262209	32.34	47.5	4221.1	2670	

Calculations for Predicted Strength Data Using obtained  
Labotatory Data Mixture B A (w/c = 0.65)

Wave Velocity Observed (km/s)	Predicted Strength (MPa) by Author			Actual Compressive Strength (Mpa)
	Yan	Qaswari	Pessiki	
2.95	5.88	-20.76	6.98	4.77
2.85	5.02	-24.46	5.99	4.30
2.74	4.21	-28.57	5.06	3.70
3.52	14.43	0.22	16.50	7.93
3.54	14.92	0.99	17.02	7.54
3.56	15.38	1.70	17.53	7.76
3.67	18.15	5.56	20.53	11.70
3.70	19.15	6.82	21.62	12.42
3.63	17.21	4.33	19.52	12.04
4.13	37.43	22.48	41.01	17.93
4.04	32.83	19.41	36.18	17.33
4.05	33.28	19.73	36.65	17.37
3.98	29.71	17.08	32.89	21.93
4.11	36.39	21.82	39.92	22.57
4.08	35.00	20.91	38.46	22.30
4.10	35.98	21.55	39.48	24.86
4.15	38.75	23.29	42.39	24.98
4.09	35.09	20.97	38.56	24.95
4.15	38.75	23.29	42.39	28.10
4.11	36.24	21.72	39.76	29.04
4.13	37.51	22.53	41.09	27.26
4.22	43.33	25.90	47.15	29.74
4.19	41.63	24.96	45.38	30.59
4.26	45.78	27.18	49.69	29.25
4.22	43.26	25.86	47.08	32.40
4.16	39.71	23.86	43.39	31.09
4.22	43.38	25.92	47.20	32.34



APPENDIX E  
LABORATORY DATA AND GRAPHICAL RESULTS OF LARGE SCALE  
SPECIMENS

Summary Sheet for Block Samples		
Summary of Block Identification and Conditioning		
Block Number	(w/c ratio)	Solution type
5	0.45	Sulfate Solution
6	0.45	Sulfate Solution
7	0.45	Lime water
8	0.45	Lime water
21	0.65	Lime water
22	0.65	Lime water
23	0.65	Sulfate Solution
24	0.65	Sulfate Solution

Date	2/9/2003	Temp	72°F	Block #	5
------	----------	------	------	---------	---

Ultrasonic Pulse Velocity Testing		
Point #	Time ( $\mu$ s)	Wave Velocity (m/s)
1	64.6	3761.6
2	64.5	3767.4
3	64.6	3761.6
4	64.8	3750.0
5	61.5	3951.2
6	61.6	3944.8
7	61.3	3964.1
8	61.4	3957.7
9	58.7	4139.7
10	58.9	4125.6
11	57.5	4226.1
12	57.3	4240.8
13	231.0	3896.1
14	226.4	3984.1
15	220.4	4101.6

Impact Echo Testing	
Reading #	Wave Velocity (m/s)
1	3519
2	3831
3	3802
4	3808
5	3831
6	3945

Date	2/13/2003	Temp	72°F	Block #	5
------	-----------	------	------	---------	---

Ultrasonic Pulse Velocity Testing		
Point #	Time ( $\mu$ s)	Wave Velocity (m/s)
1	64.4	3773.3
2	64.1	3791.0
3	64.3	3779.2
4	62.3	3900.5
5	59.7	4070.4
6	59.6	4077.2
7	59.8	4063.5
8	60.0	4050.0
9	58.4	4161.0
10	58.3	4168.1
11	59.3	4097.8
12	60.0	4050.0
13	223.2	4032.3
14	218.0	4137.6
15	213.1	4242.1

Impact Echo Testing	
Reading #	Wave Velocity (m/s)
1	3672
2	3751
3	3887
4	3918
5	4285
6	4187

Date	2/21/2003	Temp	72°F	Block #	5
------	-----------	------	------	---------	---

Ultrasonic Pulse Velocity Testing		
Point #	Time ( $\mu$ s)	Wave Velocity (m/s)
1	59.4	4090.9
2	60.0	4050.0
3	60.2	4036.5
4	59.9	4056.8
5	58.0	4189.7
6	58.1	4182.4
7	58.2	4175.3
8	58.4	4161.0
9	55.8	4354.8
10	56.1	4331.6
11	56.6	4293.3
12	56.1	4331.6
13	224.7	4005.3
14	217.3	4150.9
15	212.8	4248.1

Impact Echo Testing	
Reading #	Wave Velocity (m/s)
1	3673
2	3751
3	4021
4	4000
5	4171
6	4287

Date	2/27/2003	Temp	72°F	Block #	5
------	-----------	------	------	---------	---

Ultrasonic Pulse Velocity Testing		
Point #	Time ( $\mu$ s)	Wave Velocity (m/s)
1	58.9	4125.6
2	58.7	4139.7
3	59.0	4118.6
4	59.2	4104.7
5	57.3	4240.8
6	57.5	4226.1
7	57.5	4226.1
8	58.3	4168.1
9	56.2	4323.8
10	56.8	4278.2
11	57.1	4255.7
12	56.3	4316.2
13	215.4	4178.3
14	211.4	4266.8
15	208.0	4346.2

Impact Echo Testing	
Reading #	Wave Velocity (m/s)
1	3913
2	3831
3	4056
4	3914
5	4312
6	4199

Date	3/7/2003	Temp	72°F	Block #	5
------	----------	------	------	---------	---

Ultrasonic Pulse Velocity Testing		
Point #	Time ( $\mu$ s)	Wave Velocity (m/s)
1	58.3	4168.1
2	57.8	4204.2
3	58.4	4161.0
4	58.6	4146.8
5	56.8	4278.2
6	56.8	4278.2
7	56.6	4293.3
8	57.4	4233.4
9	55.0	4418.2
10	55.4	4386.3
11	55.6	4370.5
12	55.2	4402.2
13	212.5	4235.3
14	210.0	4295.2
15	206.6	4375.6

Impact Echo Testing	
Reading #	Wave Velocity (m/s)
1	3977
2	4000
3	3999
4	4101
5	4287
6	4390

Date	3/27/2003	Temp	72°F	Block #	5
------	-----------	------	------	---------	---

Ultrasonic Pulse Velocity Testing		
Point #	Time ( $\mu$ s)	Wave Velocity (m/s)
1	58.1	4182.4
2	57.8	4204.2
3	58.3	4168.1
4	58.4	4161.0
5	57.0	4263.2
6	56.9	4270.7
7	56.4	4308.5
8	57.1	4255.7
9	54.8	4434.3
10	56.0	4339.3
11	56.9	4270.7
12	55.5	4378.4
13	211.0	4265.4
14	208.2	4332.4
15	203.9	4433.5

Impact Echo Testing	
Reading #	Wave Velocity (m/s)
1	3913
2	3826
3	4187
4	4301
5	4392
6	4388

Date 4/17/2003	Temp 72°F	Block # 5
----------------	-----------	-----------

Ultrasonic Pulse Velocity Testing		
Point #	Time ( $\mu$ s)	Wave Velocity (m/s)
1	58.1	4182.4
2	57.9	4196.9
3	58.2	4175.3
4	58.4	4161.0
5	57.1	4255.7
6	56.7	4285.7
7	56.4	4308.5
8	56.7	4285.7
9	55.0	4418.2
10	55.2	4402.2
11	55.9	4347.0
12	54.6	4450.5
13	210.7	4271.5
14	207.6	4344.9
15	200.4	4511.0

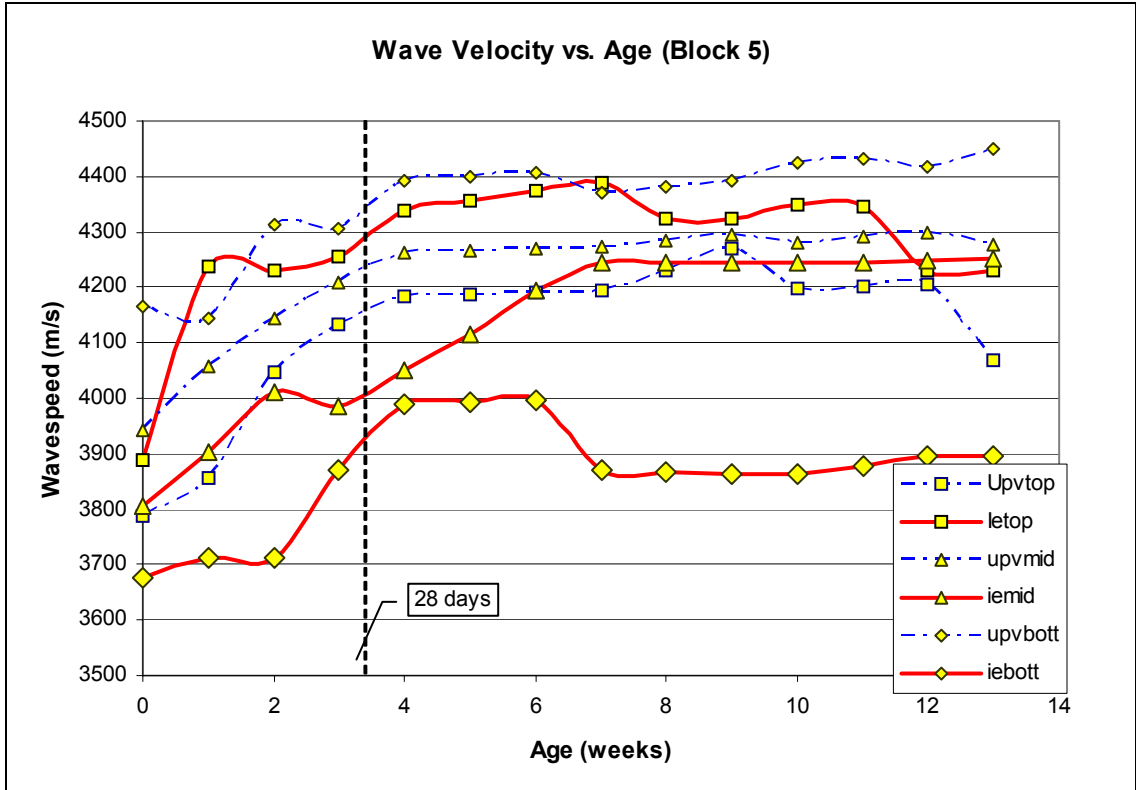
Impact Echo Testing	
Reading #	Wave Velocity (m/s)
1	3983
2	3741
3	4255
4	4233
5	4307
6	4393

Date 5/1/2003	Temp 72°F	Block # 5
---------------	-----------	-----------

Ultrasonic Pulse Velocity Testing		
Point #	Time ( $\mu$ s)	Wave Velocity (m/s)
1	58.3	4168.1
2	57.9	4196.9
3	58.2	4175.3
4	58.3	4168.1
5	56.7	4285.7
6	56.7	4285.7
7	56.6	4293.3
8	56.8	4278.2
9	54.7	4442.4
10	55.3	4394.2
11	55.2	4402.2
12	54.8	4434.3
13	210.4	4277.6
14	207.5	4347.0
15	202.7	4459.8

Impact Echo Testing	
Reading #	Wave Velocity (m/s)
1	3788
2	3936
3	4101
4	4387
5	4176
6	4287

Tomography Data Sheet for Test blocks.					
Date		5/8/2003			
Block #		5			
Point #	Time ( $\mu$ s)	Point #	Time ( $\mu$ s)	Point #	Time ( $\mu$ s)
A1	61.0	B1	58.4	C1	57.0
A2	60.0	B2	58.1	C2	57.1
A3	58.1	B3	57.6	C3	56.8
A4	59.6	B4	57.5	C4	56.8
A5	60.6	B5	57.6	C5	56.7
A6	59.9	B6	57.8	C6	56.7
A7	58.6	B7	57.5	C7	56.8
A8	59.5	B8	58.1	C8	57.0
A9	60.1	B9	58.3	C9	56.5
D1	55.6	E1	55.2		
D2	57.0	E2	53.5		
D3	55.6	E3	54.5		
D4	56.3	E4	55.1		
D5	55.4	E5	55.3		
D6	55.6	E6	54.9		
D7	56.1	E7	54.9		
D8	56.6	E8	53.7		
D9	55.1	E9	54.6		
X1	111.4	Y1	113.1	Z1	111.0
X2	112.6	Y2	111.9	Z2	111.6
X3	111.2	Y3	110.8	Z3	111.3
X4	113.0	Y4	111.5	Z4	111.4
X5	112.9	Y5	112.3	Z5	112.6
X6	112.6	Y6	111.9	Z6	113.5
X7	113.5	Y7	110.6	Z7	110.9
X8	112.2	Y8	112.1	Z8	112.8
X9	110.9	Y9	110.1	Z9	108.4
XA	214.6	YA	214.6	ZA	215.5
XB	210.4	YB	211.1	ZB	211.5
XC	210.6	YC	208.7	ZC	208.9
XD	206.9	YD	207.7	ZD	205.6
XE	196.2	YE	202.3	ZE	201.6



Date	2/9/2003	Temp	72°F	Block #	6
------	----------	------	------	---------	---

Ultrasonic Pulse Velocity Testing		
Point #	Time ( $\mu$ s)	Wave Velocity (m/s)
1	63.5	3811.0
2	63.3	3823.1
3	63.4	3817.0
4	63.1	3835.2
5	63.1	3835.2
6	63.6	3805.0
7	62.7	3859.6
8	63.6	3805.0
9	63.6	3805.0
10	63.6	3805.0
11	63.6	3805.0
12	63.6	3805.0
13	231.4	3889.4
14	227.0	3967.0
15	222.3	4053.1

Impact Echo Testing	
Reading #	Wave Velocity (m/s)
1	3345
2	3454
3	3477
4	3526
5	3840
6	4092

Date	2/13/2003	Temp	72°F	Block #	6
------	-----------	------	------	---------	---

Ultrasonic Pulse Velocity Testing		
Point #	Time ( $\mu$ s)	Wave Velocity (m/s)
1	61.9	3909.5
2	65.0	3723.1
3	64.3	3763.6
4	62.0	3903.2
5	61.5	3935.0
6	61.8	3915.9
7	61.8	3915.9
8	60.8	3980.3
9	59.5	4067.2
10	60.4	4006.6
11	59.8	4046.8
12	58.6	4129.7
13	222.9	4037.7
14	218.7	4117.5
15	215.6	4179.0

Impact Echo Testing	
Reading #	Wave Velocity (m/s)
1	3396
2	3461
3	3462
4	3672
5	3828
6	4100

Date	2/21/2003	Temp	72°F	Block #	6
------	-----------	------	------	---------	---

Ultrasonic Pulse Velocity Testing		
Point #	Time ( $\mu$ s)	Wave Velocity (m/s)
1	63.3	3823.1
2	60.9	3973.7
3	61.2	3954.2
4	61.0	3967.2
5	60.5	4000.0
6	60.8	3980.3
7	60.7	3986.8
8	59.9	4040.1
9	58.7	4122.7
10	62.3	3884.4
11	64.0	3781.3
12	59.7	4053.6
13	217.6	4136.0
14	214.0	4207.9
15	210.8	4274.2

Impact Echo Testing	
Reading #	Wave Velocity (m/s)
1	3648
2	3555
3	3914
4	3821
5	4090
6	3913

Date	2/27/2003	Temp	72°F	Block #	6
------	-----------	------	------	---------	---

Ultrasonic Pulse Velocity Testing		
Point #	Time ( $\mu$ s)	Wave Velocity (m/s)
1	59.3	4080.9
2	59.9	4040.1
3	59.4	4074.1
4	59.9	4040.1
5	58.6	4129.7
6	59.3	4080.9
7	59.6	4060.4
8	59.6	4060.4
9	57.0	4245.6
10	58.2	4158.1
11	58.4	4143.8
12	57.6	4201.4
13	215.3	4180.2
14	212.0	4247.6
15	209.6	4298.7

Impact Echo Testing	
Reading #	Wave Velocity (m/s)
1	3597
2	3704
3	4021
4	3945
5	4187
6	4091

Date	3/7/2003	Temp	72°F	Block #	6
------	----------	------	------	---------	---

Ultrasonic Pulse Velocity Testing		
Point #	Time ( $\mu$ s)	Wave Velocity (m/s)
1	58.6	4129.7
2	58.7	4122.7
3	59.2	4087.8
4	58.6	4129.7
5	58.7	4122.7
6	58.8	4115.6
7	58.7	4122.7
8	57.8	4186.9
9	56.6	4275.6
10	57.3	4223.4
11	57.0	4245.6
12	56.0	4321.4
13	213.3	4219.4
14	211.4	4259.7
15	207.0	4352.7

Impact Echo Testing	
Reading #	Wave Velocity (m/s)
1	3673
2	3751
3	3829
4	4092
5	4186
6	4188

Date	3/27/2003	Temp	72°F	Block #	6
------	-----------	------	------	---------	---

Ultrasonic Pulse Velocity Testing		
Point #	Time ( $\mu$ s)	Wave Velocity (m/s)
1	59	4101.7
2	58.8	4115.6
3	59.2	4087.8
4	58.7	4122.7
5	58.9	4108.7
6	58.6	4129.7
7	58.7	4122.7
8	57.9	4179.6
9	57.6	4201.4
10	58.3	4150.9
11	58.3	4150.9
12	56.5	4283.2
13	210.5	4275.5
14	209.0	4308.6
15	206.3	4367.4

Impact Echo Testing	
Reading #	Wave Velocity (m/s)
1	3841
2	3912
3	4009
4	4000
5	4114
6	4235

Date	4/17/2003	Temp	72°F	Block #	6
------	-----------	------	------	---------	---

Ultrasonic Pulse Velocity Testing		
Point #	Time ( $\mu$ s)	Wave Velocity (m/s)
1	58.4	4143.8
2	58.7	4122.7
3	58.9	4108.7
4	58.6	4129.7
5	58.9	4108.7
6	58.7	4122.7
7	58.5	4136.8
8	57.8	4186.9
9	56.4	4290.8
10	57.1	4238.2
11	56.7	4268.1
12	55.9	4329.2
13	210.8	4269.4
14	207.8	4333.5
15	204.9	4397.3

Impact Echo Testing	
Reading #	Wave Velocity (m/s)
1	3989
2	4001
3	4211
4	4090
5	4186
6	4175

Date	5/1/2003	Temp	72°F	Block #	6
------	----------	------	------	---------	---

Ultrasonic Pulse Velocity Testing		
Point #	Time ( $\mu$ s)	Wave Velocity (m/s)
1	58.8	4115.6
2	58.6	4129.7
3	59.3	4080.9
4	58.7	4122.7
5	58.9	4108.7
6	58.6	4129.7
7	58.3	4150.9
8	57.6	4201.4
9	56.7	4268.1
10	58.3	4150.9
11	56.9	4253.1
12	56.0	4321.4
13	210.1	4283.7
14	207.3	4343.9
15	204.6	4403.7

Impact Echo Testing	
Reading #	Wave Velocity (m/s)
1	
2	
3	
4	
5	
6	

## Tomography Data Sheet for Test blocks.

Date	5/9/2003
Block #	6

Point #	Time ( $\mu$ s)	Point #	Time ( $\mu$ s)
A1	59.6	B1	58.4
A2	59.3	B2	58.1
A3	58.3	B3	58.4
A4	59.1	B4	59.4
A5	58.9	B5	58.9
A6	58.5	B6	59.0
A7	59.0	B7	58.6
A8	58.9	B8	58.2
A9	59.8	B9	58.0

Point #	Time ( $\mu$ s)
C1	57.9
C2	58.6
C3	58.6
C4	58.5
C5	58.5
C6	58.5
C7	58.0
C8	57.9
C9	57.6

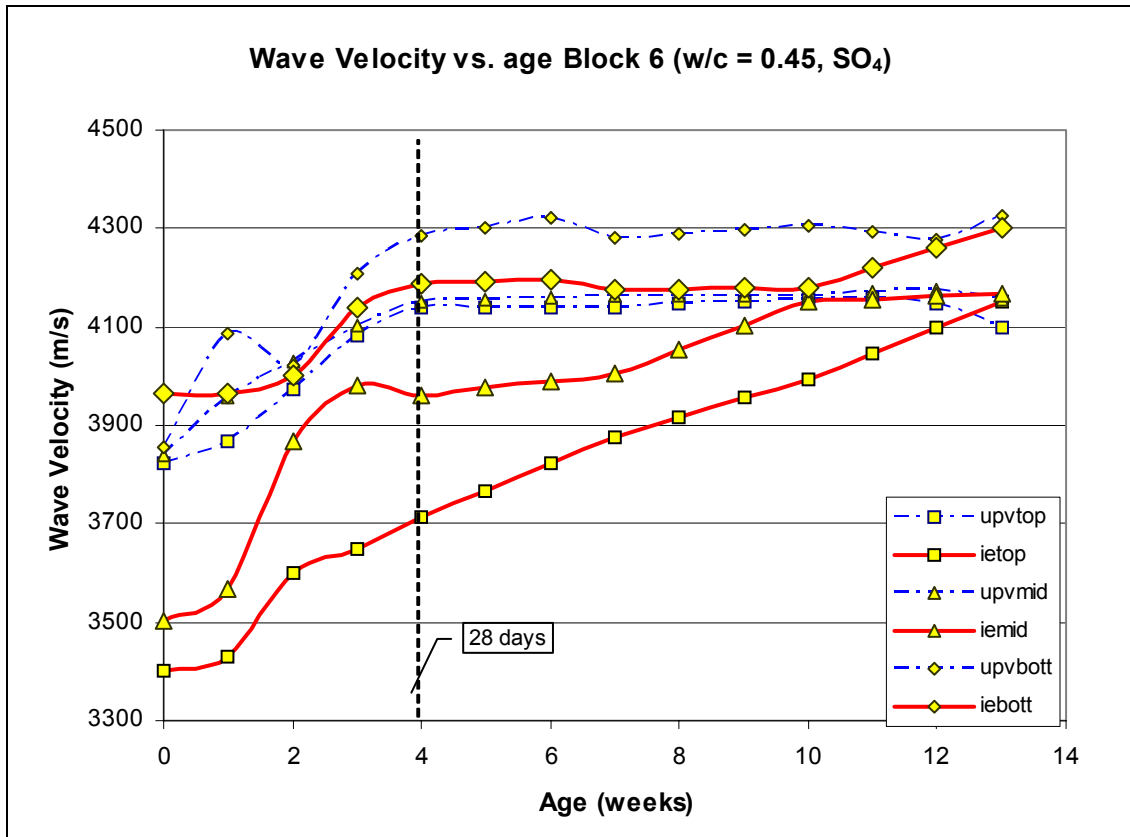
D1	55.8	E1	55.5
D2	57.6	E2	55.6
D3	57.8	E3	57.2
D4	57.9	E4	56.7
D5	57.8	E5	56.5
D6	58.4	E6	56.4
D7	57.3	E7	56.1
D8	57.2	E8	55.1
D9	55.9	E9	54.4

X1	108.2	Y1	109.8
X2	111.7	Y2	111.6
X3	111.9	Y3	110.9
X4	113.5	Y4	112.8
X5	114.5	Y5	113.5
X6	112.8	Y6	113.0
X7	112.5	Y7	112.4
X8	111.2	Y8	113.3
X9	112.2	Y9	111.3

Z1	110.1
Z2	111.3
Z3	110.9
Z4	113.7
Z5	114.9
Z6	115.2
Z7	111.2
Z8	111.8
Z9	112.4

XA	214.7	YA	214.5
XB	211.5	YB	209.3
XC	208.9	YC	207.9
XD	205.2	YD	205.0
XE	198.0	YE	202.5

ZA	214.5
ZB	212.0
ZC	209.4
ZD	205.8
ZE	201.2



Date	2/9/2003	Temp	72°F	Block #	7
------	----------	------	------	---------	---

Ultrasonic Pulse Velocity Testing		
Point #	Time ( $\mu$ s)	Wave Velocity (m/s)
1	61.5	3935.0
2	61.5	3935.0
3	60.8	3980.3
4	61.4	3941.4
5	62.0	3919.4
6	61.5	3951.2
7	61.6	3944.8
8	61.7	3938.4
9	61.5	3967.5
10	61.4	3973.9
11	61.4	3973.9
12	61.5	3967.5
13	224.0	4031.3
14	221.8	4080.3
15	216.4	4191.3

Impact Echo Testing	
Reading #	Wave Velocity (m/s)
1	3692
2	3645
3	3674
4	3840
5	3850
6	3674

Date	2/13/2003	Temp	72°F	Block #	7
------	-----------	------	------	---------	---

Ultrasonic Pulse Velocity Testing		
Point #	Time ( $\mu$ s)	Wave Velocity (m/s)
1	60.3	4013.3
2	61.0	3967.2
3	60.2	4019.9
4	63.0	3841.3
5	61.0	3983.6
6	60.4	4023.2
7	61.1	3977.1
8	60.4	4023.2
9	59.3	4114.7
10	60.0	4066.7
11	60.6	4026.4
12	59.3	4114.7
13	215.7	4186.4
14	214.5	4219.1
15	211.3	4292.5

Impact Echo Testing	
Reading #	Wave Velocity (m/s)
1	3673
2	3653
3	3680
4	3966
5	3900
6	4185

Date	2/21/2003	Temp	72°F	Block #	7
------	-----------	------	------	---------	---

Ultrasonic Pulse Velocity Testing		
Point #	Time ( $\mu$ s)	Wave Velocity (m/s)
1	58.0	4172.4
2	57.7	4194.1
3	57.0	4245.6
4	58.0	4172.4
5	58.4	4161.0
6	57.5	4226.1
7	57.6	4218.8
8	57.5	4226.1
9	56.7	4303.4
10	57.4	4250.9
11	57.5	4243.5
12	57.6	4236.1
13	210.8	4283.7
14	209.5	4319.8
15	206.0	4402.9

Impact Echo Testing	
Reading #	Wave Velocity (m/s)
1	3691
2	3684
3	3893
4	3924
5	4100
6	4285

Date	2/28/2003	Temp	72°F	Block #	7
------	-----------	------	------	---------	---

Ultrasonic Pulse Velocity Testing		
Point #	Time ( $\mu$ s)	Wave Velocity (m/s)
1	57.8	4186.9
2	57.8	4186.9
3	57.6	4201.4
4	57.6	4201.4
5	58.0	4189.7
6	57.8	4204.2
7	57.8	4204.2
8	57.4	4233.4
9	57.0	4280.7
10	57.3	4258.3
11	57.7	4228.8
12	56.8	4295.8
13	209.3	4314.4
14	208.4	4342.6
15	204.9	4426.5

Impact Echo Testing	
Reading #	Wave Velocity (m/s)
1	3600
2	3902
3	4090
4	3810
5	4393
6	4007

Date	3/6/2003	Temp	72°F	Block #	7
------	----------	------	------	---------	---

Ultrasonic Pulse Velocity Testing		
Point #	Time ( $\mu$ s)	Wave Velocity (m/s)
1	57.3	4223.4
2	57.1	4238.2
3	57.1	4238.2
4	57.2	4230.8
5	57.4	4233.4
6	57.3	4240.8
7	57.5	4226.1
8	57.4	4233.4
9	56.5	4318.6
10	57.3	4258.3
11	57.3	4258.3
12	57.3	4258.3
13	207.8	4345.5
14	207.1	4369.9
15	202.4	4481.2

Impact Echo Testing	
Reading #	Wave Velocity (m/s)
1	3831
2	3749
3	4091
4	4090
5	4390
6	4187

Date	3/20/2003	Temp	72°F	Block #	7
------	-----------	------	------	---------	---

Ultrasonic Pulse Velocity Testing		
Point #	Time ( $\mu$ s)	Wave Velocity (m/s)
1	57.1	4238.2
2	56.7	4268.1
3	56.5	4283.2
4	56.7	4268.1
5	57.5	4226.1
6	57	4263.2
7	57.3	4240.8
8	57.2	4248.3
9	57.4	4250.9
10	57.1	4273.2
11	57.4	4250.9
12	57.9	4214.2
13	206.4	4375.0
14	205.6	4401.8
15	200.9	4514.7

Impact Echo Testing	
Reading #	Wave Velocity (m/s)
1	3770
2	3902
3	4101
4	4186
5	4357
6	4287

Date 3/27/2003	Temp 72°F	Block # 7
----------------	-----------	-----------

Ultrasonic Pulse Velocity Testing		
Point #	Time ( $\mu$ s)	Wave Velocity (m/s)
1	57.3	4223.4
2	57.1	4238.2
3	57.1	4238.2
4	57.0	4245.6
5	57.6	4218.8
6	57.2	4248.3
7	57.5	4226.1
8	57.5	4226.1
9	56.3	4333.9
10	57.3	4258.3
11	57.4	4250.9
12	57.7	4228.8
13	206.0	4383.5
14	205.1	4412.5
15	202.1	4487.9

Impact Echo Testing	
Reading #	Wave Velocity (m/s)
1	
2	
3	
4	
5	
6	

Date 4/10/2003	Temp 72°F	Block # 7
----------------	-----------	-----------

Ultrasonic Pulse Velocity Testing		
Point #	Time ( $\mu$ s)	Wave Velocity (m/s)
1	57.2	4230.8
2	57.4	4216.0
3	57.2	4230.8
4	57.2	4230.8
5	57.6	4218.8
6	57.4	4233.4
7	57.6	4218.8
8	57.5	4226.1
9	56.7	4303.4
10	57.7	4228.8
11	59.0	4135.6
12	58.3	4185.2
13	206.2	4379.2
14	204.6	4423.3
15	202.5	4479.0

Impact Echo Testing	
Reading #	Wave Velocity (m/s)
1	3900
2	3800
3	4104
4	4116
5	4272
6	4429

Date 4/24/2003	Temp 72°F	Block # 7
----------------	-----------	-----------

Ultrasonic Pulse Velocity Testing		
Point #	Time ( $\mu$ s)	Wave Velocity (m/s)
1	57.2	4230.8
2	57.2	4230.8
3	57.2	4230.8
4	57.2	4230.8
5	57.8	4204.2
6	57.4	4233.4
7	57.7	4211.4
8	57.5	4226.1
9	57.5	4243.5
10	58.5	4170.9
11	58.0	4206.9
12	58.3	4185.2
13	208.2	4337.2
14	204.7	4421.1
15	202.4	4481.2

Impact Echo Testing	
Reading #	Wave Velocity (m/s)
1	3861
2	3954
3	4114
4	4092
5	4300
6	4388

## Tomography Data Sheet for Test blocks.

Date 5/7/2003  
 Block # 7

Point #	Time ( $\mu$ s)
A1	57.7
A2	57.1
A3	56.7
A4	56.4
A5	57.2
A6	56.4
A7	56.9
A8	56.9
A9	56.8

Point #	Time ( $\mu$ s)
B1	56.0
B2	56.5
B3	56.4
B4	56.6
B5	56.8
B6	56.2
B7	56.6
B8	56.3
B9	56.3

Point #	Time ( $\mu$ s)
C1	55.5
C2	56.9
C3	56.5
C4	56.5
C5	56.8
C6	56.8
C7	57.0
C8	56.8
C9	55.9

D1	54.5
D2	56.2
D3	56.5
D4	57.1
D5	56.4
D6	56.6
D7	56.5
D8	56.5
D9	54.4

E1	53.7
E2	54.8
E3	55.7
E4	55.8
E5	55.8
E6	56.2
E7	56.1
E8	54.3
E9	52.6

X1	113.0
X2	114.7
X3	114.1
X4	114.8
X5	115.7
X6	114.9
X7	114.2
X8	112.9
X9	113.2

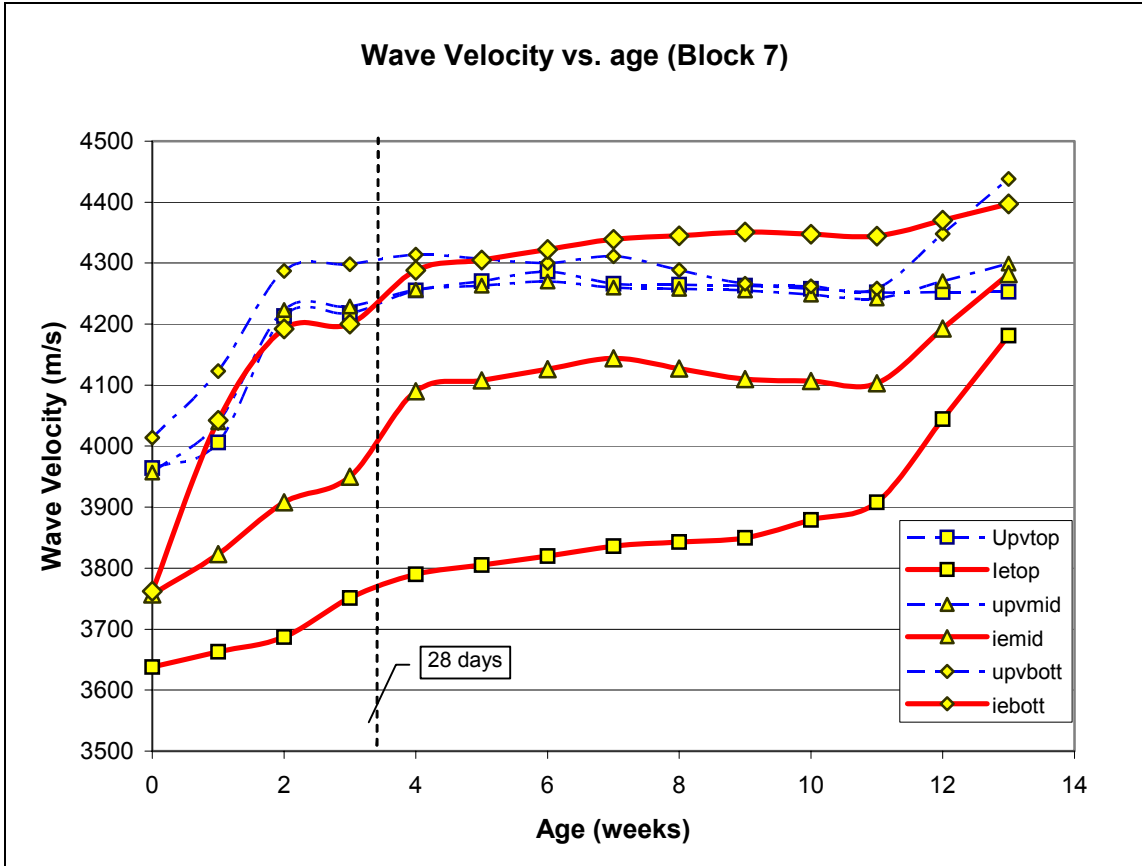
Y1	110.7
Y2	114.7
Y3	113.2
Y4	113.0
Y5	113.4
Y6	113.1
Y7	113.3
Y8	112.6
Y9	112.6

Z1	113.7
Z2	115.3
Z3	114.7
Z4	113.8
Z5	115.2
Z6	114.2
Z7	114.7
Z8	113.1
Z9	113.3

XA	208.5
XB	206.1
XC	205.8
XD	201.4
XE	195.4

YA	206.8
YB	203.6
YC	202.8
YD	203.4
YE	198.1

ZA	208.3
ZB	205.4
ZC	204.2
ZD	202.4
ZE	197.4



Date	2/9/2003	Temp	72°F	Block #	8
------	----------	------	------	---------	---

Ultrasonic Pulse Velocity Testing		
Point #	Time ( $\mu$ s)	Wave Velocity (m/s)
1	63.5	3779.5
2	60.7	3953.9
3	64.0	3750.0
4	63.4	3785.5
5	63.6	3773.6
6	60.6	3960.4
7	61.0	3934.4
8	63.8	3761.8
9	59.9	4006.7
10	61.0	3934.4
11	57.6	4166.7
12	60.1	3993.3
13	227.0	3964.8
14	218.2	4136.1
15	212.3	4262.8

Impact Echo Testing	
Reading #	Wave Velocity (m/s)
1	3684
2	3349
3	3610
4	3630
5	3655
6	3674

Date	2/13/2003	Temp	72°F	Block #	8
------	-----------	------	------	---------	---

Ultrasonic Pulse Velocity Testing		
Point #	Time ( $\mu$ s)	Wave Velocity (m/s)
1	62.8	3821.7
2	60.9	3940.9
3	58.8	4081.6
4	59.8	4013.4
5	58.8	4081.6
6	58.2	4123.7
7	58.8	4081.6
8	59.4	4040.4
9	57.3	4188.5
10	57.6	4166.7
11	56.6	4240.3
12	57.2	4195.8
13	216	4166.7
14	215.1	4195.7
15	210.8	4293.2

Impact Echo Testing	
Reading #	Wave Velocity (m/s)
1	
2	
3	
4	
5	
6	

Date	2/21/2003	Temp	72°F	Block #	8
------	-----------	------	------	---------	---

Ultrasonic Pulse Velocity Testing		
Point #	Time ( $\mu$ s)	Wave Velocity (m/s)
1	57.5	4173.9
2	57.6	4166.7
3	57.4	4181.2
4	57.6	4166.7
5	56.8	4225.4
6	56	4285.7
7	56.4	4255.3
8	56.9	4217.9
9	54.1	4436.2
10	53.9	4452.7
11	54.3	4419.9
12	54.3	4419.9
13	210.7	4271.5
14	210.4	4289.4
15	206.4	4384.7

Impact Echo Testing	
Reading #	Wave Velocity (m/s)
1	3645
2	3682
3	3849
4	3789
5	3913
6	4093

Date	2/28/2003	Temp	72°F	Block #	8
------	-----------	------	------	---------	---

Ultrasonic Pulse Velocity Testing		
Point #	Time ( $\mu$ s)	Wave Velocity (m/s)
1	56.9	4217.9
2	56.6	4240.3
3	56.5	4247.8
4	57.0	4210.5
5	56.3	4262.9
6	55.9	4293.4
7	56.3	4262.9
8	56.7	4232.8
9	54.6	4395.6
10	54.3	4419.9
11	54.9	4371.6
12	54.9	4371.6
13	209.1	4304.2
14	208.6	4326.5
15	204.5	4425.4

Impact Echo Testing	
Reading #	Wave Velocity (m/s)
1	3830
2	3828
3	3882
4	3918
5	4092
6	4186

Date	3/6/2003	Temp	72°F	Block #	8
------	----------	------	------	---------	---

Ultrasonic Pulse Velocity Testing		
Point #	Time ( $\mu$ s)	Wave Velocity (m/s)
1	57.0	4210.5
2	56.4	4255.3
3	56.4	4255.3
4	56.9	4217.9
5	56.3	4262.9
6	56.0	4285.7
7	56.3	4262.9
8	56.7	4232.8
9	53.7	4469.3
10	53.7	4469.3
11	54.9	4371.6
12	54.6	4395.6
13	208.8	4310.3
14	207.7	4345.2
15	204.6	4423.3

Impact Echo Testing	
Reading #	Wave Velocity (m/s)
1	3674
2	3914
3	3914
4	3977
5	4401
6	4284

Date	3/20/2003	Temp	72°F	Block #	8
------	-----------	------	------	---------	---

Ultrasonic Pulse Velocity Testing		
Point #	Time ( $\mu$ s)	Wave Velocity (m/s)
1	56.7	4232.8
2	56.4	4255.3
3	56.2	4270.5
4	56.3	4262.9
5	55.9	4293.4
6	55.6	4316.5
7	55.8	4301.1
8	56.5	4247.8
9	54.5	4403.7
10	54.7	4387.6
11	54.3	4419.9
12	54.3	4419.9
13	205.8	4373.2
14	205.4	4393.9
15	202.5	4469.1

Impact Echo Testing	
Reading #	Wave Velocity (m/s)
1	3808
2	3749
3	3914
4	3829
5	4390
6	4300

Date 3/27/2003	Temp 72°F	Block # 8
----------------	-----------	-----------

Ultrasonic Pulse Velocity Testing		
Point #	Time ( $\mu$ s)	Wave Velocity (m/s)
1	56.6	4240.3
2	56.4	4255.3
3	56.4	4255.3
4	56.5	4247.8
5	56.2	4270.5
6	56.1	4278.1
7	56.4	4255.3
8	56.7	4232.8
9	54.8	4379.6
10	55.2	4347.8
11	55.3	4340.0
12	54.6	4395.6
13	206.6	4356.2
14	205.0	4402.4
15	201.9	4482.4

Impact Echo Testing	
Reading #	Wave Velocity (m/s)
1	
2	
3	
4	
5	
6	

Date 4/10/2003	Temp 72°F	Block # 8
----------------	-----------	-----------

Ultrasonic Pulse Velocity Testing		
Point #	Time ( $\mu$ s)	Wave Velocity (m/s)
1	56.8	4225.4
2	56.6	4240.3
3	56.3	4262.9
4	56.3	4262.9
5	56.2	4270.5
6	55.6	4316.5
7	56.0	4285.7
8	56.5	4247.8
9	54.9	4371.6
10	54.6	4395.6
11	55.7	4308.8
12	54.6	4395.6
13	206.8	4352.0
14	204.9	4404.6
15	201.5	4491.3

Impact Echo Testing	
Reading #	Wave Velocity (m/s)
1	3933
2	4114
3	4012
4	4080
5	4285
6	4365

Date 4/24/2003	Temp 72°F	Block # 8
----------------	-----------	-----------

Ultrasonic Pulse Velocity Testing		
Point #	Time ( $\mu$ s)	Wave Velocity (m/s)
1	56.9	4217.9
2	56.7	4232.8
3	56.7	4232.8
4	56.6	4240.3
5	56.9	4217.9
6	55.7	4308.8
7	56.4	4255.3
8	56.8	4225.4
9	55.0	4363.6
10	55.0	4363.6
11	55.6	4316.5
12	55.5	4324.3
13	206.6	4356.2
14	204.0	4424.0
15	200.4	4516.0

Impact Echo Testing	
Reading #	Wave Velocity (m/s)
1	4033
2	3967
3	4100
4	4100
5	4285
6	4315

## Tomography Data Sheet for Test blocks.

Date 5/8/2003

Block # 8

Point #	Time ( $\mu$ s)	Point #	Time ( $\mu$ s)
A1	58.2	B1	56.9
A2	57.2	B2	56.7
A3	57.3	B3	56.2
A4	57.7	B4	56.1
A5	57.4	B5	56.2
A6	57.4	B6	56.2
A7	57.4	B7	56.5
A8	57.3	B8	56.7
A9	58.3	B9	55.8

Point #	Time ( $\mu$ s)
C1	55.8
C2	56.8
C3	56.0
C4	55.8
C5	56.4
C6	56.2
C7	56.5
C8	56.6
C9	55.1

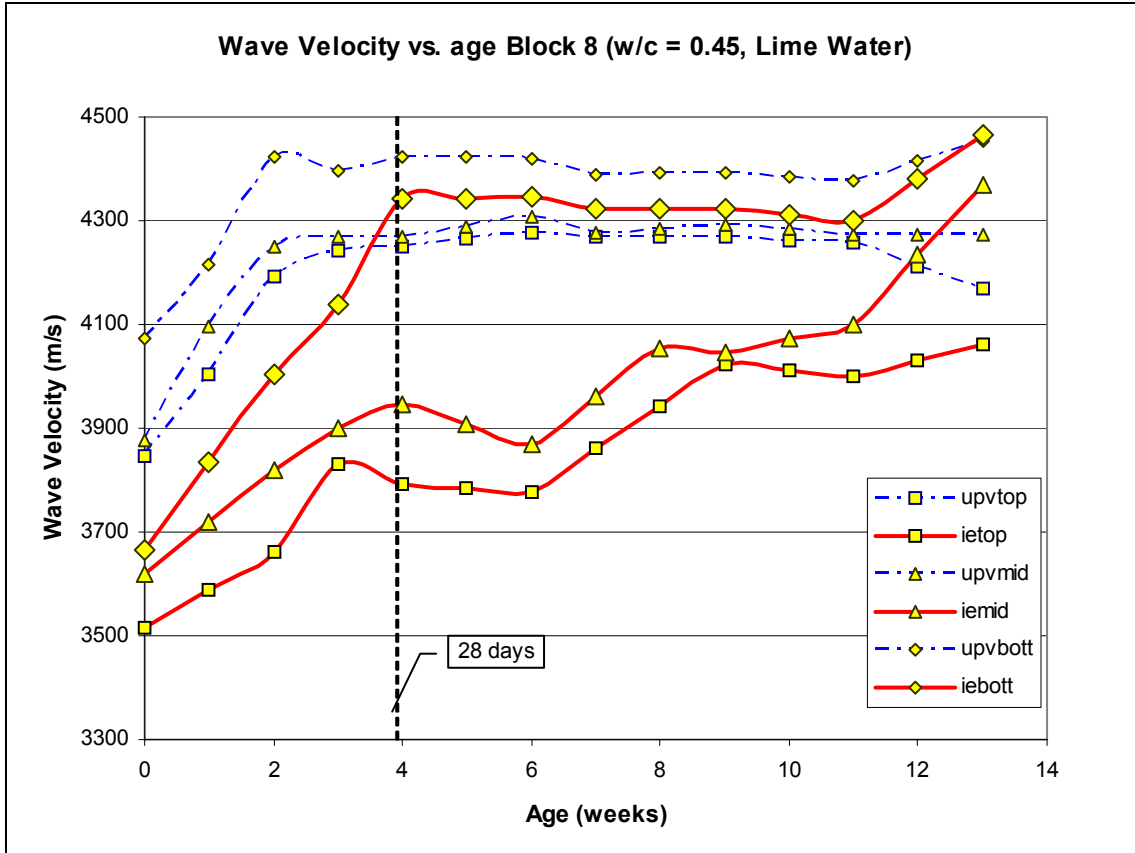
D1	55.0	E1	53.2
D2	55.2	E2	53.6
D3	55.1	E3	54.5
D4	55.2	E4	53.9
D5	55.5	E5	54.2
D6	55.1	E6	54.3
D7	56.1	E7	54.6
D8	55.2	E8	53.6
D9	54.1	E9	53.0

X1	113.3	Y1	113.7
X2	112.7	Y2	112.7
X3	112.8	Y3	112.9
X4	113.4	Y4	113.8
X5	113.9	Y5	113.3
X6	113.7	Y6	112.7
X7	112.6	Y7	112.6
X8	112.7	Y8	111.7
X9	110.8	Y9	113.5

Z1	113.6
Z2	113.6
Z3	114.2
Z4	113.4
Z5	114.1
Z6	113.7
Z7	113.6
Z8	112.7
Z9	110.0

XA	213.1	YA	211.3
XB	210.3	YB	207.5
XC	206.7	YC	206.9
XD	200.9	YD	204.9
XE	199.7	YE	202.7

ZA	210.8
ZB	208.1
ZC	208.3
ZD	204.5
ZE	199.8



Date 2/16/2003	Temp 72°F	Block # 21
----------------	-----------	------------

Ultrasonic Pulse Velocity Testing		
Point #	Time ( $\mu$ s)	Wave Velocity (m/s)
1		
2		
3		
4		
5		
6		
7		
8		
9		
10		
11		
12		
13		
14		
15		

Impact Echo Testing	
Reading #	Wave Velocity (m/s)
1	3273
2	3213
3	3389
4	3333
5	3462
6	3528

Date 2/21/2003	Temp 72°F	Block # 21
----------------	-----------	------------

Ultrasonic Pulse Velocity Testing		
Point #	Time ( $\mu$ s)	Wave Velocity (m/s)
1	67.8	3628.3
2	69.3	3549.8
3	69.2	3554.9
4	68.4	3596.5
5	65.6	3750.0
6	66.6	3693.7
7	67.0	3671.6
8	67.0	3671.6
9	62.4	3942.3
10	63.5	3874.0
11	64.3	3825.8
12	61.2	4019.6
13	240.4	3743.8
14	233.6	3874.1
15	226.9	4010.6

Impact Echo Testing	
Reading #	Wave Velocity (m/s)
1	3404
2	3600
3	3600
4	3530
5	3601
6	3850

Date	2/27/2003	Temp	72°F	Block #	21
------	-----------	------	------	---------	----

Ultrasonic Pulse Velocity Testing		
Point #	Time ( $\mu$ s)	Wave Velocity (m/s)
1	66.8	3682.6
2	70.4	3494.3
3	67.0	3671.6
4	66.8	3682.6
5	64.6	3808.0
6	65.1	3778.8
7	64.4	3819.9
8	65.2	3773.0
9	61.3	4013.1
10	63.5	3874.0
11	64.2	3831.8
12	61.1	4026.2
13	234.7	3834.7
14	229.0	3952.0
15	221.6	4106.5

Impact Echo Testing	
Reading #	Wave Velocity (m/s)
1	3500
2	3506
3	3660
4	3533
5	3799
6	3799

Date	3/6/2003	Temp	72°F	Block #	21
------	----------	------	------	---------	----

Ultrasonic Pulse Velocity Testing		
Point #	Time ( $\mu$ s)	Wave Velocity (m/s)
1	65.0	3784.6
2	66.0	3727.3
3	65.7	3744.3
4	65.3	3767.2
5	67.0	3671.6
6	63.8	3855.8
7	63.6	3867.9
8	63.3	3886.3
9	60.0	4100.0
10	60.6	4059.4
11	62.4	3942.3
12	59.4	4141.4
13	232.6	3869.3
14	225.6	4011.5
15	218.2	4170.5

Impact Echo Testing	
Reading #	Wave Velocity (m/s)
1	3396
2	3529
3	3529
4	3670
5	4001
6	4092

Date 3/13/2003	Temp 72°F	Block # 21
----------------	-----------	------------

Ultrasonic Pulse Velocity Testing		
Point #	Time ( $\mu$ s)	Wave Velocity (m/s)
1	63.7	3861.9
2	64.2	3831.8
3	64.8	3796.3
4	63.5	3874.0
5	62.0	3967.7
6	62.5	3936.0
7	62.7	3923.4
8	62.2	3955.0
9	58.6	4198.0
10	59.8	4113.7
11	59.8	4113.7
12	58.1	4234.1
13	228.0	3947.4
14	223.1	4056.5
15	216.7	4199.4

Impact Echo Testing	
Reading #	Wave Velocity (m/s)
1	3529
2	3600
3	3752
4	3433
5	3913
6	3913

Date 3/27/2003	Temp 72°F	Block # 21
----------------	-----------	------------

Ultrasonic Pulse Velocity Testing		
Point #	Time ( $\mu$ s)	Wave Velocity (m/s)
1	65.1	3778.8
2	65.9	3732.9
3	65.7	3744.3
4	64.5	3814.0
5	63.2	3892.4
6	64.4	3819.9
7	64.1	3837.8
8	63.2	3892.4
9	59.5	4134.5
10	60.0	4100.0
11	61.0	4032.8
12	59.6	4127.5
13	228.8	3933.6
14	222.7	4063.8
15	216.6	4201.3

Impact Echo Testing	
Reading #	Wave Velocity (m/s)
1	3611
2	3461
3	3752
4	3598
5	4005
6	3996

Date	4/17/2003	Temp	72°F	Block #	21
------	-----------	------	------	---------	----

Ultrasonic Pulse Velocity Testing		
Point #	Time ( $\mu$ s)	Wave Velocity (m/s)
1	65.0	3784.6
2	66.9	3677.1
3	65.9	3732.9
4	64.9	3790.4
5	62.9	3911.0
6	63.6	3867.9
7	63.3	3886.3
8	63.2	3892.4
9	59.5	4134.5
10	60.1	4093.2
11	61.0	4032.8
12	58.8	4183.7
13	228.5	3938.7
14	221.6	4083.9
15	216.2	4209.1

Impact Echo Testing	
Reading #	Wave Velocity (m/s)
1	3600
2	3529
3	3789
4	3749
5	4002
6	3996

Date	5/1/2003	Temp	72°F	Block #	21
------	----------	------	------	---------	----

Ultrasonic Pulse Velocity Testing		
Point #	Time ( $\mu$ s)	Wave Velocity (m/s)
1	64.5	3814.0
2	65.3	3767.2
3	65.3	3767.2
4	65.0	3784.6
5	61.9	3974.2
6	62.2	3955.0
7	62.5	3936.0
8	63.3	3886.3
9	59.1	4162.4
10	60.4	4072.8
11	61.9	3974.2
12	59.2	4155.4
13	228.7	3935.3
14	222.1	4074.7
15	216.5	4203.2

Impact Echo Testing	
Reading #	Wave Velocity (m/s)
1	
2	
3	
4	
5	
6	

Date	5/1/2003	Temp	72°F	Block #	21
------	----------	------	------	---------	----

Ultrasonic Pulse Velocity Testing		
Point #	Time ( $\mu$ s)	Wave Velocity (m/s)
1	64.5	3814.0
2	65.3	3767.2
3	65.3	3767.2
4	65.0	3784.6
5	61.9	3974.2
6	62.2	3955.0
7	62.5	3936.0
8	63.3	3886.3
9	59.1	4162.4
10	60.4	4072.8
11	61.9	3974.2
12	59.2	4155.4
13	228.7	3935.3
14	222.1	4074.7
15	216.5	4203.2

Impact Echo Testing	
Reading #	Wave Velocity (m/s)
1	
2	
3	
4	
5	
6	

## Tomography Data Sheet for Test blocks.

Date 5/13/2003

Block # 21

Point #	Time ( $\mu$ s)	Point #	Time ( $\mu$ s)
A1	64.8	B1	62.5
A2	64.6	B2	63.6
A3	65.5	B3	64.2
A4	66.5	B4	64.2
A5	65.8	B5	65.0
A6	65.9	B6	64.9
A7	65.5	B7	64.8
A8	65.4	B8	64.5
A9	66.4	B9	63.5

Point #	Time ( $\mu$ s)
C1	60.2
C2	62.5
C3	62.9
C4	63.3
C5	63.5
C6	63.4
C7	63.6
C8	62.8
C9	62.5

D1	60.3	E1	56.7
D2	60.7	E2	58.6
D3	61.2	E3	60.6
D4	61.6	E4	59.8
D5	62.4	E5	61.0
D6	62.6	E6	60.1
D7	62.1	E7	58.6
D8	60.9	E8	58.6
D9	59.5	E9	58.4

X1	117.2	Y1	118.2
X2	119.6	Y2	118.8
X3	120.4	Y3	119.1
X4	120.9	Y4	121.0
X5	122.7	Y5	120.8
X6	120.6	Y6	121.9
X7	119.0	Y7	117.9
X8	118.9	Y8	118.3
X9	116.5	Y9	118.7

Z1	116.4
Z2	118.6
Z3	120.2
Z4	120.7
Z5	121.6
Z6	122.1
Z7	119.4
Z8	118.3
Z9	116.6

XA	237.5	YA	231.1
XB	229.1	YB	225.5
XC	223.5	YC	221.3
XD	217.6	YD	218.2
XE	209.2	YE	213.0

ZA	235.4
ZB	227.8
ZC	222.0
ZD	214.3
ZE	209.5

Date	2/16/2003	Temp	72°F	Block #	22
------	-----------	------	------	---------	----

Ultrasonic Pulse Velocity Testing		
Point #	Time (μs)	Wave Velocity (m/s)
1		
2		
3		
4		
5		
6		
7		
8		
9		
10		
11		
12		
13		
14		
15		

Impact Echo Testing	
Reading #	Wave Velocity (m/s)
1	3396
2	3348
3	3529
4	3272
5	3461
6	3528

Date	2/20/2003	Temp	72°F	Block #	22
------	-----------	------	------	---------	----

Ultrasonic Pulse Velocity Testing		
Point #	Time (μs)	Wave Velocity (m/s)
1	70	3485.7
2	67.3	3625.6
3	68.3	3572.5
4	69.7	3500.7
5	65.1	3748.1
6	66.3	3680.2
7	63.8	3824.5
8	63.6	3836.5
9	63	3873.0
10	62.8	3885.4
11	62.3	3916.5
12	60.5	4033.1
13	240.8	3737.5
14	233.7	3861.8
15	228.7	3957.1

Impact Echo Testing	
Reading #	Wave Velocity (m/s)
1	3389
2	3397
3	3788
4	3839
5	3852
6	3831

Date	2/27/2003	Temp	72°F	Block #	22
------	-----------	------	------	---------	----

Ultrasonic Pulse Velocity Testing		
Point #	Time ( $\mu$ s)	Wave Velocity (m/s)
1	64.6	3777.1
2	64.8	3765.4
3	65	3753.8
4	65	3753.8
5	62.1	3929.1
6	62.1	3929.1
7	61.6	3961.0
8	61.6	3961.0
9	61.2	3986.9
10	61.6	3961.0
11	60.4	4039.7
12	58.8	4149.7
13	232.3	3874.3
14	226.7	3981.0
15	220.5	4104.3

Impact Echo Testing	
Reading #	Wave Velocity (m/s)
1	3662
2	3893
3	3798
4	4104
5	3894
6	4285

Date	3/6/2003	Temp	72°F	Block #	22
------	----------	------	------	---------	----

Ultrasonic Pulse Velocity Testing		
Point #	Time ( $\mu$ s)	Wave Velocity (m/s)
1	64.3	3794.7
2	64.7	3771.3
3	64.3	3794.7
4	67	3641.8
5	64.6	3777.1
6	64.6	3777.1
7	60.7	4019.8
8	60.2	4053.2
9	61.1	3993.5
10	60.9	4006.6
11	58.8	4149.7
12	58.4	4178.1
13	230.8	3899.5
14	225.3	4005.8
15	218.7	4138.1

Impact Echo Testing	
Reading #	Wave Velocity (m/s)
1	3600
2	3600
3	4092
4	3674
5	4114
6	3902

Date 3/12/2003	Temp 72°F	Block # 22
----------------	-----------	------------

Ultrasonic Pulse Velocity Testing		
Point #	Time ( $\mu$ s)	Wave Velocity (m/s)
1		
2		
3		
4		
5		
6		
7		
8		
9		
10		
11		
12		
13		
14		
15		

Impact Echo Testing	
Reading #	Wave Velocity (m/s)
1	3396
2	3672
3	3913
4	3935
5	4090
6	3998

Date 3/27/2003	Temp 72°F	Block # 22
----------------	-----------	------------

Ultrasonic Pulse Velocity Testing		
Point #	Time ( $\mu$ s)	Wave Velocity (m/s)
1	63.9	3818.5
2	63.7	3830.5
3	63.7	3830.5
4	63.7	3830.5
5	60.6	4026.4
6	60.4	4039.7
7	60.6	4026.4
8	60.6	4026.4
9	58.9	4142.6
10	59.1	4128.6
11	57.6	4236.1
12	57.0	4280.7
13	227.4	3957.8
14	220.6	4091.1
15	215.4	4201.5

Impact Echo Testing	
Reading #	Wave Velocity (m/s)
1	3600
2	3463
3	3751
4	3749
5	4091
6	3913

Date 4/17/2003	Temp 72°F	Block # 22
----------------	-----------	------------

Ultrasonic Pulse Velocity Testing		
Point #	Time ( $\mu$ s)	Wave Velocity (m/s)
1	63.4	3848.6
2	64.1	3806.6
3	63.3	3854.7
4	63.6	3836.5
5	60.9	4006.6
6	60.4	4039.7
7	60.3	4046.4
8	60.1	4059.9
9	58.5	4170.9
10	59.2	4121.6
11	57.3	4258.3
12	56.9	4288.2
13	227.3	3959.5
14	219.5	4111.6
15	214.3	4223.1

Impact Echo Testing	
Reading #	Wave Velocity (m/s)
1	3600
2	3601
3	3841
4	3828
5	3913
6	4068

Date 5/1/2003	Temp 72°F	Block # 22
---------------	-----------	------------

Ultrasonic Pulse Velocity Testing		
Point #	Time ( $\mu$ s)	Wave Velocity (m/s)
1	64.0	3812.5
2	64.4	3788.8
3	63.2	3860.8
4	64.0	3812.5
5	60.4	4039.7
6	59.6	4094.0
7	59.7	4087.1
8	59.2	4121.6
9	61.8	3948.2
10	59.9	4073.5
11	57.9	4214.2
12	58.1	4199.7
13	225.6	3989.4
14	219.3	4115.4
15	215.2	4205.4

Impact Echo Testing	
Reading #	Wave Velocity (m/s)
1	
2	
3	
4	
5	
6	

## Tomography Data Sheet for Test blocks.

Date 5/13/2003

Temp 72°F

Block # 22

Point #	Time (μs)
A1	64.1
A2	64.4
A3	64.9
A4	65.1
A5	65.3
A6	65.7
A7	65.2
A8	64.4
A9	65.4

Point #	Time (μs)
B1	61.2
B2	61.7
B3	62.0
B4	61.6
B5	61.5
B6	61.4
B7	62.3
B8	61.7
B9	62.1

Point #	Time (μs)
C1	59.4
C2	60.7
C3	60.5
C4	60.4
C5	60.2
C6	60.4
C7	60.6
C8	60.4
C9	60.0

D1	58.5
D2	59.5
D3	59.8
D4	59.7
D5	59.3
D6	59.1
D7	59.0
D8	58.4
D9	58.6

E1	55.9
E2	56.9
E3	56.9
E4	58.2
E5	58.6
E6	57.4
E7	57.6
E8	56.8
E9	55.4

X1	112.1
X2	115.9
X3	117.3
X4	118.3
X5	117.6
X6	116.8
X7	117.1
X8	116.7
X9	116.5

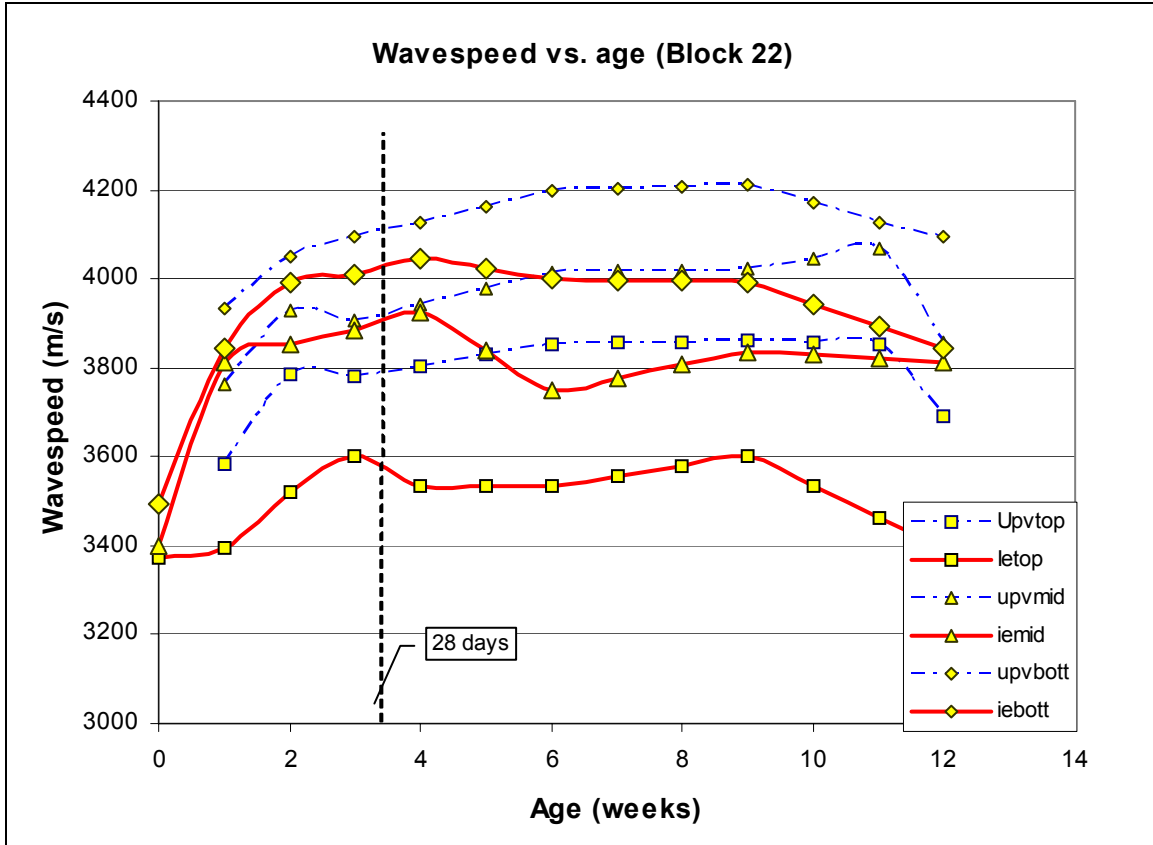
Y1	115.0
Y2	115.7
Y3	117.0
Y4	118.7
Y5	117.8
Y6	118.0
Y7	115.9
Y8	115.7
Y9	117.3

Z1	112.4
Z2	115.0
Z3	117.0
Z4	118.1
Z5	117.5
Z6	117.9
Z7	116.4
Z8	116.5
Z9	116.8

XA	235.2
XB	225.8
XC	219.1
XD	214.4
XE	208.4

YA	232.0
YB	223.8
YC	219.1
YD	217.2
YE	211.3

ZA	236.5
ZB	226.7
ZC	220.5
ZD	214.7
ZE	208.0



Date	2/10/2003	Temp	72°F	Block #	23
------	-----------	------	------	---------	----

Ultrasonic Pulse Velocity Testing		
Point #	Time ( $\mu$ s)	Wave Velocity (m/s)
1		
2		
3		
4		
5		
6		
7		
8		
9		
10		
11		
12		
13		
14		
15		

Impact Echo Testing	
Reading #	Wave Velocity (m/s)
1	3287
2	3272
3	3470
4	3430
5	3674
6	3600

Date	1/20/2003	Temp	72°F	Block #	23
------	-----------	------	------	---------	----

Ultrasonic Pulse Velocity Testing		
Point #	Time ( $\mu$ s)	Wave Velocity (m/s)
1	68.7	3493.4
2	70	3428.6
3	68.6	3498.5
4	67.5	3555.6
5	65.3	3706.0
6	65.7	3683.4
7	65.6	3689.0
8	65.1	3717.4
9	61.5	3967.5
10	64.4	3788.8
11	64.5	3782.9
12	63.7	3830.5
13	245.6	3664.5
14	235.8	3829.5
15	224.8	4030.2

Impact Echo Testing	
Reading #	Wave Velocity (m/s)
1	3272
2	3328
3	3653
4	3768
5	4090
6	3789

Date	2/28/2003	Temp	72°F	Block #	23
------	-----------	------	------	---------	----

Ultrasonic Pulse Velocity Testing		
Point #	Time (μs)	Wave Velocity (m/s)
1	66.5	3609.0
2	66.7	3598.2
3	67.7	3545.1
4	65.1	3686.6
5	64.3	3763.6
6	63.2	3829.1
7	63.6	3805.0
8	62.2	3890.7
9	60.0	4066.7
10	62.0	3935.5
11	62.6	3897.8
12	61.7	3954.6
13	234.8	3833.0
14	226.7	3983.2
15	218.5	4146.5

Impact Echo Testing	
Reading #	Wave Velocity (m/s)
1	3462
2	3601
3	4000
4	3830
5	4002
6	4090

Date	3/6/2003	Temp	72°F	Block #	23
------	----------	------	------	---------	----

Ultrasonic Pulse Velocity Testing		
Point #	Time (μs)	Wave Velocity (m/s)
1	65.4	3669.7
2	65.6	3658.5
3	64.7	3709.4
4	63.4	3785.5
5	62.4	3878.2
6	62.4	3878.2
7	63.3	3823.1
8	62.0	3903.2
9	58.3	4185.2
10	61.5	3967.5
11	61.2	3986.9
12	60.8	4013.2
13	232.1	3877.6
14	224.6	4020.5
15	216.3	4188.6

Impact Echo Testing	
Reading #	Wave Velocity (m/s)
1	3397
2	3670
3	3752
4	3751
5	4009
6	4001

Date 3/20/2003	Temp 72°F	Block # 23
----------------	-----------	------------

Ultrasonic Pulse Velocity Testing		
Point #	Time ( $\mu$ s)	Wave Velocity (m/s)
1	63.7	3767.7
2	63.6	3773.6
3	63.3	3791.5
4	62.6	3833.9
5	60.8	3980.3
6	60.6	3993.4
7	60.5	4000.0
8	59.6	4060.4
9	57.4	4250.9
10	59.7	4087.1
11	59.9	4073.5
12	59.5	4100.8
13	228.2	3943.9
14	219.6	4112.0
15	212.0	4273.6

Impact Echo Testing	
Reading #	Wave Velocity (m/s)
1	3513
2	3751
3	3831
4	3749
5	4176
6	4185

Date 3/27/2003	Temp 72°F	Block # 23
----------------	-----------	------------

Ultrasonic Pulse Velocity Testing		
Point #	Time ( $\mu$ s)	Wave Velocity (m/s)
1	64.8	3703.7
2	64.8	3703.7
3	64.8	3703.7
4	63.9	3755.9
5	62.2	3890.7
6	61.6	3928.6
7	61.9	3909.5
8	60.8	3980.3
9	58.7	4156.7
10	60.9	4006.6
11	61.6	3961.0
12	61.0	4000.0
13	228.6	3937.0
14	220.5	4095.2
15	211.9	4275.6

Impact Echo Testing	
Reading #	Wave Velocity (m/s)
1	
2	
3	
4	
5	
6	

Date 4/10/2003	Temp 72°F	Block # 23
----------------	-----------	------------

Ultrasonic Pulse Velocity Testing		
Point #	Time ( $\mu$ s)	Wave Velocity (m/s)
1	65.6	3658.5
2	65.6	3658.5
3	65.6	3658.5
4	64.2	3738.3
5	62.1	3896.9
6	61.9	3909.5
7	63.1	3835.2
8	62.1	3896.9
9	60.0	4066.7
10	62.4	3910.3
11	61.9	3941.8
12	61.0	4000.0
13	227.0	3964.8
14	220.2	4100.8
15	214.3	4227.7

Impact Echo Testing	
Reading #	Wave Velocity (m/s)
1	3598
2	3599
3	3693
4	3674
5	4298
6	4287

Date 4/24/2003	Temp 72°F	Block # 23
----------------	-----------	------------

Ultrasonic Pulse Velocity Testing		
Point #	Time ( $\mu$ s)	Wave Velocity (m/s)
1	65.8	3647.4
2	65.8	3647.4
3	65.1	3686.6
4	64.1	3744.1
5	61.7	3922.2
6	62.5	3872.0
7	63.7	3799.1
8	61.3	3947.8
9	60.0	4066.7
10	61.0	4000.0
11	62.3	3916.5
12	62.4	3910.3
13	227.3	3959.5
14	220.6	4093.4
15	213.5	4243.6

Impact Echo Testing	
Reading #	Wave Velocity (m/s)
1	3618
2	3581
3	3693
4	3680
5	4050
6	4150

## Tomography Data Sheet for Test blocks.

Date 5/13/2003

Block # 23

Point #	Time ( $\mu$ s)	Point #	Time ( $\mu$ s)
A1	67.0	B1	61.7
A2	66.9	B2	63.2
A3	67.0	B3	64.3
A4	67.6	B4	64.5
A5	66.5	B5	63.3
A6	65.9	B6	63.9
A7	65.4	B7	63.3
A8	65.4	B8	63.2
A9	66.7	B9	64.3

Point #	Time ( $\mu$ s)
C1	60.4
C2	61.9
C3	62.5
C4	62.0
C5	62.3
C6	62.1
C7	62.4
C8	60.8
C9	60.8

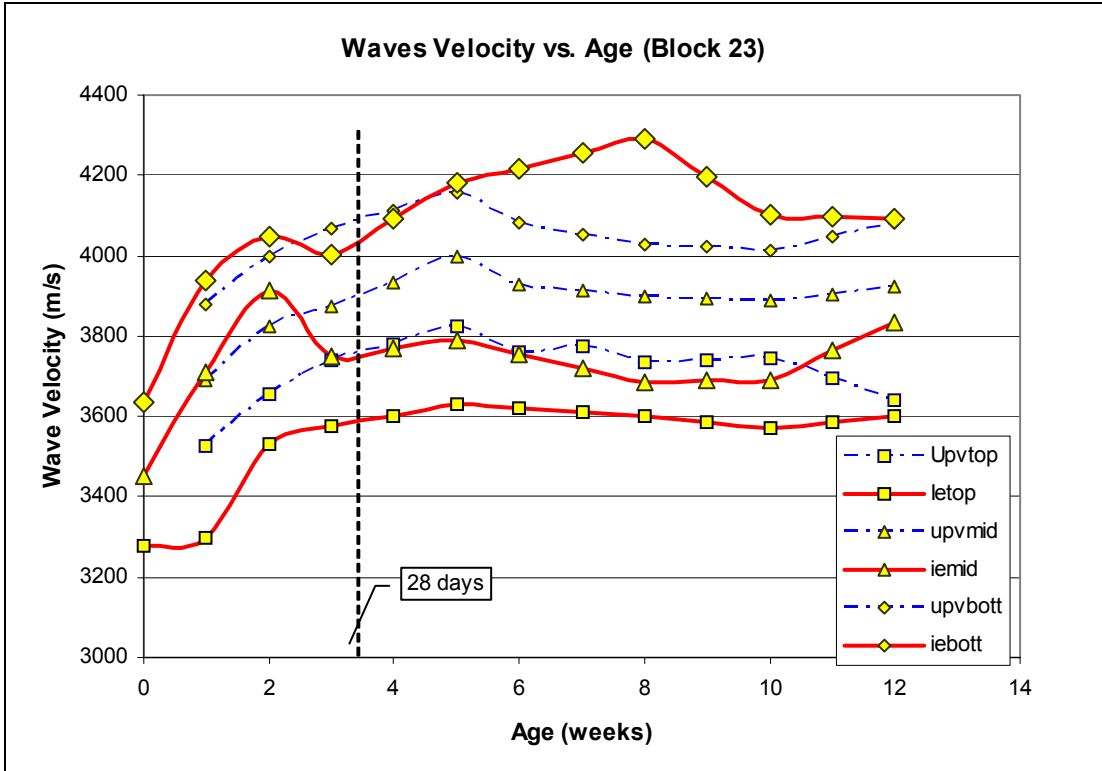
D1	58.1	E1	56.4
D2	59.6	E2	57.8
D3	60.7	E3	59.0
D4	61.3	E4	60.9
D5	61.3	E5	60.9
D6	61.1	E6	61.1
D7	61.2	E7	61.2
D8	60.6	E8	59.5
D9	58.7	E9	57.2

X1	115.7	Y1	116.2
X2	117.4	Y2	116.6
X3	118.4	Y3	116.8
X4	119.5	Y4	119.2
X5	119.3	Y5	118.5
X6	118.5	Y6	117.7
X7	117.6	Y7	116.4
X8	118.4	Y8	116.2
X9	115.9	Y9	116.5

Z1	117.0
Z2	118.8
Z3	118.1
Z4	119.3
Z5	118.6
Z6	118.5
Z7	118.5
Z8	117.3
Z9	116.0

XA	237.9	YA	233.5
XB	28.4	YB	225.6
XC	222.6	YC	220.2
XD	214.7	YD	216.4
XE	208.5	YE	211.0

ZA	239.5
ZB	226.8
ZC	220.4
ZD	214.9
ZE	207.4



Date	2/10/2003	Temp	72°F	Block #	24
------	-----------	------	------	---------	----

Ultrasonic Pulse Velocity Testing		
Point #	Time ( $\mu$ s)	Wave Velocity (m/s)
1		
2		
3		
4		
5		
6		
7		
8		
9		
10		
11		
12		
13		
14		
15		

Impact Echo Testing	
Reading #	Wave Velocity (m/s)
1	3348
2	3332
3	3531
4	3547
5	3692
6	3674

Date	2/21/2003	Temp	72°F	Block #	24
------	-----------	------	------	---------	----

Ultrasonic Pulse Velocity Testing		
Point #	Time ( $\mu$ s)	Wave Velocity (m/s)
1	67	3641.8
2	67.8	3598.8
3	70.9	3441.5
4	68.2	3577.7
5	66.5	3669.2
6	66.3	3680.2
7	67.4	3620.2
8	65.1	3748.1
9	60.2	4053.2
10	61.5	3967.5
11	62.2	3922.8
12	61	4000.0
13	244.3	3684.0
14	232.2	3882.4
15	225.4	4006.2

Impact Echo Testing	
Reading #	Wave Velocity (m/s)
1	3599
2	3530
3	3944
4	3555
5	4000
6	3617

Date	2/28/2003	Temp	72°F	Block #	24
------	-----------	------	------	---------	----

Ultrasonic Pulse Velocity Testing		
Point #	Time ( $\mu$ s)	Wave Velocity (m/s)
1	65.8	3708.2
2	65.4	3730.9
3	65.7	3713.9
4	65.3	3736.6
5	62.5	3904.0
6	62.2	3922.8
7	61.0	4000.0
8	61.6	3961.0
9	59.1	4128.6
10	59.6	4094.0
11	59.6	4094.0
12	58.0	4206.9
13	235.6	3820.0
14	227.6	3960.9
15	219.7	4110.2

Impact Echo Testing	
Reading #	Wave Velocity (m/s)
1	3601
2	3600
3	3731
4	3675
5	4000
6	4009

Date	3/6/2003	Temp	72°F	Block #	24
------	----------	------	------	---------	----

Ultrasonic Pulse Velocity Testing		
Point #	Time ( $\mu$ s)	Wave Velocity (m/s)
1	64.0	3812.5
2	64.3	3794.7
3	64.7	3771.3
4	65.0	3753.8
5	61.1	3993.5
6	61.1	3993.5
7	62.0	3935.5
8	62.3	3916.5
9	57.9	4214.2
10	58.8	4149.7
11	58.7	4156.7
12	57.7	4228.8
13	234.5	3838.0
14	224.5	4015.6
15	219.4	4115.8

Impact Echo Testing	
Reading #	Wave Velocity (m/s)
1	3599
2	3529
3	3752
4	3672
5	4080
6	4090

Date 3/20/2003	Temp 72°F	Block # 24
----------------	-----------	------------

Ultrasonic Pulse Velocity Testing		
Point #	Time ( $\mu$ s)	Wave Velocity (m/s)
1	62.2	3922.8
2	62.5	3904.0
3	63.3	3854.7
4	63.7	3830.5
5	59.0	4135.6
6	59.1	4128.6
7	60.6	4026.4
8	60.9	4006.6
9	57.5	4243.5
10	59.2	4121.6
11	58.5	4170.9
12	57.8	4221.5
13	229.9	3914.7
14	220.4	4090.3
15	214.7	4205.9

Impact Echo Testing	
Reading #	Wave Velocity (m/s)
1	3601
2	3601
3	3758
4	3735
5	4135
6	4138

Date 3/27/2003	Temp 72°F	Block # 24
----------------	-----------	------------

Ultrasonic Pulse Velocity Testing		
Point #	Time ( $\mu$ s)	Wave Velocity (m/s)
1	63.3	3854.7
2	63.3	3854.7
3	63.8	3824.5
4	64.8	3765.4
5	60.0	4066.7
6	59.9	4073.5
7	60.9	4006.6
8	61.6	3961.0
9	60.0	4066.7
10	59.4	4107.7
11	59.2	4121.6
12	58.8	4149.7
13	230.4	3906.3
14	221.5	4070.0
15	214.0	4219.6

Impact Echo Testing	
Reading #	Wave Velocity (m/s)
1	
2	
3	
4	
5	
6	

Date 4/10/2003	Temp 72°F	Block # 24
----------------	-----------	------------

Ultrasonic Pulse Velocity Testing		
Point #	Time ( $\mu$ s)	Wave Velocity (m/s)
1	63.8	3824.5
2	63.8	3824.5
3	64.0	3812.5
4	65.0	3753.8
5	60.5	4033.1
6	60.5	4033.1
7	60.5	4033.1
8	61.0	4000.0
9	59.8	4080.3
10	60.3	4046.4
11	60.0	4066.7
12	59.2	4121.6
13	229.5	3921.6
14	221.6	4068.1
15	215.3	4194.1

Impact Echo Testing	
Reading #	Wave Velocity (m/s)
1	3770
2	3581
3	3600
4	3674
5	3829
6	3947

Date 4/24/2003	Temp 72°F	Block # 24
----------------	-----------	------------

Ultrasonic Pulse Velocity Testing		
Point #	Time ( $\mu$ s)	Wave Velocity (m/s)
2	63.4	3848.6
3	64.6	3777.1
4	65.3	3736.6
5	59.9	4073.5
6	60.4	4039.7
7	60.9	4006.6
8	62.0	3935.5
9	58.9	4142.6
10	62.7	3891.5
11	60.1	4059.9
12	60.9	4006.6
13	229.8	3916.4
14	219.1	4114.6
15	215.1	4198.0

Impact Echo Testing	
Reading #	Wave Velocity (m/s)
2	3461
3	3602
4	3545
5	3742
6	3913

## Side Tomography Data Sheet for Test blocks.

Date		5/13/2003	
Block #		24	
Point #	Time (ms)	Point #	Time (ms)
A1	68.7	B1	63.9
A2	66.3	B2	63.5
A3	66.5	B3	63.9
A4	66.3	B4	64.1
A5	66.1	B5	62.7
A6	66.4	B6	63.3
A7	65.4	B7	63.1
A8	66.6	B8	63.0
A9	69.0	B9	63.7

Point #	Time (ms)
C1	60.3
C2	61.4
C3	61.6
C4	61.0
C5	61.5
C6	60.7
C7	60.5
C8	60.9
C9	61.1

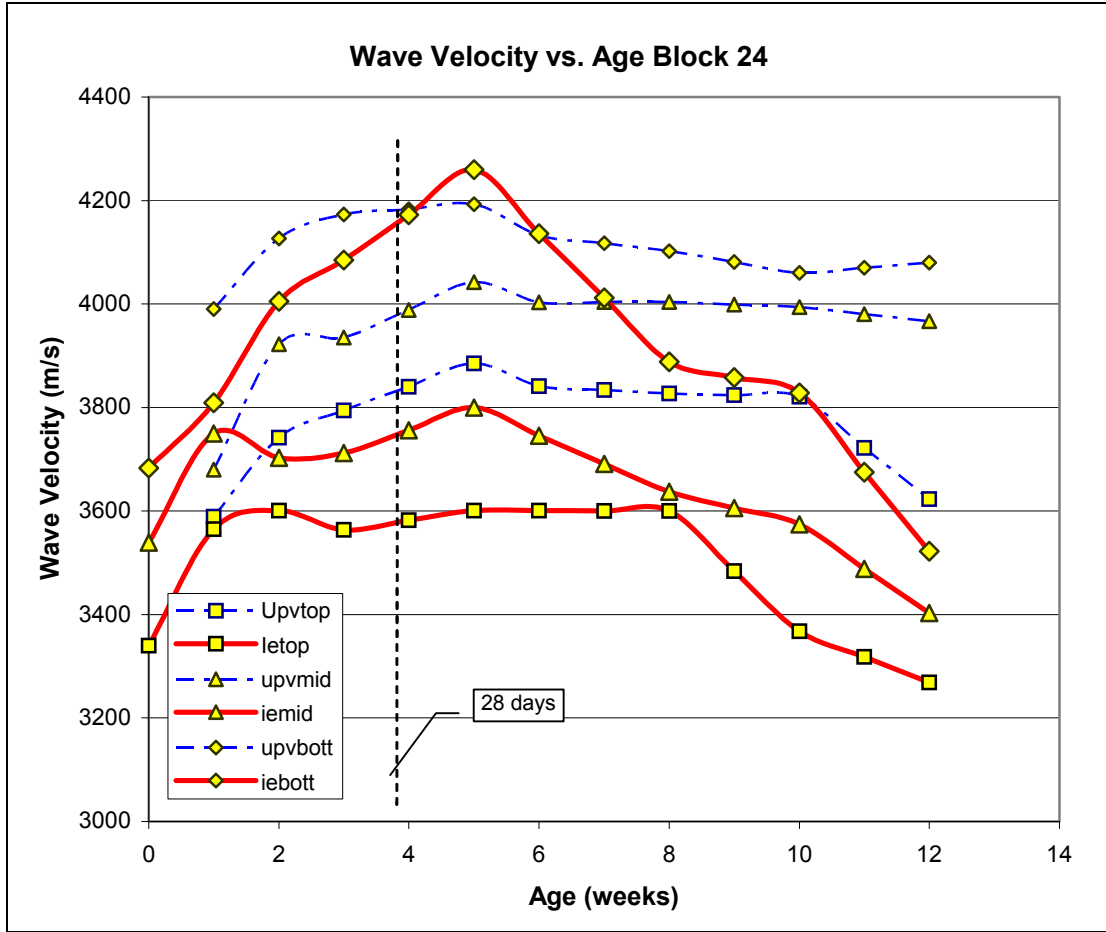
D1	58.3	E1	56.7
D2	59.2	E2	56.5
D3	59.0	E3	57.9
D4	59.7	E4	58.5
D5	59.5	E5	59.0
D6	59.4	E6	58.3
D7	58.9	E7	56.9
D8	59.7	E8	56.1
D9	59.0	E9	58.1

X1	116.1	Y1	117.9
X2	117.8	Y2	117.0
X3	118.8	Y3	117.4
X4	118.0	Y4	118.7
X5	118.2	Y5	118.0
X6	117.9	Y6	118.8
X7	118.4	Y7	117.4
X8	118.2	Y8	117.5
X9	118.1	Y9	118.7

Z1	116.3
Z2	118.3
Z3	119.1
Z4	120.1
Z5	119.4
Z6	120.0
Z7	118.0
Z8	117.9
Z9	118.1

XA	238.1	YA	234.3
XB	229.1	YB	226.2
XC	223.0	YC	220.2
XD	215.4	YD	216.0
XE	209.3	YE	212.3

ZA	238.7
ZB	229.3
ZC	222.1
ZD	213.6
ZE	207.0



APPENDIX F  
SUMMARY OF STASTICAL RESULTS OF ULTRASONIC PULSE VELOCITY  
DATA

ANOVA Summary Table (Block 5)  
Ultrasonic Pulse Velocity Results

Date	One Way ANOVA		Bartlet's Test for Equal Variances		Coefficient of Variation			
	P-Value	Are means significantly different? (P < 0.05)	Bartlet's Statistic	P-Value	Are variances significantly different? (P < 0.05)	Coefficient of Variation for top row of block	Coefficient of Variation for middle row of block	Coefficient of Variation for bottom row of block
9-Feb	0.0001	Yes	0.0474		Yes	1.61%	0.38%	1.50%
13-Feb	0.0002	Yes	0.1160		No	2.90%	0.83%	1.77%
21-Feb	0.0001	Yes	0.2238		No	0.77%	0.38%	0.97%
27-Feb	0.0001	Yes	0.8623		No	0.68%	0.86%	0.85%
7-Mar	0.0001	Yes	0.5068		No	0.86%	0.58%	0.45%
27-Mar	0.0005	Yes	0.3502		No	1.00%	0.77%	1.55%
17-Apr	0.0001	Yes	0.5198		No	1.03%	0.77%	1.37%
1-May	0.0001	Yes	0.5807		No	1.12%	0.62%	0.91%
10-May	0.0001	Yes	0.0002		Yes	1.85%	0.52%	1.44%

ANOVA Summary Table (Block 6)  
Ultrasonic Pulse Velocity Results

Date	One Way ANOVA		Bartlet's Test for Equal Variances		Coefficient of Variation			
	P-Value	Are means significantly different? (P < 0.05)	Bartlet's Statistic	P-Value	Are variances significantly different? (P < 0.05)	Coefficient of Variation for top row of block	Coefficient of Variation for middle row of block	Coefficient of Variation for bottom row of block
9-Feb								
13-Feb	0.0126	Yes	0.4935		No	3.26%	2.14%	1.68%
21-Feb	0.7103	No	0.3387		No	2.80%	2.35%	4.84%
27-Feb	0.0303	Yes	0.8246		No	1.41%	1.92%	1.52%
7-Mar	0.0026	Yes	0.8970		No	1.18%	1.49%	1.24%
27-Mar	0.2654	No	0.9266		No	1.85%	1.97%	2.21%
17-Apr	0.0162	Yes	0.6985		No	1.57%	2.20%	1.43%
1-May	0.0919	No	0.9351		No	1.90%	2.25%	2.17%
10-May	0.0001	Yes	0.0503		No	1.32%	2.06%	2.47%

## ANOVA Summary Table (Block 7)

## Ultrasonic Pulse Velocity Results

One Way ANOVA		Bartlet's Test for Equal Variances			Coefficient of Variation		
Date	P-Value	Are means significantly different? (P < 0.05)	Bartlet's Statistic P-Value	Are variances significantly different? (P < 0.05)	Coefficient of Variation for top row of block	Coefficient of Variation for middle row of block	Coefficient of Variation for bottom row of block
9-Feb	0.4840	No	0.2859	No	1.05%	1.63%	2.46%
13-Feb	0.2617	No	0.8967	No	3.09%	2.46%	2.47%
21-Feb	0.1622	No	0.8008	No	1.17%	1.35%	1.63%
27-Feb	0.1643	No	0.8100	No	1.29%	1.47%	1.77%
7-Mar	0.3820	No	0.4426	No	1.19%	1.44%	2.24%
20-Mar	0.9304	No	0.2673	No	1.22%	1.67%	2.82%
27-Mar	0.6364	No	0.6740	No	1.55%	1.93%	2.46%
10-Apr	0.9988	No	0.3947	No	1.53%	2.09%	3.14%
24-Apr	0.9923	No	0.2143	No	1.12%	2.14%	3.01%
10-May	0.0001	Yes	0.0100	No	1.03%	1.47%	2.50%

## ANOVA Summary Table (Block 8)

## Ultrasonic Pulse Velocity Results

One Way ANOVA		Bartlet's Test for Equal Variances			Coefficient of Variation		
Date	P-Value	Are means significantly different? (P < 0.05)	Bartlet's Statistic P-Value	Are variances significantly different? (P < 0.05)	Coefficient of Variation for top row of block	Coefficient of Variation for middle row of block	Coefficient of Variation for bottom row of block
9-Feb	0.0178	Yes	0.7487	No	2.70%	3.93%	3.45%
13-Feb	0.0088	Yes	0.1292	No	3.30%	1.43%	1.19%
21-Feb	0.0001	Yes	0.4125	No	0.38%	0.78%	0.57%
27-Feb	0.0001	Yes	0.7654	No	0.87%	0.83%	0.58%
7-Mar	0.0001	Yes	0.9828	No	0.93%	0.98%	0.99%
20-Mar	0.0013	Yes	0.5167	No	1.27%	1.23%	0.69%
27-Mar	0.0145	Yes	0.8310	No	1.12%	1.55%	1.30%
10-Apr	0.0171	Yes	0.8580	No	1.15%	1.42%	1.49%
24-Apr	0.0635	Yes	0.7266	No	1.33%	1.98%	1.85%
10-May	0.0001	Yes	0.9636	No	1.10%	1.15%	1.70%

## ANOVA Summary Table (Block 21)

## Ultrasonic Pulse Velocity Results

One Way ANOVA			Bartlet's Test for Equal Variances		Coefficient of Variation		
Date	P-Value	Are means significantly different? (P < 0.05)	Bartlet's Statistic P-Value	Are variances significantly different? (P < 0.05)	Coefficient of Variation for top row of block	Coefficient of Variation for middle row of block	Coefficient of Variation for bottom row of block
21-Feb	0.0002	Yes	0.9871	No	2.19%	2.29%	2.15%
27-Feb	0.0027	Yes	0.6170	No	3.29%	1.91%	2.87%
6-Mar	0.0006	Yes	0.3567	No	1.46%	3.15%	2.18%
13-Mar	0.0001	Yes	0.9910	No	1.46%	1.32%	1.32%
27-Mar	0.0001	Yes	0.6936	No	2.13%	2.47%	1.48%
17-Apr	0.0001	Yes	0.8296	No	2.58%	2.25%	1.71%
1-May	0.0002	Yes	0.8383	No	1.85%	1.75%	2.22%
10-May	0.0001	Yes	0.3301	No	2.24%	2.89%	3.02%

## ANOVA Summary Table (Block 22)

## Ultrasonic Pulse Velocity Results

One Way ANOVA			Bartlet's Test for Equal Variances		Coefficient of Variation		
Date	P-Value	Are means significantly different? (P < 0.05)	Bartlet's Statistic P-Value	Are variances significantly different? (P < 0.05)	Coefficient of Variation for top row of block	Coefficient of Variation for middle row of block	Coefficient of Variation for bottom row of block
21-Feb	0.0001	Yes	0.662	No	2.86%	1.97%	1.64%
27-Feb	0.0001	Yes	0.0981	No	1.35%	0.57%	1.95%
6-Mar	0.0023	Yes	0.6142	No	2.43%	3.50%	2.11%
13-Mar	0.0001	Yes	0.311	No	1.52%	0.69%	1.52%
27-Mar	0.0001	Yes	0.5793	No	1.50%	0.94%	1.59%
17-Apr	0.0004	Yes	0.0926	No	2.10%	0.79%	2.81%
1-May	0.0001	Yes	0.1732	No	2.02%	3.23%	3.16%

## ANOVA Summary Table (Block 23)

## Ultrasonic Pulse Velocity Results

Date	One Way ANOVA		Bartlet's Test for Equal Variances		Coefficient of Variation		
	P-Value	Are means significantly different? (P < 0.05)	Bartlet's Statistic P-Value	Are variances significantly different? (P < 0.05)	Coefficient of Variation for top row of block	Coefficient of Variation for middle row of block	Coefficient of Variation for bottom row of block
21-Feb	0.0002	Yes	0.5129	No	2.51%	1.61%	2.89%
27-Feb	0.0006	Yes	0.8762	No	3.06%	2.22%	2.58%
6-Mar	0.0004	Yes	0.7510	No	2.45%	1.87%	2.69%
20-Mar	0.0001	Yes	0.5818	No	1.91%	1.38%	2.33%
27-Mar	0.0017	Yes	0.6626	No	2.69%	2.08%	3.24%
10-Apr	0.0072	Yes	0.8664	No	3.55%	2.57%	3.13%
24-Apr	0.0192	Yes	0.8980	No	3.32%	2.89%	3.59%
10-May	0.0001	Yes	0.0430	Yes	2.44%	2.24%	3.79%

## ANOVA Summary Table (Block 24)

## Ultrasonic Pulse Velocity Results

Date	One Way ANOVA		Bartlet's Test for Equal Variances		Coefficient of Variation		
	P-Value	Are means significantly different? (P < 0.05)	Bartlet's Statistic P-Value	Are variances significantly different? (P < 0.05)	Coefficient of Variation for top row of block	Coefficient of Variation for middle row of block	Coefficient of Variation for bottom row of block
21-Feb	0.0001	Yes	0.3826	No	2.56%	2.73%	1.21%
27-Feb	0.0001	Yes	0.9023	No	1.21%	0.95%	1.14%
6-Mar	0.0001	Yes	0.8016	No	0.88%	1.07%	1.13%
20-Mar	0.0001	Yes	0.7788	No	1.04%	1.44%	1.14%
27-Mar	0.0001	Yes	0.9671	No	1.34%	1.24%	1.38%
10-Apr	0.0001	Yes	0.2259	No	1.57%	0.60%	1.43%
24-Apr	0.002	Yes	0.4473	No	1.80%	1.69%	2.94%
10-May	0.0001	Yes	0.1508	No	2.66%	1.32%	1.98%

## LIST OF REFERENCES

- American Concrete Institute. Committee 224. (1993). *Causes, Evaluation and Repair of Cracks in Concrete Structures* (No. 0-87031-006-2). Detroit, Michigan: American Concrete Institute.
- American Concrete Institute. Committee 546. (1996). *Concrete Repair Guide* (No. 0-87031-022-4). Detroit, Michigan: American Concrete Institute.
- American Concrete Institute. Committee 224. (1998). *Nondestructive Test Methods for Evaluation of Concrete in Structures* Detroit, Michigan: American Concrete Institute.
- ASTM (2001a). *Standard Test for the Compressive Strength of Cylindrical Concrete Specimens*, C39-01. West Conshohocken, Pennsylvania: American Society for Testing and Materials.
- ASTM (2001b). *Standard Test for the Fundamental Transverse, Longitudinal and Torsional Resonant Frequencies of Concrete Specimens*, C215-97. West Conshohocken, Pennsylvania: American Society for Testing and Materials.
- ASTM (2001c). *Standard Test Method for Liquid Penetrant Examination*, E165-95. West Conshohocken, Pennsylvania: American Society for Testing and Materials.
- ASTM (2001d). *Standard Test for the Pulse Velocity Through Concrete*, C597-97. West Conshohocken, Pennsylvania: American Society for Testing and Materials.
- ASTM (2002a). *Dye Penetration of Solid Fiberglass Reinforced Pultruded Stock*, D5117-96. West Conshohocken, Pennsylvania: American Society for Testing and Materials.
- ASTM (2002b). *Standard Guide for Acoustic Examination of Small Parts*, E1932-97. West Conshohocken, Pennsylvania: American Society for Testing and Materials.
- ASTM (2002c). *Standard Guide for Mounting Piezoelectric Acoustic Emission Sensors* E650-97. West Conshohocken, Pennsylvania: American Society for Testing and Materials.
- ASTM (2002d). *Standard Practice for Characterizing Acoustic Emission Instrumentation*, E750-98. West Conshohocken, Pennsylvania: American Society for Testing and Materials.

- ASTM (2002e). *Standard Practices for Thermal Neutron Radiography of Materials*, E748-02. West Conshohocken, Pennsylvania: American Society for Testing and Materials.
- Benedetti, A. (1998). On the Ultrasonic Pulse Propagation into Fire Damaged Concrete. *ACI Structural Journal*, 95(3), 259-271.
- Bergander, M. J. (2003). EMAT Thickness Measurement for Tubes in Coal-fired Boilers. *Applied Energy*, 74(3-4), 439-444.
- Bhide, S. (2001). *Material Usage and Condition of Existing Bridges in the U.S.* Skokie, Illinois: Portland Cement Association.
- Binda, L., Lenzi, G., & Saisi, A. (1998). NDE of Masonry Structures: Use of Radar Tests for the Characterization of Stone Masonries. *NDT & E International*, 31(6), 411-419.
- Binda, L., Saisi, A., & Tiraboschi, C. (2001). Application of Sonic Tests to the Diagnosis of Damaged and Repaired Structures. *NDT & E International*, 34(2), 123-138.
- Boving, K. G. (1989). *NDE Handbook : Non-Destructive Examination Methods for Condition Monitoring*. London: Butterworths.
- Boyd, A. J., Mindess, S., & Skalny, J. (2001). Designing Concrete for Durability. *Materiales De Construccion*, 51(263-64), 37-53.
- Carino N.J. 2001, "The Impact-Echo Method: An Overview" Buildings and Fire Research Laboratory, NIST Gaithersburg, MD. Reprinted from the Proceedings of the 2001 Structures Congress and Exposition, ASCE, May 21-23 Washington D.C. Chang P.C. Editor.
- Casas, J. R., Klaiber, F. W., Mari, A. R., Universidad Politecnica de Catalunya, & Iowa State University. (1996). *Recent Advances in Bridge Engineering: Evaluation, Management and Repair: Proceedings of the US-Europe Workshop on Bridge Engineering, Barcelona, 15-17 July 1996* (1st ed.). Barcelona, Spain: Artes Graficas Torres.
- Casper, J. (2002). *Human-Robot Interactions During the Robot-Assisted Urban Search and Rescue Response at the World Trade Center*. Thesis (M.S.C.S.) University of South Florida.
- Cawley, P., & Adams, R. D. (1988). The Mechanics of the Coin-Tap Method of Non-Destructive Testing. *Journal of Sound and Vibration*, 122(2), 299-316.
- Colla, C., Burnside, C. D., Clark, M. R., Broughton, K. J., & Forde, M. C. (1998). Comparison of Laboratory and Simulated Data for Radar Image Interpretation. *NDT & E International*, 31(6), 439-444.

- Cornwell, I., & McNab, A. (1999). Towards Automated Interpretation of Ultrasonic NDT Data. *NDT & E International*, 32(2), 101-107.
- Davis, A. G. (1997). A Place for Nondestructive Evaluation in the Maintenance of Our Concrete Infrastructure. *Materials Evaluation*, 55(11), 1234-1237.
- Davis, A. G. (1999). Review of Nondestructive Evaluation Techniques of Civil Infrastructure. *Journal of Performance of Constructed Facilities*, 11(4), 47-48.
- Davis, A. G. (2003). The Nondestructive Impulse Response Test in North America: 1985-2001. *NDT & E International*, 36(4), 185-193.
- Davis, A. G., Evans, J. G., & Hertlein, B. H. (1997). Nondestructive Evaluation of Concrete Radioactive Waste Tanks. *Journal of Performance of Constructed Facilities*, 11(4), 161-167.
- Davis, A. G., Olson, C. A., & Michols, K. A. (2001). *Evaluation of Historic Reinforced Concrete Bridges*. Paper Presented at the Proceedings of the 2001 Structural Congress and Exposition, held May 21-23, 2001, Washington, D.C.
- FHWA, U.S. Department of Transportation. Federal Highway Administration. (1995). *Recording and Coding Guide for the Structure Inventory and Appraisal of the Nations Bridges* (No. FHWA-PD-96-001). Washington, DC: U.S. Department of Transportation.
- Green, R. E. (2002). Noncontact Acoustical Techniques for Nondestructive Characterization of Materials and Structures. *International Applied Mechanics*, 38(3), 253-259.
- Gudra, T., & Stawiski, B. (2000). Non-Destructive Strength Characterization of Concrete Using Surface Waves. *NDT & E International*, 33(1), 1-6.
- Guenther, N. (1999). *Internship Report* (No. SS99). Soquel, California: Ultrasonic Devices, Inc.
- Halliday, D., Resnick, R., & Walker, J. (1997). *Fundamentals of Physics* (5th ed.). New York: Wiley.
- Hamilton, H. R., & Levar, J. M. (2003). Nondestructive Evaluation of Carbon Fiber-Reinforced Polymer-Concrete Bond Using Infrared Thermography. *ACI Materials Journal*, 100(1), 63-72.
- Hearn, S. W., & Shield, C. K. (1997). Acoustic Emission Monitoring as a Nondestructive Testing Technique in Reinforced Concrete. *ACI Materials Journal*, 94(6), 510-519.
- Hellier, C. (2001). *Handbook of Nondestructive Evaluation*. New York: McGraw-Hill.

- Institute of British Standards. (1986). *Recommendations for Surface Hardness Testing by Rebound Hammer* (No. 1881 pt. 202:1986). United Kingdom: British Standards Institute.
- Kaiser, H., & Karbhari, V. M. (2002). *Quality and Monitoring of Structural Rehabilitation Measures* (Contract #18347): Oregon Department of Transportation.
- Kearl, P. M. (1997). Observations of Particle Movement in a Monitoring Well Using the Colloidal Borescope. *Journal of Hydrology*, 200(1-4), 323-344.
- Krause, H. J., Wolf, W., Glaas, W., Zimmermann, E., Faley, M. I., Sawade, G., et al. (2002). SQUID Array for Magnetic Inspection of Prestressed Concrete Bridges. *Physica C*, 368(1-4), 91-95.
- Krause, M., Mielentz, F., Milman, B., Muller, W., Schmitz, V., & Wiggenhauser, H. (2001). Ultrasonic Imaging of Concrete Members Using an Array System. *NDT & E International*, 34(6), 403-408.
- Krautkramer, J., & Krautkramer, H. (1990). *Ultrasonic Testing of Materials* (4th fully rev. ed.). New York: Springer-Verlag.
- Kulynyak, D. (2000). Ivan Pului, the Discoverer of X-rays. *The Ukrainian Weekly*, 68(28).
- Lane, D. S. (1998). *Evaluation of Concrete Characteristics for Rigid Pavements*. Charlottesville, Virginia: Virginia Transportation Research Council.
- Lew, H. S., & ACI Committee 228 - Nondestructive Testing of Concrete. (1988). *Nondestructive Testing*. Detroit: American Concrete Institute.
- Li, F. M., & Li, Z. J. (2000). Acoustic Emission Monitoring of Fracture of Fiber-Reinforced Concrete in Tension. *ACI Materials Journal*, 97(6), 629-636.
- Maldague, X. (2001). *Theory and Practice of Infrared Technology for Nondestructive Testing*. New York: Wiley.
- Malhotra, V. M. (1984). *In Situ/Nondestructive Testing of Concrete*. Detroit, Michigan: American Concrete Institute.
- Malhotra, V. M., & Carino, N. J. (1991). *CRC Handbook on Nondestructive Testing of Concrete*. Boca Raton: CRC Press.
- Malhotra, V. M., & Mehta, P. K. (1994). *Concrete Technology: Past, Present, and Future: Proceedings of V. Mohan Malhotra Symposium*. Detroit, Michigan: American Concrete Institute.

- Martin, J., Broughton, K. J., Giannopolous, A., Hardy, M. S. A., & Forde, M. C. (2001). Ultrasonic Tomography of Grouted Duct Post-Tensioned Reinforced Concrete Bridge Beams. *NDT & E International*, 34(2), 107-113.
- Miller, R. K. (1985). *Bridge Testing* (No. TR-103-68-12/85). Princeton Junction, New Jersey: Physical Acoustic Corporation.
- Mindess, S., Young, J. F., & Darwin, D. (2003). *Concrete* (2nd ed.). Upper Saddle River, New Jersey: Prentice Hall.
- Murphy, R. (2000). *Introduction to AI Robotics*. Cambridge, Massachusetts: MIT Press.
- NBI (2003) [http://www.nationalbridgeinventory.com/new\\_page\\_1.htm](http://www.nationalbridgeinventory.com/new_page_1.htm) Last accessed August 20, 2003
- Neville, A. M. (1996). *Properties of Concrete* (4th and final ed.). New York: J. Wiley.
- NOAA (2003) <http://www.srh.noaa.gov/tulsa/climate/rh.html> Last accessed August 20, 2003
- Ohtsu, M., Uchida, M., Okamoto, T., & Yuyama, S. (2002). Damage Assessment of Reinforced Concrete Beams Qualified by Acoustic Emission. *ACI Structural Journal*, 99(4), 411-417.
- Papadakis, E. P. (1999). *Ultrasonic Instruments and Devices: Reference for Modern Instrumentation, Techniques, and Technology*. San Diego, California: Academic Press.
- Pessiki, S. P., & Carino, N. J. (1988). Setting Time and Strength of Concrete Using the Impact-Echo Method. *ACI Materials Journal*, 85(5), 389-399.
- Popovics, J. S., Achenbach, J. D., & Song, W. J. (1999). Application of New Ultrasound and Sound Generation Methods for Testing Concrete Structures. *Magazine of Concrete Research*, 51(1), 35-44.
- Popovics, S. (2001). Analysis of the Concrete Strength Versus Ultrasonic Pulse Velocity Relationship. *Materials Evaluation*, 59(2), 123+.
- Popovics, S., Bilgutay, N. M., Karaoguz, M., & Akgul, T. (2000). High-Frequency Ultrasound Technique for Testing Concrete. *ACI Materials Journal*, 97(1), 58-65.
- Qasrawi, H. Y. (2000). Concrete Strength by Combined Nondestructive Methods - Simply and Reliably Predicted. *Cement and Concrete Research*, 30(5), 739-746.
- Reese, R. T., Kawahara, W. A., & Society for Experimental Mechanics (U.S.). (1993). *Handbook on Structural Testing*. Englewood Cliffs, New Jersey: Fairmont Press.
- Ryall, M. J. (2001). *Bridge Management*. Boston: Butterworth-Heinemann.

- Salawu, O. S. (1997). Detection of Structural Damage through Changes in Frequency: A Review. *Engineering Structures*, 19(9), 718-723.
- Sansalone, M., & Streett, W. B. (1997). *Impact-Echo: Non-Destructive Evaluation of Concrete and Masonry*. Ithaca, New York: Bullbrier Press.
- Scott, I. G. (1991). *Basic Acoustic Emission*. New York: Gordon and Breach Science Publishers.
- Shaw, R. E. (2002). Ultrasonic Testing Procedures, Technician Skills, and Qualifications. *Journal of Materials in Civil Engineering*, 14(1), 62-67.
- Sison, M., Duke, J. C., Clemena, G., & Lozev, M. G. (1996). Acoustic Emission: A Tool for the Bridge Engineer. *Materials Evaluation*, 54(8), 888+.
- Sypeck, D. J. (1996). *Damage Evolution In Titanium Matrix Composites*. Unpublished Ph.D. Dissertation, University of Virginia, Charlottesville.
- Tam, M. T., & Weng, C. C. (1995). Acoustic-Emission Kaiser Effect in Fly-Ash Cement Mortar under Compression. *Journal of Materials in Civil Engineering*, 7(4), 212-217.
- Washer, G. A. (1998). Developments for the Non-Destructive Evaluation of Highway Bridges in the USA. *NDT & E International*, 31(4), 245-249.
- Weil, G. J., & Rowe, T. J. (1998). Nondestructive Testing and Repair of the Concrete Roof Shell at the Seattle Kingdome. *NDT & E International*, 31(6), 389-400.
- Wells, P. N. T. (1974). Medical Ultrasonic Diagnostics. *Electronics and Power*, 20(9), 367-370.
- Wu, H. D., & Siegel, M. (2000). Correlation of Accelerometer and Microphone Data in the "Coin Tap Test". *IEEE Transactions on Instrumentation and Measurement*, 49(3), 493-497.
- Wu, K., Chen, B., & Yao, W. (2000). Study on the AE Characteristics of Fracture Process of Mortar, Concrete and Steel-Fiber-Reinforced Concrete Beams. *Cement and Concrete Research*, 30(9), 1495-1500.
- Yan, T Lin, Y. C., & Lai, C. P., (2003). Prediction of Ultrasonic Pulse Velocity (UPV) in Concrete. *ACI Materials Journal*, 100(1), 21-28.
- Yeih, W., & Huang, R. (1998). Detection of the Corrosion Damage in Reinforced Concrete Members by Ultrasonic Testing. *Cement and Concrete Research*, 28(7), 1071-1083.
- Young, J. F., Mindess, S., Gray, R. J., & Bentur, A. (1998). *The Science and Technology of Civil Engineering Materials*: Prentice Hall.

Yuyama S., Okamoto, T., Tomita, R., Fujiwara, H., Kajio S., Ohtsu, S., & Shigeishi M. (1992). *Discrimination of Cracking Width Developed in Reinforced Concrete Structures by Acoustic Emission*. Seattle, Washington: Physical Acoustics Corporation.

## BIOGRAPHICAL SKETCH

Christopher C. Ferraro was born March 1, 1974, in Huntington, New York, to Ronald and Victoria Ferraro. He graduated from Walt Whitman High School in June 1992. He received his Associate of Arts degree in December of 1994 from Palm Beach Community College, and transferred to the University of Florida to pursue a Bachelor of Science in Civil Engineering in the summer of 1995. While attending the University of Florida full time, Christopher worked part time for the Department of Civil Engineering, for two years as a teaching assistant and research assistant for Dr. Fazil T. Najafi. He received his Bachelor of Science in Civil Engineering in May of 1998, graduating with honors.

Upon graduation he relocated to Long Island, New York, and worked full time in Manhattan, New York, as an Engineer Intern for Law Engineering Inc. After a year with Law, he transferred to STV Incorporated where he worked on several inspection projects under the supervision of Ms. Marjorie M. Lynch, P.E. who aided him in gaining expertise and knowledge which inspired him to resume his education.

Christopher continued with his education, entering graduate school to pursue a Master of Engineering in the Materials Group of the Civil and Coastal Engineering Department in August 2000. After graduating from the University of Florida with a Master of Engineering, Christopher plans on working with Andrew Boyd in the Department of Civil and Coastal Engineering for the fall of 2003, after which he plans to

pursue a career in the exciting and challenging field of civil engineering inspection, research and design.